# PERFORMANCE EVALUATION OF CORROSION INHIBITORS FOR LOCAL CONDITIONS

BY

KHALED AHMED ALAWI AL-SODANI

A Thesis Presented to the
DEANSHIP OF GRADUATE STUDIES

**KING FAHD UNIVERSITY OF PETROLEUM & MINERALS**

DHAHRAN, SAUDI ARABIA

In Partial Fulfillment of the
Requirements for the Degree of

# MASTER OF SCIENCE

In

CIVIL ENGINEERING

MAY 2014

KING FAHD UNIVERSITY OF PETROLEUM & MINERALS

DHAHRAN 31261, SAUDI ARABIA

**DEANSHIP OF GRADUATE STUDIES**

This thesis, written by **Khaled Ahmed Alawi Al-Sodani** under the direction of his thesis advisor and approved by his thesis committee, has been presented and accepted by the Dean of Graduate Studies, in partial fulfillment of the requirements for the degree of **MASTER OF SCIENCE IN CIVIL ENGINEERING.**

**Thesis Committee**

Prof. Omar S. Baghabra Al-Amoudi
(Advisor)

Prof. Mohammed Maslehuddin
(Co-Advisor)

08 JUN 2014

Prof. Nedal T. Ratrout
Department Chairman

Dr. Ahmad Saad Al-Gahtani
(Member)

Prof. Salam A. Zummo
Dean of Graduate Studies

Dr. Salah U. Al-Dulaijan
(Member)

3/6/14

Date

Dr. Shamshad Ahmad
(Member)

*In the Name of Allah, Most Gracious, Most Merciful.*

*Dedicated to:*

*My beloved parents, wife and children*
*for their love, sacrifices and prayers*

# ACKNOWLEDGMENTS

All praises and thanks are due to Allah (subhana wa taala) for bestowing me with health, knowledge and patience to complete this work. May the peace and blessing of Allah be upon Prophet Muhammad (PBUH), his family and his companions. Thereafter, I acknowledge KFUPM for the support given to this research through its tremendous facilities and for granting me the opportunity to pursue graduate studies with financial support. Moreover, I acknowledge the financial support given by Thamar University.

I acknowledge, with deep gratitude and appreciation, encouragement, the inspiration, valuable time and guidance given to me by my Advisor, Prof. Omar S. Baghabra Al-Amoudi. Special thanks are due to Co-Adviser, Prof. Mohammed Maslehuddin, for his continuous encouragement, moral support, valuable time and guidance during this research work.

I am grateful to my Committee members, Dr. Ahmed S. Al-Gahtani, Dr. Salah U. Al-Dulaijan and Dr. Shamshad Ahmad for their constructive guidance and technical support.

Deep thanks are to Department of Civil and Environmental Engineering particularly the chairman Prof. Nedal T. Ratrout, and the other faculty members for their support and encourgment. Thanks are extended to the Research Institute researchers: Eng. Mohammed Shameem, Eng. Abdul Quddus, Eng. Mohammed Bari, Eng. Mohammed Ibrahim, Eng. Hatim and Eng. Mohammad Rizwan, for their sincere and untiring efforts and supplying me with needed materials. Thanks are also due to the laboratory

personnel, Eng. Imran, Mr. Mohammed Showikhat, Mr. Hussain, and Mr. Alam who assisted me in the experimental work.

Finally, my heartfelt gratitude is given to my parents and beloved wife, and my children Mohammed and Omar, who always supported me with their love, patience, encouragement and constant prayers. I would like to thank my brother, sisters, and all members of my family in Yemen.

# TABLE OF CONTENTS

# LIST OF FIGURES

# LIST OF TABLES

# LIST OF PHOTOS

# LIST OF ABBREVIATIONS

| | | |
|---|---|---|
| LPR | : | Linear polarization resistance |
| SCPS | : | Simulated concrete pore solution |
| $E_{corr}$ | : | Corrosion potential (V) |
| $I_{corr}$ | : | Corrosion current density ($\mu A/cm^2$) |
| SEM | : | Scanning electron microscopy |
| T | : | Temperature |
| $^oC$ | : | degree centigrade |
| Fig. | : | Figure |
| *R*p | : | Polarization resistance |
| SCPS | : | Simulated concrete pore solution |
| PDP | : | Potentio-dynamic polarization |
| EDS | : | Systems include a sensitive x-ray detector, liquid nitrogen for cooling, and software to collect and analyze energy spectra. |
| NaCl | : | Sodium chloride: |
| SCE | : | Saturated calomel electrode |

# THESIS ABSTRACT (ENGLISH)

**Name :** **KHALED AHMED ALAWI AL-SODANI**

**Thesis Title :** **PERFORMANCE EVALUATION OF CORROSION INHIBITORS FOR LOCAL CONDITIONS**

**Major Field :** **CIVIL ENGINEERING (STRUCTURES)**

**Date of Degree :** **May 2014**

Deterioration of concrete structures due to reinforcement corrosion is noted in many industrial and non-industrial structures in the coastal areas of Saudi Arabia. Considerable resources are being expended to repair and rehabilitate the deteriorated concrete structures. While deteriorating concrete structures need to be repaired for meeting their design life, preventive measures need also to be taken to avoid deterioration in new construction. Some of the protective measures include: use of fusion-bonded-epoxy coated (FBEC) bars or chemical inhibitors. However, under severe exposure conditions, the service life of structures built with FBEC steel bars can be limited due to the detrimental effect of damage to the FBEC. Consequently, there is an increasing trend towards utilizing corrosion inhibitors to minimize reinforcement corrosion.

Though there is some information on the use of corrosion inhibitors, both locally and in other countries, several aspects, such as the exposure temperature and the combined presence of chloride and sulfate ions, on the effectiveness of inhibitors have not been studied. Consequently, there is an urgent need to study the performance of inhibitors in the presence of temperature and chloride and sulfate concentration.

This research program was conducted into two parts. The first part consisted of preparing a set of 66 steel specimens immersed in simulated concrete pore solution and varying the three key exposure parameters (chloride and/or sulfate concentration, inhibitor type and exposure temperature) using potentio-dynamic polarization method. In the second part of this research, a set of 36 mixtures of concrete specimens was prepared to evaluate the performance of the selected inhibitors in both sound and cracked concrete specimens according to ASTM G 109.

Potentio-dynamic polarization results showed that all the inhibitors perform well in minimizing corrosion. However, their performance decreased with increasing the chloride and/or sulfate concentration and exposure temperature. The corrosion in ASTM G 109 uncracked specimens with the selected corrosion inhibitors was less than that in the control specimens (around three to four times lower). Further, in case of cracked concrete specimens, Inhibitor IV and Inhibitor V exhibited the best corrosion protection. However, the specimens incorporating Inhibitors I, II and III provided no or at best limited protection to the reinforcing steel. The data developed in this study were used in the selection of appropriate inhibitors for the local conditions.

**MASTER OF SCIENCE DEGREE**
**KING FAHD UNIVERSITY OF PETROLEUM AND MINERALS**
**Dhahran, Saudi Arabia**

# ملخص الرسالة

**الاســم : خالد أحمد علوي السوداني**

**عنوان الرسـالة: تقييم أداء موانع الصدأ في البيئات المحليّة**

**التـــخصـــص: هندسة مدنية (إنشاءات)**

**تاريخ الدرجة العلمية: مايو 2014**

لوحظ تدهور المنشآت الخرسانية بسبب تآكل حديد التسليح في العديد من المنشآت الصناعية وغير الصناعية في المناطق الساحلية من المملكة العربية السعودية. وكما هو معلوم، يتم إنفاق موارد ضخمة لإصلاح وإعادة تأهيل المنشآت الخرسانية المتدهورة، والتي تحتاج إلى إصلاح لتلبية عمرها التصميمي. كما تحتاج المنشآت الجديدة إلى اتخاذ التدابير الوقائية اللازمة لتفادي التدهور. وتشمل بعض التدابير الوقائية ما يلي: استخدام القضبان المطلية بالايبوكسي (FBEC) أو الموانع الكيميائية. وفي ظل ظروف التعرض القاسية، فان العمر الافتراضي للمنشآت الخرسانية المبنية باستخدام القضبان المطلية يمكن أن يكون محدوداً نظرا للتأثير الضار للأضرار التي قد تلحق بالقضبان المطلية. وبالتالي، فإن هناك اتجاها متزايدا نحو استخدام موانع الصدأ في تقليل تآكل حديد التسليح.

وعلى الرغم من وجود بعض المعلومات عن استخدام موانع الصدأ، سواء محليا اوفي دول أخرى، فان هناك العديد من الجوانب، مثل تأثير درجة الحرارة ووجود ايونات الكلورايدات والكبريتات جنبا إلى جنب، على فعالية موانع الصدأ التي لم يتم دراستها. ولذلك، فان هناك حاجة ملحة لدراسة أداء موانع الصدأ في وجود درجة الحرارة ، الكلوريدات و الكبريتات.

تم اجراء هذا البحث والذي يتكون من جزئين. الجزء الأول يتكون من تجهيز مجموعة من 66 عينة من حديد التسليح و التي تم غمرها في محلول يحاكي المحلول المائي للخرسانة وتغيير المعايير الثلاثة الرئيسية

للتعرض (كلورايد و/أو كبريتات، مانع الصدأ ودرجة الحرارة) باستخدام طريقة Potentio-dynamic. وفي الجزء الثاني من هذا البحث، تم تجهيز مجموعة من 36 عينه خرسانيه لتقييم أداء الموانع المختارة في كل من العينات السليمة والمشققة طبقا للمواصفة ASTM G 109.

وأظهرت نتائج (Potentio-dynamic Polarization) أن أداء جميع موانع الصدأ كان جيداً في التقليل من التآكل. ومع ذلك، فقد انخفض اداء هذه الموانع مع زيادة تركيز كلورايد و/أو الكبريتات ودرجة حرارة التعرض. وكان التآكل في عينات ASTM G 109 الغير مشققه والتي تحتوي على موانع الصدأ أقل من ذلك في العينات التي لا تحتوي على موانع الصدأ (حوالي 3 الى 4 مرات أقل). علاوة على ذلك، فان عينات الخرسانة المتشققة التي تحتوي على الموانع الرابع والخامس أظهرت حماية افضل. إلا ان العينات التي تتضمن المثبطات الأول والثاني والثالث لم تنجح في توفير الحماية الكافية او في احسن الاحوال وفرت حماية محدودة لحديد التسليح. وقد استخدمت البيانات التي تم تطويرها في هذه الدراسة في اختيار موانع الصدأ الملائمة للظروف المحلية.

**ماجستير بالعلوم الهندسية**
**جامعة الملك فهد للبترول والمعادن**
**الظهران- المملكة العربية السعودية**

# CHAPTER 1

# INTRODUCTION

## 1.1 Durability

Reinforced concrete is widely utilized in the construction of most of the facilities all over the world. It is the most versatile construction material, hence, no significant structure is being built anywhere in the world without the use of concrete in one way or the other. This wide use of concrete is attributed to four specific characteristics. Firstly, concrete can be molded into different sizes and shapes either in a precast concrete plant or on the site. Its second characteristic is the protection it provides to steel against corrosion and the third is its low-cost. The fourth characteristic is the easy availability of its constituent materials. Added to the above advantages, concrete has good fire-resistance, excellent compressive strength, low maintenance requirements, long service-life, and high water resistance. Due to all these advantages, concrete has established itself as a major construction material.

Although concrete has many advantages, it has its own disadvantages. The typical tensile strength of concrete is 8% to 15% of its compressive strength, which is low compared to its compressive strength [1]. This weakness of the concrete has been overcome by the addition of reinforcing steel bars (rebars), so that rebars resist shear and tensile stresses and concrete primarily resists compressive stresses.

Reinforced concrete is expected to show long term durability; however, sometimes it does not perform sufficiently as a result of improper construction, inadequate materials selection, harsh environment, inferior design, or a combination of these factors. The infrequent inferior durability of concrete is the major problem facing the construction industry all over the world, particularly in aggressive exposure conditions. Substantial resources have to be diverted towards the rehabilitation and repair of the deteriorated reinforced concrete structures. These structures are sometimes affected by many processes leading to loss of serviceability or, in extreme cases, to structural collapse. The most common problems are freeze-thaw damage, corrosion of steel reinforcement, alkali-aggregate reactions, high temperature and sulfate attack [2].

Corrosion of reinforcing steel is the most common cause of concrete deterioration. Further, it mainly reduces the useful service life of reinforced concrete structures. Corrosion of reinforcing steel is caused by the diffusion of chloride ions or carbon dioxide to the steel surface. In the arid and semi-arid regions, reinforcement corrosion is accentuated by the high temperature and humidity.

Deterioration of reinforced concrete in the coastal areas of the Arabian Gulf is often noted within a short span of 5 to 10 years. Field studies indicate that the deterioration of structures in this region is mainly attributed to: (i) inappropriate materials specifications, (ii) inadequate construction practices, and (iii) severe environment and geomorphic conditions. The environmental conditions of Saudi Arabia are characterized by a large variation in the daily and seasonal temperature. The ambient temperature in the summer is as high as 45 to 55 °C and the relative humidity ranges between 40 to 95% over a period of 24 hours [3].

The temperature on the concrete surface at this ambient temperature may be as high as 70°C due to solar radiation. The variation in the day to night temperature may be as much as 20°C. This high variation in the day and night temperature leads to the formation of micro-cracks in the concrete that accelerate the diffusion of aggressive species, such as oxygen, chlorides, moisture, and carbon dioxide, to the steel surface thereby promoting corrosion of reinforcing steel. This corrosion is accompanied with substantial expansive forces that result in cracking and spalling of concrete [4].

## 1.2 Improvement of Concrete Durability

Unless proper precautions are taken at the design stage, a reduction in the design life of the structures is to be expected under the severe exposure conditions of the Arabian region. Therefore, concrete quality should be specified in terms of permeability and diffusion indices rather than strength in order to improve its durability [4].

Some of the precautionary measures to improve the concrete quality include: use of dense and impermeable concrete, use of fusion-bonded epoxy-coated (FBEC) bars or chemical inhibitors. FBEC steel bars have been used worldwide for more than three decades to enhance the useful service life of reinforced concrete structures serving in aggressive environments [5-7]. However, they also have a limited life, particularly in severe environments, due to the expected surface damage to the coating. Consequently, corrosion inhibitors are being actively considered for minimizing reinforcement corrosion. The corrosion inhibitors prevent the electrochemical reactions, associated with reinforcement corrosion, from proceeding. They can inhibit the anodic or cathodic reactions or both. While some data exist on the use of chemical inhibitors both in the

Arabian Gulf and in other countries, there is a need for a more detailed study to evaluate the effectiveness of inhibitors under the concomitant effect of different chloride and sulfate concentrations and temperature that prevail in eastern Saudi Arabia.

This study was planned to assess the performance of proprietary and generic inhibitors in minimizing reinforcement corrosion under the conjoint effect of chloride and sulfate and temperature. Based on the data developed in this study, an attempt would be made to determine the service life extension of concrete structures due to the use of corrosion inhibitors. The findings of the study would also be useful in updating the local and international building codes.

## 1.3 Research Objectives

The overall objective of this study was to assess the corrosion protection provided by chemical inhibitors in concrete. The specific objectives are the following:

1. To assess the effect of inhibitor type on the corrosion behavior of steel bars under varying exposure temperature, and chloride and sulfate concentration.
2. To evaluate the chloride threshold in both sound and cracked concrete in the presence of corrosion inhibitors,
3. To study the mechanisms of corrosion protection provided by selected corrosion inhibitors; and
4. To provide recommendations on appropriate avenues of utilizing chemical inhibitors.

# CHAPTER 2

# LITERATURE REVIEW

The premature deterioration of reinforced concrete construction has resulted in considerable resources to be diverted towards the repair and rehabilitation of these structures. Hence, deterioration of concrete structures due to reinforcement corrosion has generated significant research interest worldwide in the past few decades. The protective measures that can be utilized to protect the reinforcing steel from corrosion include the following: (i) production of dense and impermeable concrete, using appropriate design and construction practices, (ii) enhancing the performance of concrete through the application of hydrophobic agents or surface coatings, and (iii) protection of steel through electro-chemical metallic or non-metallic coatings or the use of chemical inhibitors [8-9]. However, there is an increasing trend towards using chemical inhibitors, which is the subject of this investigation.

## 2.1 Mechanism of Reinforcement Corrosion

Corrosion, in general terms, means destruction or deterioration of a material due to a reaction with its environment [10]. Also, metallic corrosion can be defined as a chemical reaction that returns the metal to compounds which are similar to the minerals from which it was extracted [11]. A refined metal, such as steel or iron, has a natural tendency to return to its stable state (iron oxide, $Fe_2O_3$) that exists in nature by corroding. The rate of steel corrosion depends on grain structure, the presence of entrained stress from

fabrication and its composition. It also depends on the nature of the surrounding environment, such as oxygen, pH, the availability of water, ionic species, and temperature [11].

Concrete normally provides a high alkalinity (pH > 13.5) which increases the reinforcing steel protection against corrosion. Under high alkalinity, steel remains passivated. Also, concrete with a low w/c ratio, well consolidated and well cured, has a low permeability that decreases the penetration of corrosion-inducing agents, for example carbon dioxide, chloride, moisture, etc., to the steel surface. In addition, the high electrical resistivity of concrete restricts corrosion rate by reducing the flow of electrical current from the anodic to the cathode electrode [11].

The presence of alkali elements, such as calcium hydroxide, sodium hydroxide, and potassium hydroxide, increase the alkalinity of the concrete pore solution (pH> 13). This high value of alkalinity results in the formation of a sub-microscopic surface layer on the embedded steel. As long as this layer is not disturbed, it keeps the steel in a passive condition and protects from corrosion.

Reinforcement corrosion is caused either by the carbonation of concrete or diffusion of chloride ions or both of them combined together. Both of these species are able to destroy the chemical protection provided by the concrete to the reinforcing steel. The ingress of chloride ions to the steel-concrete interface or carbonation leads to the depassivation of steel.

### 2.1.1 Basic Principles of Corrosion

The most common form of reinforcement corrosion in aqueous medium is of an electrochemical nature in which the corroding metal behaves like a small electrochemical cell. It requires an anode (where oxidation takes place), a cathode (where reduction occurs), an electrical conductor (steel reinforcement), and an electrolyte (concrete). At the anode, oxidation is the principal reaction (loss of electron) [12]. Corrosion starts at the anode when the electrochemical process is initiated by the oxidation of the iron (i.e. loss of electrons). Oxidation is the process when an oxidizing agent (oxygen in this case) takes electrons from the iron atoms transitioning them into soluble ions that enter the solution as shown in Equation 2.1.

$$\boldsymbol{Fe \rightarrow Fe^{++} + e^{-2}} \qquad (\textbf{Oxidation}) \qquad (\boldsymbol{2.1})$$

At the cathode, reduction is the principal reaction whereby the dissolved oxygen in the electrolyte is reduced by the electrons supplied by the anodic reaction to form hydroxyl ions:

$$\boldsymbol{\frac{1}{2}\,O_2 + H_2O + 2e^- \rightarrow 2OH} \qquad (\textbf{Oxygen reduction}) \qquad (\boldsymbol{2.2})$$

This $OH^-$ flows back to the anode through the concrete to complete the circuit. The transfer rate of $OH^-$ depends on moisture content, electrical resistivity of concrete, temperature, and ionic concentration. Then, $OH^-$ ions at the anode combine with the $Fe^{++}$, as shown in Equation 2.3, to form a fairly soluble ferrous hydroxide, $Fe(OH)_2$ [12]. Figure 2.1 schematically represents the mechanisms of reinforcement corrosion.

$$Fe^{++} + 2OH^{-} \rightarrow Fe(OH)_2 \qquad (2.3)$$

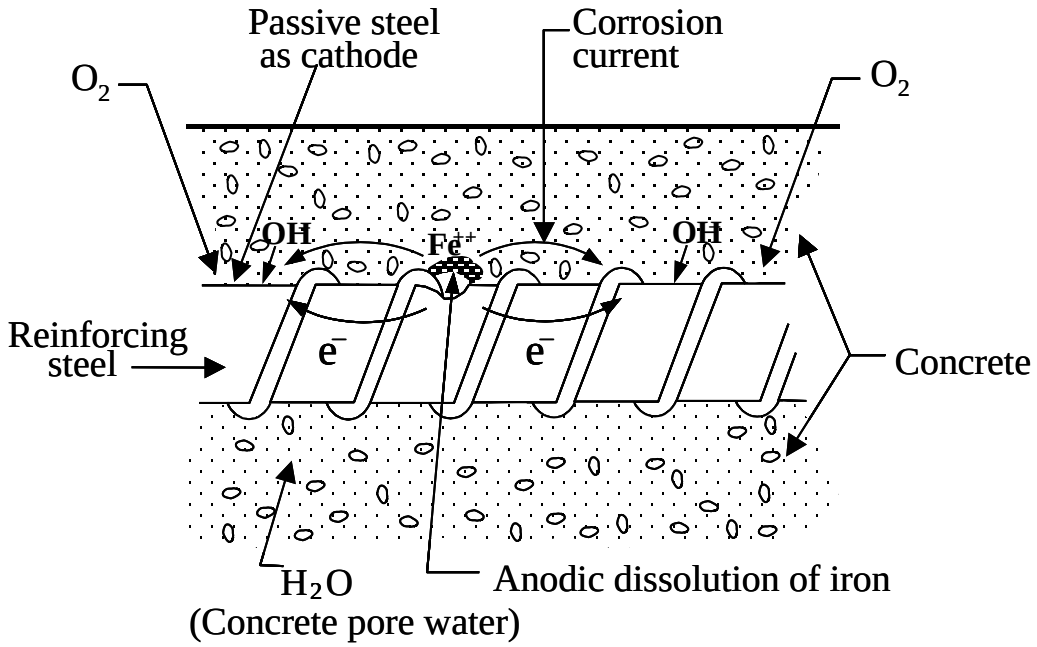


Figure 2.1: Schematic Representation of Mechanism of Reinforcement Corrosion [12].

If there is sufficient oxygen available, this product can further be more oxidized to form insoluble hydrated red rust. The rust thus developed can have a volume 2 to 10 times of the parent iron from which it is formed, depending on the type of oxide formed, as shown in Figure 2.2 [12]. This rust product can exert tensile stresses which is roughly equal to 10 times the tensile strength of concrete. This excessive tensile pressure causes the concrete cover to crack. This leads to eventual spalling off the cover concrete at an advanced stage of the corrosion process, and it may be lead to a reduction in the cross-sectional area of the structural member [12].

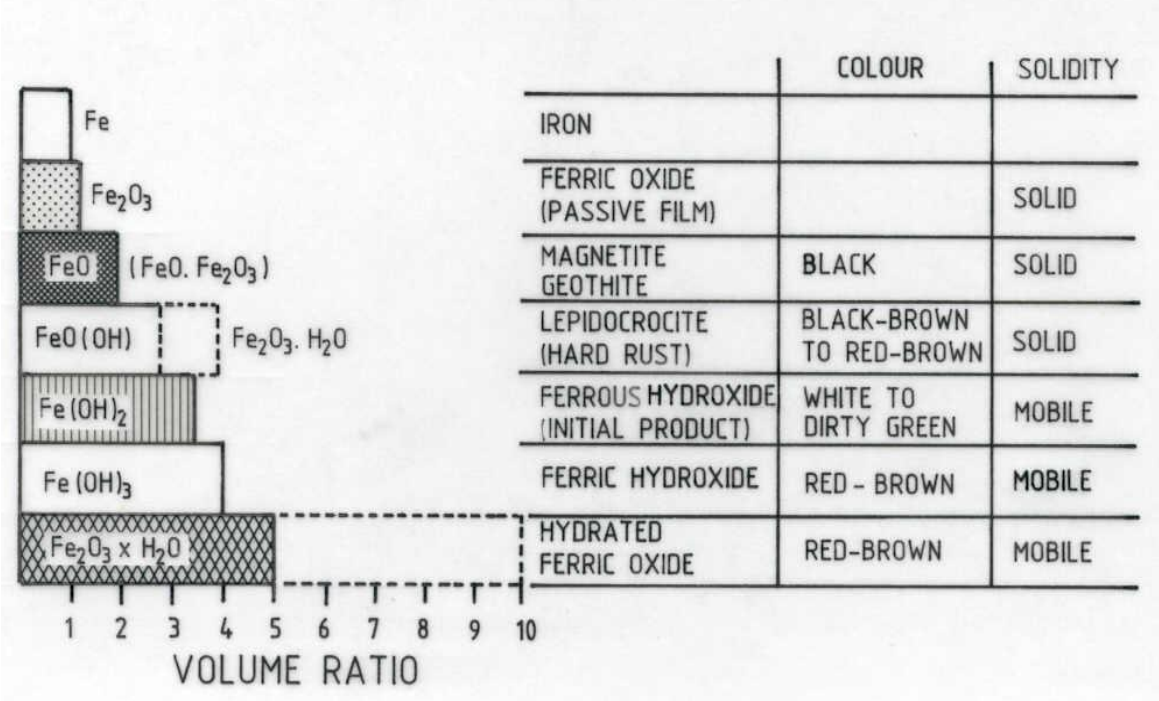


Figure 2.2: Volume of Various Oxides Formed due to Corrosion of Iron [12]

### 2.1.2 Effect of Chloride on Reinforcement Corrosion

Chloride ions in concrete can be contributed from different sources including: contaminated aggregates, salts in chemicals that are applied to the concrete surface, air born salts, salts in ground water, mixing water, and chloride containing admixtures which are used to accelerate curing. The chloride ions from these sources slowly attack the concrete through the pores in the hydrated cement paste till they eventually reach the steel bars. At certain level of concentration, the protective film will be destroyed and the steel will start to corrode when sufficient moisture and oxygen are present at the steel-concrete interface.

The chloride ions initiate corrosion of steel reinforcement by destroying the natural submicroscopic oxide film on the steel surface, allowing the iron to dissolve into solution. Once chloride ions reach the steel surface, they oxidize iron, as

shown in Equation 2.4, to form $FeCl_3$. At the cathode, reduction is the principal reaction; dissolved oxygen in the electrolyte is reduced by the electrons supplied by the anodic reaction to form hydroxyl ions, as shown in Equation 2.5. Thereafter, $FeCl_3$ drags its unstable ferrous ions into solution, where they react with the available hydroxyl ions to form $Fe(OH)_2$. This reaction releases $Cl^-$ ions into the solution and consumes the hydroxyl ions, as shown in Equation 2.6.

$$\mathbf{2Fe + 6Cl^- \rightarrow 2FeCl_3^- + 4e^-} \quad (\mathbf{2.4})$$

$$\mathbf{2H_2 + O_2 + 4\,e^- \rightarrow 4OH^-} \quad (\mathbf{2.5})$$

$$\mathbf{FeCl_3^- + 2OH^- \rightarrow Fe(OH)_2 + 3Cl^-} \quad (\mathbf{2.6})$$

During the oxidation reaction, electrons are released then flow through the steel bar to the cathode. This process results in an increase in the concentration of the chloride ions and a reduction of the pH at the points of corrosion initiation, which may probably lead to the process of pitting corrosion.

"The chloride ions play a dominant role in the initiation of reinforcement corrosion. From this perspective, ACI 318 limits the water-soluble chlorides to 0.15% by weight of cement. ACI Committee 224, adopting a more conservative approach, has suggested that the acid-soluble chloride content should not be more than 0.2% by weight of cement. The British Standard, (BS 8110) allows a maximum total chloride content of 0.4%" [12]. Hausmann [13] suggested that the critical $Cl^-/OH^-$ ratio is about 0.6. Amoudi et al. [14] reported that minimal reinforcement corrosion in blast furnace slag and silica fume cement mortar specimens placed in the aggressive environment of sabkha has been observed even at $Cl^-/OH^-$ ratios of 6.5 and 3.3, respectively.

### 2.1.3 Effect of Sulfate Ions on Reinforcement Corrosion

In sabkha soils and marine environment, sulfates and chlorides are present together and they considerably affect the durability of concrete. Studies conducted by Holden et al. [15] on the pore solution composition of pastes prepared with fixed quantities of sulfates and chlorides indicate an increase in the $OH^-$ concentration due to the addition of sulfates as compared to the alkalinity of pore solution of cement contaminated with similar quantities of chloride salts alone. These results showed the tendency of sulfates ion to reacts preferentially with the $C_3A$ in cement. Hence, corrosion risk is probably to be significantly increased in environments where concrete is subjected to both chloride and sulfate salts [15].

Al-Amoudi and Maslehuddin [16] investigated reinforcement corrosion in cement paste specimens immersed in sulfate, chloride, and sulfate plus chloride environments. It was reported that while the sulfate ions alone were not able to induce reinforcement corrosion while substantial corrosion activity was observed in the specimens immersed in sulfate plus chloride solution.

### 2.1.4 Effect of Temperature on Reinforcement Corrosion

Most regions in the Kingdom of Saudi Arabia are exposed to relatively high temperature of 40 to 50 $^oC$ especially in the summer. The temperature of concrete surface reaches 70 to 75 $^oC$ due to solar radiation. Mehta and Gerwica [17] reported that an increase in temperature increases the kinetics of corrosion reaction and respective factors such as corrosion rate and corrosion current density. They investigated the concrete with high quantity of cement 375 $kg/m^3$ and w/c ratio of 0.45 which was used in beams of San

Mateo Bridge. All beams were exposed to the same environment, however, after 17 years; the steam-cured beams were damaged due to corrosion impact and needed to be repaired. However, the naturally-cured beams showed no corrosion damage. They reported that the micro-cracking in the steam cured beams due to temperature gradients made them more permeable to oxygen and chloride, thus accelerating the corrosion process.

The data available for the performance of concrete under high temperature is very little. It was reported that the initiation time for the corrosion of reinforcement at 10 ºC is approximately three times lower than that at 30º C [18].

## 2.2 Use of Corrosion Inhibitors

A corrosion inhibitor is a chemical compound that, when added in the form of gas, or liquid, reduces the corrosion rates of a material, typically an alloy or a metal. The advantages of using inhibitors to provide corrosion protection are that they are uniformly distributed throughout the concrete matrix, protecting the entire steel surface; and that the concrete's low permeability prevents the inhibitor from leaching out [19]. Reinforced concrete is extensively used in of Saudi Arabia, due to its cost and durability advantages over other structural materials. However, the presence of chloride-contaminated concrete ingredients and severe exposure conditions causes premature deterioration of reinforced concrete, mainly due to reinforcement corrosion, is definite if additional corrosion protection measures are not implemented [19]. In situations where sulfate and chloride contamination is inevitable, one of the main ways of protecting reinforcing steel from corrosion is to add a chemical corrosion inhibitor to the concrete. While a large number

of inhibitors have been produced, only a small group of these inhibitors have been critically studied, and only a few of these inhibitors are used commercially [20].

Over the past fifteen years, corrosion inhibitors have been used extensively for long-term protection of reinforced concrete structures in many applications, for example highway bridges, marine structures and parking garages, etc. In the Middle East, corrosion inhibitors have also been used. In the UAE, according to Matta and Berke [21], more than 100,000 $m^3$ of concrete containing calcium nitrite have been used to build swimming pools, power stations, sea walls, and other residential structures. Studies were also conducted at King Fahd University of Petroleum and Minerals (KFUPM) to assess the usefulness of chemical inhibitors in the aggressive environments of the Arabian Gulf. In the earliest study conducted at KFUPM [22], the effectiveness of selected inhibitors in decreasing reinforcement corrosion in concrete incorporating unwashed aggregates, brackish water or seawater was investigated. The results of that study indicated that calcium nitrate was effective in delaying the onset of reinforcement corrosion in the concrete specimens incorporating seawater, chloride solution or chloride plus sulfate solution. In the concrete specimens prepared with brackish water or unwashed aggregates, all the inhibitors were generally effective in delaying the onset of reinforcement corrosion [22].

The time to initiation of reinforcement corrosion was also calculated by measuring the corrosion current density ($I_{corr}$). Corrosion was assumed to have been initiated when $I_{corr}$ was more than 0.3 $\mu A/cm^2$. Corrosion initiation was indicated only in the control concrete specimens incorporating chloride, chloride plus sulfate or seawater, as a

contamination. All the inhibitors were effective in delaying the onset of reinforcement corrosion, even in the presence of chloride or chloride plus sulfate contamination [22].

## 2.3 Types of Corrosion Inhibitors

Corrosion inhibitors can be divided into three types: anodic, cathodic, and mixed, depending on whether they interface with the corrosion reaction preferentially at the anodic or cathodic sites or whether both are involved [23]. Each of these corrosion inhibitor groups may include materials which mitigate reinforcement corrosion by one of the following mechanisms: (a) formation of layers; (b) oxidation by passivation of the surface, and (c) inhibiting the environment in contact with the metal.

**Anodic types** of corrosion inhibitors are materials that work as inhibitors due to their ability to accept electrons. They operate their action by stifling the reaction at the anode. Anodic inhibitors are usually used in near-neutral solutions where a sparingly soluble corrosion product, such as hydroxides, oxides or salts are formed. Most of these types of inhibitors are effective only when used in high concentrations. The required concentration is often dependent on the level of chlorides at the bar level. The most materials belonging to anodic inhibitors group are sodium nitrite, calcium nitrite, sodium benzoate and sodium chromate [23]. Figure 2.3 shows Evans diagram for the effect of anodic inhibitor.

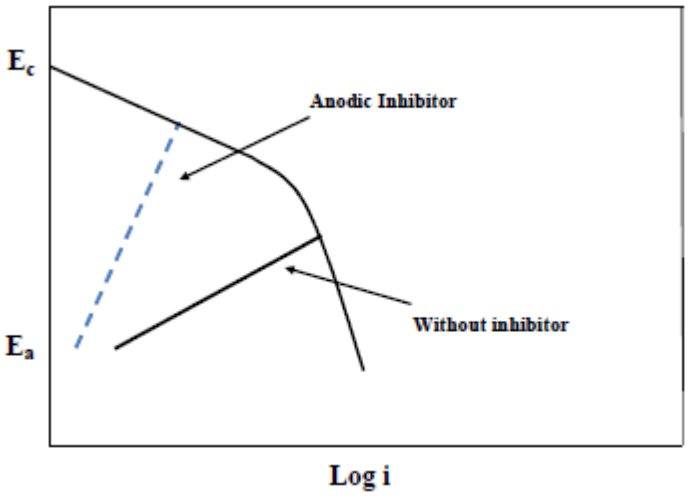


Figure 2.3: Evans Diagram Showing the Effect of Anodic Inhibitor (adapted from Wranglen, 1985)

**Cathodic inhibitors**: These inhibitors operate either by selectively hasten at the cathodic sites or by slowing the cathodic reaction. Most of the materials of this group are strong acceptors for protons and their action, in contrary to anodic inhibitors, is usually indirect.

Cathodic inhibitor is effective in prevent oxygen reduction by the formation of protective inhibitor film at cathodic sites. Hence, it is commonly used in cooling water treatment. The most commonly used materials in this group are bases, like NaOH, $NH_4OH$ or $Na_2CO_3$, that increase the pH of the concrete medium and thereby reducing the solubility of the ferrous ions [23]. Figure 2.4 shows Evans diagram by Revie (2011) showing the effective of cathodic inhibitor in reducing the corrosion rate. These types of corrosion inhibitors shift corrosion potential to the positive side hence reduce corrosion current density and corrosion rate.

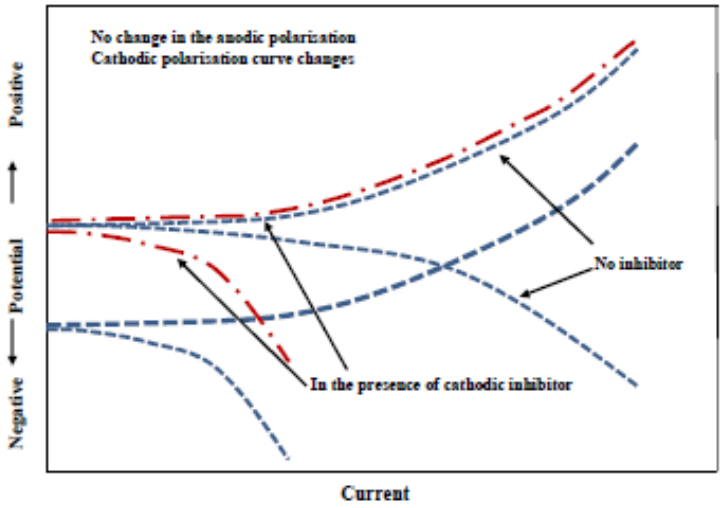


Figure 2.4: Effect of Cathodic Inhibitor in Reduce Corrosion Rate (Revie, 2011)

**Mixed inhibitors:** These inhibitors may simultaneously affect both the cathodic and anodic processes. A mixed inhibitor is usually highly desirable because its effect is all encompassing, including corrosion resulting from microcells on the metal surface as well as that due to chloride attack. These types of inhibitors contain molecules in which the electron density distribution makes the inhibitor to be attracted to both the cathodic and anodicd sites [23]. There are many types of this inhibitor such as zinc phosphonate and molybdate – phosphonate. Figure 2.5 shows corrosion kinetics of mixed inhibitor.

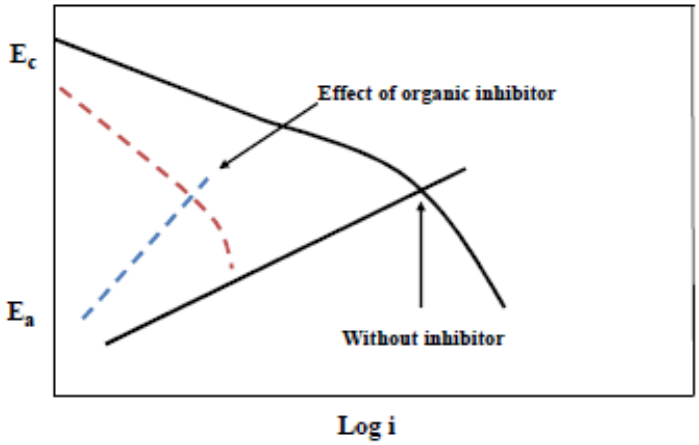


Figure 2.5: Corrosion Kinetics of Mixed Inhibitor (adapted from Wranglen, 1985)

## 2.4 Previous Studies on Corrosion Inhibitors

Several studies have been conducted to evaluate the effectiveness of chemical admixtures in inhibiting reinforcement corrosion [24-29]. Early studies were concentrated on sodium nitrite, potassium chromate, sodium benzoate, and stannous chloride. Later work concentrated mainly on calcium nitrate. El-Jazairi et al. [30] from their work on calcium nitrate concluded that, for effective performance of calcium nitrate exposed to aggressive environments, it is essential to use good quality concrete. They indicated that the use of adequate dosage of the corrosion inhibiting admixture based on calcium nitrate in good quality concrete provides additional safe guard and protection to reinforcing steel in concrete exposed to aggressive environments. According to them, calcium nitrate-based admixture has no detrimental effect on the durability of reinforced concrete even at reduced levels [30]. It enhances the early strength development of concrete and provides long-term protection to reinforcement.

The effect of calcium nitrate-based corrosion inhibitor and crack width on reinforcement corrosion in high performance concrete was investigated by Montes et al. [31]. They reported that the inhibitor alone does not always provide corrosion protection to the reinforcing steel in the concrete. The inhibitor failed to protect the reinforcing steel even in uncracked concrete. However, in combination with good quality concrete, incorporating fly ash, the inhibitor was found to be effective in reducing the effect of chloride-induced reinforcement corrosion.

Maeder [32] investigated the effectiveness of some mixed types of organic inhibitors in inhibiting reinforcement corrosion. These inhibitors were amines and alkanolamines and their salts were organic and inorganic acids. According to the author, the unique

feature of these inhibitors is their ability to diffuse a considerable distance through concrete because of their high vapor pressure. When these inhibitors are added to concrete, they do not delay the time of set. They diffuse to both anodic and cathodic sites and provide protection to reinforcing steel. Furthermore, the author indicates that these inhibitors are preferable over nitrites as they are non-toxic.

The effectiveness of amino-alcohol-based mixed corrosion inhibitors in reducing the rate of reinforcement corrosion was studied by Wombacher et al. [33]. The inhibiting properties were assessed in concrete and in an alkaline electrolyte. Results indicated a delay in the onset of reinforcement corrosion and a decrease in its rate. According to the authors, the inhibitor can be applied on the surface of existing concrete structures, in repair mortars or in grouts for rock bolts and anchors [33]. Also, Jamil et al. [34] conducted electro-chemical impedance measurements in order to obtain information on the corrosion behavior of reinforcing steel in the presence of a penetrating amino-alcohol corrosion inhibitor. The investigation was performed in solutions contaminated with chlorides, in the presence of the inhibitor. The electro-chemical results indicated that the inhibitor is able to penetrate through mortar, minimizing steel corrosion.

Scott et al. [35] conducted a long-term corrosion study to determine the effectiveness of calcium nitrate, silica fume, fly ash, ground granulated blast furnace slag, and disodium tetrapropenyl succinte (DSS) in reducing corrosion of reinforcing steel in concrete. Mixture proportions included: single, double, and triple combinations of these admixtures. Non-cracked and pre-cracked slab specimens were evaluated by visual inspection, macrocell readings, half-cell potentials and autopsies. Triple combinations of calcium nitrate, silica fume, and either fly ash or ground granulated blast furnace slag, as

well as a double combination of calcium nitrate and ground granulated blast furnace slag, performed very well and were recommended in concrete mixtures exposed to severe corrosive environments. DSS outperformed the other admixtures in corrosion prevention. However, it resulted in somewhat lower compressive strength and was not fully tested for effects on other concrete properties.

Qian and Cusson [36] stated that conclusions from previous studies on the effectiveness and field performance of inhibitors on corrosion of reinforcing steel are controversial. They investigated eight commercial corrosion-inhibiting systems using them in a newly reconstructed barrier wall of a highway bridge. Results from a 5-year field survey and laboratory electro-chemical study were presented revealed that low corrosion rates in all spans and more time were needed to induce the significant corrosion activity. Laboratory tests showed cementitious inhibitor coatings applied directly on the rebar could reduce or delay corrosion compared with the cement-coated samples at equivalent NaCl concentrations in a saturated $Ca(OH)_2$ solution.

Malik et al. [37] investigated the performance of dimethyl ethanol amine-based and triethanol amine-based migratory corrosion inhibitors when applied on the surface of concrete. Reinforced concrete specimens coated with migratory inhibitors were exposed to 5% NaCl solution and to the Arabian Gulf seawater for up to 12 months. The condition of the steel bars was evaluated by physical examination and electro-chemical measurements. The results indicated that the corrosion inhibitors utilized were generally able to decrease the corrosion rate of steel in concrete. However, the effect of inhibitors on reinforcement corrosion was not significantly noticeable due to the small period, i.e., 12 months, of exposure.

Al-Mehthel et al. [38] conducted a study to evaluate the improvement in corrosion resistance of chloride-contaminated silica fume cement concrete due to the use of corrosion inhibitors. Three proprietary inhibitors and one generic corrosion inhibitor were evaluated for their performance in inhibiting reinforcement corrosion in the silica fume cement concrete specimens contaminated with 0.4%, 1% and 2% chloride concentration, by weight of cementations materials. Some of the specimens were subjected to wetting and drying cycles and reinforcement corrosion was monitored by measuring the corrosion potentials and corrosion current density. Another batch of concrete specimens was partially immersed in the chloride solution and reinforcement corrosion was accelerated by impressing an anodic potential of 2V. The extent of corrosion increased with increasing chloride contamination in the concrete specimens. Incorporation of inhibitor generally decreased the rate of reinforcement corrosion. The rate of reinforcement corrosion in the concrete specimens incorporating an organic inhibitor that was added to the concrete during mixing was the least followed by that in the concrete specimens on which a penetrating corrosion inhibitor was applied.

Investigation of five corrosion inhibitors was carried out by Belew [39]. The results showed that only calcium nitrite was effective, based on testing performed on concrete samples which were prepared according to ASTM G 109 and cracked beam testing [39].

Different types of commercially available corrosion inhibiting admixtures which can be used in concretes made with basalt aggregates common to Hawaii and Pacific Islands were evaluated by the Hawaii Department of Transportation [40]. These inhibitors were categorized into two main types. Type I admixtures attempt to decrease the concrete permeability that included: latex modifier, Xypex Admix C-2000, Kryton KIM, fly ash

and silica fume. Type II admixtures tend to increase the chloride concentration threshold: Rheocrete CNI, Darex Corrosion Inhibitor (DCI), FerroGard 901and Rheocrete 222. The results showed that Panel with Type 1 admixtures revealed significantly lower half-cell potentials than the corresponding control panel whereas the panels with Type 2 admixtures showed varying degrees of corrosion probability based on half-cell measurements [40].

A recent study was performed by Qian and Cusson to evaluate corrosion protection methods for reinforced concrete bridges, in the presence of chemical corrosion inhibitors utilizing ASTM G 109 concrete samples [41]. Furthermore, on-site measurements were also carried out. The results indicated that ASTM G 109 concrete samples containing corrosion inhibitors did not show any activation after long period of testing (10 years). The control concrete samples which did not contain any chemical inhibitors showed corrosion activation after seven years of testing [41].

Carvallo et al. [42] evaluated the effectiveness of three different types of commercially available corrosion inhibitors for steel in concrete, Ferro Gard 901, Rheocrete $222^{+}$ and DCI (calcium nitrite-based). The results showed that calcium nitrite was the most effective of the three selected chemical inhibitors in mitigating corrosion, while the other two inhibitors were ineffective regardless of concrete quality. Both fly ash and silica fume were ineffective in improving the long term corrosion performance of the embedded bars in concrete. They also reported that no one of the three corrosion inhibitors affected sulfate resistance, strength, and chloride penetration in concrete [42].

Muralidharan et al. [43] evaluated the performance of admixed and migrating inhibitors for reinforcement embedded in portland pozzolona cement (PPC), ordinary

portland cement (OPC), and portland slag cement (PSC) concretes by using macro cell corrosion set-up. The results revealed that migrating corrosion inhibitor performed better than admixed inhibitor in decreasing the corrosion rate of steel bars embedded in different types of concretes under macro cell set up.

Laboratory studies were carried out to evaluate the performance of four commercially available corrosion inhibitors, Rheocrete 222+, DCI–S, Ferrogard 901 and XYPEX C1000 [44]. All concrete samples were prepared according to ASTM G 109. The results gave the following list from the best performance to the worst: XYPEX C-1000, Rheocrete 222-t, DCI-S, Ferrogard 901and the control [44].

Three corrosion inhibitors, sodium nitrite ($NaNO_2$), sodium phosphate ($Na_3PO_4$), and benzotriazole (BTA), in simulated concrete pore solutions were investigated [45]. Corrosion behavior of steel was studied by means of linear polarization resistance (LPR), corrosion potential ($E_{corr}$), electrochemical impedance spectroscopy (EIS), and potentio-dynamic polarization (PDP). Scanning electron microscope (SEM) was used for noticing the morphology and microstructures of corrosion products of steel. The results indicated that BTA may be a potentially effective inhibitor to prevent corrosion of steel in simulated concrete pore solutions, while sodium nitrite ($NaNO_2$) and sodium phosphate ($Na_3PO_4$) are not good corrosion inhibitors [45].

Corrosion rate of reinforcing steels was measured in solutions simulating electrolytic chloride environments in the presence of sodium nitrite as corrosion inhibitor [46]. The presence of sodium nitrite significantly reduced the corrosion rate at low chloride contents, but this efficiency decreases when the pH was decreased [46].

Polarization study has been done to evaluate the corrosion behavior of mild steel in electrolyte simulating concrete pore solution with various water samples such as different types of ions such as well water, rainwater and seawater [47]. The corrosion resistance of mild steel bar in simulated concrete pore solution is as follows: Rainwater > Well water > Seawater. This is evaluated by corrosion current values and linear polarization resistance values [47].

The effect of Benzotriazole and four other Benzotriazole derivatives on the steel corrosion resistance in simulated concrete pore solution was evaluated [48]. Electro-chemical impedance, potentio-dynamic polarization, electro-chemical impedance polarization and Fourier transform infrared spectroscopy (FTIR) were used to assess the steel corrosion protection systems. The potentio-dynamic polarization studies indicated an increase in the pitting potential for all selected protection systems. These inhibitors provided good protection to steel in simulated concrete pore solution [48].

Investigation of the corrosion behavior of carbon steel in the presence of alkaline medium with very low concentration of polymeric nanoaggregates as corrosion inhibitors [49]. The steel electrodes were investigated in chloride-containing and chloride-free cement extracts. The electro-chemical impedance spectroscopy, potentio-dynamic polarization measurements indicated that the presence of polymeric nanoaggregates (micelles) increased corrosion resistance of the carbon steel [49].

Evaluation of an imidazoline derivative for corrosion inhibition activity was carried out for carbon steel in presence of 5% NaCl in simulated concrete pore solution using electro-chemical measurements [50]. The results showed that imidazoline derivative acts as a cathodic type inhibitor and an effective inhibitor in protecting carbon steel from corrosion in alkaline chloride solution [50].

Pereira et al. [51] evaluated the efficiency of two organic corrosion inhibitors, a migratory and an admixed, by electro-chemical techniques in solutions simulating the interstitial electrolyte of concrete and on concrete slabs exposed to natural environmental conditions over a five-year period. From the obtained results, the usefulness of the two products was discussed in view of their application in new structures to prevent chloride-induced corrosion and as a curative method for repairing reinforced concrete structures contaminated with chlorides and affected by reinforcement corrosion.

Ormellese et al. [52] studied the inhibitive action of organic substances on carbon steel in alkaline environment. The effect of aminic and carboxylic groups was investigated through electro-chemical potentio-dynamic polarisation tests in simulated concrete pore solution in the presence of chlorides. They reported that amines showed poor inhibition effect, with very scattered results when their volatility increased. Aminoacids were reported to show some inhibition effect, but not sufficient for industrial applications. Carboxylate substances, especially poly-carboxylates, showed very good inhibition effectiveness, making them the most promising candidates among the tested substances. However, the authors recommend confirmation tests on concrete to check the compatibility of studied inhibitors with concrete and long-term effectiveness of the organic inhibitors [52].

In a study by Mennucci et al. [53], benzotriazole (BTAH), a well-known corrosion inhibitor for copper, was evaluated as a possible corrosion inhibitor of carbon steel (CA-50) in concrete. BTAH was added to a simulated pore solution of an aged concrete with the addition of 3.5 wt% NaCl to imitate marine environments. The effect of BTAH in a concentration of 1.5 wt% on the corrosion resistance of CA-50 carbon steel was

investigated by electro-chemical impedance spectroscopy (EIS) and potentio-dynamic polarization tests. The improvement of the corrosion resistance due to BTAH addition was superior to that associated with nitrite in similar concentration, suggesting that BTAH is a potentially attractive alternative to nitrites for inhibiting corrosion of reinforcing steel in concrete.

Nguyen and Shi [54] evaluated the role of salt contamination and corrosion inhibiting admixtures on reinforcement corrosion. Cement mortar specimens were prepared with NaCl and one of the three admixed corrosion inhibitors, sodium nitrite, disodium β-glycerophosphate, or N,N′-dimethylethanolamine. After 28 days of curing, all steel-mortar samples were ponded with 3% NaCl solution and electro-chemical impedance spectroscopy (EIS) measurements were conducted periodically during the first 48 days. After 60 days of ponding by 3% NaCl solution, field-emission scanning electron microscopy (FESEM) analyses were conducted on the fracture surface of the steel-mortar sample. They reported that admixed chlorides and inhibitors in fresh mortar changed the morphology and cement hydration product of hardened mortar at the steel-mortar interface [54]. The EIS data indicated that all inhibitors increased the polarization resistance of steel, implying reduced corrosion rate of the steel over 48-day exposure to salt ponding. 0.05 M N,N′-dimethylethanolamine was reported to be the most effective corrosion inhibitor, followed by 0.5 M sodium nitrite; whereas 0.05 M disodium β-glycerophosphate was a slower and less capable corrosion inhibitor.

The influence of alkaline nitrites on the inhibition of corrosion of steel in binary and ternary cement environments was evaluated by Song et al. [55]. pH measurements carried out for binary and ternary cement extracts were reported to show that the alkalinity of the

cement was not affected by making use of binary and ternary cements. Gravimetric measurements showed that the decrease in the corrosion rate of steel in different systems follows the order: Ternary > Ordinary Portland cement (OPC) + Portland slag cement (PSC) > (OPC) + Portland pozzalona cement (PPC) > (PPC + PSC). Potential-time studies indicated that the ability to maintain the passivity of steel in different systems also follows the order as above. Potentio-dynamic polarization studies for steel in binary and ternary cement environments showed the favorable influence of the presence of higher amounts of chlorides. The authors reported that nitrites of sodium, potassium and calcium act as anodic inhibitors and they compete with chloride ions for the ferrous ions at the steel to form a film of ferric oxide [55]. An efficiency, as high as 91%, was reported for the ternary system containing 1% chloride and 0.5% nitrite. The degree of surface coverage showed a maximum value for the ternary system (>0.9) even in the presence of a higher amount of chloride thereby indicating the better performance of the system.

Mechmeche et al. [56] studied the effective modes of use of an amino-alcohol based mixed corrosion inhibitor. The inhibitor was tested in fresh pore concrete simulating solutions. The effectiveness of the corrosion inhibitor was investigated through corrosion potential measurements, polarization curves and microscopic observations. The authors reported that the best inhibiting capacity was noted when the inhibitor was introduced in the solution before the contamination with chlorides [56]. The efficiency of the inhibitor was demonstrated even in the case of chloride presence.

Ann and Buenfeld [57] conducted laboratory studies to assess the effect of calcium nitrite-based corrosion inhibitors in raising the chloride threshold level (CTL) for the corrosion of steel embedded in concrete and, hence, the time to corrosion initiation.

Concrete specimens with a centrally located steel rebar were cast with 0, 1, 2, 2.5, and 5.0% nitrite by weight of cement and were cured for 4 weeks. They were then immersed in 4M sodium chloride solution and the galvanic current between the embedded steel and an external cathode was monitored. The CTL of nitrite-free specimens was reported to be typically doubled and trebled by 2.5% nitrite and 5% nitrite, respectively. It was reported that the time to corrosion depended on the cement content. Use of low cement content (282 kg/$m^3$) increased the CTL as the dosage of nitrite in concrete increased, but did not extend the time to corrosion because it accelerated chloride penetration. For a richer mix (350 kg/$m^3$), the time to corrosion increased with the dosage of calcium nitrite. After corrosion initiation, the corrosion rate for specimens containing calcium nitrite was typically two to three times higher than for nitrite-free specimens.

Berke and Hicks [58] published long-term data to show the levels of chloride that a given level of calcium nitrate can protect. They also indicated that once corrosion is initiated, the rates are lower with the addition of calcium nitrate. Justnes and Hygaard [59] used calcium nitrate as a corrosion inhibitor in their research work. The scope of their work was to determine the effect of calcium nitrate on both the chloride-binding capacity and chloride-induced reinforcement corrosion. They concluded that addition of 3.85% calcium nitrate to 1:3 mortars, with and without silica fume, tends to reduce the 1-day strength, but increases the compressive strength from 8 until 56 days of curing. The corrosion rate of embedded steel was; however, five times lower than that in an identical mortar without calcium nitrate.

Nmai [60] studied the multi-functional benefits of a water-based organic corrosion inhibitor. The organic inhibitor investigated consisted of amines of fatty acid esters. The

time to corrosion data indicated that the inhibitor is effective in both the moderate (w/c: 0.5) and high (w/c: 0.4) quality concretes. The permeability-reducing characteristic of the inhibitor was also helpful in reducing the deterioration due to the ingress of other aggressive species, such as sulfates and sulfuric acid.

American Engineering and Testing made a comparative study on cracked beam for three commercial corrosion inhibitors. These inhibitors include Rheocrete 222+, DCI and MCI 2005 NS. The test is a modified ASTM G 109 test using 6% salt solution for ponding and week-long test cycles (instead of 3.5% salt solution and two week cycles). The results showed that MCI 2005 NS is approximately twice as effective as Rheocrete 222+ and DCI in preventing corrosion [61].

## 2.5 Significance of This Research

The literature review, mostly cited in the previous section, reported that several chemical admixtures have been used in concrete construction to retard or inhibit reinforcement corrosion. However, several aspects, such as the exposure temperature and the combined presence of chloride and sulfate ions, on the effectiveness of corrosion inhibitors have not been well studied. The performance of corrosion inhibitors exposed to temperature variation, representative of the environmental conditions of the Arabian Gulf needs to be investigated. Such a study is essential for the Arabian Gulf countries. Consequently, there is an urgent need to study the performance of various types of inhibitors under the local exposure conditions.

# CHAPTER 3

# METHODOLOGY OF RESEARCH

This chapter outlines the materials and the test methods utilized to fulfill the objectives of the present study. In this study, the effect of inhibitor type on corrosion behavior of steel bars under varying exposure conditions in terms of temperature and chloride and sulfate concentration was evaluated. Also, the mechanisms of corrosion protection provided by the selected corrosion inhibitors were evaluated by measuring the corrosion rate using potentio-dynamic scanning and linear polarization techniques on steel specimens immersed in simulated concrete pore solution (SCPS) incorporating one of the selected corrosion inhibitors. Furthermore, macro-cell current, corrosion potential and total corrosion in both sound and cracked ASTM G 109 concrete specimens in the presence of corrosion inhibitors were evaluated. In order to fulfill all the above-mentioned tasks, the following sections describe the materials and various techniques.

## 3.1 Materials

The materials that were used in this investigation are detailed in the following sub-sections.

### 3.1.1 Corrosion Inhibitors

Based on a local market survey and literature review, five corrosion inhibitors were selected. A brief description of each type of the selected inhibitors is as follows:

(i) **Inhibitor I** is a liquid concrete admixture based on calcium nitrite. The manufacturer has claimed that Inhibitor I can be used in conjunction with other concrete admixtures. Also, it acts as a corrosion inhibitor for steel embedded in concrete structures. Furthermore, it does not affect the strength or workability of concrete. The recommended dosage is in the range of 7.5 to 22.5 l/m³ (about 2-6% by weight of the cementitious materials).

(ii) **Inhibitor II** is a liquid concrete admixture based on calcium nitrite. The manufacturer has claimed that Inhibitor II is able to form effective surface barrier for protecting the steel embedded in concrete from chlorides. Moreover, it increases the compressive strength of concrete. The recommended dosage is in the range of 10.0 to 38.0 l/m³ of concrete depending upon the chloride rate.

(iii) **Inhibitor III** is a liquid concrete admixture based on amine carboxylate type. It is claimed that this inhibitor is able to protect steel reinforcing, carbon steel, galvanized steel and any other metals from corrosion induced by chloride, carbonation and atmospheric attack. It is recommended for all reinforced concrete, prestressed, post-tensioned, precast, or marine concrete structures. The recommended dosage is 0.6 l/$m^3$.

(iv) **Inhibitor IV** is a liquid concrete admixture based on modified amino alcohol". The manufacturer has been claimed that this inhibitor can be used as a corrosion inhibitor to protect steel embedded in concrete structures. Furthermore, the manufacturer reported that "because of its high affinity to

steel, Inhibitor IV is able to displace chloride ions from the metal surface to protect concrete from chloride induced corrosion." The recommended dosage is in the range of 3-4% by weight of cementitious materials.

(v) **Inhibitor V** is a liquid concrete admixture based on calcium nitrite. The manufacturer has claimed that this inhibitor effectively inhibits corrosion in all types of metals embedded in concrete structures including pre-stressed, precast and post-tensioned concrete. It is claimed that it is able to extend the service life of concrete structures. The typical dosage of this inhibitor is in the range of 10.0 to 30.0 $l/m^3$ of concrete depending upon the severity of environment.

### 3.1.2 Aggregates

Crushed limestone aggregates with maximum size of 1/2 inch (12.5 mm) obtained from quarries in Abu-Hadriyah were used. It was first sieved into different size fractions and then washed with potable water to remove salt and dust contamination. Thereafter, it was air-dried for 48 hours and stored till used. The absorption and bulk specific gravity of the coarse aggregate were determined as per ASTM C 127 and were found to be 2.9% and 2.60, respectively. Also, dune sand with an average absorption of 0.57% and specific gravity of 2.56 was used as fine aggregate. Table 3.1 shows the grading of the coarse aggregates used in preparing the concrete specimens based on ASTM C 33. Potable water was used for mixing the concrete constituents for all ASTM G 109 specimens.

Table 3.1: Grading of the Coarse Aggregates Used in the Preparing Concrete Specimens

| Size | Wt. Retained % | Cum. Weight. Retained | Passing % | ASTM C 33, No. 7 |
|---|---|---|---|---|
| 3/4” | 0 | 0 | 100 | - |
| 1/2” | 40 | 40 | 60 | 25-60 |
| 3/8” | - | - | - | - |
| 3/16” | 50 | 90 | 10 | 0-10 |
| 3/32” | 10 | 100 | 0 | 0-5 |

### 3.1.3 Cement

ASTM C 150 Type I and silica fume were used in preparing all concrete mixes. Table 3.2 shows the chemical composition of Portland cement and silica fume.

Table 3.2: Chemical Composition of Portland Cement and Silica Fume

| Constituents (wt %) | Type I Cement | Silica Fume |
|---|---|---|
| $SiO_2$ | 19.92 | 98.7 |
| $Al_2O_3$ | 6.54 | 0.21 |
| $Fe_2O_3$ | 2.09 | 0.046 |
| CaO | 64.70 | 0.024 |
| MgO | 1.84 | - |
| $SO_3$ | 2.61 | 0.015 |
| $K_2O$ | 0.56 | 0.048 |
| $Na_2O$ | 0.28 | 0.085 |
| $C_3S$ | 55.9 | - |
| $C_2S$ | 19 | - |
| $C_3A$ | 7.5 | - |
| $C_4AF$ | 9.8 | - |

### 3.1.4 Steel

Deformed mild steel bars produced by the Saudi Iron and Steel Company (HADEED) with a diameter of 16 mm were used to prepare all the steel specimens for potentio-dynamic test in the simulated concrete pore solution analysis (SCPS), while 12 mm steel bars were used for preparing the concrete specimens according to ASTM G 109.

## 3.2 Test Variables

In order to fulfil the objectives of this investigation, the following test variables were selected to simulate moderate and severe environmental conditions in the eastern province of Saudi Arabia:

1) Type of corrosion inhibitor (Five different types of corrosion inhibitor).
2) Temperature (25, 40 and 55 ºC).
3) Chloride concentration (1000, 1500 and 2000 ppm).
4) Sulfate concentration (500 and 2000 ppm).

Tables 3.3 through 3.5 show the types of inhibitor, temperature range and chloride sulfate concentration and the relevant tests, while Tables 3.6 and 3.7 show the details of concrete specimens for determining the chloride threshold values.

Table 3.3: Potentio-Dynamic Tests on Steel Samples in Presence of Chloride and Varying Temperature

| Inhibitor | Chloride Concentration (ppm) | Temperature (°C) | Evaluation Test |
|---|---|---|---|
| None (Control) | 1000 | 25 | - Potentio-dynamic technique.<br>- Linear polarization method. |
| | 1500 | 40 | |
| | 2000 | 55 | |
| Inhibitor I | 1000 | 25 | |
| | 1500 | 40 | |
| | 2000 | 55 | |
| Inhibitor II | 1000 | 25 | |
| | 1500 | 40 | |
| | 2000 | 55 | |
| Inhibitor III | 1000 | 25 | |
| | 1500 | 40 | |
| | 2000 | 55 | |
| Inhibitor IV | 1000 | 25 | |
| | 1500 | 40 | |
| | 2000 | 55 | |
| Inhibitor V | 1000 | 25 | |
| | 1500 | 40 | |
| | 2000 | 55 | |

Table 3.4: Details of Potentio-Dynamic Tests on Steel Samples in the Presence of Chloride and Sulfate

| Inhibitor | Chloride Concentration (ppm) | Sulfate Concentration (ppm) | Temperature (°C) | Evaluation Test |
|---|---|---|---|---|
| **None (Control)** | 1000 | 500<br>2000 | 40 | - Potentio-dynamic technique.<br>-Linear polarization method. |
| **Inhibitor I** | 1000 | 500<br>2000 | 40 | |
| **Inhibitor II** | 1000 | 500<br>2000 | 40 | |
| **Inhibitor III** | 1000 | 500<br>2000 | 40 | |
| **Inhibitor IV** | 1000 | 500<br>2000 | 40 | |
| **Inhibitor V** | 1000 | 500<br>2000 | 40 | |

Table 3.5: Details of Steel Samples for SEM

| Inhibitor | Chloride Concentration (ppm) | Sulfate Concentration (ppm) | Temperature (°C) | No. of Steel Specimens | Evaluation Properties |
|---|---|---|---|---|---|
| **None(Control)** | 1500 | - | 25<br>55 | 2 | **Microstructure** |
| **Inhibitor I** | 1500 | - | 25<br>55 | 2 | |
| **Inhibitor II** | 1500 | - | 25<br>55 | 2 | |
| **Inhibitor III** | 1500 | - | 25<br>55 | 2 | |
| **Inhibitor IV** | 1500 | - | 25<br>55 | 2 | |
| **Inhibitor V** | 1500 | - | 25<br>55 | 2 | |
| **None(Control)** | 1000 | 2000 | 40 | 1 | |
| **Inhibitor I** | 1000 | 2000 | 40 | 1 | |
| **Inhibitor II** | 1000 | 2000 | 40 | 1 | |
| **Inhibitor III** | 1000 | 2000 | 40 | 1 | |
| **Inhibitor IV** | 1000 | 2000 | 40 | 1 | |
| **Inhibitor V** | 1000 | 2000 | 40 | 1 | |

Table 3.6 : Concrete Specimens (without Crack) for Laboratory Exposure

| Inhibitor | No. of Prismatic Specimens | Dimensions in (mm) | Test | Evaluation Properties |
|---|---|---|---|---|
| **None (Control)** | 3 | 280 x 150 x 115 | ASTM G 109 | Chloride threshold |
| **Inhibitor I** | 3 | 280 x 150 x 115 | | |
| **Inhibitor II** | 3 | 280 x 150 x 115 | | |
| **Inhibitor III** | 3 | 280 x 150 x 115 | | |
| **Inhibitor IV** | 3 | 280 x 150 x 115 | | |
| **Inhibitor V** | 3 | 280 x 150 x 115 | | |

Table 3.7: Cracked Concrete Specimens for Laboratory Exposure

| Inhibitor | No. of prismatic Specimens | Dimensions in (mm) | Test | Evaluation Properties |
|---|---|---|---|---|
| **None (Control)** | 3 | 280 x 150 x 115 | ASTM G 109 "with artificial crack" | Chloride threshold |
| **Inhibitor I** | 3 | 280 x 150 x 115 | | |
| **Inhibitor II** | 3 | 280 x 150 x 115 | | |
| **Inhibitor III** | 3 | 280 x 150 x 115 | | |
| **Inhibitor IV** | 3 | 280 x 150 x 115 | | |
| **Inhibitor V** | 3 | 280 x 150 x 115 | | |

## 3.3 Electro-Chemical Testing

### 3.3.1 Steel Specimens Design

Steel specimens of 28 mm length and 16 mm diameter were prepared and the surface of each sample was cleaned by using sand paper and acetone. Both ends of the steel samples were coated with epoxy resin, as shown in Figure 3.1. The top side of steel specimen was drilled to be fitted with coarse-thread stainless steel holder. The exposed area of the reinforcing steel was in the range of (14.50 to 14.75) $cm^2$. Completed specimens are shown in Figure 3.2.

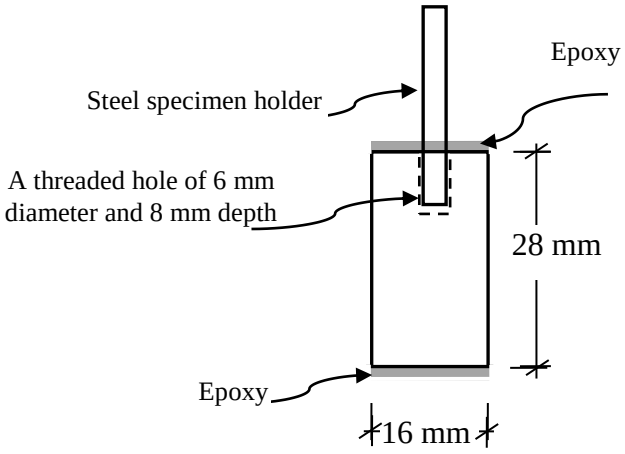


Figure 3.1: Schematic Representation Steel Specimen

Figure 3.2: Specimens Ready for Testing

### 3.3.2 Simulated Concrete Pore Solution

The simulated concrete pore solution was prepared based on the analysis of concrete specimens at KFUPM which indicates that one liter of concrete pore solution contains 974 g of distilled water, 14 g of potassium hydroxide (KOH), 10 g of sodium hydroxide (NaOH), and 2 g of calcium hydroxide [$Ca(OH)_2$]. The simulated concrete pore solution has a pH of more than 13.4. Reagent grade chemicals of KOH, NaOH and Ca $(OH)_2$ were utilized to prepare the concrete pore solution.

### 3.3.3 Test procedures

The steel specimens, as described in Section 3.3.1, were placed in the corrosion cell containing simulated concrete pore solution incorporating one type of corrosion inhibitor and varying temperature and sulfate and/or chloride concentration. Thereafter, potentio-dynamic polarization test was conducted.

In order to conduct the proposed test procedures, specialized equipment was used (ACM instrument). The main components of this system included: computer operated potentiostat, controlled magnetic stirring table for stirring the solution during test period, corrosion cell, and thermometer for measuring the temperature of the solution.

### 3.3.4 Description of the Corrosion Cell Preparation and Curing of Specimens

A three electrodes cell was used for the potentio-dynamic measurement. It mainly consists of three electrodes which are immersed in the solution as follows:

- Stainless steel plate was used as concrete electrode.
- Saturated calomel electrode (SCE) used as the reference electrode.

- Working electrode (the tested steel specimen itself).

The steel samples were prepared as described in 3.3.1. In order to attach the steel specimen to the specimen holder, a threaded hole of 6 mm diameter and 8 mm deep was drilled in each sample. The specimen holder was covered with a Teflon tube to prevent any possibility of crevice corrosion. The electrolyte level was kept below the attaching point all the time. Figure 3.3 shows the working electrode, reference and counter electrode.

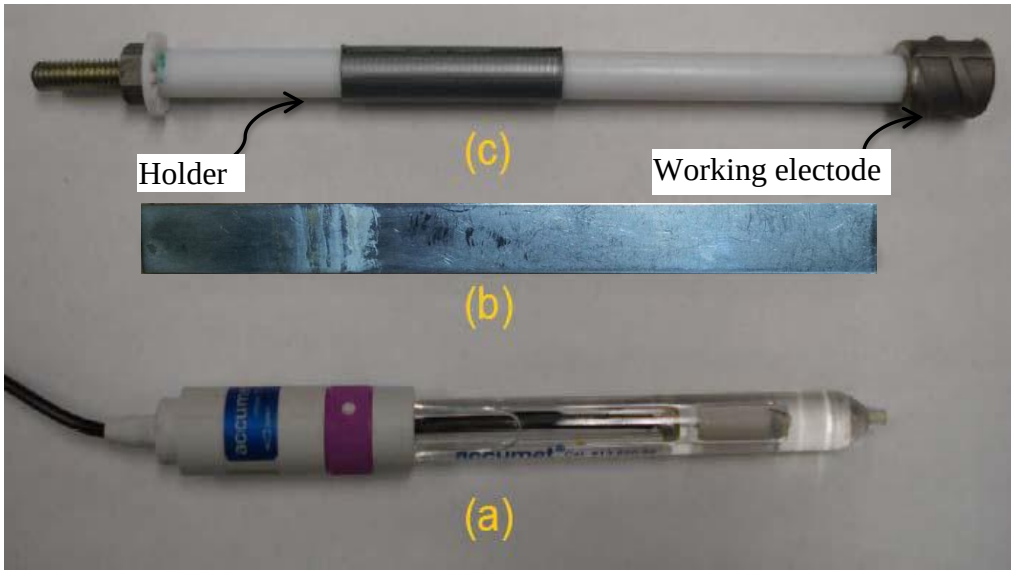


Figure 3.3: The Electrodes Used (a) Reference Electrode (b) Counter Electrode (c) Working Electrode Attached to its Holder

### 3.3.5 Potentio-dynamic Testing

The potentio-dynamic method measures the current for a large potential sweep from the cathodic to the anodic region of the corrosion potential. The potentio-dynamic studies were conducted on bare steel exposed to electrolyte representing the concrete pore solution admixed with the selected inhibitors, selected chloride concentration and

selected temperature. The potentio-dynamic potential-current curves were recorded by changing the electrode potential from -900 to +900 mV with a scan rate of 15 mV/minute, as shown in Figure 3.4. The schematic illustration in Figure 3.5a displays the main terminologies for a typical potentio-dynamic polarization diagram (PDP), which is plotted in terms of applied potential vs the logarithm of the measured corrosion current density. From this Figure, we can notice many futures which can be used to interpret the behavior of steel specimens under PDP test. The open circuit potential is located at Point (A) at which the sum of cathodic and anodic reaction on the working electrode is zero (often this point equals to corrosion potential). As the applied potential increases from A to B, anodic polarization moves to region (B), which is the passive region (increase in the applied potential without increase in the measured current). Point (C) is known as the active potential, and as the applied potential increases above this value, the current moves to region (D), which is called active region. At region (D), the current density increases with the increase in the applied potential and steel oxidation is the dominant reaction taking place. The increase in current continues with the increase in the applied potential till it reaches point (E), which is the limit point of anodic scan. In some cases, sudden increase in the measured current may be noted without an increase in the potential, which indicates presence of pitting corrosion and the corresponding potential called the pitting potential, as shown in Figure 3.5b.

In the cathodic scan, the applied potential increased in the negative direction, as anodic scan point (A) represents the open circuit potential. As the applied potential increases in the negative direction the current moves into region (F), which represents the

oxygen reduction reaction (cathodic polarization). This increase continues till point (H), which is the limit point for cathodic scan.

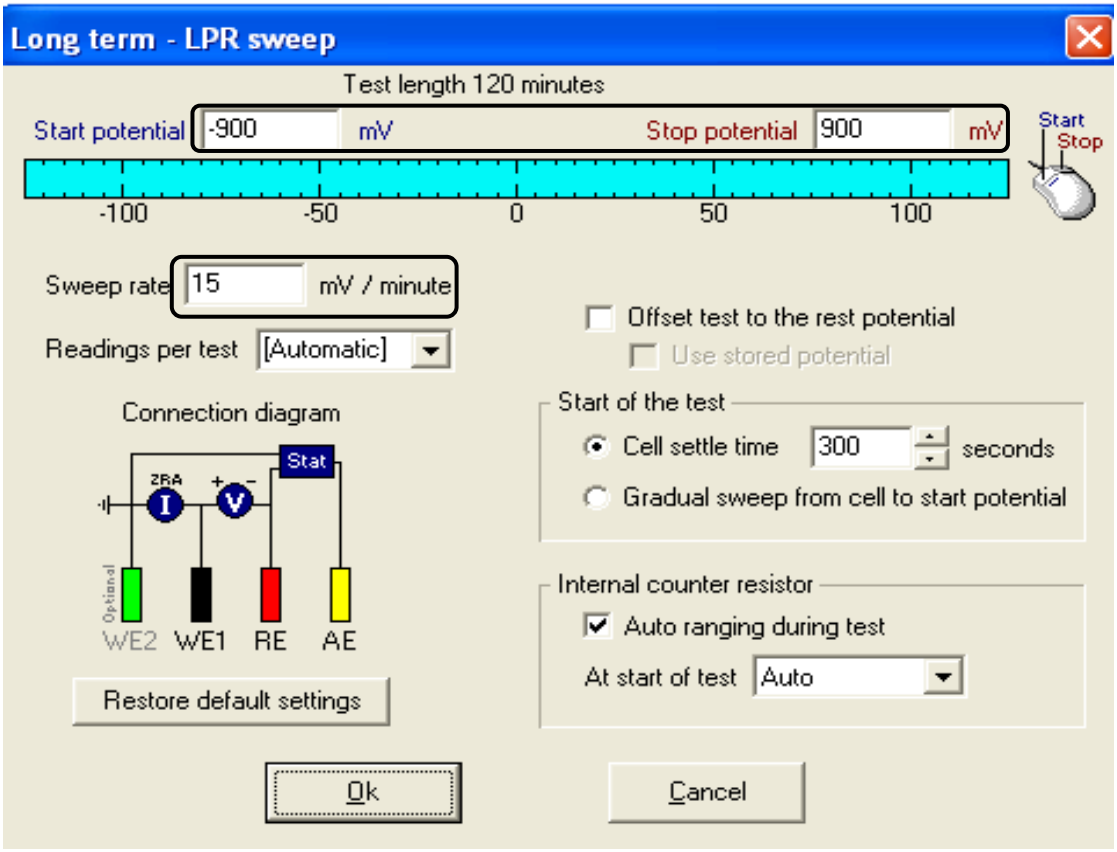


Figure 3.4: Potential Range and Scanning Rate as Appeared

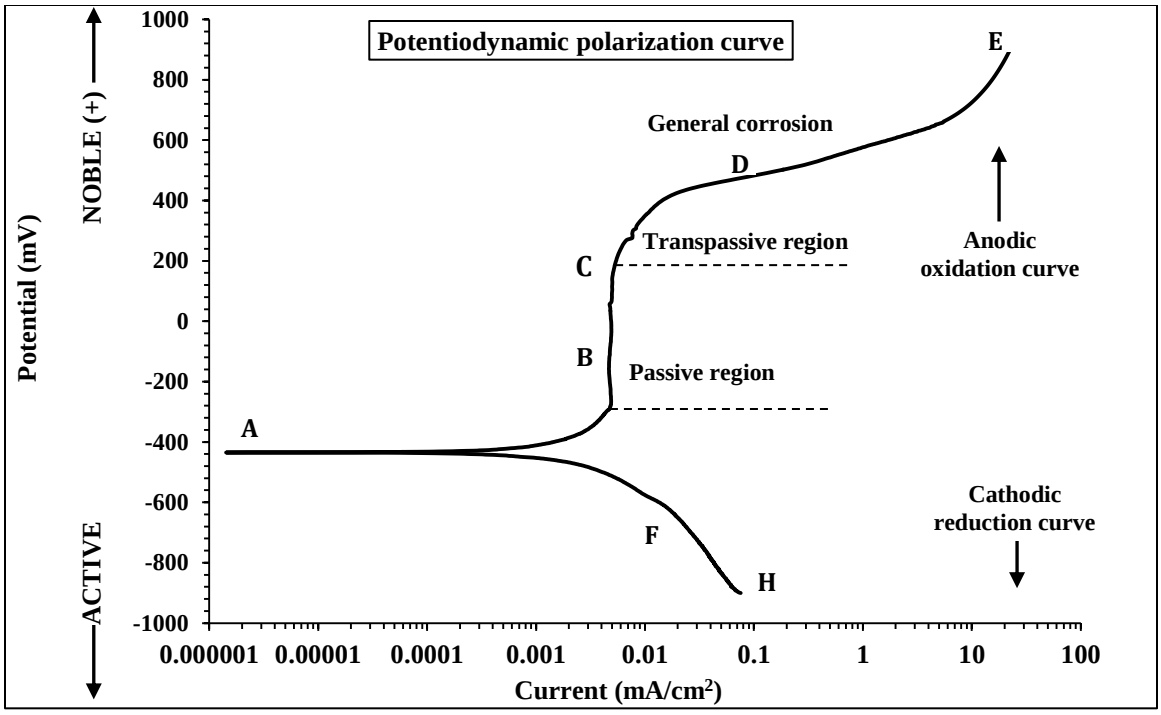


Figure 3.5a: Schematic Illustration of Potentio-Dynamic Polarization with Various Terminologies

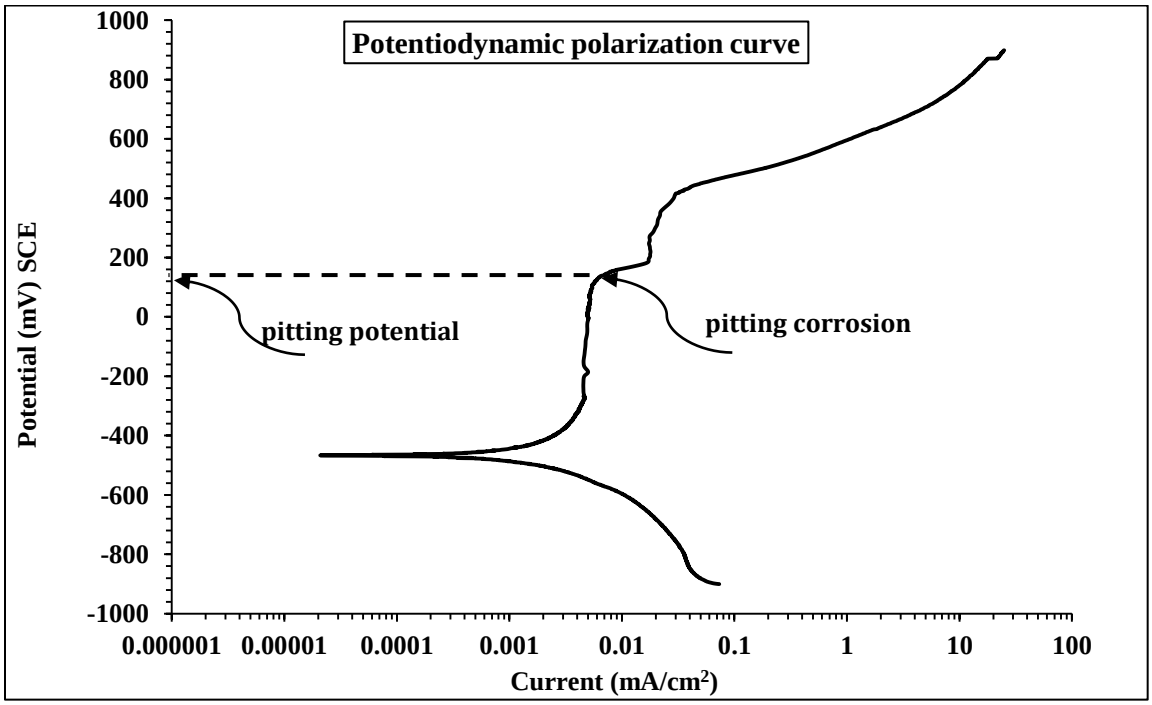


Figure 3.5b: Schematic Illustration of Potentio-Dynamic Polarization with Pitting Corrosion

Significant information can be obtained from the potentio-dynamic polarization scan, some of which include the following:

i. The potential area over which the metal remains at passive stage.
ii. The corrosion rate of the metal sample in the passive area and the ability of the metal sample to be passivated,
iii. The localized corrosion of metal samples, and
iv. Passivity condition.

### 3.3.6 Corrosion Current Density

For this test, ACM instrument with three electrodes was used to conduct the potentio-dynamic scan. The steel specimen with 28 mm length and 16 mm diameter, as described in Section 3.3.1, was connected to the working electrode terminal while reference electrode and small steel plate were connected to the respective terminals of the potentiostat. This specimen was polarized by applying a potential of ±900 mV of the corrosion potential with scan rate of 15 mV/minute and the resulting current between the working and counter electrodes is measured. Figure 3.6 shows a schematic representation of the set-up which was used to measure the corrosion current density. Also, Figure 3.7 show general view of the experimental setup of corrosion current density test.

Figure 3.8 depicted the main terminologies in a polarization diagram which is plotted between the applied potential and log measured current. The solid lines represent cathodic and anodic reactions, whereas the dashed lines represent the linear part of each reaction. The intersection of these dashed lines gives the open circuit potential ($E_{corr}$) on

the vertical excise and corrosion current density on the horizontal axis. The anodic polarization curve is predominant at positive direction (Nobel), while cathodic polarization curve is predominant at negative direction (active). Then, the corrosion current density can be calculated using the Stern-Geary formula [63]:

$$I_{corr} = B/R_p \qquad (3.1)$$

Where:

$I_{corr}$ = corrosion current density ($\mu A/cm^2$);

$R_p$ = polarization resistance, KOhms-$cm^2$;

$B = (\beta a * \beta c)/(2.3(\beta a+\beta c))$;

Where:

$\beta c$ and $\beta a$ are the cathodic and anodic Tafel constants, respectively.

The Tafel constants can be determined either by polarizing the steel to ±250 mV of the corrosion potential or polarizing the steel to ±900 mV of the corrosion potential (potentio-dynamic). In case of the absence of sufficient data on tafel constants, "a value of 100 mV is to be used for steel in a highly resistant medium" [64]. A good correlation between the linear polarization technique and the weight loss determined by gravimetric methods was observed by Gonzalez et al [65] by using a B value of 52 mV in the passive state and 26 mV for steel in the active state. In our investigation, $\beta c = \beta a = 120$ mV was used throughout which corresponds to B = 26 mV. These values have been found to be useful in the corrosion experiments at KFUPM.

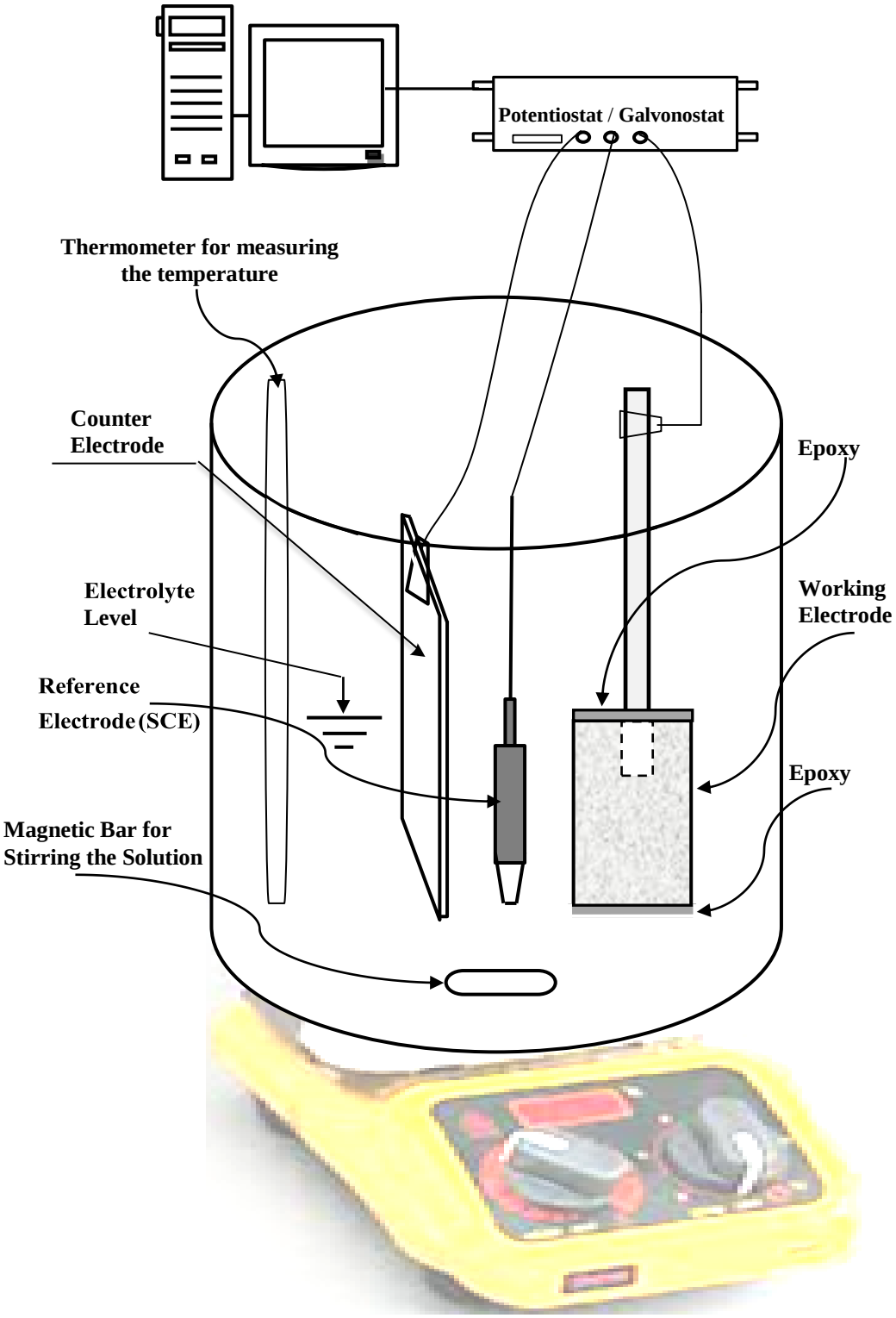


Figure 3.6: Schematic Representation of the Experimental Setup Used for Electro-Chemical Measurements

Figure 3.7: General View of the Experimental Setup for Electro-Chemical Measurements

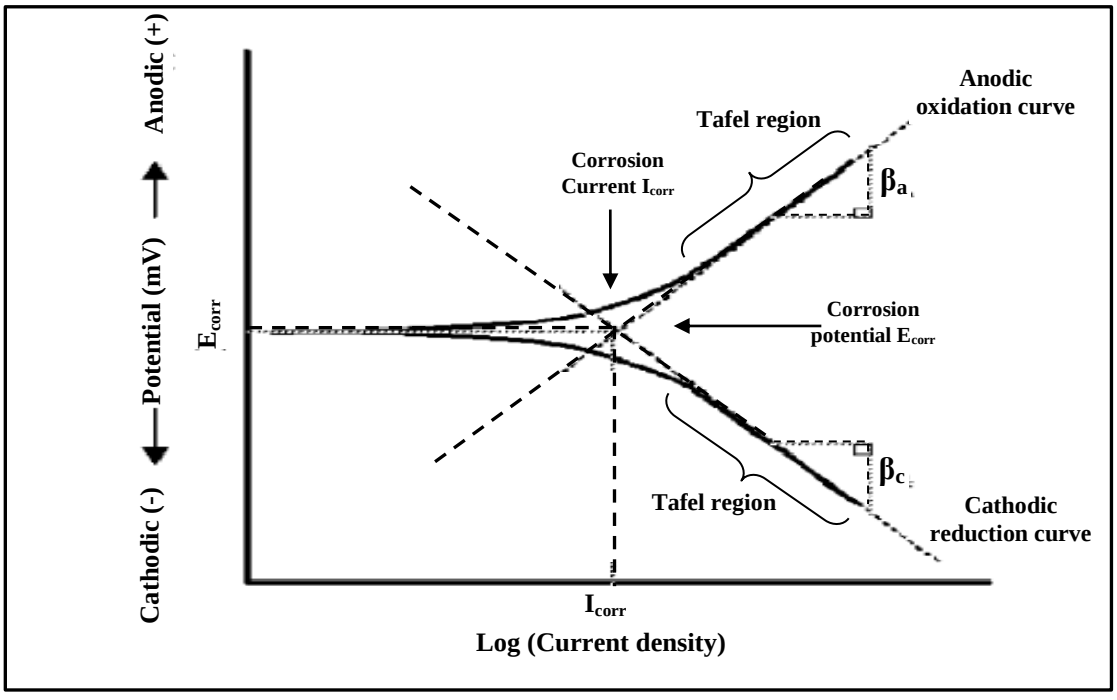


Figure 3.8: The Main Terminologies in Tafel Polarization Diagram

### 3.3.7 Corrosion Potentials

Corrosion is an electro-chemical process in which the corroding metal behaves like a small electro-chemical cell. This process of corrosion generates electrical potentials which can be detected and categorized by the half-cell. The equipment and method of measurment are presented in ASTM C 876 [62]. The free corrosion potential of the steel bar can be measured by determining the voltage difference between the steel bar and reference electrode which are immerged in electrolyte representing concrete pore solution. Also, the free corrosion potential of the steel bar for ASTM G 109 specimens was measured by determining the voltage difference between the top steel bar and reference electrode which are immerged in electrolyte representing distilled water with 3% NaCl. The more negative the reading means greater corrosion probability.

### 3.3.8 Scanning Electron Microscopy (SEM)

The scanning electron microscope (SEM) uses beam of high-energy electrons instead of light to generate variety of signals at the surface of solid samples. These signals reveal information about the sample including its chemical composition, external morphology (texture), and orientation of materials making up the sample, and crystalline structure. In this research, the surface of mild steel samples exposed to simulated concrete pore solution at different temperatures and chloride or chloride plus sulfate concentrations with and without inhibitor were evaluated using SEM to know the surface conditions. In order to conduct the proposed SEM test procedures, specialized equipment (JSM-5800LV SEM instrument) was used. The main components of this system includes: sample chamber, electron column, three visual display monitors and EDS detector, as shown in Figure 3.9.

Figure 3.9: Photographic Documentation of SEM Instrument showing the main Components

## 3.4 Preparation of Concrete Specimens

Two types of concrete specimens were prepared with one dosage of the five different corrosion inhibitors. The dosage of the proprietary inhibitors was that recommended by their manufacturers.

### 3.4.1 Concrete Specimens Design

The first type of concrete specimens was designed according to ASTM G 109, with a 12 mm diameter steel bars. These bars were cut into 14-in (360 mm) long pieces. One end of steel specimen was drilled and tapped to be fitted with a coarse-thread stainless. The steel screwed bars were cleaned with acetone. Electroplater's tape was used to cover 78 mm from each end of the steel samples leaving 204 mm long piece of sample exposed

for testing. Electrical connections and the ends of steel bars were coated with a two-part epoxy. Then, the steel bars were placed into wooden molds with the following dimensions: 280 x 150 x 115 mm (inner dimensions) in two layers. These bars must be placed in the middle of the mold. The top layer consisted of one steel reinforcement bar with a clear cover depth of 25.4 mm. While the bottom reinforcement layer consisted of two steel reinforcement bars that were placed 31.75 mm from bottom of the mold. Figure 3.10 is a schematic representation of an ASTM G 109 test specimen. Photographic documentation of the completed specimens is shown in Figure 3.11.

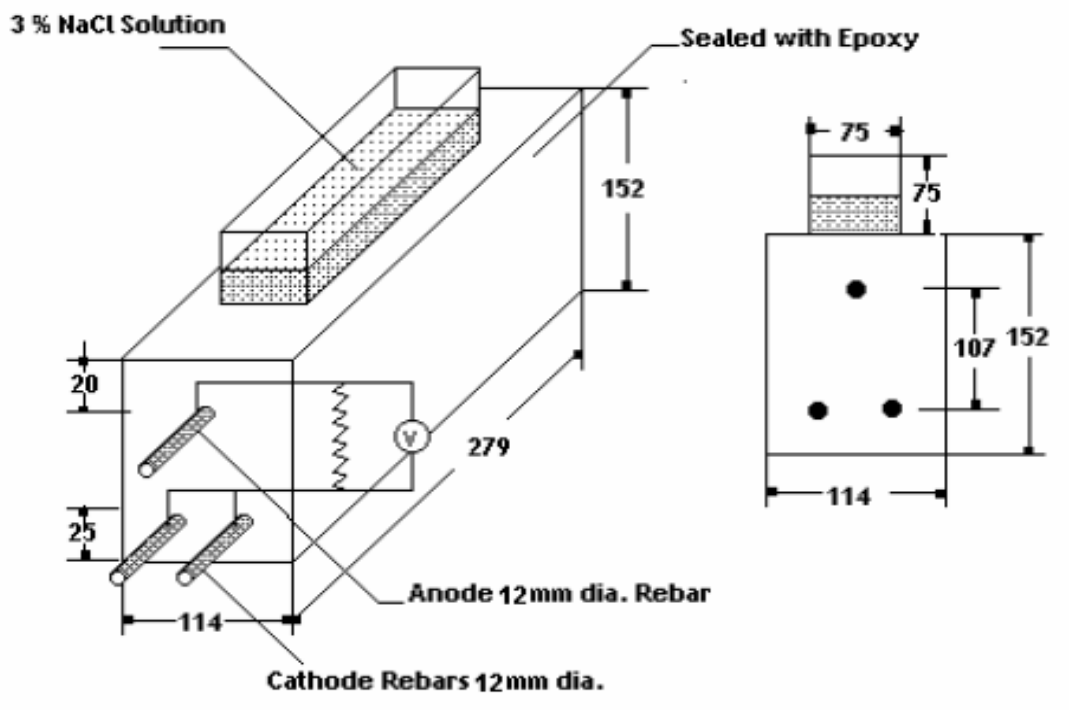


Figure 3.10: Schematic Representation of ASTM G 109 Specimen

Figure 3.11: Completed G 109 Concrete Specimens

The second type of concrete specimens was designed according to ASTM G 109 but with a crack. Reinforced concrete specimens were prepared as described earlier. However, artificial crack was simulated in the concrete parallel to and above the top bar using a 0.30 mm wide, 203 mm long stainless steel shim cast into the concrete specimens. The shim was removed 4 hours after casting, as shown in Figures 3.12 and 3.13.

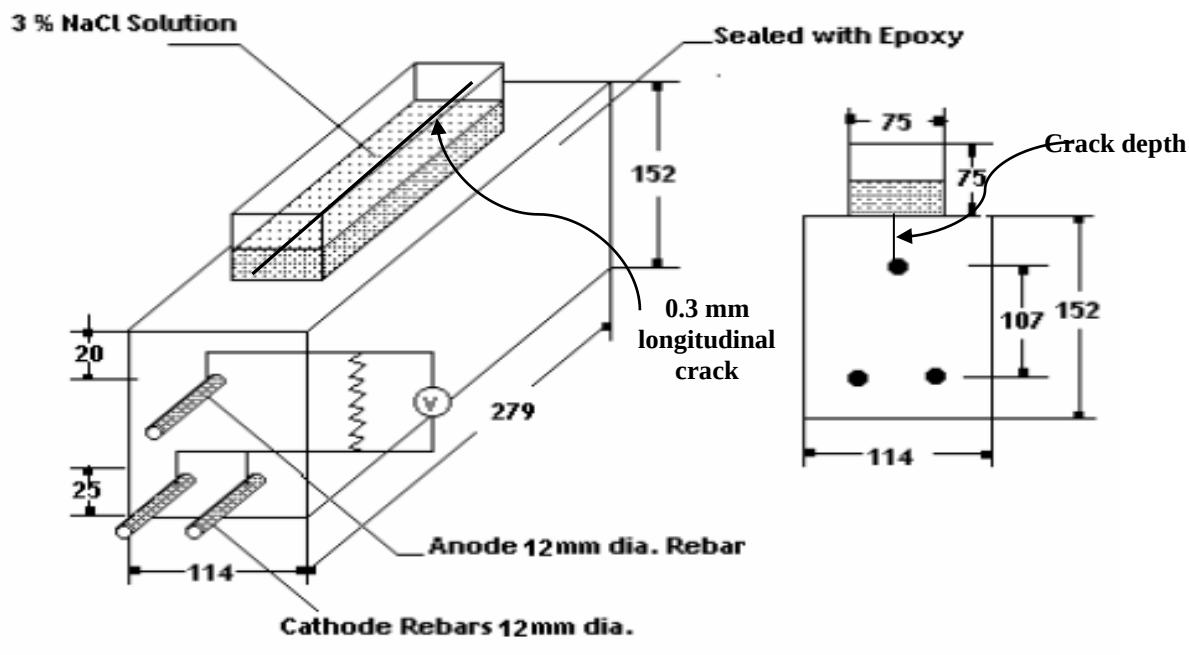


Figure 3.12: Schematic Representation ASTM G 109 Specimen with Longitudinal Crack.

Figure 3.13: ASTM G109 Concrete Specimen with a Longitudinal Crack

### 3.4.2 Concrete Proportioning

Twelve concrete mixtures were used to cast the cracked, uncracked and control concrete specimens. ASTM C 150 Type I (ordinary Portland) cement and silica fume were used in all of the concrete mixtures. The coarse aggregate used was crushed limestone with a maximum size of 12.5 mm. Also, dune sand with an average absorption of 0.57% and specific gravity of 2.56 was used as fine aggregate. Each concrete mixture contained one type of the five selected corrosion inhibitors. The concrete specimens were prepared with the mix design shown in Table 3.8 while table 3.9 shows the dosage of each of the five corrosion inhibitors.

Table 3.8: Concrete Mixture Proportions for ASTM G 109 Specimens

| **Quantities per cubic meter** | **For both cracked and uncracked concrete specimens** | |
|---|---|---|
| **Cement (kg)** | **355** | |
| **Water (kg)** | **170** | |
| **Silica fume (kg)** | **25** | |
| **Coarse aggregate** | **Opening Size (mm)** | **Weight (kg)** |
| | **19** | **0.0** |
| | **12.5** | **449.09** |
| | **9.5** | **449.09** |
| | **4.75** | **112.27** |
| | **2.36** | **112.27** |
| **Sand (kg)** | **748.48** | |
| **W/(C+SF) ratio** | **0.444** | |
| **Corrosion inhibitor** | **The dosage depends on the selected corrosion inhibitor as shown in Table 3.9** | |

Table 3.9: Dosage of Corrosion Inhibitor per Cubic Meter of Concrete

| Corrosion inhibitor name | Quantities per cubic meter of concrete (l) * |
|---|---|
| **Inhibitor V** | **15** |
| **Inhibitor II** | **15** |
| **Inhibitor I** | **15** |
| **Inhibitor IV** | **15** |
| **Inhibitor III** | **0.6** |

* As recommend by the manufacturers

### 3.4.3 Fabrication of Specimens

A band saw used to cut all reinforcement to the required length (360 mm). Thereafter, reinforcing was drilled on a lathe, and using drill press the threads were tapped. Both ends of all reinforcing bars were wrapped with electroplaters tape for a length of 76 mm (3 in) from each end of the steel samples, as shown in Figures 3.14 and 3.15. A 89 mm piece of neoprene tubing (12.5mm internal diameter, 19 mm outer diameter) was then placed on each end to provide a second barrier layer and to protect the tape from any physical damage during handling (see Figure 3.16). A stainless steel screw with stainless steel nut was threaded into one end of the bar, and then two part waterproof epoxy was placed on one end of each bar, covering both the tubing and steel. The bars were then placed into the wooden mold so that an equal length was protruding from both ends, as shown in Figure 3.17. For ASTM G 109 test, the bottom two reinforcing bars are the cathode and the top reinforcing bar is the anode.


Figure 3.14: Reinforcing Bars for ASTM G 109 Specimens

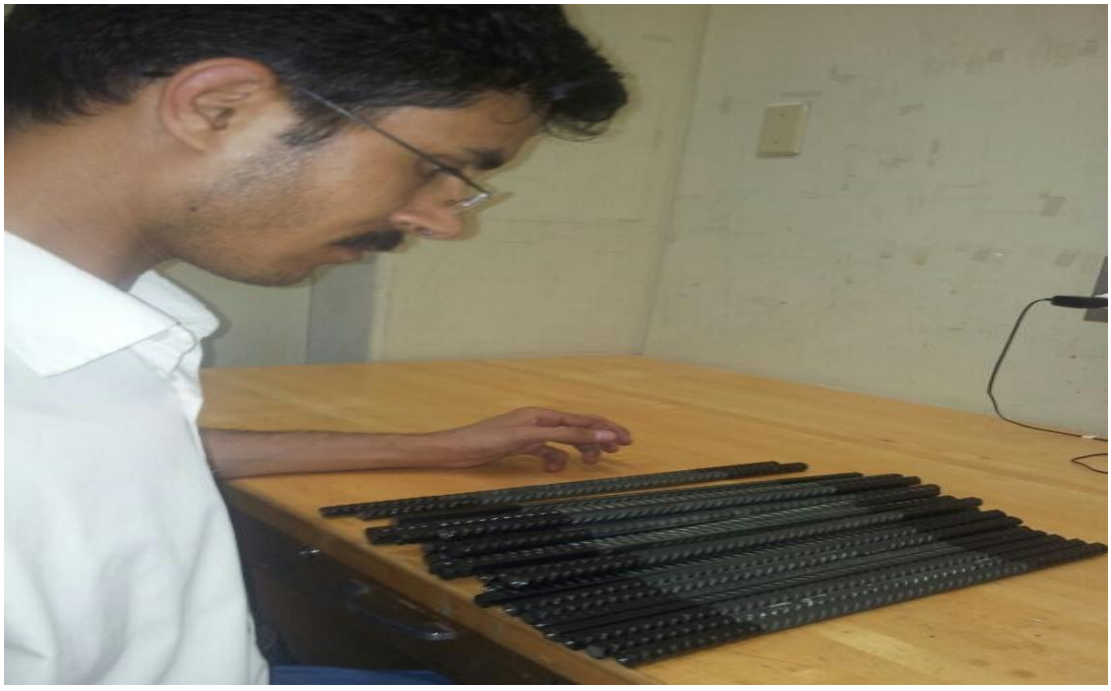

Figure 3.15: Wrapping Bars End with Electroplaters Tape

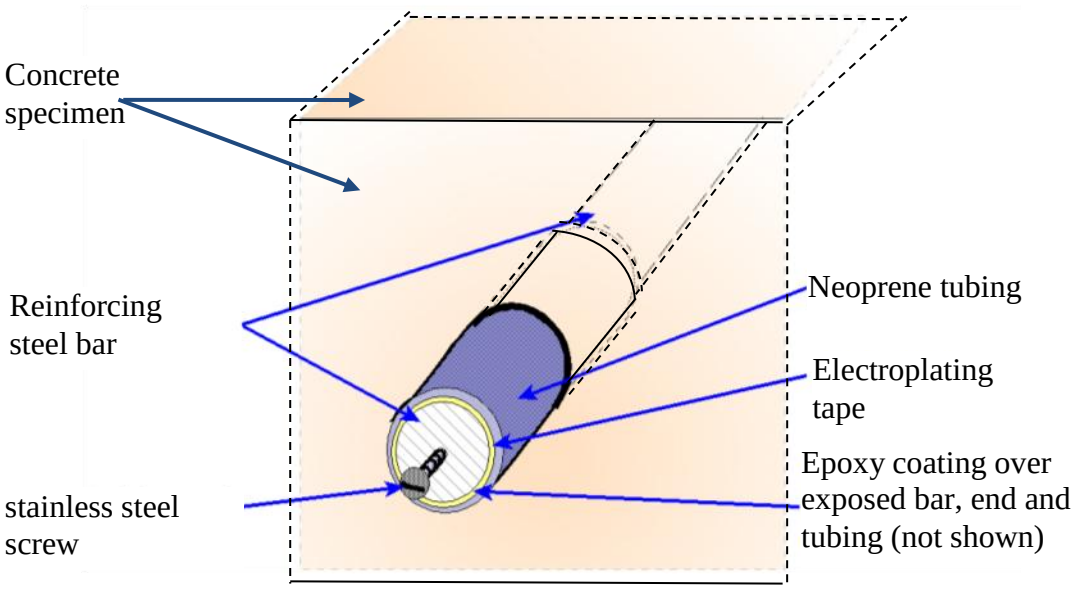


Figure 3.16: Reinforcing Bar End Treatment

Figure 3.17: Completed Reinforcing Bars in Formwork

### 3.4.4 Mixing and Casting

The concrete constituents were mixed in a revolving drum type mixer (Figure 3.18) for about 4 to 5 minutes till a uniform mixture was achieved. The corrosion inhibitors were added to the mixes by dissolving them in the mixing water. Thereafter, the molds were filled with concrete in roughly two equal layers (76.2 mm height each layer) and vibrated for consolidation by using a small vibrating table, as shown in Figure 3.19. ASTM G 109 requires three replicates to be made, hence three uncracked and three cracked specimens were cast for each type of corrosion inhibitor. The top of the specimens were finished with a steel float, as shown in Figure 3.20.

Figure 3.18: Photograph for Revolving Drum Mixer

Figure 3.19: Concrete Specimens on the Vibrating Table

Figure 3.20: Finishing the Surface of Concrete Specimens

### 3.4.5 Curing

After casting, the concrete specimens were cured by covering them with plastic sheet for approximately 24 hours. Then, the specimens were demolded and cured by covering them with wet burlap for 28 days. A total of 36 specimens were covered with wet burlap and plastic sheets, as shown in Figures 3.21 and 3.22. These burlaps were wetted twice daily (at early morning and evening). After two weeks of drying, as shown in Figure 3.23, the four vertical sides and the top, except on the inside of the plexiglass dams were sealed with epoxy. Then, wires were attached to each of the screws on one end of each top reinforcing bars (anode electrode), and the bottom two wires were connected together to form one wire (cathode electrode). A 100 Ohm resister was connected between the bottom and the top wires. Completed specimens are shown in Figure 3.24.

Figure 3.21: Curing of Concrete Specimens by Covering them with Plastic Sheets

Figure 3.22: Curing of Specimens by Covering them with Wet Burlap

Figure 3.23: Drying the Specimens after 28 Days of Curing

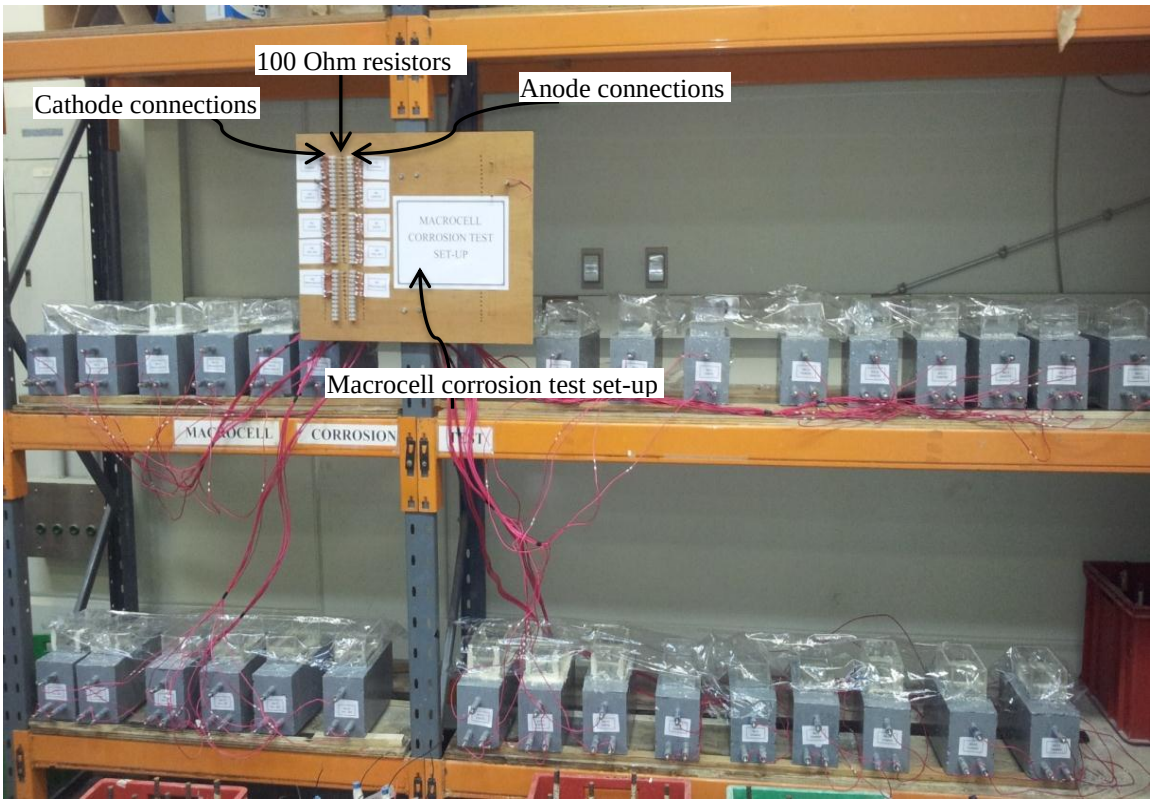


Figure 3.24: Specimens Ready for Measurements

## 3.5 Testing

The concrete specimens were stored on steel shelves in the laboratory to ensure their bottom surfaces are exposed to air during all period of the test. The specimens were ponded with 400 ml (half the height of plexiglass dam) of 3% (by weight of distilled water) NaCl solution for two weeks. At the end of the two weeks of ponding, the solution was removed by vacuuming it off. Thereafter, specimens were allowed to dry for further two weeks. Thereafter, specimens were ponded again, and this cycle of wetting and drying was repeated for six months.

### 3.5.1 Corrosion Potential

The corrosion potential of each specimen was measured with respect to the reference saturated calomel electrode (SCE). Since measuring the potential requires a path of moisture between the concrete and the electrode, corrosion potentials were only measured during the ponding period. One reading was taken over the top reinforcing bar at the beginning of the second week of wetting cycle (i.e. the bottom bar was cathode). Measurement of corrosion potential is shown in Figure 3.25.

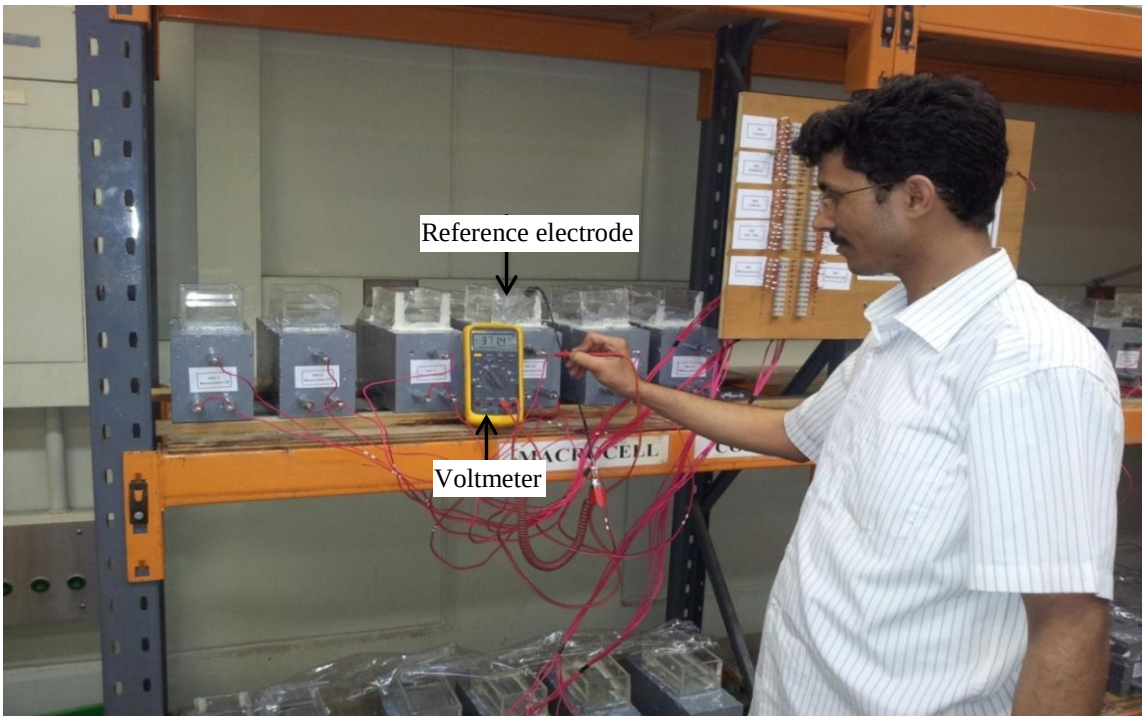


Figure 3.25: Measurement of Corrosion Potentials.

### 3.5.2 Macro-Cell Current Measurement

Macro-cell corrosion current was measured between the top and bottom layers of the reinforcing steel. The test measures the current flowing from the top bar which is being exposed to a chloride environment, while the bottom bars were free of chloride

environment because they acted as the cathode, and the top steel was the anode. The 100-Ohm resistor connects the top and bottom layers of steel, and the voltage readings were measured across the resistors with a high impedance voltmeter. Then, using Ohm's Law, the macro-cell current was calculated (the voltage was divided by the resistance values of the resistor to obtain current). Measurement of macro-cell corrosion current is shown in Figure 3.26.

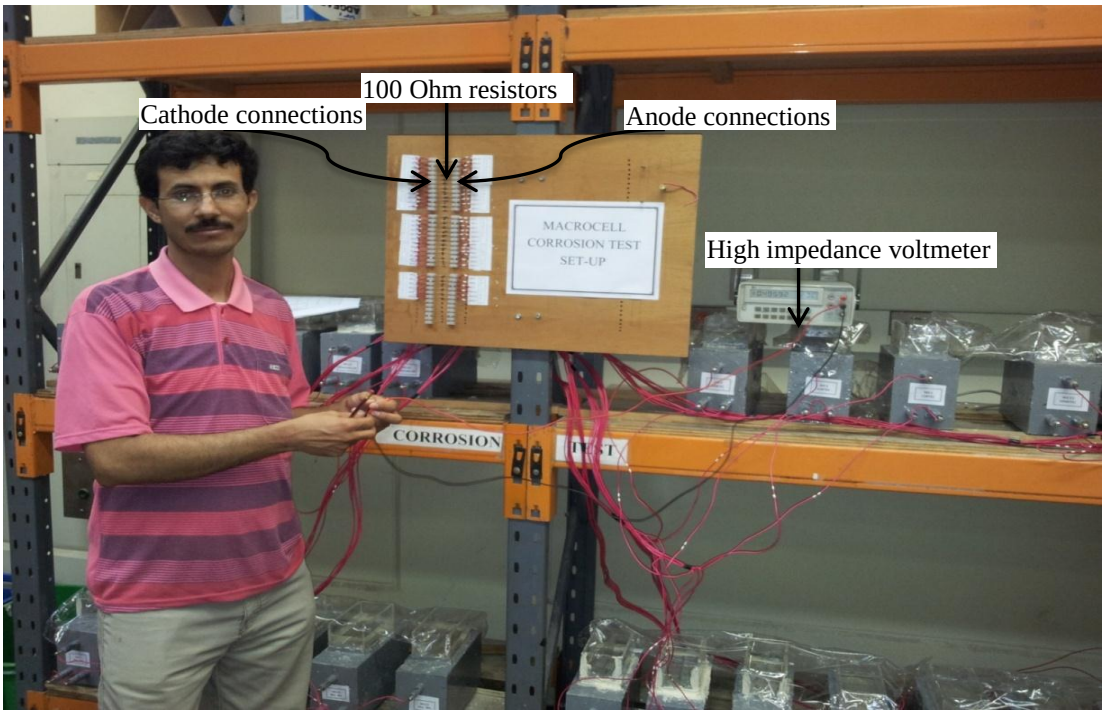


Figure 3.26: Measurements of Macro-Cell Corrosion Current.

### 3.5.3 Determination of Chloride Concentration

For each ASTM G 109 specimen tested, the chloride concentration at the rebar level was determined. A 19 mm diameter hole was drilled above the top reinforcing bar to obtain at least 3 grams of concrete powder up to a depth of 20 mm from the top surface. The loose dust was blown out of the hole just before reaching the 20 mm depth in order

to collect the right sample. Then, the dust was collected by drilling vertically between 20 to 25 mm in a sequential process. Each sample was stored in a plastic bag until all the samples were taken. For the determination of free chloride content, 3 grams of concrete powder was transferred to a 100-ml beaker and 50 ml of hot distilled water was added. The sample was heated gently and thoroughly mixed by a stirrer. The solution was allowed to settle for 24 hours and filtered using No. 1 filter paper. After that, the filtered solution was poured into 100 ml flask then, distilled water was added to make the solution 100 ml (standardization of volume) [66,67]. A 0.1 ml of solution was mixed with 2 ml of ferric ammonium sulfate plus 2 ml of mercuric thiocyanate. Finally, the above solution was pleased in the compartment of Spectronic 21 (spectrophotometer machine) [67, 73]. This machine is equipped with a screen display that can be programmed to display the chloride absorption value automatically when appropriate inputs are fed. Figure 3.27 shows the spectrophotometer machine used in the investigation.


Figure 3.27: Spectronic 21 Machine

# CHAPTER 4

# RESULTS AND DISCUSSION

This chapter presents the results of the tests conducted on the selected inhibitors and their possible interpretation. Broadly speaking, the data developed fall in the following categories.

1. Combined effect of sulfate and/or chloride and temperature on the mechanism of corrosion in the presence or absence of the selected corrosion inhibitors using PDP test.
2. Effect of the selected inhibitors on reinforcement corrosion of both sound and cracked concrete specimens using ASTM G 109.

## 4.1 Performance of Steel Specimens in SCPS without Corrosion Inhibitor

Potentio-dynamic polarization (PDP) technique is considered as a reliable method to evaluate the mechanism of corrosion. The PDP curves can be utilized to determine the nature and extent of corrosion. The effect of chloride and/or sulfate and temperature on the mechanism of corrosion of mild steel placed in simulated concrete pore solution (SCPS) without inhibitor is described in the following sub-sections.

### 4.1.1 Effect of Chloride and Temperature on Corrosion Mechanism

The PDP curves for mild steel specimens placed in SCPS without any inhibitor are depicted in Figures 4.1 through 4.3. These curves are for the specimens immersed in SCPS contaminated with 1000, 1500 and 2000 ppm of chloride, respectively, and temperatures of 25, 40 and 55 ºC.

The PDP curves for steel specimens exposed to chloride concentration of 1000 at 25, 40 and 55 ºC exhibits general corrosion (Figure 4.1). The current required for transition from anodic to cathodic polarization varies from 0.09 to 0.0819 µA with increase the temperature. The polarizing potentials were around -377, -377 and -346 mV, respectively.

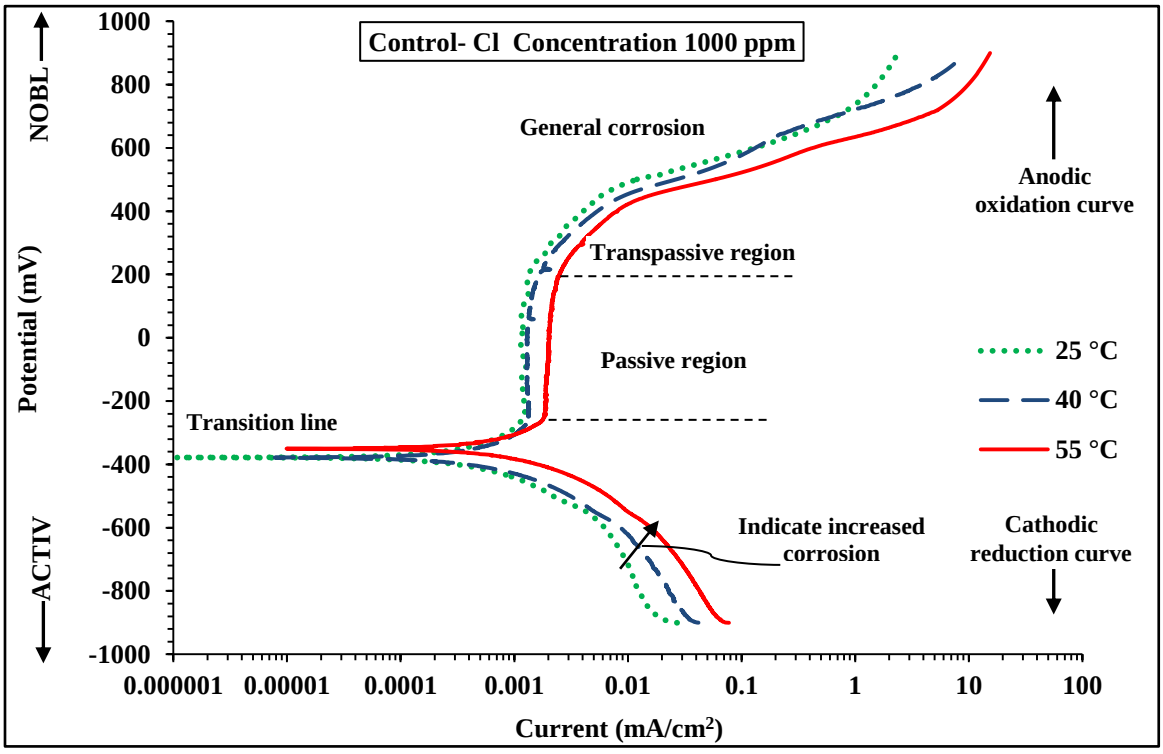


Figure 4.1: Potentio-Dynamic Polarization Curves for Mild Steel in SCPS with 1000 ppm of Cl Concentration without Corrosion Inhibitor

As expected, the rate of corrosion increased with an increase in the temperature. There was almost a uniform increase in the corrosion activity with an increase in the temperature.

Figure 4.2 shows the PDP curves for steel specimens exposed to chloride concentration of 1500 ppm at different temperatures (25, 40 and 55 °C) also exhibits general corrosion. The polarizing potentials in these groups of specimens were around -404, -384 and -432 mV, respectively and the polarization curve is also similar as in the other group of specimens (1000 ppm $Cl^-$).

The PDP drifts towards the anodic region with increasing the temperature of the pore solution. While there was no significant difference in the anodic behavior of solution exposed to 25 or 40 ºC the PDP for 55 ºC tends to be more than the other two curves. Figure 4.3 shows the PDPs for steel specimens placed in SCPS with 2000 ppm chloride. General corrosion was noted in both the specimens exposed to temperature of 25 or 40 ºC and the polarizing potential is around -405 and -439 mV, respectively. However, when temperature was increased to 55 ºC, there was pitting corrosion and the pitting potential is around 160 mV. The transition curve slightly decreased with increasing the temperature. This is the result of conjoint effect of temperature and increased chloride concentration.

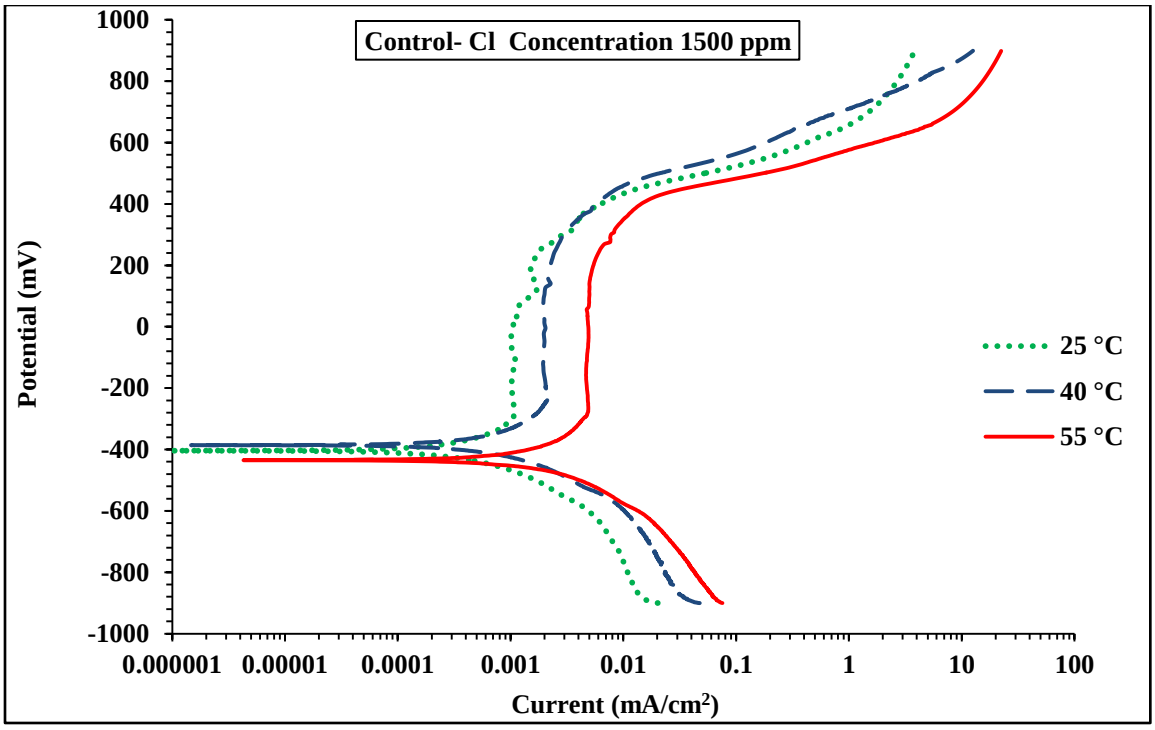


Figure 4.2: Potentio-Dynamic Polarization Curves for Mild Steel in SCPS with 1500 ppm of Cl Concentration without Corrosion Inhibitor

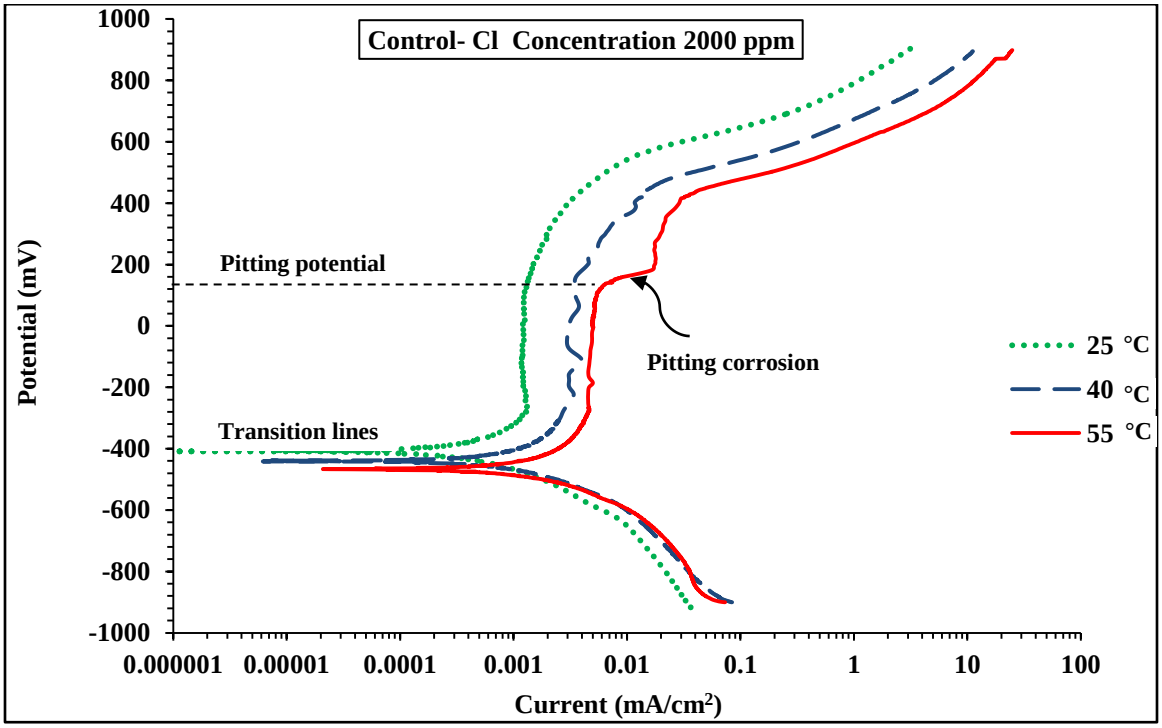


Figure 4.3: Potentio-Dynamic Polarization Curves for Mild Steel in SCPS with 2000 ppm of Cl Concentration without Corrosion Inhibitor

Figure 4.1 through 4.3 were utilized to determine the corrosion polarization parameters for the specimens exposed SCPS without inhibitor. These data are summarized in Table 4.1. The data in this table revealed that an increase in temperature increased the corrosion current density ($I_{corr}$). This can be explained by the fact that an increase in temperature usually accelerates the corrosive processes [70]. This leads to higher dissolution rates of the metal. While there was slight increase in $I_{corr}$ when the temperature was increased from 25 to 40 ºC, the increase in $I_{corr}$ was significant around three to five times when the temperature was increased from 40 to 55 ºC.

Figure 4.4 summarizes the combined effect of temperature and chloride concentration on the $I_{corr}$. It is evident that a temperature of 55 ºC has significant effect (around six times) on $I_{corr}$ compared to 25 and 40 ºC.

Table 4.1: Potentio-Dynamic Polarization Results for Steel Specimens Immersed in SCPS without Corrosion Inhibitor

| **Temperature (ºC)** | **Chloride Concentration (ppm)** | **$E_{corr}$ (mV)** | **Rp Ohm.cm$^2$** | **$I_{corr}$ (µA/cm$^2$)** | **Corrosion Rate (mm/year)** |
|---|---|---|---|---|---|
| **25** | **1000** | **-377.17** | **27937.10** | **0.9336** | **0.0108** |
| | **1500** | **-404.83** | **23913.34** | **1.0904** | **0.0126** |
| | **2000** | **-405.36** | **19704.16** | **1.3233** | **0.0153** |
| **40** | **1000** | **-377.12** | **23843.26** | **1.0938** | **0.0127** |
| | **1500** | **-384.3** | **18596.02** | **1.4027** | **0.0163** |
| | **2000** | **-439.89** | **10517.26** | **2.4801** | **0.0287** |
| **55** | **1000** | **-346.03** | **3801.99** | **6.8562** | **0.0795** |
| | **1500** | **-432.79** | **3472.76** | **7.49** | **0.0871** |
| | **2000** | **-460.38** | **3392.46** | **7.6849** | **0.0891** |

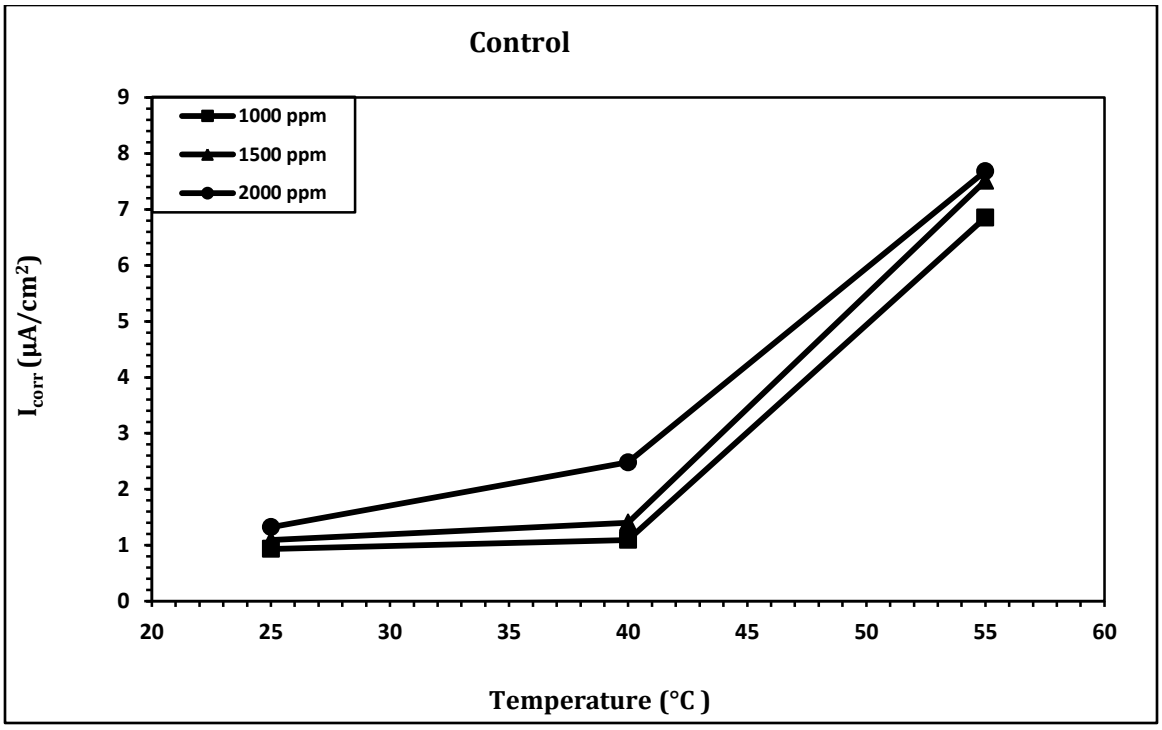


Figure 4.4: Effect of Chloride and Temperature on Corrosion Current Density

### 4.1.2 Effect of Sulfate and/or Chloride and Temperature on Corrosion Mechanism

Figure 4.5 shows a PDP for control specimens immersed in SCPS contaminated with 1000 ppm Cl and various sulfate concentrations (0, 500 and 2000) ppm at 40 ºC. The polarization potentials were around -377, -418 and -496 mV, respectively in all solutions. However, the PDP for steel in 2000 ppm sulfate is more anodic than the one immersed in 500 ppm sulfate. This indicates that sulfate has an effect to similar to that of temperature. The polarization data are summarized in table 4.2 which shows the increase in $I_{corr}$ from 1.094 to 1.548 μA/cm$^2$ for the increase in $SO_4$ from 0 to 2000 ppm. The increase in $I_{corr}$ due to incorporation of $SO_4$ is depicted in Figure 4.6.

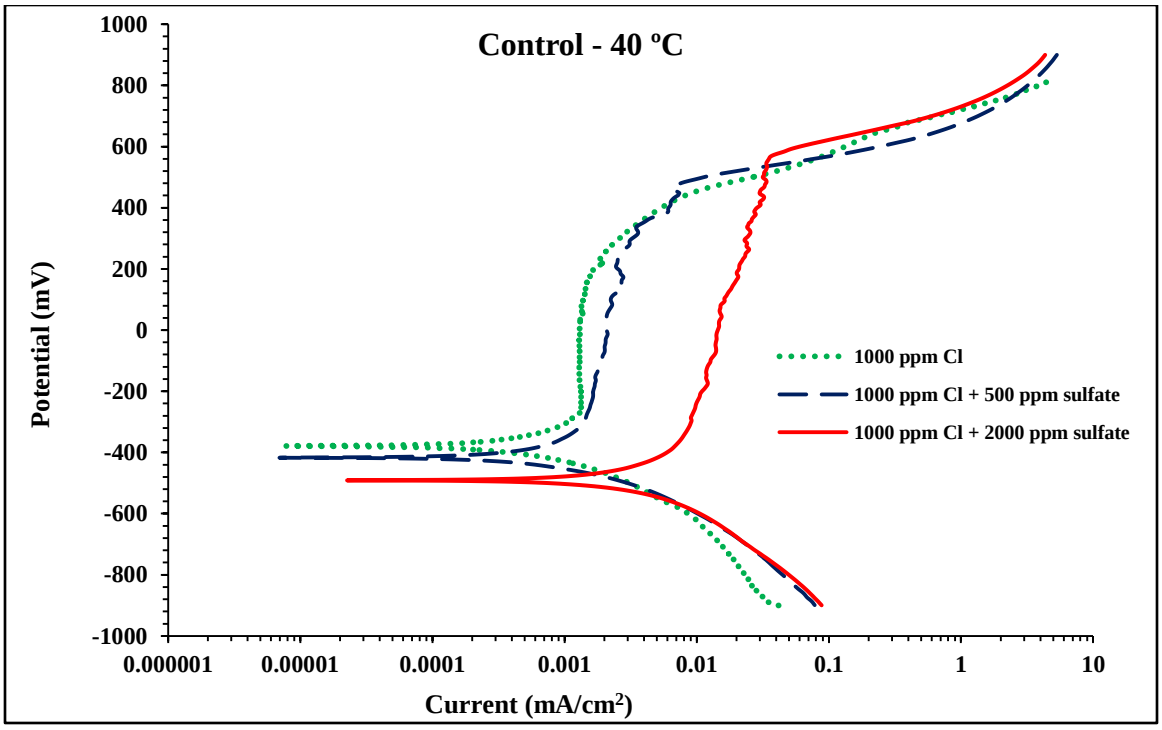


Figure 4.5: Potentio-Dynaimic Polarization Curves for Control Specimens at 1000 ppm Cl plus (0, 500 and 2000) ppm $SO_4$

Table 4.2: Potentio-Dynamic Polarization Results of Steel Specimens Immersed in SCPS without Corrosion Inhibitor (Control) at 40 ºC

| Chloride + Sulfate Concentration (ppm) | $E_{corr}$ (mV) | $R_p$ (Ohm.cm$^2$) | $I_{corr}$ (µA/cm$^2$) | Corrosion rate (mm/year) |
|---|---|---|---|---|
| 1000 + 0 | -377.12 | 23843.26 | 1.0938 | 0.0127 |
| 1000 + 500 | -418 | 23066.54 | 1.1308 | 0.0131 |
| 1000 +2000 | -496 | 16851.32 | 1.5481 | 0.0179 |

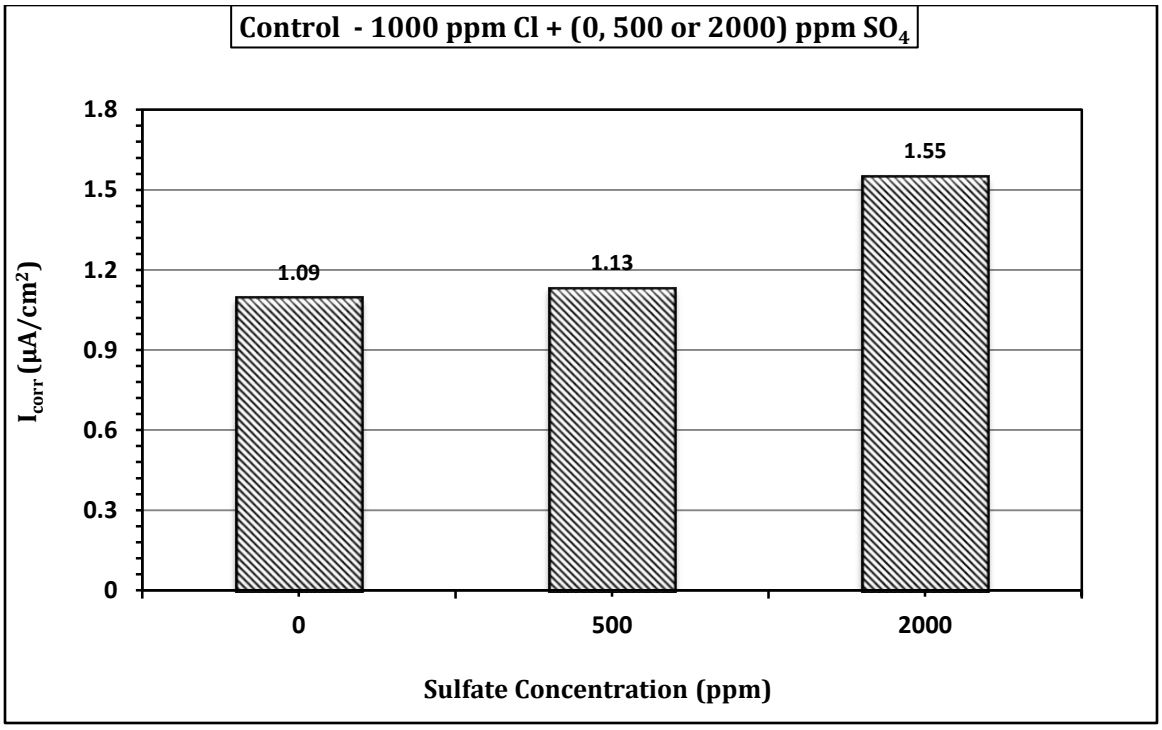


Figure 4.6: Combined Effect of Chloride, Sulfate and Temperature on Corrosion Current Density (40 °C)

### 4.1.3 Scanning Electron Microscopy of Steel Specimens Immersed in SCPS without Inhibitor

The scanning electron micrographs of the polished surface of mild steel specimens exposed to SCPS contaminated with sulfate and/or chloride ions (no inhibitor) are shown in Figures 4.7 through 4.9. There was general corrosion in all the specimens. The steel surface was rough and covered with corrosion products. However, shallow pits were noted on the specimens immersed in SCPS contaminated with 1,500 ppm chloride and exposed to 25 ºC (Figure 4.7).

Figure 4.8 shows the SEM of the mild steel specimen immersed in SCPS without corrosion inhibitor and contaminated with 1,500 ppm Cl and exposed to temperature of

55 ºC. General corrosion was noted in this specimen as well. However, there was severe damage of the surface.

Figure 4.9 is the SEM micrograph of specimen immersed in SCPS without corrosion inhibitor and contaminated with 1000 ppm Cl and 2000 ppm sulfate and exposure temperature of 40 ºC. There was general corrosion on the specimen with is noted spots on the surface. These spots might be the sulfate deposits.

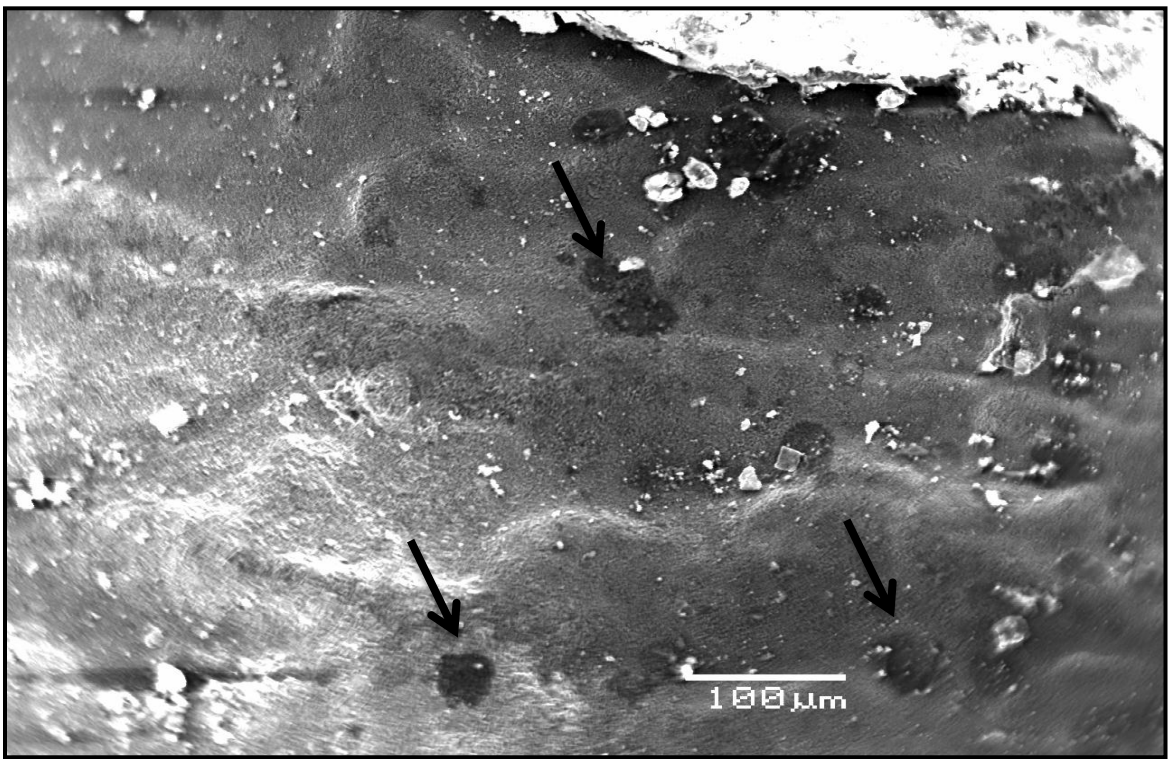


Figure 4.7: Close up Picture of SEM (180X) for Control Specimen in SCPS Contaminated with 1500 ppm Cl at 25 ºC

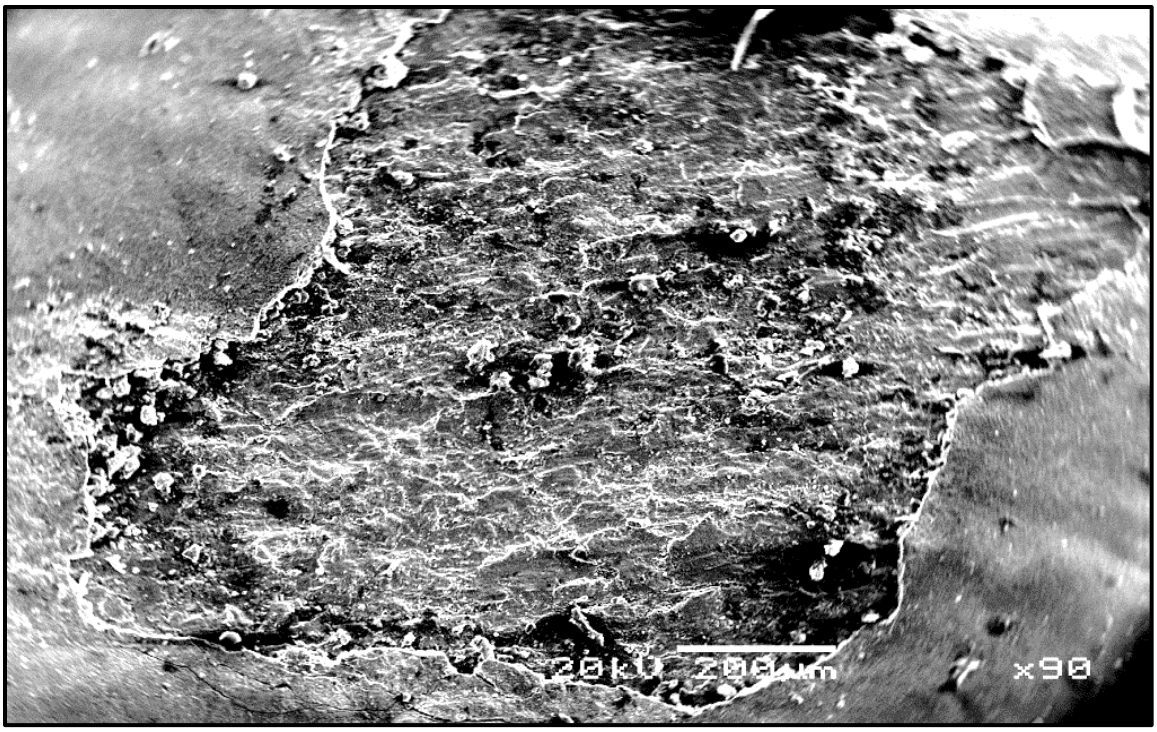


Figure 4.8: Close up Picture of SEM (90X) for Control Specimen in SCPS Contaminated with 1500 ppm Cl at 55 ºC

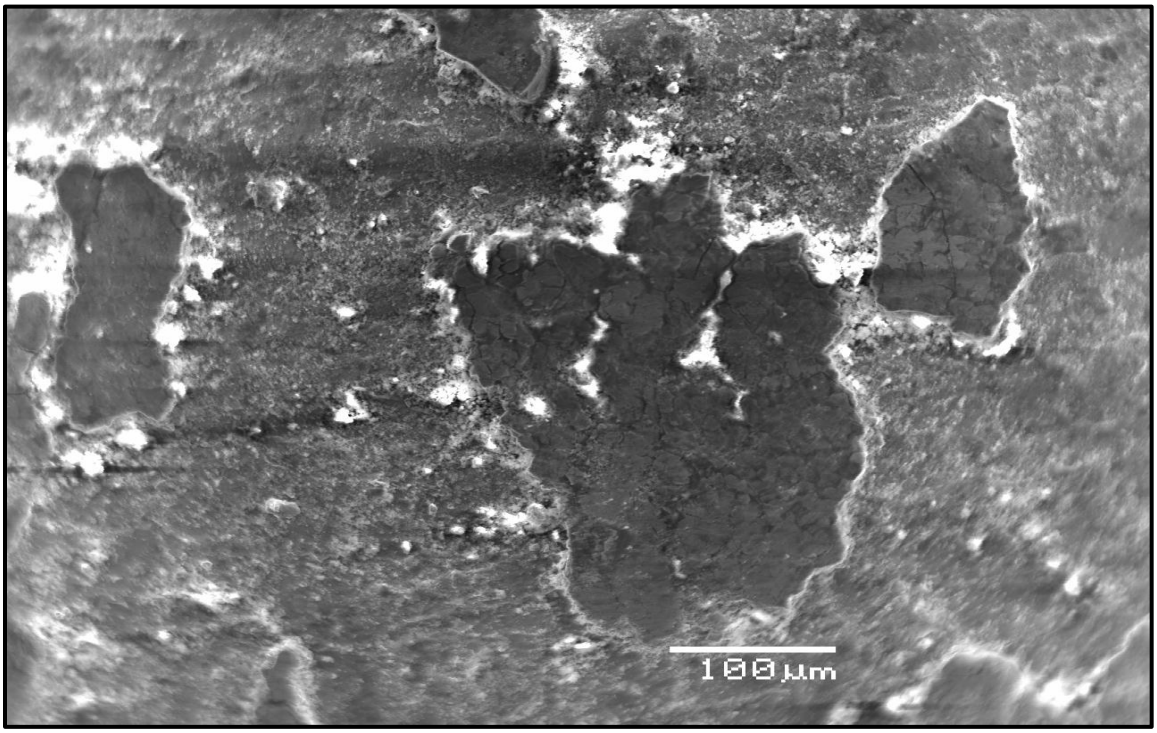


Figure 4.9: SEM (180X) for Control Specimen in SCPS Contaminated with 1000 ppm Cl + 2000 ppm Sulfate at 40 ºC.

## 4.2 Performance of Steel Specimens in Presence of Inhibitor I

The effect of Inhibitor I on the corrosion behavior of steel immersed in SCPS for various sulfate and/or chloride concentrations and temperatures was evaluated using PDP technique. The results of these techniques are summarized in the following sub-sections.

### 4.2.1 Effect of Chloride and Temperature on Corrosion Mechanism

The PDP curves for mild steel specimens placed in SCPS incorporating Inhibitor I as a corrosion inhibitor are displayed in Figures 4.10 through 4.12. These curves are for specimens immersed in SCPS incorporating Inhibitor I and contaminated with 1000, 1500 and 2000 ppm chloride and at temperatures of 25, 40 and 55 ºC.

The PDP curves for steel specimens exposed to chloride concentration of 1000 ppm exhibits general corrosion for all exposure temperatures (Figure 4.10). The current required for transition from cathodic to anodic polarization decreases from 0.045 to 0.0423 $\mu A/cm^2$ with increasing temperature from 25 to 55 °C. The polarization potentials were around -335, -366 and -460 mV, respectively. As expected, the rate of corrosion increased with an increase in the temperature. Although there was a slight increase in the corrosion current density from 0.132 to 0.135 $\mu A/cm^2$ when the temperature was increased from 25 to 40 ºC. However, the increase in $I_{corr}$ when the temperature was increased to 55 ºC was significant (0.45 $\mu A/cm^2$).

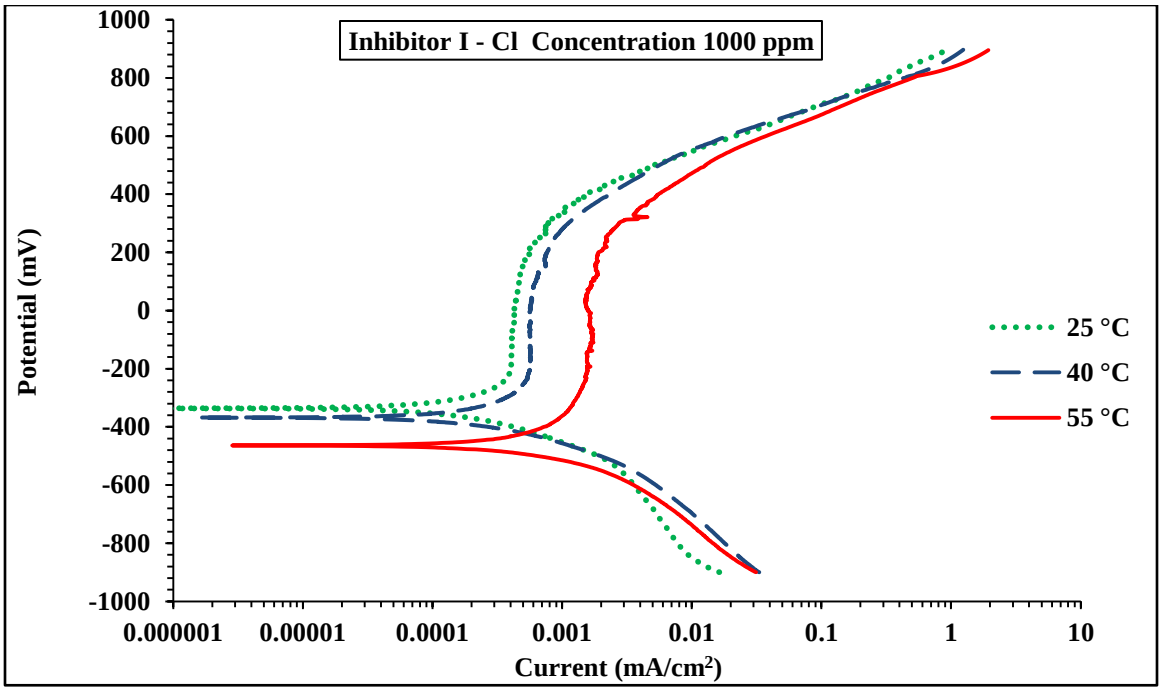


Figure 4.10: Potentio-Dynamic Polarization Curves for Mild Steel in SCPS Incorporated Inhibitor I and 1000 ppm Cl Concentration.

Figure 4.11 shows the PDP curves for steel specimens immersed in SCPS incorporating Inhibitor I and exposed to chloride concentration of 1500 ppm at different temperatures. The data in this figure indicate that the steel specimens exhibit general corrosion for all exposure temperatures (25, 40 and 55 °C). The polarizing potentials in these groups of specimens were around -426, -433 and -446 mV, respectively and the polarization curve is also similar to those in the other group of specimens (1000 ppm $Cl^-$).

The PDP drifts towards anodic region with increasing the temperature of the pore solution. While there was no significance difference in the anodic behavior of solution exposed to 25 or 40 ºC, the PDP for 55 ºC tends to be more than the other two curves (exposed to 25 and 40 °C, respectively). Figure 4.12 shows the PDPs for steel specimens placed in SCPS contaminated with 2000 ppm chloride. General corrosion was noted in all

the specimens. However, the transition line decreases from 0.09 to 0.0819 μA/cm$^2$ with increasing the temperature from 25 to 55 °C. This is the result of conjoint effect of temperature and increased chloride concentration.

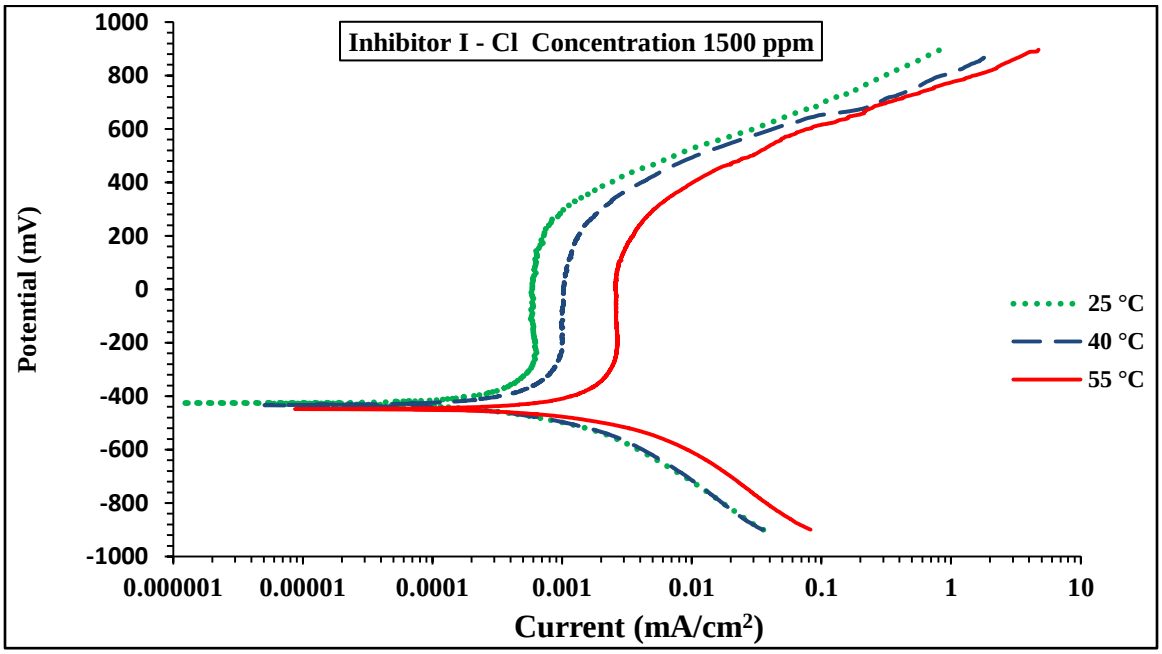


Figure 4.11: Potentio-Dynamic Polarization Curves for Mild Steel in SCPS Incorporated Inhibitor I and 1500 ppm Cl Concentration.

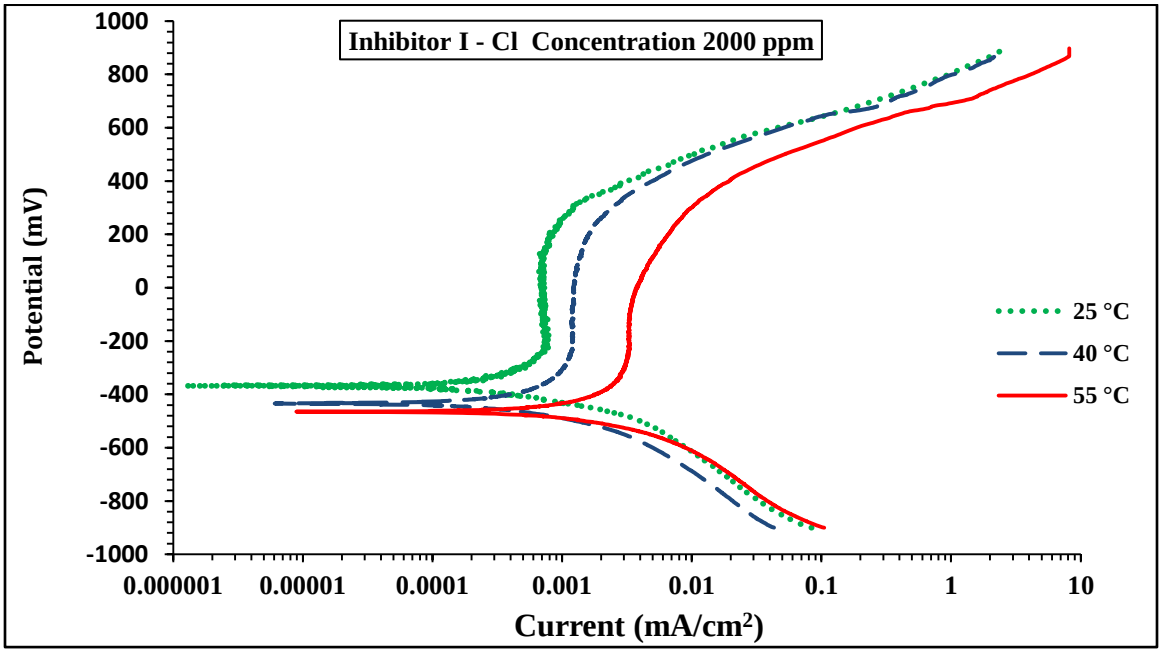


Figure 4.12: Potentio-Dynamic Polarization Curves for Mild Steel in SCPS Incorporated Inhibitor I and 2000 ppm Cl Concentration.

Figure 4.10 through 4.12 were utilized to determine the corrosion polarization parameters for the specimens exposed SCPS incorporating Inhibitor I. These data are summarized in Table 4.3. The data in this table also revealed that an increase in temperature and chloride concentration tends to increase the corrosion current density. The effect of chloride content and temperature on $I_{corr}$ determined by PDP technique is plotted in Figure 4.13. The increase in $I_{corr}$ with chloride concentration and temperature is visible in these data.

Table 4.3: Potentio-Dynamic Polarization Results for Steel Specimens Immersed in SCPS Incorporating Inhibitor I.

| Temperature (°C) | Chloride Concentration (ppm) | $E_{corr}$ (mV) | $R_p$ (Ohm.cm$^2$) | $I_{corr}$ (µA/cm$^2$) | Corrosion Rate (mm/year) | Inhibitor Efficiency in Reducing $I_{corr}$ % |
|---|---|---|---|---|---|---|
| 25 | 1000 | -335.4 | 197625.60 | 0.1320 | 0.0015 | 85.86 |
| | 1500 | -425.98 | 164994.60 | 0.1581 | 0.0018 | 85.50 |
| | 2000 | -366.75 | 105633.92 | 0.2470 | 0.0029 | 81.34 |
| 40 | 1000 | -366.69 | 193552.20 | 0.1348 | 0.0016 | 87.68 |
| | 1500 | -432.96 | 130272.88 | 0.2002 | 0.0023 | 85.72 |
| | 2000 | -429.53 | 56386.66 | 0.4626 | 0.0054 | 81.35 |
| 55 | 1000 | -460.64 | 57969.30 | 0.4500 | 0.0052 | 93.44 |
| | 1500 | -446.75 | 52247.56 | 0.4993 | 0.0058 | 93.35 |
| | 2000 | -464.03 | 19728.98 | 1.3219 | 0.0153 | 82.81 |

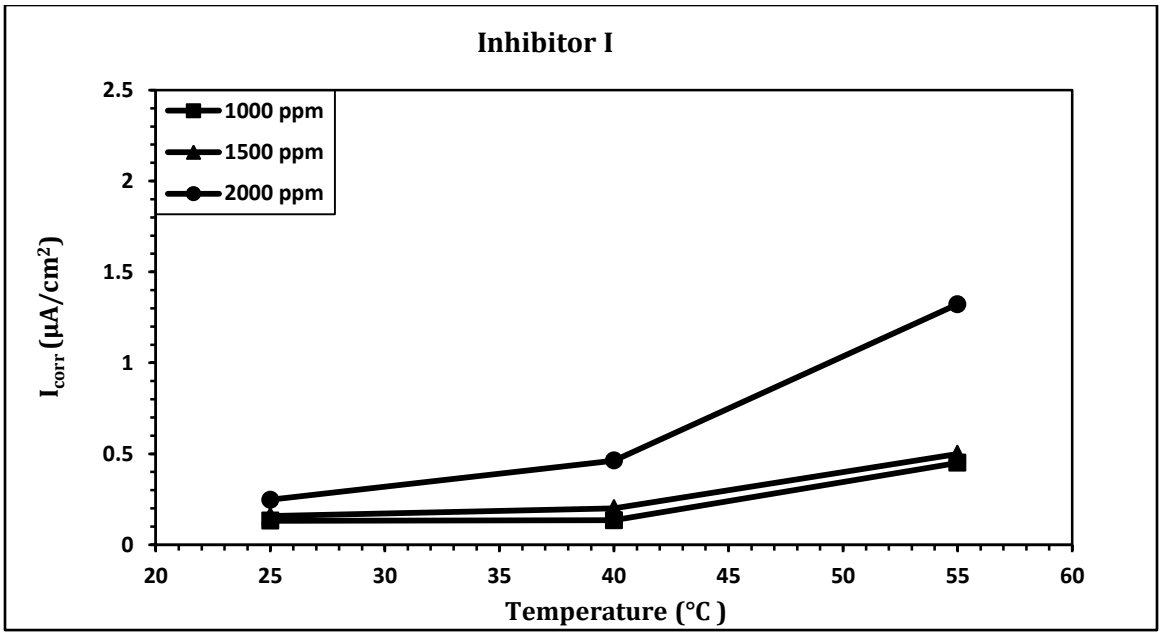


Figure 4.13: Effect of Chloride Concentration on Corrosion Current Density in the Presence for Various Temperatures.

### 4.2.2 Effect of Sulfate and/or Chloride and Temperature on Corrosion Mechanism

Figure 4.14 displays PDP plot for steel exposed to SCPS incorporating Inhibitor I and contaminated with 1000 ppm Cl and 0 or 500 or 2000 ppm $SO_4$ at a temperature of 40 ºC. The PDP curves indicate general corrosion in all the specimens. The polarization potentials for 0, 500 and 2000 ppm $SO_4$ are around -366, -436 and -554 mV, respectively. This increase in corrosion potential in the negative direction indicates an increase in the corrosion process. Further, the current required for transition from cathodic to anodic region was smaller (0.0933 μA/cm$^2$) in the specimens exposed to 2000 ppm $SO_4$ than that exposed to 500 ppm $SO_4$ (0.0937 μA/cm$^2$).

The combined effect of sulfate and/or chloride on corrosion of steel specimens immersed in SCPS incorporating Inhibitor I and contaminated with 1000 ppm Cl and various sulfate concentrations (500 and 2000) ppm at 40 ºC is summarized in the Table

4.4. The data showed significant increase in the corrosion current density from 0.135 to 0.309 μA/cm$^2$ with the increase in sulfate concentration from 0 to 2000 ppm. The increase in $I_{corr}$ due to incorporation of $SO_4$ is depicted in Figure 4.15.

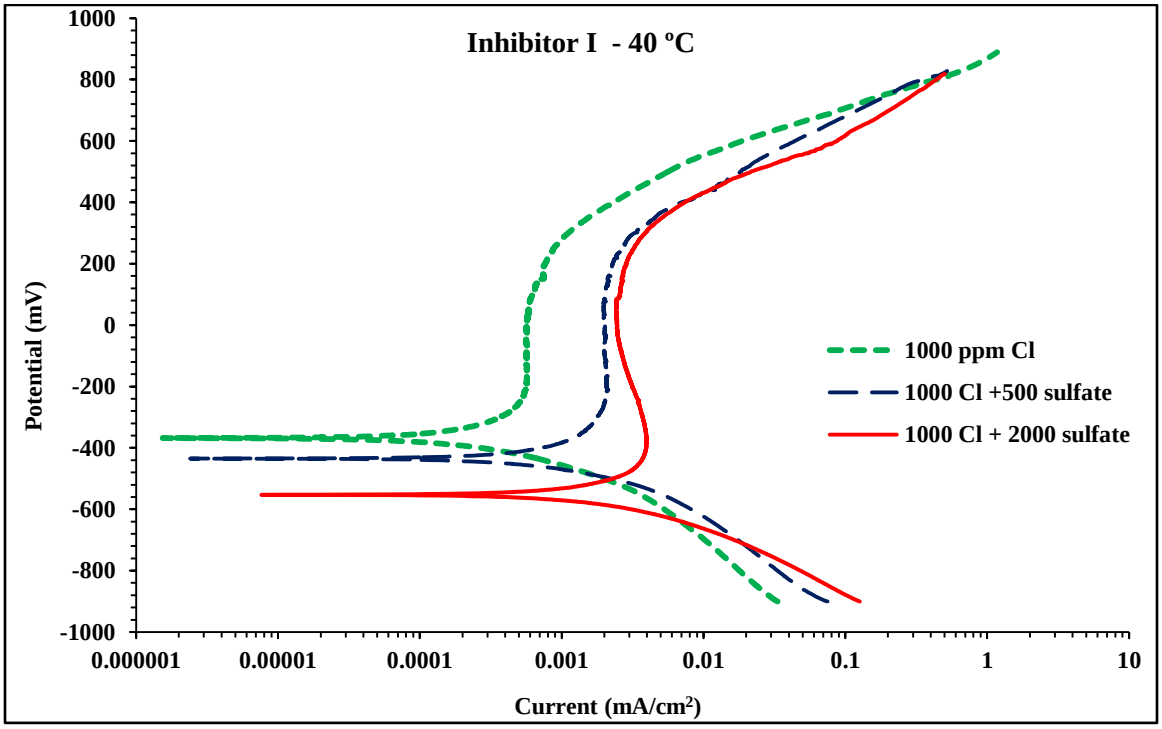


Figure 4.14: Potentio-Dynaimic Polarization Curves for Specimens Immersed in SCPS Incorporating Inhibitor I and 1000ppm Cl plus (0, 500 and 2000) ppm $SO_4$

Table 4.4: Potentio-Dynamic Polarization Results of Steel Specimens Immersed in SCPS Incorporating Inhibitor I at 40 ºC.

| Chloride + Sulfate Concentration (ppm) | $E_{corr}$ (mV) | $R_p$ (Ohm.cm$^2$) | $I_{corr}$ (μA/cm$^2$) | Corrosion rate (mm/year) | Inhibitor Efficiency in Reducing $I_{corr}$ % |
|---|---|---|---|---|---|
| 1000 + 0 | -366.69 | 193537.60 | 0.1347 | 0.0016 | 87.68 |
| 1000 + 500 | -436.38 | 154395.00 | 0.1689 | 0.0020 | 85.06 |
| 1000 + 2000 | -554.59 | 84300.40 | 0.3095 | 0.0036 | 80.01 |

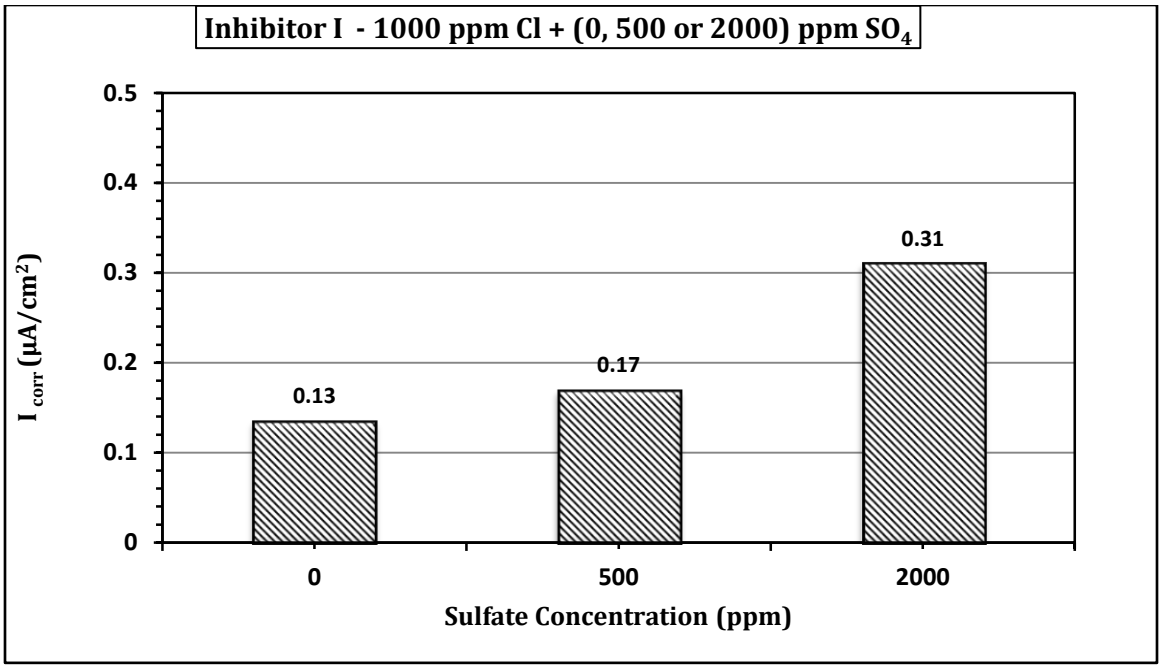


Figure 4.15: Combined Effect of Chloride, Sulfate and Temperature on Corrosion Current Density (40 °C).

### 4.2.3 Scanning Electron Microscopy of Steel Specimens Immersed in SCPS Incorporating Inhibitor I

The scanning electron micrographs of the mild steel specimens exposed to SCPS incorporating Inhibitor I and contaminated with sulfate and/or chloride ions are shown in Figures 4.16 through 4.18. There was general corrosion in all the specimens. The SEM in Figure 4.16 (Cl: 1,500; temperature: 25 ºC) exhibits general corrosion and a good protective adsorbed film is formed on the surface of the specimen, which decreases the corrosion current density and corrosion rate of steel in alkaline environment. The micrograph also shows that the steel surface is better in the presence of Inhibitor I compared to the surface of control specimen (Figure 4.7) which was rough and covered with the corrosion products.

Figure 4.17 shows the SEM of the polished surface of mild steel specimen immersed in SCPS incorporating Inhibitor I and contaminated with 1500 ppm Cl and exposed to a temperature of 55 ºC. General corrosion was noted in this specimen also. However, there were corrosion products on the surface of steel specimen. This might be due to the effect of chloride and elevated exposure temperature.

Figure 4.18 is the SEM of steel immersed in SCPS incorporating Inhibitor I and contaminated with 1000 ppm Cl and 2000 ppm sulfate and exposure temperature of 40 ºC. General corrosion and a good protective adsorbed film is noted on the surface of the specimen. The SEM in Figures 4.16 through 4.18 indicate that Inhibitor I can minimize corrosion of steel bars.

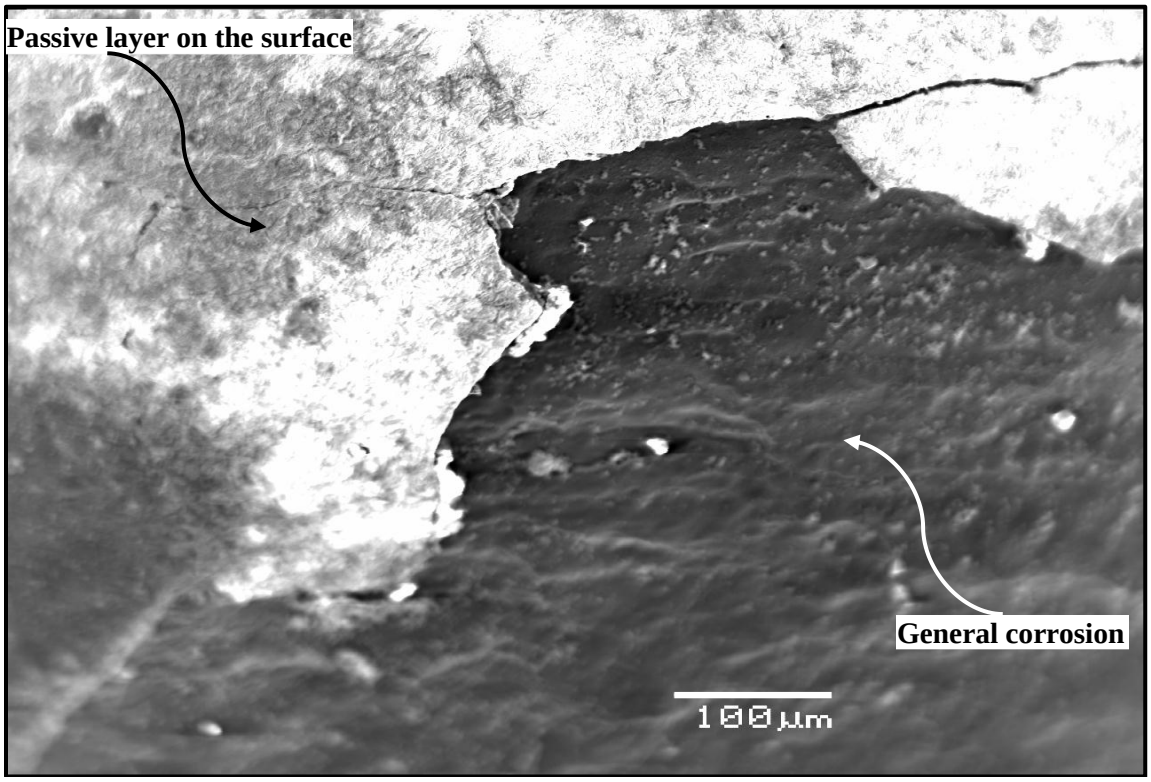


Figure 4.16: SEM (180X) for Steel Specimen in SCPS Incorporating Inhibitor I and Contaminated with 1500 ppm Cl at 25 ºC

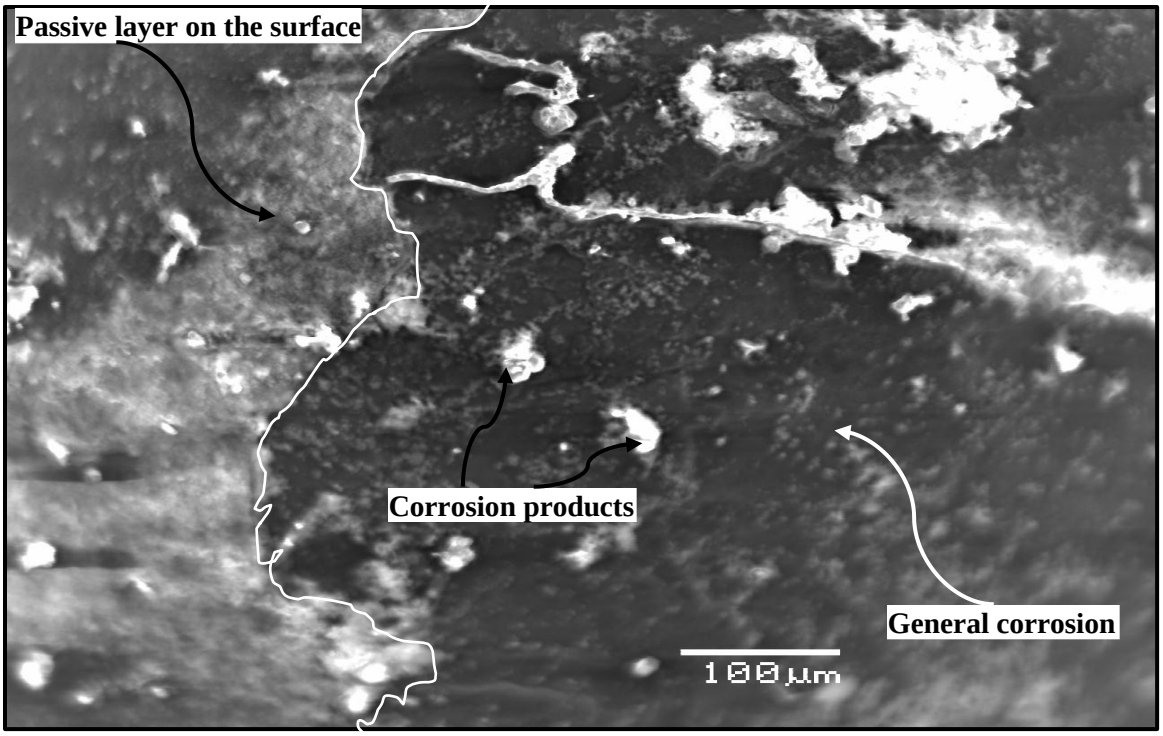


Figure 4.17: SEM (180X) for Steel Specimen in SCPS Incorporating Inhibitor I and Contaminated with 1500 ppm Cl at 55 ºC

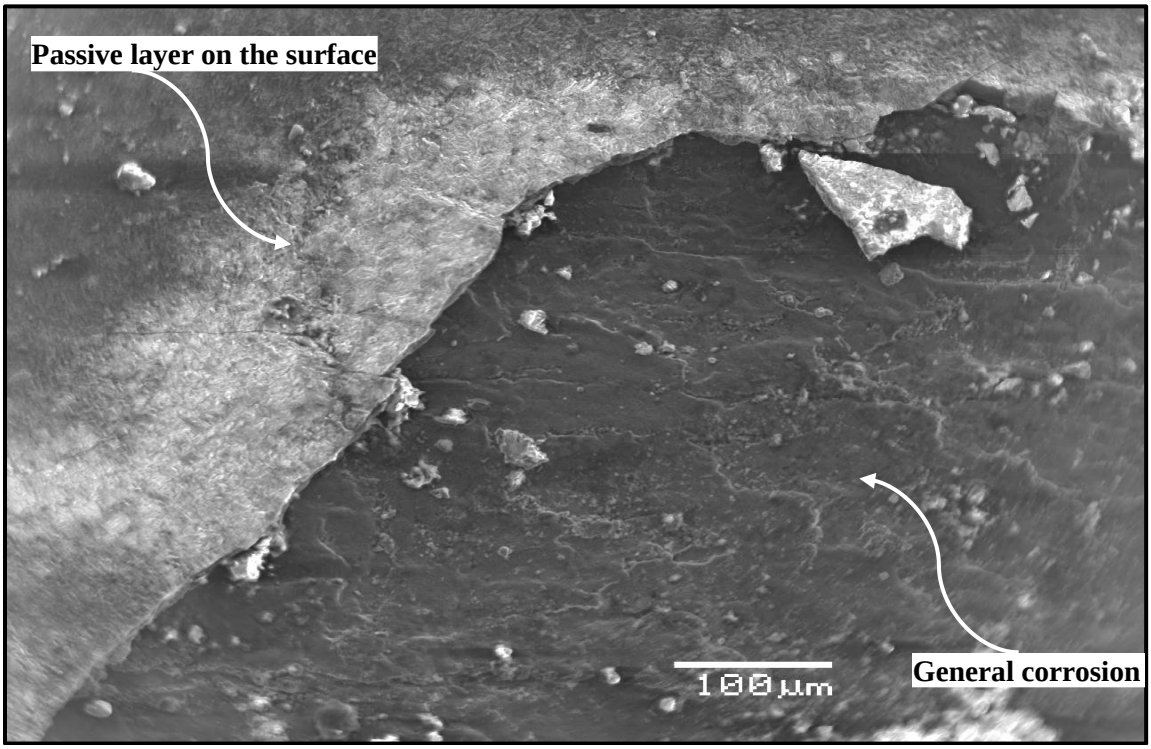


Figure 4.18: SEM (180X) for Steel Specimen in SCPS Incorporating Inhibitor I and Contaminated with 1000 ppm Cl + 2000 ppm Sulfate at 40 ºC

## 4.3 Performance of Steel Specimens in the Presence of Inhibitor II

In order to evaluate the protective effect of Inhibitor II inhibitor on corrosion mechanism and rate, PDP test was performed on steel specimens immersed in SCPS contaminated with various sulfate and/or chloride concentrations at different exposure temperatures. The results of these tests are described in the following sub-sections.

### 4.3.1 Effect of Chloride and Temperature on Corrosion Mechanism

The PDP curves for mild steel specimens placed in SCPS incorporating Inhibitor II inhibitor are displayed in Figures 4.19 through 4.21. These curves are for the specimens immersed in SCPS incorporating Inhibitor II and contaminated with 1000, 1500 and 2000 ppm chloride, respectively and at temperatures of 25, 40 and 55 ºC.

The PDP curves for steel specimens exposed to chloride concentration of 1000 exhibits general corrosion for all the exposure temperatures (Figure 4.19). The current required for transition from cathodic to anodic region varies with the temperature from 0.0648 to 0.0621 $\mu A/cm^2$. The polarizing potential is around -400 mV in all the specimens. As expected, the rate of corrosion increased with an increase in the temperature. Although there was a slight increase in the corrosion current density when temperatures were 25 and 40 ºC for 1000 ppm chloride concentration (0.146 to 0.168) $\mu A/cm^2$, the increase was significant when temperature was increased to 55 ºC (0.549 $\mu A/cm^2$).

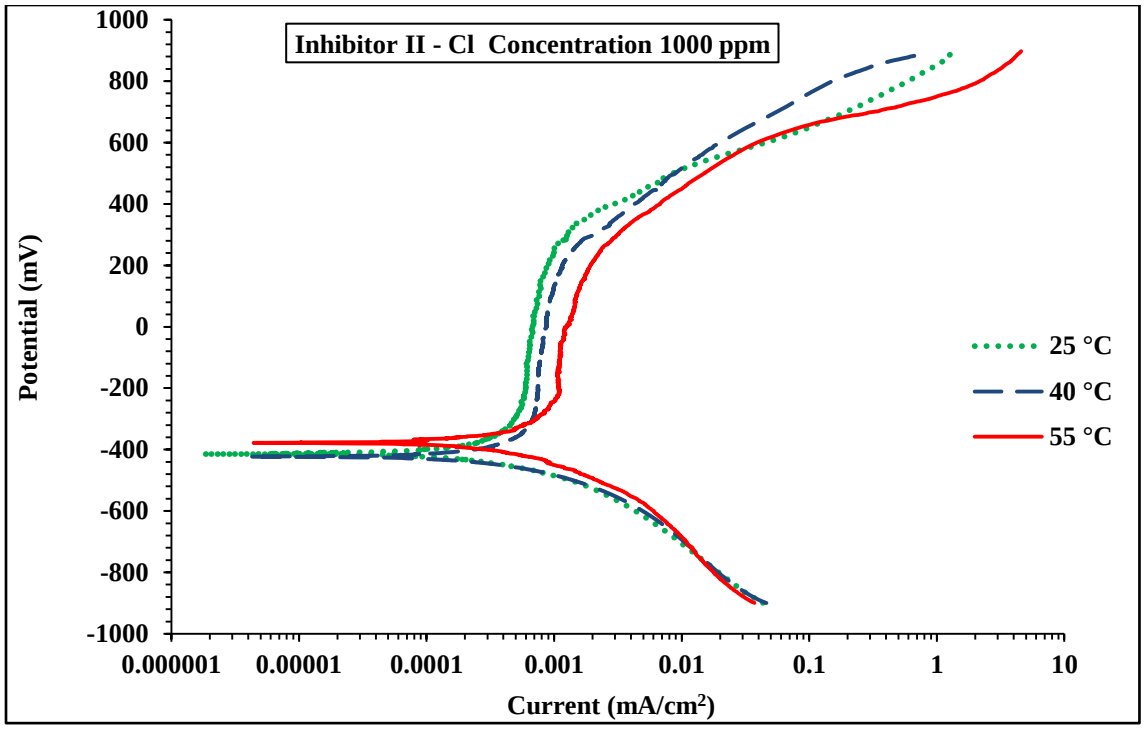


Figure 4.19: Potentio-Dynamic Polarization Curves for Mild Steel in SCPS Incorporated Inhibitor II and 1000 ppm of Cl.

Figure 4.20 shows the PDP curves for steel specimens immersed in SCPS incorporating Inhibitor II and exposed to chloride concentration of 1500 ppm at different temperatures (25, 40 and 55 °C). The data therein exhibit general corrosion. The polarizing potential in these groups of specimens is also around -430 mV for the exposure temperatures of 25 and 40 ºC and decreased to around -502 mV when the exposure temperature was increased to 55 ºC and the polarization curve is also similar as in the other group of specimens (1000 ppm $Cl^-$). While there was no significance difference in the anodic behavior of solution exposed to 25 or 40 ºC, the PDP for 55 ºC tends to be more than that for the temperatures at high potential.

Figure 4.21 shows the PDPs for steel specimens placed in SCPS contaminated with 2000 ppm chloride. General corrosion was noted in all the specimens. The polarizing potential is around -485 mV for the exposure temperature of 25 ºC and decreased to around -579 mV when the exposure temperature was increased to 55 ºC, which indicates an increase in the corrosion process. There was almost a uniform increase in the corrosion activity with an increase in the temperature. The required current for transition from cathodic to anodic varies from 0.09675 to 0.08775 μA/cm$^2$ with increasing the temperature from 25 to 55 ºC. This is the result of conjoint effect of temperature and increased chloride concentration.

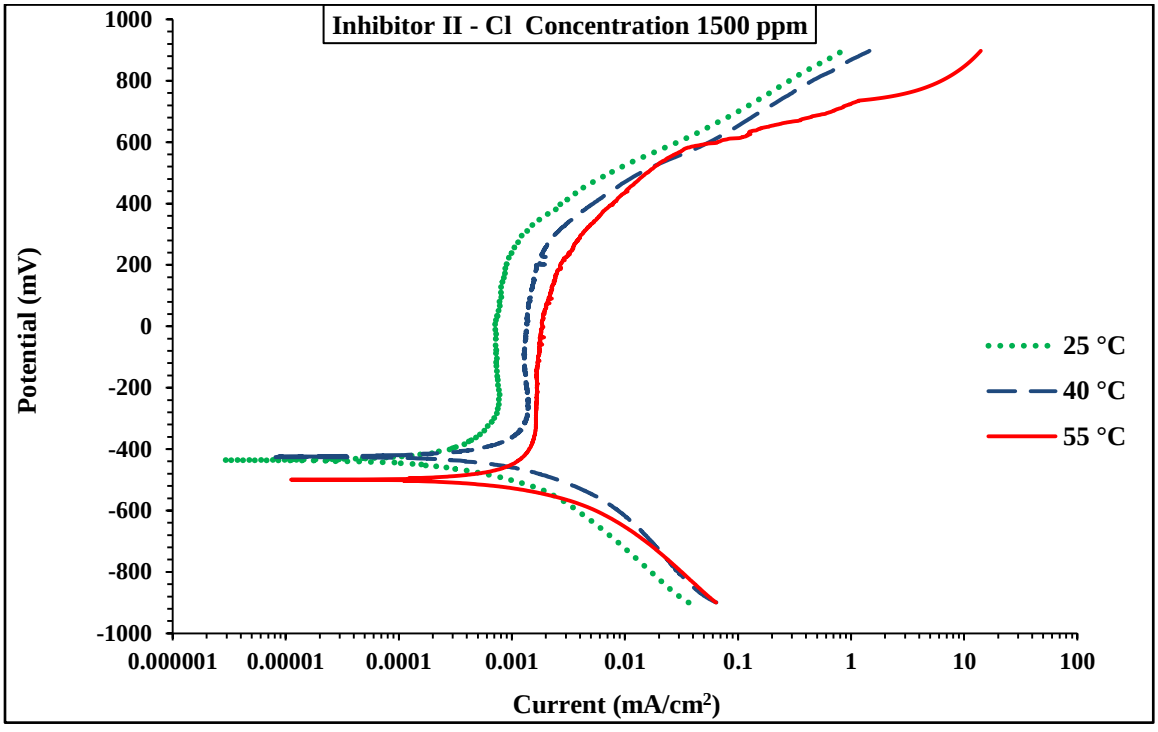


Figure 4.20: Potentio-Dynamic Polarization Curves for Mild Steel in SCPS Incorporated Inhibitor II and 1500 ppm of Cl

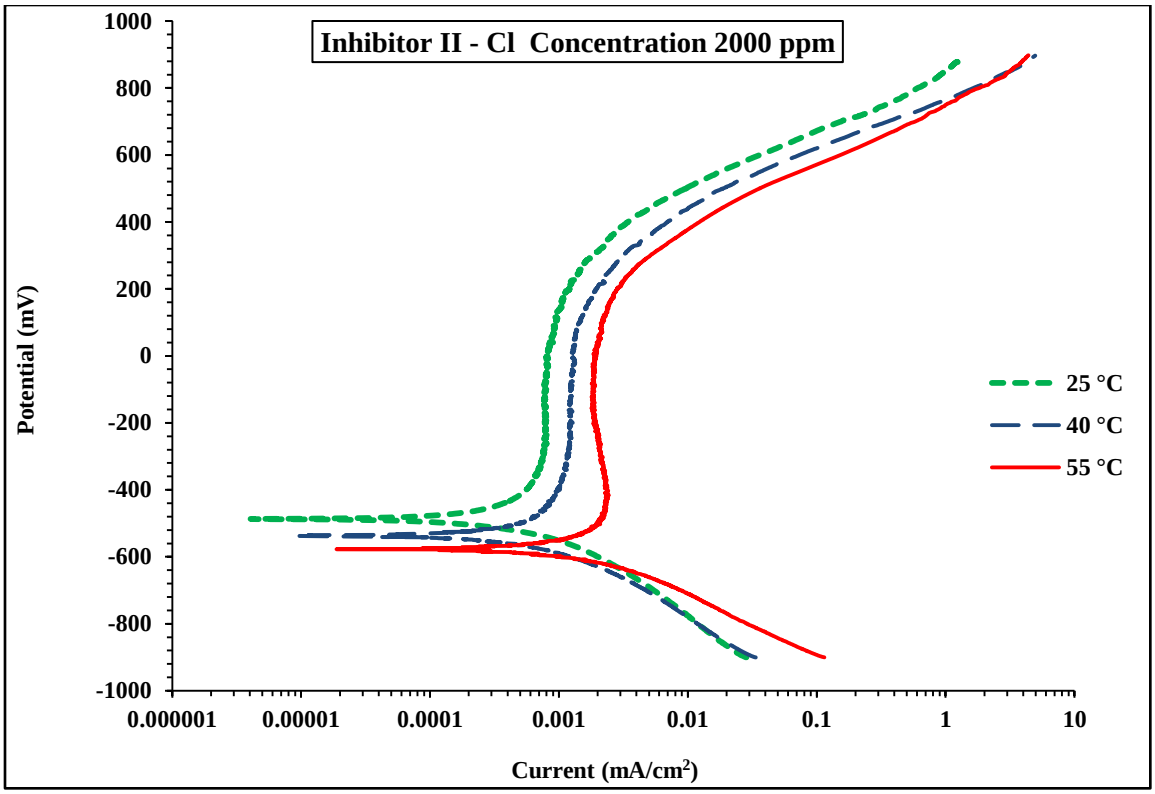


Figure 4.21: Potentio-Dynamic Polarization Curves for Mild Steel in SCPS Incorporated Inhibitor II and 2000 ppm of Cl.

The data in Figure 4.19 through 4.21 were utilized to determine the corrosion polarization parameters for the specimens exposed SCPS incorporating Inhibitor II. These data are summarized in Table 4.5. The data in Table 4.5 revealed that an increase in temperature and chloride concentration increases the corrosion current density. The effect of chloride content and temperature on $I_{corr}$ determined by PDP technique is plotted in Figure 4.22. The increase in $I_{corr}$ with chloride concentration and temperature is visible in these data.

Table 4.5 : Potentio-Dynamic Polarization Results for Steel Specimens Immersed in SCPS Incorporating Inhibitor II

| Temperature (°C) | Chloride Concentration (ppm) | $E_{corr}$ (mV) | $R_p$ (Ohm.cm$^2$) | $I_{corr}$ (µA/cm$^2$) | Corrosion Rate (mm/year) | Inhibitor Efficiency in Reducing $I_{corr}$ % |
|---|---|---|---|---|---|---|
| 25 | 1000 | -412.05 | 179069.00 | 0.1457 | 0.0017 | 84.40 |
| | 1500 | -432.3 | 108199.14 | 0.2411 | 0.0028 | 77.89 |
| | 2000 | -485.13 | 84998.28 | 0.3069 | 0.0036 | 76.82 |
| 40 | 1000 | -419.12 | 155314.80 | 0.1680 | 0.0019 | 84.65 |
| | 1500 | -429.61 | 86118.10 | 0.3029 | 0.0035 | 78.40 |
| | 2000 | -537.27 | 47261.66 | 0.5520 | 0.0064 | 77.75 |
| 55 | 1000 | -373.8 | 47495.26 | 0.5492 | 0.0064 | 91.99 |
| | 1500 | -502.7 | 40392.36 | 0.6458 | 0.0075 | 91.41 |
| | 2000 | -579.4 | 25352.90 | 1.0289 | 0.0119 | 86.62 |

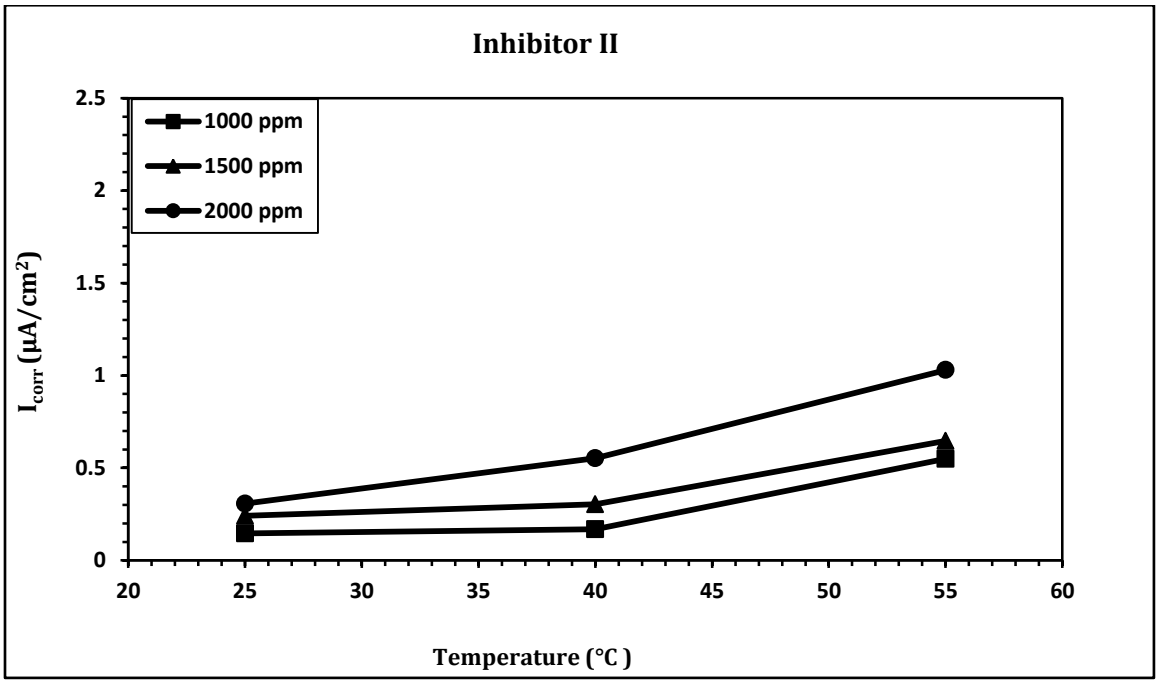


Figure 4.22: Effect of Chloride Concentration on Corrosion Current Density in Presence of Inhibitor II for Various Temperatures

### 4.3.2 Effect of Sulfate and/or Chloride and Temperature on Corrosion Mechanism

The concomitant effect of chloride and sulfate concentrations and temperature on corrosion mechanism of steel immersed in SCPS incorporating Inhibitor II and contaminated with chloride and/or sulfate was investigated. Figure 4.23 displays PDP plot for steel exposed to SCPS incorporating Inhibitor II and contaminated with 1000 ppm Cl plus 0, 500 and 2000 ppm $SO_4$ and 40 ºC. The PDP curves indicate general corrosion in both the specimens. The polarization potentials were -474.62 and -554.64 mV for the 500 and 2000 ppm $SO_4$, respectively. Further, current required for transition from cathodic to anodic region was smaller in the specimens exposed to 2000 ppm $SO_4$ than that exposed to 500 ppm $SO_4$ 0.0612 and 0.0693, respectively $\mu A/cm^2$. The combined effect of sulfate and/or chloride on corrosion of steel specimens immersed in SCPS incorporating Inhibitor II and contaminated with 1000 ppm Cl and various sulfate concentrations 0, 500 or 2000 ppm at 40 ºC is summarized in the Table 4.6. The data showed significant increase in the corrosion current density with the increase in sulfate concentration from 500 to 2000 ppm. The increase in $I_{corr}$ due to incorporation of $SO_4$ is depicted in Figure 4.24.

Table 4.6 : Potentio-Dynamic Polarization Results of Steel Specimens Immersed in SCPS Incorporating Inhibitor II at 40 ºC.

| **Chloride + Sulfate Concentration (ppm)** | **$E_{corr}$ (mV)** | **$R_p$ ($Ohm.cm^2$)** | **$I_{corr}$ ($\mu A/cm^2$)** | **Corrosion rate (mm/year)** | **Inhibitor Efficiency in Reducing $I_{corr}$ %** |
|---|---|---|---|---|---|
| **1000 + 0** | **-419.12** | **155314.80** | **0.1680** | **0.0019** | **84.64** |
| **1000 + 500** | **-474.62** | **83328.04** | **0.3130** | **0.0036** | **72.32** |
| **1000 + 2000** | **-554.64** | **59940.30** | **0.4352** | **0.0050** | **71.88** |

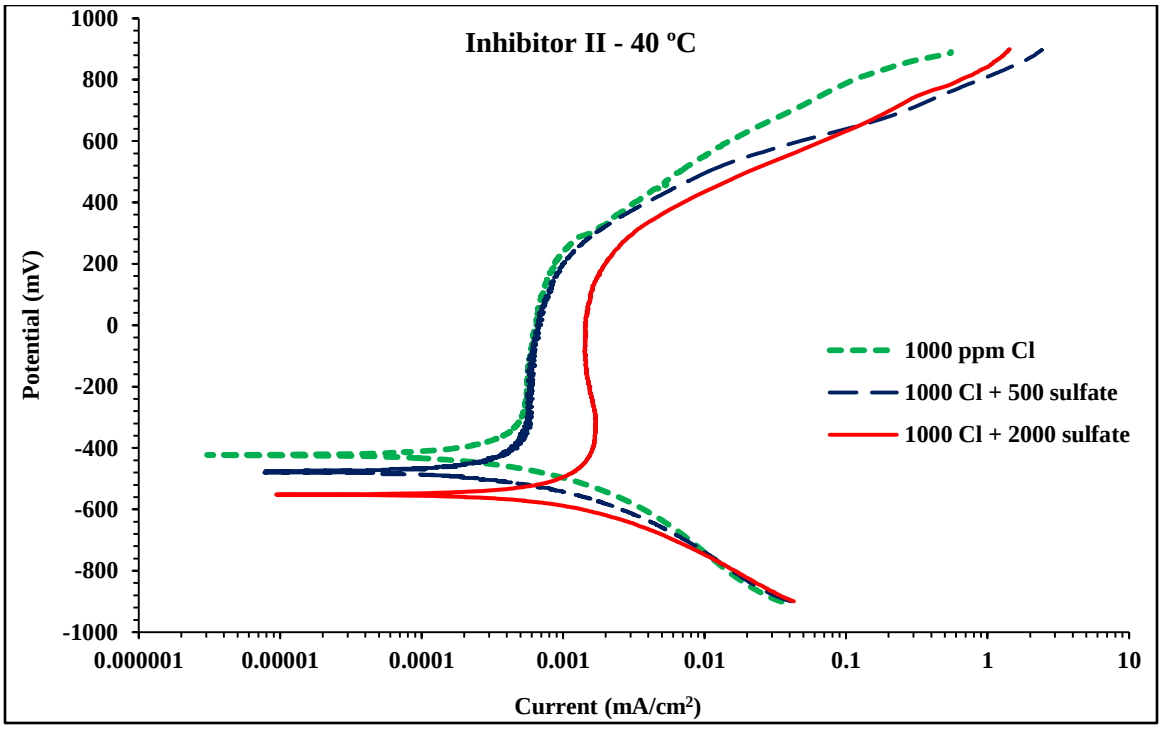


Figure 4.23: Potentio-Dynaimic Polarization Curves for Specimens Immersed in SCPS Incorporating Inhibitor II and 1000 ppm Cl plus (0, 500 and 2000) ppm $SO_4$

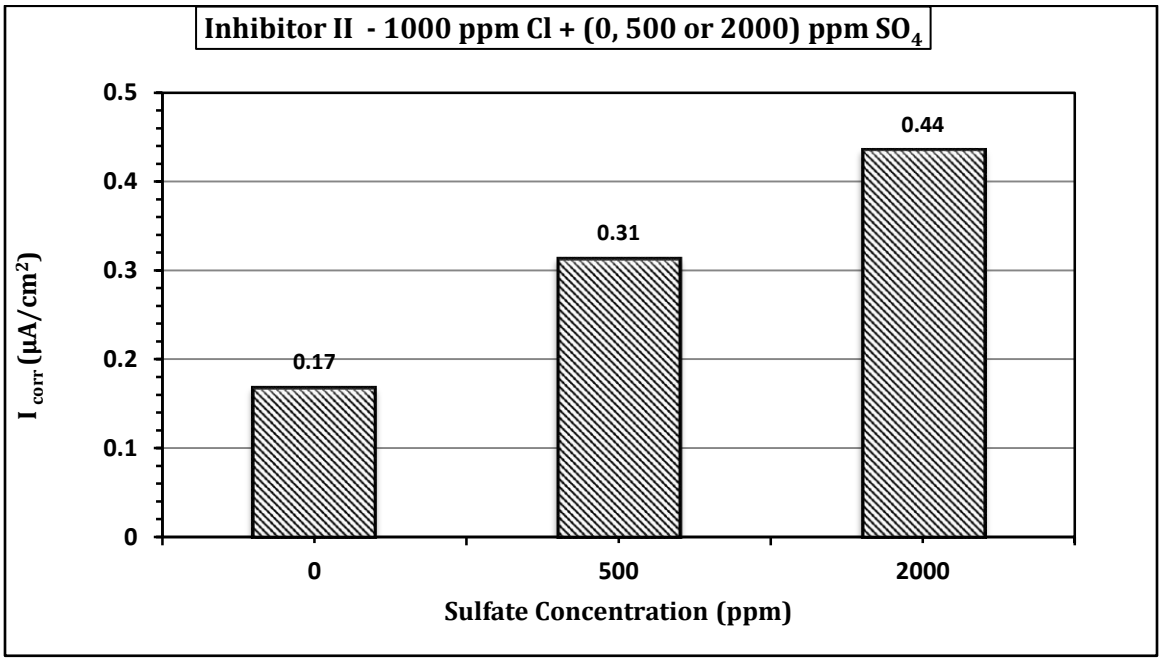


Figure 4.24: Combined Effect of Chloride, Sulfate and Temperature on Corrosion Current Density (40 °C).

### 4.3.3 Scanning Electron Microscopy of Steel Specimens Immersed in SCPS Incorporating Inhibitor II

The scanning electron micrographs of the mild steel specimen exposed to SCPS incorporating Inhibitor II and contaminated with sulfate and/or chloride ions are shown in Figures 4.25 through 4.27. There was general corrosion in all the specimens due to the presence of Inhibitor II in the SCPS. The SEM in Figure 4.25 (Cl: 1,500; temperature: 25 ºC) exhibits general corrosion. Comparison of the SEM micrograms for the control specimen and the specimen immersed in SCPS incorporating Inhibitor II, there was a rough surface on mild steel in the control specimen. In addition, the specimen surface was strongly damaged. However, the specimen immersed in SCPS incorporating Inhibitor II revealed that a good protective adsorbed film has been formed on the surface of the specimens, which confirms the fact that the inhibited corrosion on the surface of mild steel in SCPS adsorption of the used corrosion inhibitor.

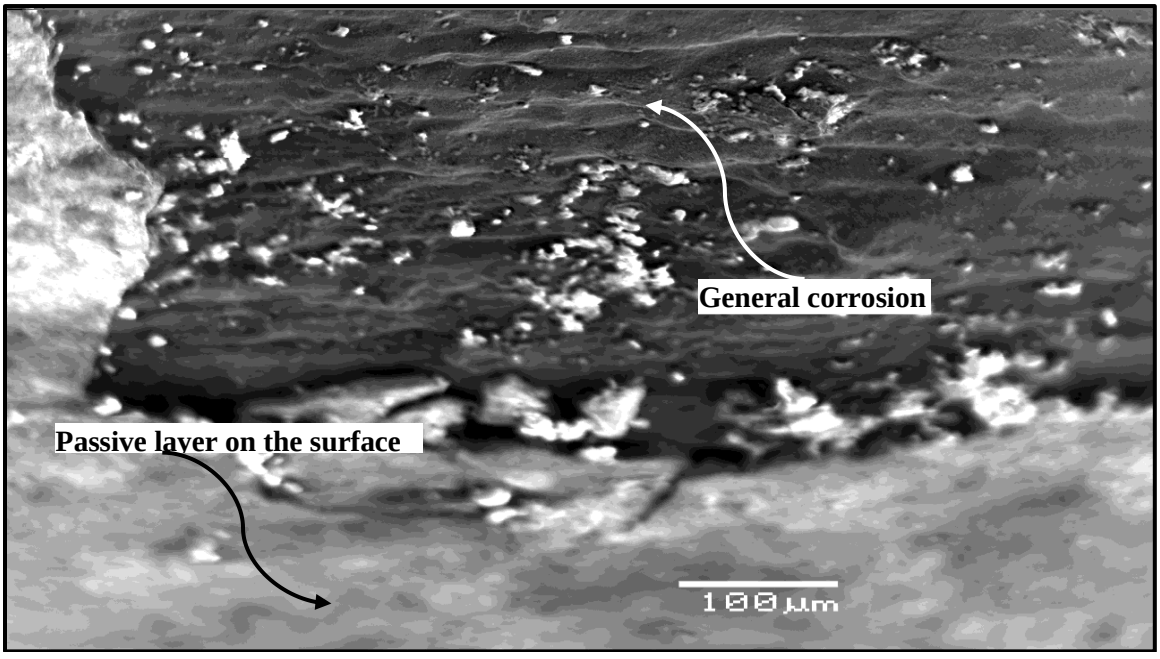


Figure 4.25: SEM (180X) for Steel Specimen in SCPS Incorporating Inhibitor II and Contaminated with 1500 ppm Cl at 25 ºC

Figure 4.26 shows the SEM of the polished surface of mild steel specimen immersed in SCPS incorporating Inhibitor II and contaminated with 1500 ppm Cl and exposed to a temperature of 55 ºC. General corrosion was also noted in this specimen. However, there were corrosion products on the surface of steel specimen. This might be due to the effect of chloride and elevated exposure temperature.

Figure 4.27 is the SEM of steel immersed in SCPS incorporating Inhibitor II and contaminated with 1000 ppm Cl and 2000 ppm sulfate and exposure temperature of 40 ºC. As the other groups of specimens, general corrosion and a good protective adsorbed film is noted on the surface of the specimen.

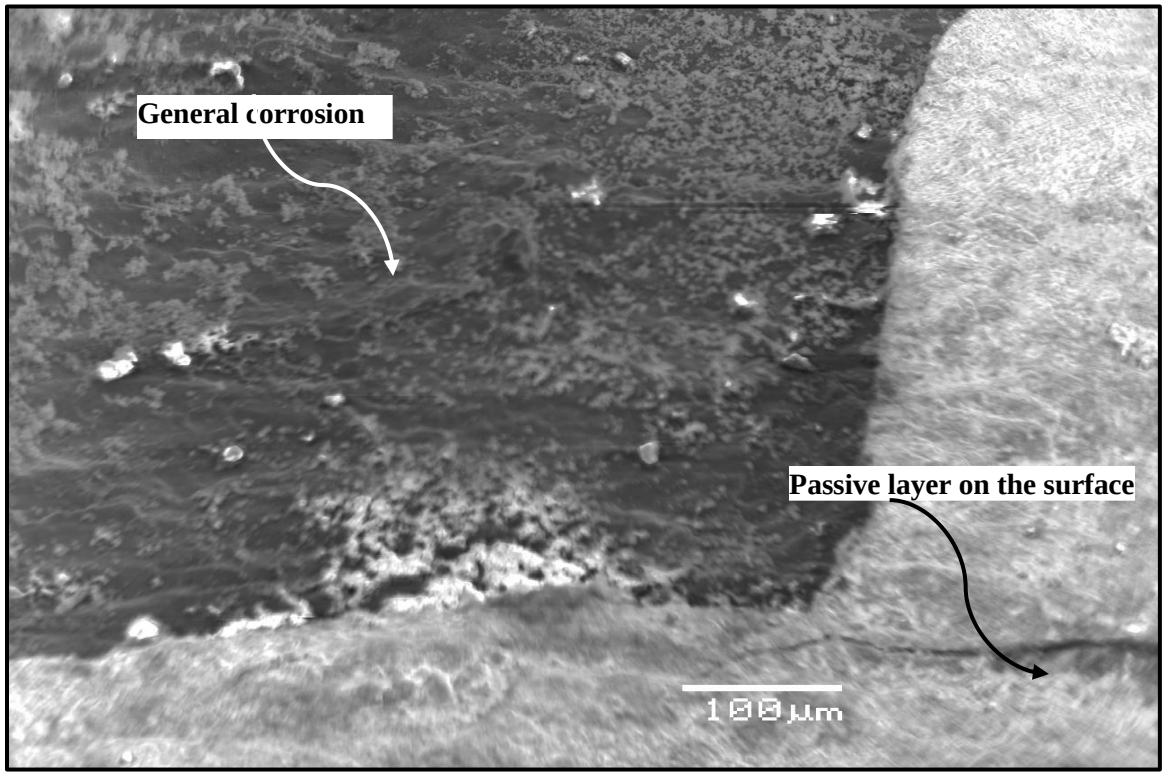


Figure 4.26: SEM (180X) for Steel Specimen in SCPS Incorporating Inhibitor II and Contaminated with 1500 ppm Cl at 55 ºC

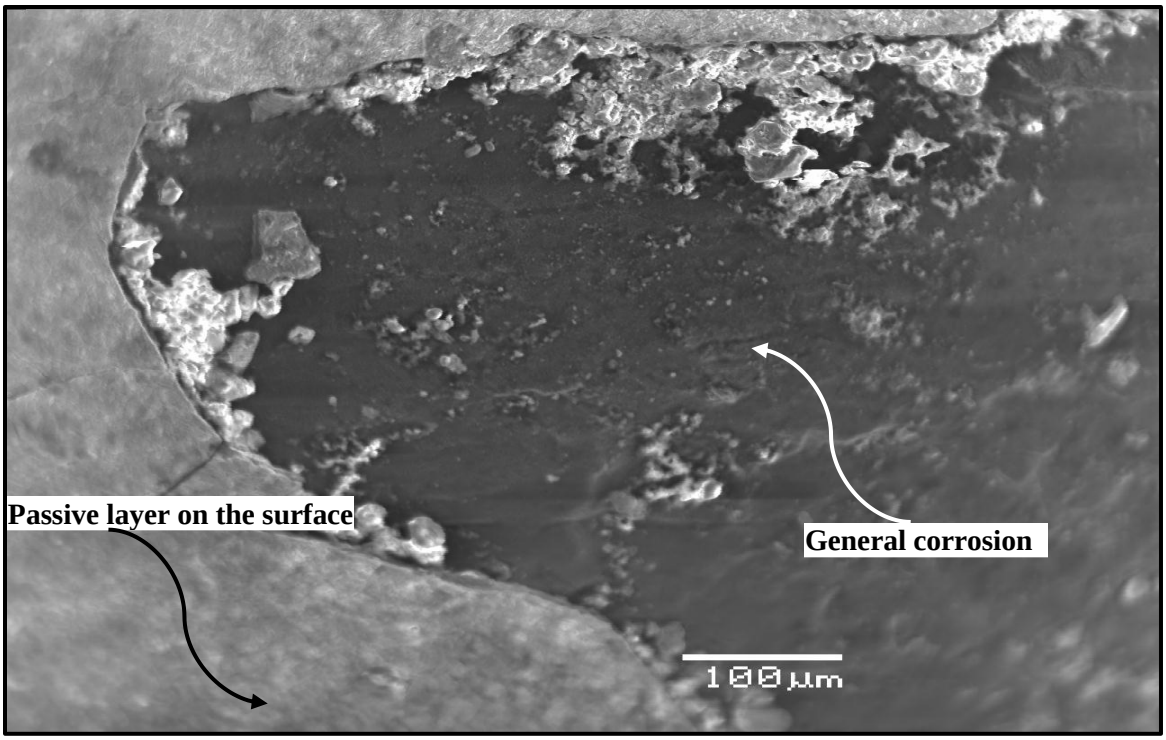


Figure 4.27: SEM (180X) for Steel Specimen in SCPS Incorporating Inhibitor II and Contaminated with 1000 ppm Cl + 2000 ppm Sulfate at 40 ºC

## 4.4 Performance of Steel Specimens in Presence of Inhibitor III

Performance evaluation of Inhibitor III as a corrosion inhibitor on the corrosion behavior of steel specimens immersed in SCPS and exposed to various sulfate and/or chloride concentrations and temperatures was evaluated using PDP technique. The results of these tests are summarized and discussed in the following sub-sections.

### 4.4.1 Effect of Chloride and Temperature on Corrosion Mechanism

The PDP curves for mild steel specimens placed in SCPS incorporating Inhibitor III as a corrosion inhibitor are displayed in Figures 4.28 through 4.30. These curves are for

specimens immersed in SCPS incorporating Inhibitor III and contaminated with 1000, 1500 and 2000 ppm chloride at temperatures of 25, 40 and 55 ºC.

The PDP curves for steel specimens exposed to chloride concentration of 1000 exhibited general corrosion for all exposure temperatures (Figure 4.28). The current required for transition from cathodic to anodic region decreased from 0.0108 to 0.0072 $\mu A/cm^2$ with increasing the temperature from 25 to 55 °C. The polarization potentials were around -270, -360 and -400 mV, respectively. As expected, the rate of corrosion increased with the increase in the temperature. Although there was a slightly increase in the corrosion current density 0.144 and 0.168 $\mu A/cm^2$, respectively when the temperature was increased from 25 to 40 ºC, the increase in $I_{corr}$ when the temperature was increased to 55 ºC was significant (0.380 $\mu A/cm^2$).

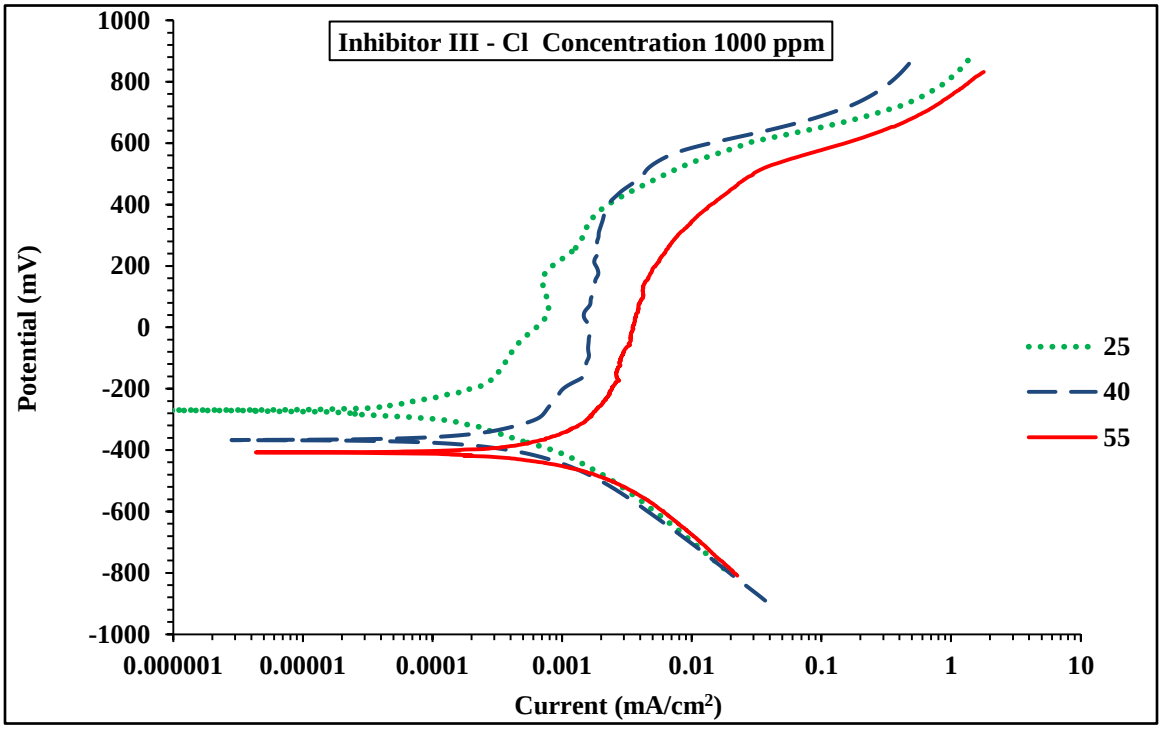


Figure 4.28: Potentio-Dynamic Polarization Curves for Mild Steel in SCPS Incorporated Inhibitor III and 1000 ppm of Cl

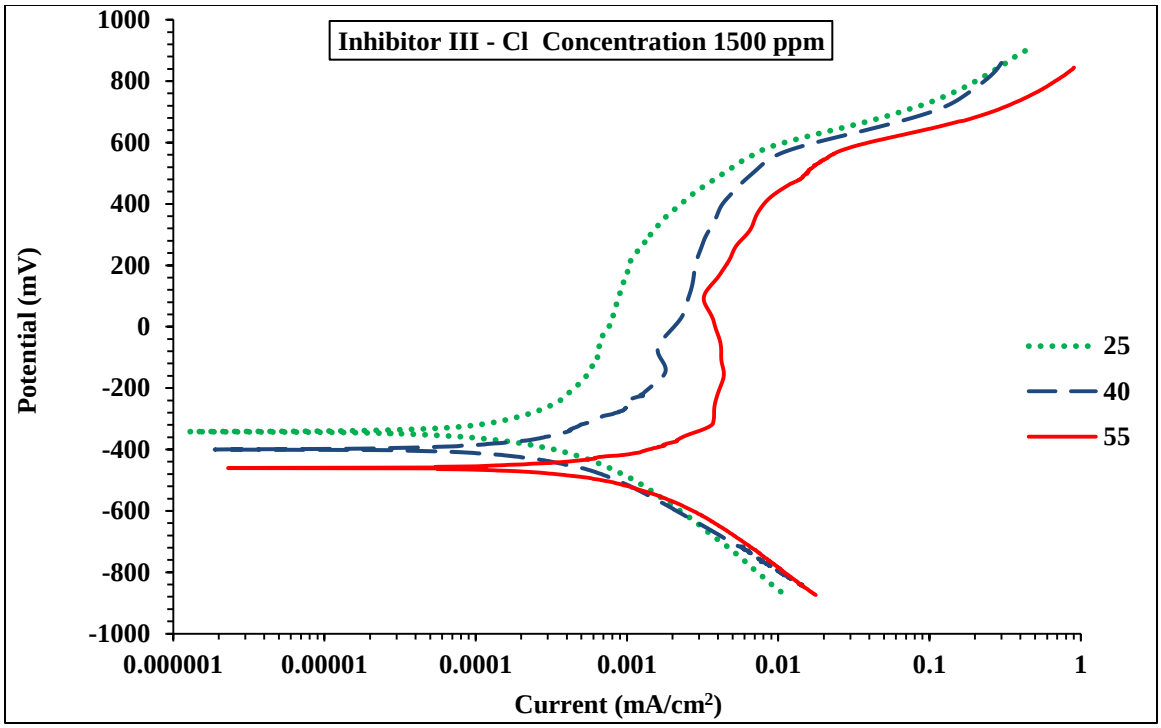


Figure 4.29: Potentio-Dynamic Polarization Curves for Mild Steel in SCPS Incorporated Inhibitor III and 1500 ppm of Cl

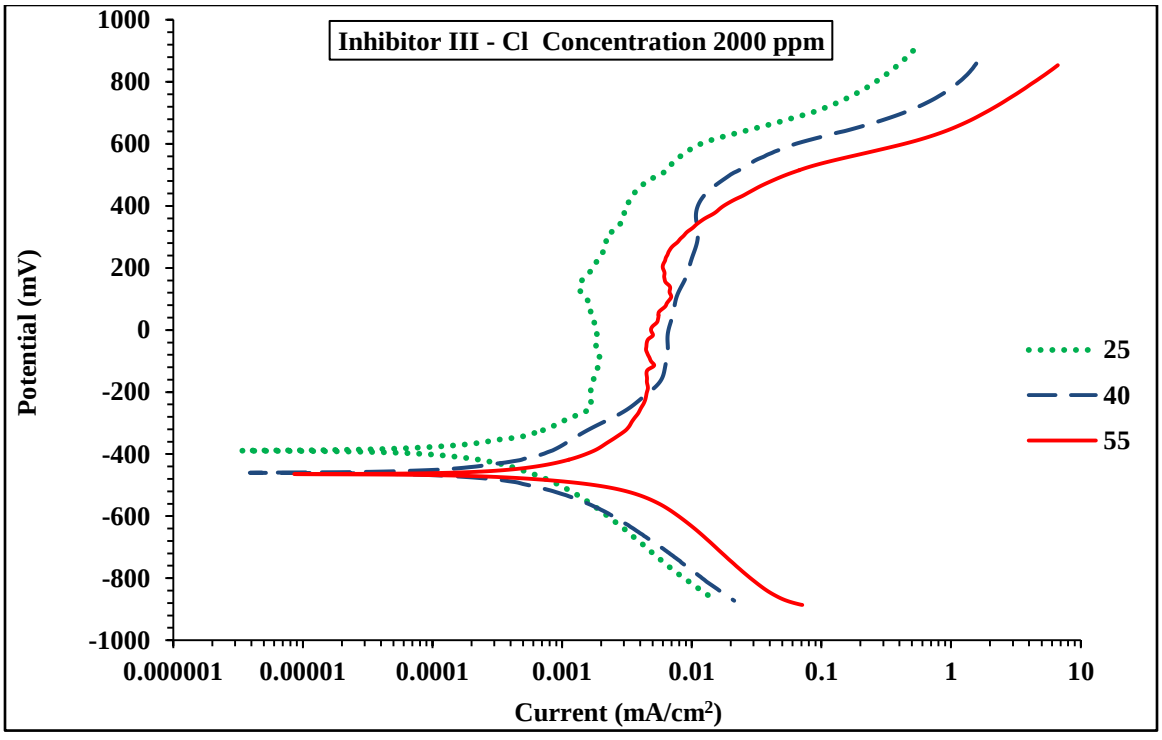


Figure 4.30: Potentio-Dynamic Polarization Curves for Mild Steel in SCPS Incorporated Inhibitor III and 2000 ppm of Cl

Figure 4.29 shows the PDP curves for steel specimens exposed to chloride concentration of 1500 ppm at different temperatures and general corrosion could be observed. The polarizing potential in this group of specimens varies from -340 to -401 with increased exposure temperature from 25 to 55 °C. However, the polarization curve is also similar as in the other group of specimens (1000 ppm $Cl^-$), there is a significant jump in PDP curve at exposure temperature of 55 ºC which might be due to the diffusion of the chloride ions in the pores of the surface of steel specimens that might have accelerated the corrosion.

Figure 4.30 shows the PDP for steel specimens placed in SCPS with 2000 ppm chloride. General corrosion was noted in all the specimens and the polarizing potentials are around -390 mV for the exposure temperatures of 25 ºC and decreased to around -479 mV when the exposure temperature was increased to 55 ºC. However, the transition line from the anodic to cathodic decreased from 0.0423 to 0.0351 μA with increasing the temperature. This is the result of conjoint effect of temperature and increased chloride concentration. The PDP drifted towards anodic region with increasing the temperature of the pore solution. While there was no significance difference in the anodic behavior of solution exposed to 40 or 55 ºC, the PDP for 25 ºC tends to be less than the other two curves. The current required for transition from cathodic to anodic polarization decreased with increase the temperature.

Figures 4.28 through 4.30 were utilized to determine the corrosion polarization parameters for the specimens exposed SCPS incorporating Inhibitor III. These data are summarized in Table 4.7 and revealed that an increase in temperature increases the corrosion current density. The effect of chloride content and temperature on $I_{corr}$

determined by PDP technique is plotted in Figure 4.31. The increase in $I_{corr}$ with chloride concentration and temperature is visible in these data.

Table 4.7: Potentio-Dynamic Polarization Results for Steel Specimens Immersed in SCPS Incorporating Inhibitor III

| Temperature (°C) | Chloride Concentration (ppm) | $E_{corr}$ (mV) | $R_p$ (Ohm.cm$^2$) | $I_{corr}$ (µA/cm$^2$) | Corrosion Rate (mm/year) | Inhibitor Efficiency in Reducing $I_{corr}$ % |
|---|---|---|---|---|---|---|
| 25 | 1000 | -270 | 180748.00 | 0.1443 | 0.0017 | 84.54 |
| | 1500 | -340 | 118792.90 | 0.2196 | 0.0025 | 79.86 |
| | 2000 | -390 | 68579.12 | 0.3804 | 0.0044 | 71.26 |
| 40 | 1000 | -360 | 155271.00 | 0.1680 | 0.0019 | 84.64 |
| | 1500 | -401 | 97430.18 | 0.2678 | 0.0031 | 80.91 |
| | 2000 | -471 | 53856.48 | 0.4844 | 0.0056 | 84.30 |
| 55 | 1000 | -400 | 68579.12 | 0.3804 | 0.0044 | 94.46 |
| | 1500 | -450 | 20847.34 | 1.2513 | 0.0145 | 83.34 |
| | 2000 | -479 | 14836.52 | 1.7583 | 0.0204 | 77.13 |

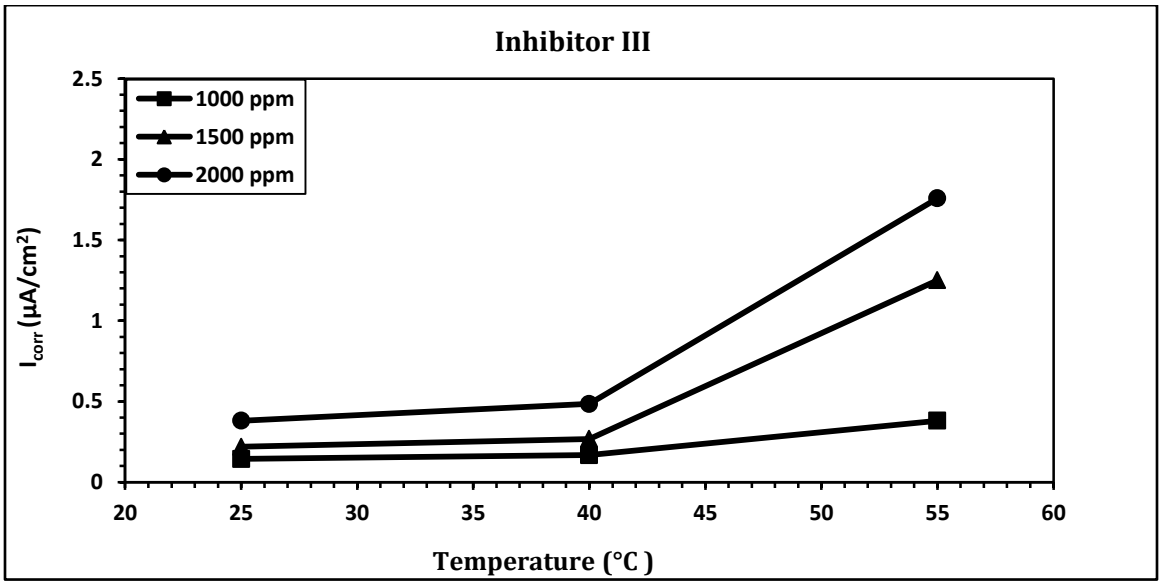


Figure 4.31: Effect of Chloride Concentration on Corrosion Current Density in the Presence of Inhibitor III for Various Temperatures

### 4.4.2 Effect of Sulfate and/or Chloride and Temperature on Corrosion Mechanism

The concomitant effect of chloride and sulfate and temperature on the corrosion mechanism and rate of steel bars immersed in SCPS incorporating Inhibitor III is shown in Figure 4.32. This Figure displays PDP plot for steel exposed to SCPS incorporating Inhibitor III contaminated with 1000 ppm Cl and 0, 500 and 2000 ppm $SO_4$ at 40 ºC. The PDP curves indicate general corrosion in all the specimens. The polarization potential varies from -360 to -400 mV with the increase in sulfate concentration from 0 to 2000 ppm. Further, the current required for transition from cathodic to anodic region varied from 0.0788 to 0.0428 $\mu A/cm^2$ with the increase of $SO_4$ concentrations from 500 to 2000 ppm.

The combined effect of sulfate and/or chloride on corrosion of steel specimens immersed in SCPS incorporating Inhibitor III and contaminated with 1000 ppm Cl and various sulfate concentrations (0, 500 and 2000) ppm at 40 ºC is summarized in the Table 4.8. The data showed significant increase in the corrosion current density with the increase in sulfate concentration from 500 to 2000 ppm. The increase in $I_{corr}$ due to incorporation of $SO_4$ is depicted in Figure 4.33.

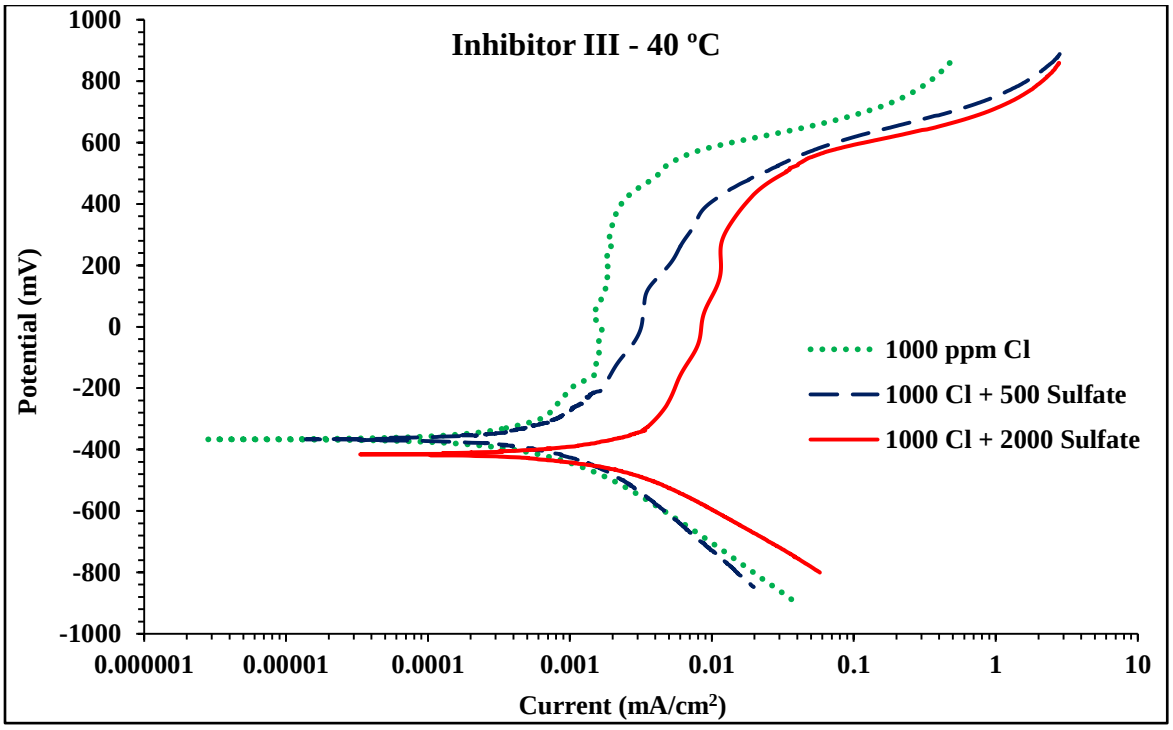


Figure 4.32: Potentio-Dynaimic Polarization Curves for Specimens Immersed in SCPS Incorporating Inhibitor III and 1000 ppm Cl plus (0, 500 and 2000) ppm $SO_4$

Table 4.8: Potentio-Dynamic Polarization Results of Steel Specimens Immersed in SCPS Incorporating Inhibitor III at 40 ºC

| Chloride + Sulfate Concentration (ppm) | $E_{corr}$ (mV) | $R_p$ (Ohm.cm$^2$) | $I_{corr}$ (µA/cm$^2$) | Corrosion Rate (mm/year) | Inhibitor Efficiency in Reduction of $I_{corr}$ % |
|---|---|---|---|---|---|
| 1000 + 0 | -360 | 155271.00 | 0.1680 | 0.0019 | 84.64 |
| 1000 + 500 | -360.1 | 93183.04 | 0.2800 | 0.0032 | 75.24 |
| 1000 + 2000 | -400.64 | 55258.08 | 0.4721 | 0.0055 | 69.50 |

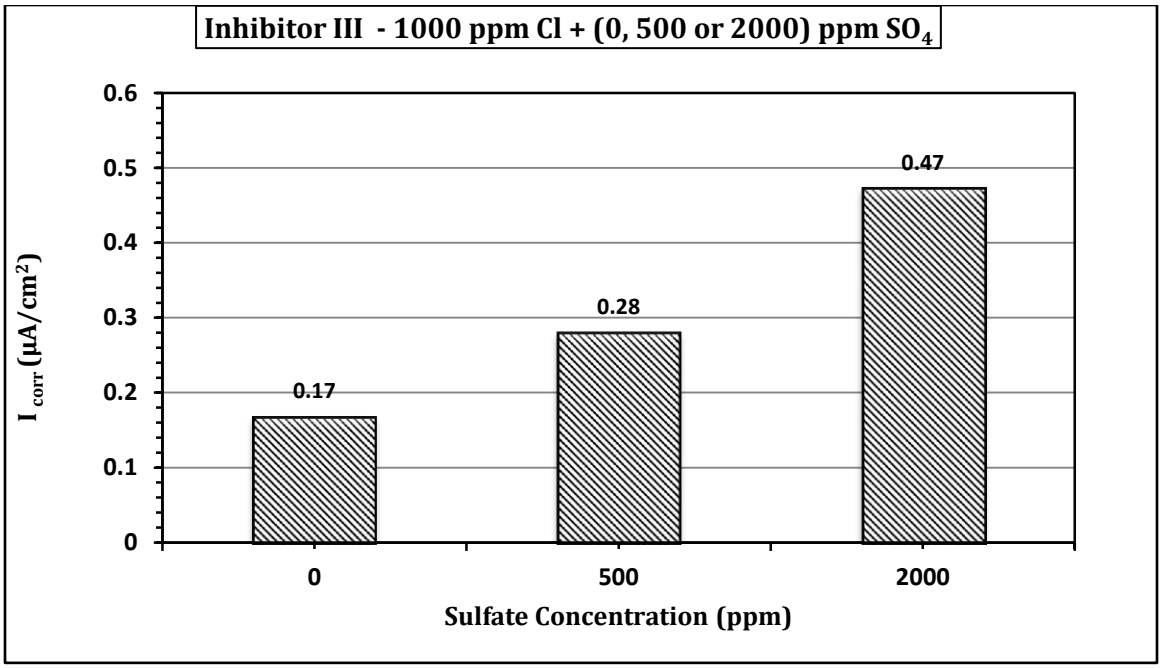


Figure 4.33: Combined Effect Of Chloride, Sulfate and Temperature on Corrosion Current Density (40 °C).

### 4.4.3 Scanning Electron Microscopy of Steel Specimens Immersed in SCPS Incorporating Inhibitor III

The scanning electron micrographs of the mild steel specimen exposed to SCPS incorporating Inhibitor III and contaminated with sulfate and/or chloride ions are shown in Figures 4.34 through 4.36. There was general corrosion in all the specimens (Figures 4.34 through 4.36). The SEM in Figure 4.34 (Cl: 1,500; temperature: 25 ºC) exhibits general corrosion and a good protective adsorbed film was formed on the surface of the specimen, which decreased the corrosion current density and corrosion rate of steel in the alkaline environment. The micrograph also shows that the steel surface was better in the presence of Inhibitor III compared to the surface of the control specimen which was rough and covered with the corrosion product.

Figure 4.35 shows the SEM of the polished surface of mild steel specimen immersed in SCPS incorporating Inhibitor III and contaminated with 1500 ppm Cl and exposed to a temperature of 55 ºC. General corrosion was noted in this specimen also. However, there were many of corrosion products on the surface of steel specimen. This might be due to the effect of chloride and elevated exposure temperature.

Figure 4.36 is a SEM of the steel immersed in SCPS incorporating Inhibitor III and contaminated with 1000 ppm Cl and 2000 ppm sulfate at an exposure temperature of 40 ºC. General corrosion and a good protective adsorbed film were noted on the surface of the specimen. The SEM in Figures 4.34 through 4.36 indicate that Inhibitor III can minimize corrosion of steel bars.

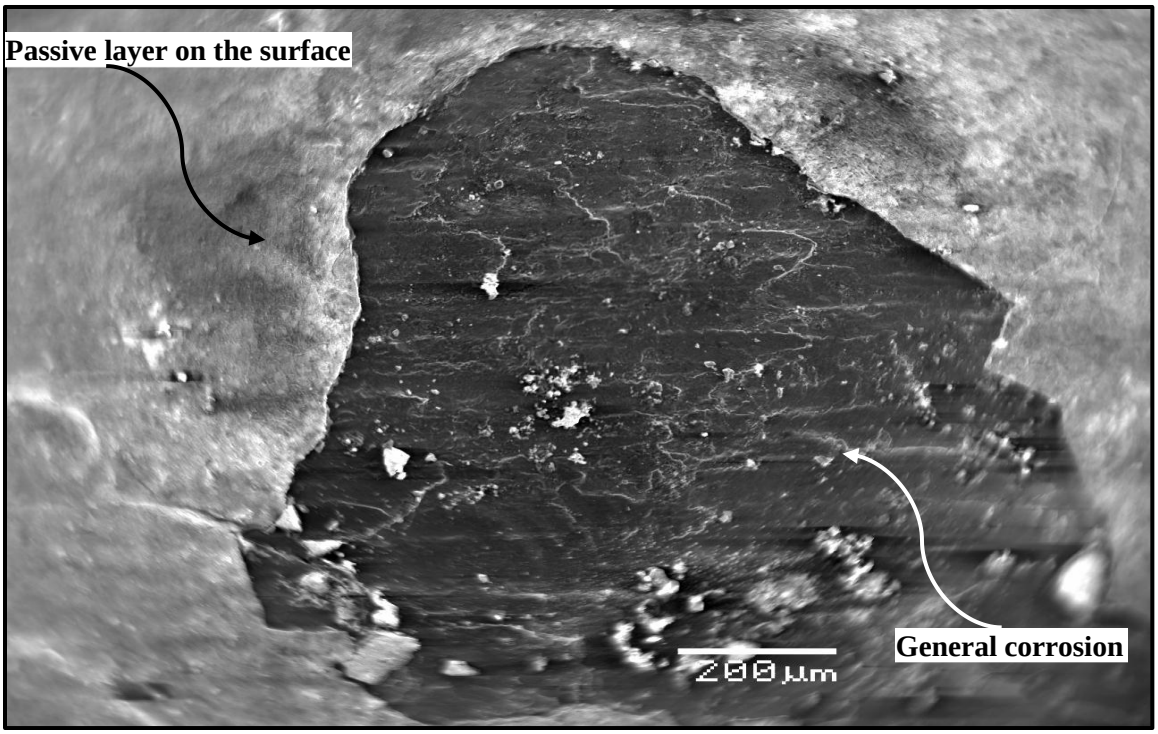


Figure 4.34: SEM (180X) for Steel Specimen in SCPS Incorporating Inhibitor III and Contaminated with 1500 ppm Cl at 25 ºC.

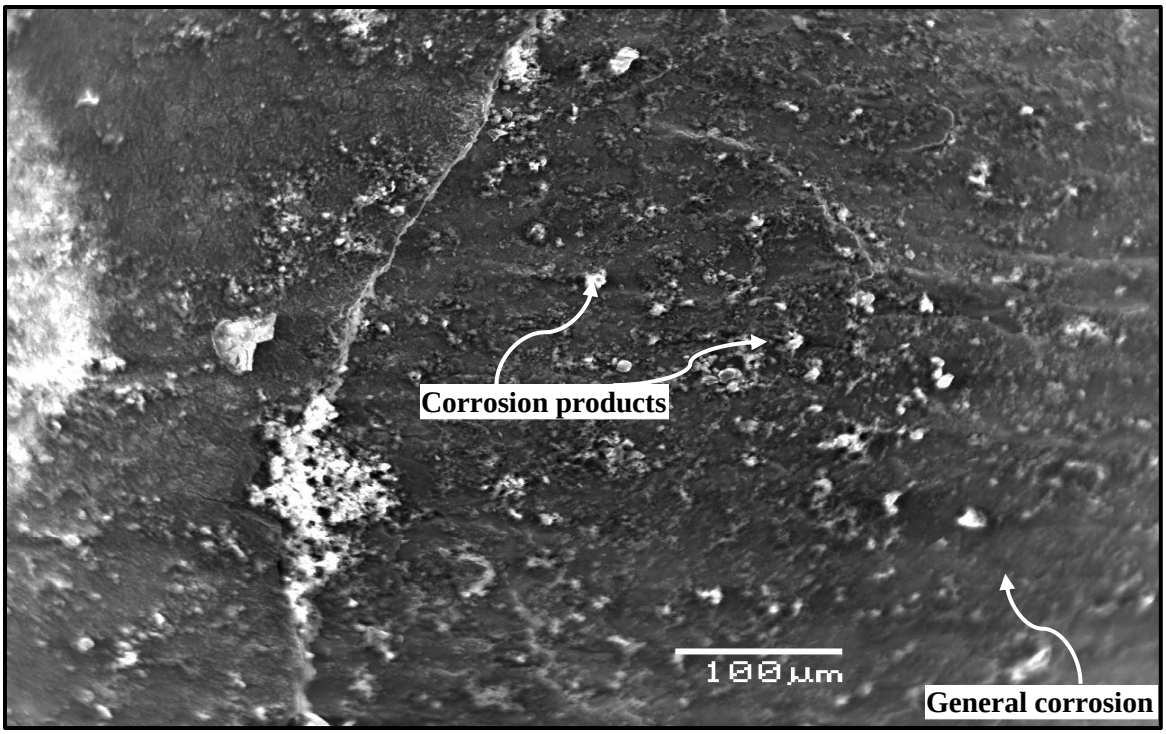


Figure 4.35: SEM (180X) for Steel Specimen in SCPS Incorporating Inhibitor III and Contaminated with 1500 ppm Cl at 55 ºC.

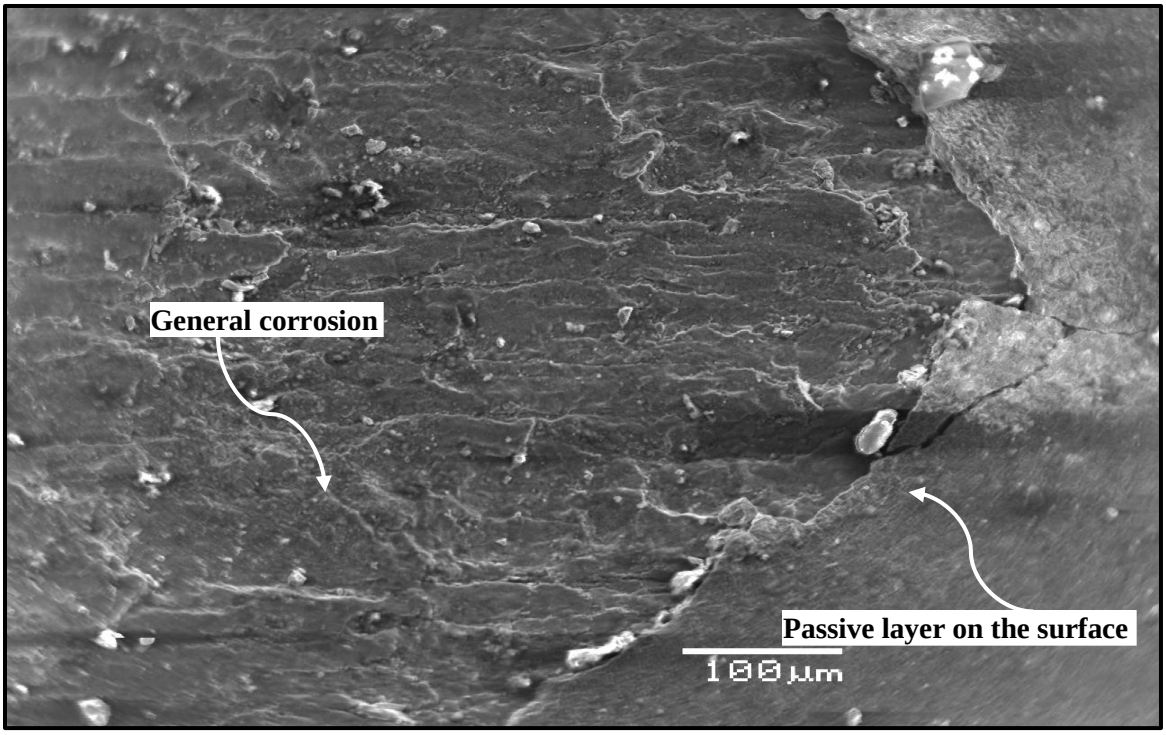


Figure 4.36: SEM (180X) for Steel Specimen in SCPS Incorporating Inhibitor III and Contaminated with 1000 ppm Cl + 2000 ppm sulfate at 40 ºC.

## 4.5 Performance of Steel Specimens in Presence of Inhibitor IV

Corrosion mechanism of steel specimens immersed in alkaline environment incorporating Inhibitor IV as a corrosion inhibitor and exposed to various temperatures was investigated using PDP technique. The results of these tests are summarized and discussed in the following sub-sections.

### 4.5.1 Effect of Chloride and Temperature on Corrosion Mechanism

The PDP curves for mild steel specimens placed in SCPS incorporating Inhibitor IV as a corrosion inhibitor are displayed in Figures 4.37 through 4.39. These curves are for the specimens immersed in SCPS incorporating Inhibitor IV and contaminated with 1000, 1500 and 2000 ppm chloride and at temperatures of 25, 40 and 55 ºC.

The PDP curves for steel specimens exposed to chloride concentration of 1000 exhibits general corrosion for all the exposure temperatures (Figure 4.37) due to the fact that Inhibitor IV is good in minimizing pitting corrosion. The current required for transition from cathodic to anodic polarization decreases from 0.0522 to 0.0162 $\mu A/cm^2$ with increasing temperature. The polarizing potential is around -380 mV at exposure temperatures of 25 and 40 ºC and -500 mV for 55 ºC. As expected, the rate of corrosion increased with an increase in the temperature.

Figure 4.38 shows the PDP curves for steel specimens immersed in SCPS incorporating Inhibitor IV and exposed to chloride concentration of 1500 ppm at different temperatures and general corrosion could be absolved. The polarizing potential in this group of specimens is also around -394 mV for the exposure temperatures of 25 ºC and decreased

to around -512 mV when the exposure temperature was increased to 55 ºC the polarization curve is also similar as in the previous group of specimens (1000 ppm $Cl^-$).

The PDP drifted towards anodic region with increasing the temperature of the pore solution. That is due to the fact that increasing the temperature leads to decrease in the pore solution resistance, hence increase corrosion process. There was uniform difference in the anodic behavior of solution for all exposed temperatures. Figure 4.39 shows the PDPs for steel specimens placed in SCPS contaminated with 2000 ppm chloride. General corrosion was noted in all the specimens and the polarizing potential is around – 450 mV. However, the transition curve decreases from 0.0977 to 0.0932 μA with increasing the temperature. This is the result of conjoint effect of temperature and increased chloride concentration.

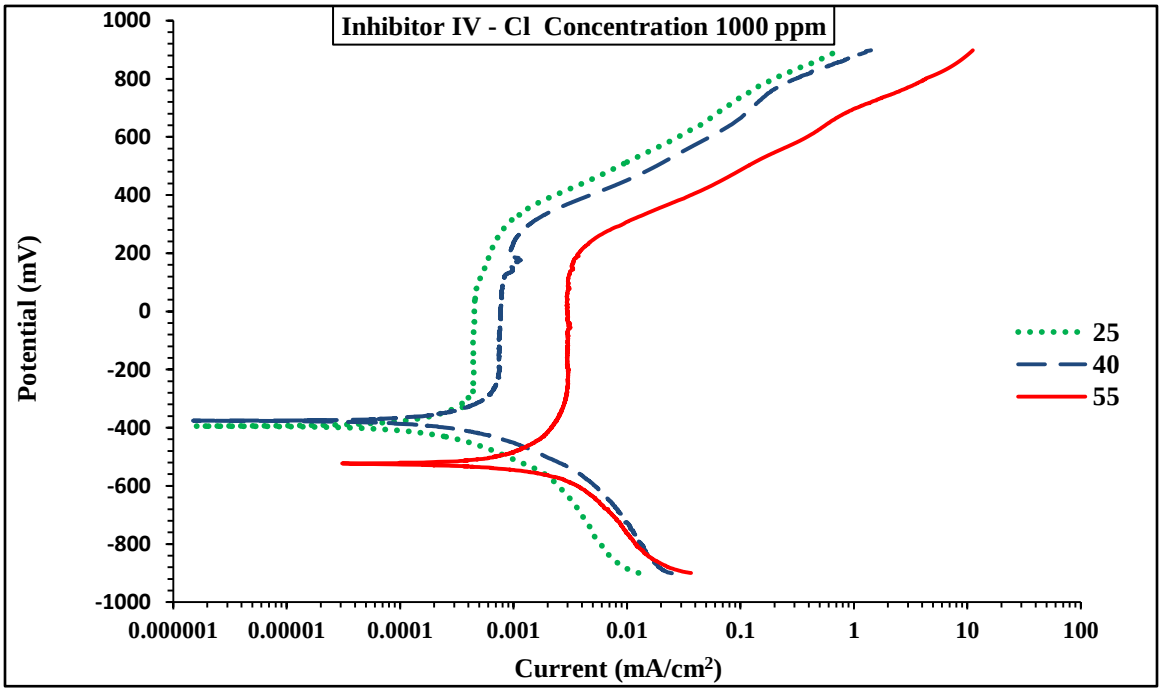


Figure 4.37: Potentio-Dynamic Polarization Curves for Mild Steel in SCPS Incorporated Inhibitor IV and 1000 ppm of Cl.

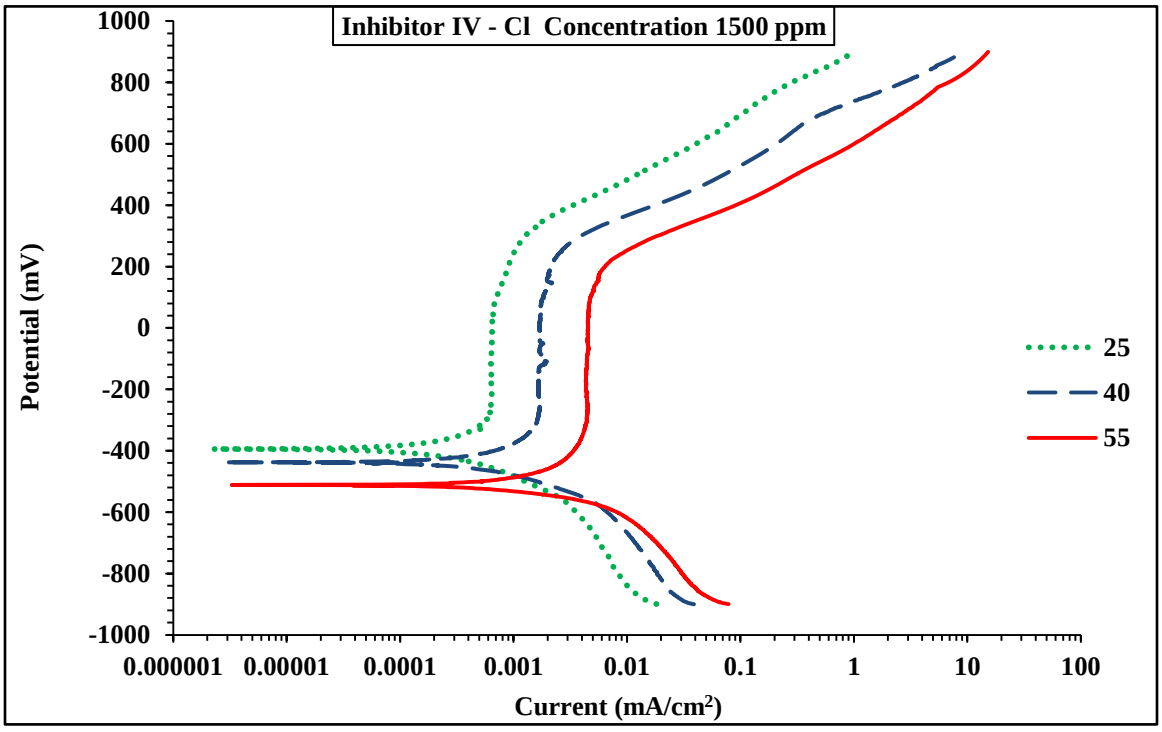


Figure 4.38: Potentio-Dynamic Polarization Curves for Mild Steel in SCPS Incorporated Inhibitor IV and 1500 ppm of Cl.

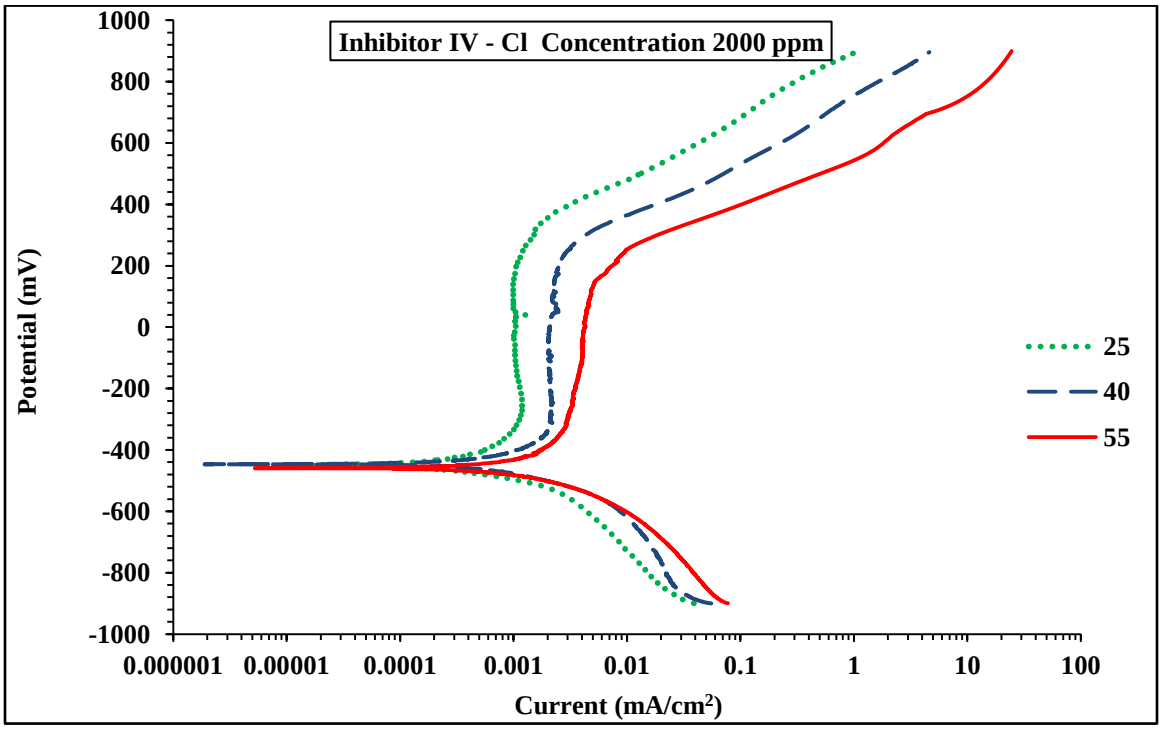


Figure 4.39: Potentio-Dynamic Polarization Curves for Mild Steel in SCPS Incorporated Inhibitor IV and 2000 ppm of Cl.

The data in Figures 4.37 through 4.39 were utilized to determine the corrosion polarization parameters for specimens exposed SCPS incorporating Inhibitor IV. These data were summarized in Table 4.9. The data in this table also revealed that an increase in temperature and chloride concentration increased the corrosion current density. The effect of chloride content and temperature on $I_{corr}$ determined by PDP technique is plotted in Figure 4.40. The increase in $I_{corr}$ with chloride concentration and temperature is visible in these data.

Table 4.9: Potentio-Dynamic Polarization Results for Steel Specimens Immersed in SCPS Incorporating Inhibitor IV.

| Temperature (ºC) | Chloride Concentration (ppm) | $E_{corr}$ (mV) | $R_p$ (Ohm.cm$^2$) | $I_{corr}$ (µA/cm$^2$) | Corrosion Rate (mm/year) | Inhibitor Efficiency in Reducing $I_{corr}$ % |
|---|---|---|---|---|---|---|
| 25 | 1000 | -394.42 | 188004.20 | 0.1387 | 0.0016 | 85.14 |
| | 1500 | -394.52 | 116957.68 | 0.2230 | 0.0026 | 79.54 |
| | 2000 | -446.82 | 89585.60 | 0.2912 | 0.0034 | 78.00 |
| 40 | 1000 | -376.46 | 106247.12 | 0.2455 | 0.0028 | 77.55 |
| | 1500 | -450.27 | 81865.12 | 0.3187 | 0.0037 | 77.28 |
| | 2000 | -446.88 | 29305.12 | 0.8902 | 0.0103 | 64.11 |
| 55 | 1000 | -523.22 | 14490.79 | 1.8002 | 0.0209 | 73.76 |
| | 1500 | -512.87 | 12511.32 | 2.0849 | 0.0242 | 72.24 |
| | 2000 | -457.26 | 6226.32 | 4.1897 | 0.0486 | 45.50 |

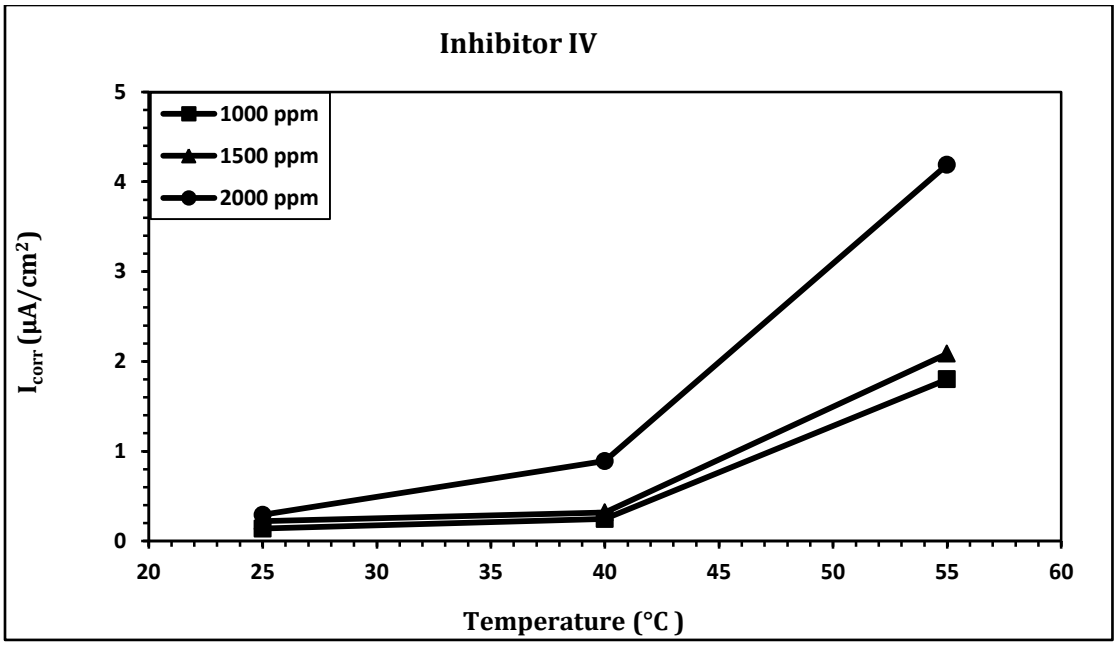


Figure 4.40 : Effect of Chloride Concentration on Corrosion Current Density for Various Temperatures

### 4.5.2 Effect of Sulfate and/or Chloride and Temperature on Corrosion Mechanism

In order to simulate most of the aggressive factors of alkaline environment, the concomitant effect of different chloride and sulfate concentrations and temperature on the performance of Inhibitor IV was performed using PDP test. Figure 4.41 displays PDP plot for steel exposed to SCPS incorporating Inhibitor IV and contaminated with 1000 ppm Cl and 0, 500 and 2000 ppm $SO_4$ at a temperature of 40 ºC. The PDP curves indicate general corrosion in all the three specimens. Further, the current required for transition from cathodic to anodic region slightly varies from a round zero to 0.055 μA with increase the sulfate concentration from 500 to 2000 ppm.

The combined effect of sulfate and/or chloride on corrosion of steel specimens immersed in SCPS incorporating Inhibitor IV and contaminated with 1000 ppm Cl and

various sulfate concentrations 500 or 2000 ppm at 40 ºC is summarized in the Table 4.10. The data showed significant increase in corrosion current density from 0.246 to 1.118 $\mu A/cm^2$ with the increase in sulfate concentration from 0 to 2000 ppm. The increase in $I_{corr}$ due to incorporation of $SO_4$ is depicted in Figure 4.42.

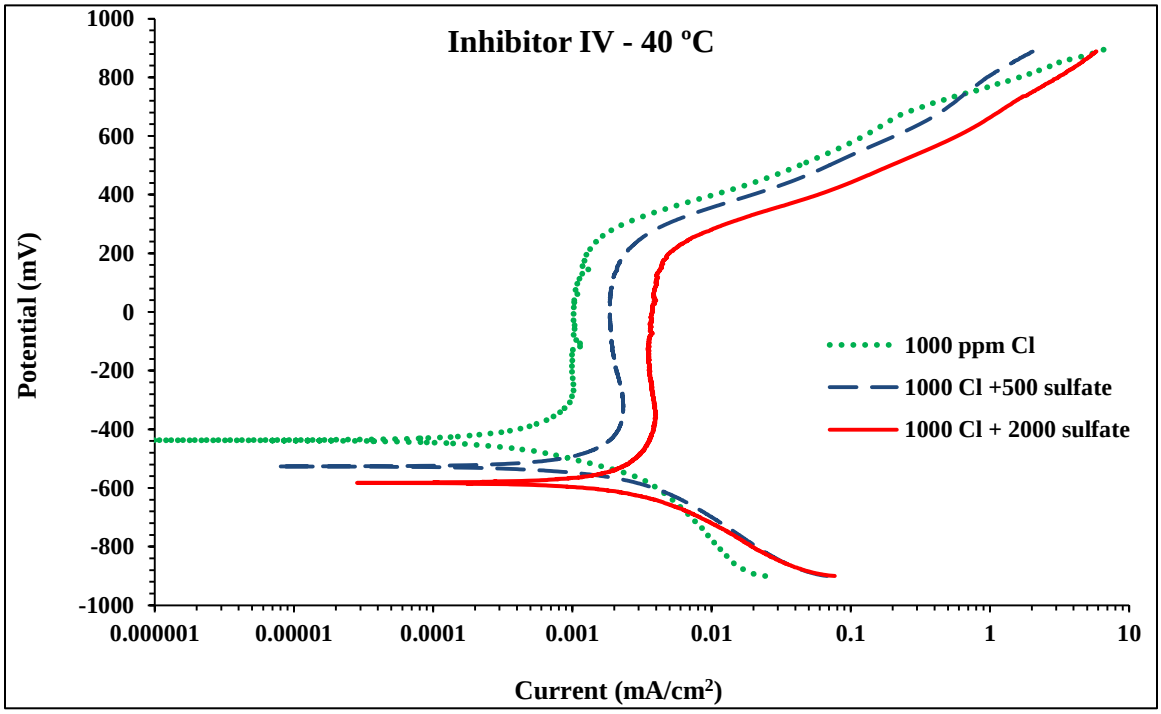


Figure 4.41: Potentio-Dynaimic Polarization Curves for Specimens Immersed in SCPS Incorporating Inhibitor IV and 1000ppm Cl plus (0, 500 and 2000) ppm $SO_4$

Table 4.10: Potentio-Dynamic Polarization Results of Steel Specimens Immersed in SCPS Incorporating Inhibitor IV at 40 ºC

| Chloride + Sulfate Concentration (ppm) | $E_{corr}$ (mV) | $R_p$ (Ohm.cm$^2$) | $I_{corr}$ ($\mu A/cm^2$) | Corrosion rate (mm/year) | Inhibitor Efficiency in Reducing $I_{corr}$ % |
|---|---|---|---|---|---|
| 1000 + 0 | -376.46 | 106247.12 | 0.246 | 0.0029 | 77.55 |
| 1000 + 500 | -482.8 | 36873.76 | 0.707 | 0.0082 | 37.49 |
| 1000 + 2000 | -523.22 | 23335.18 | 1.118 | 0.0130 | 27.79 |

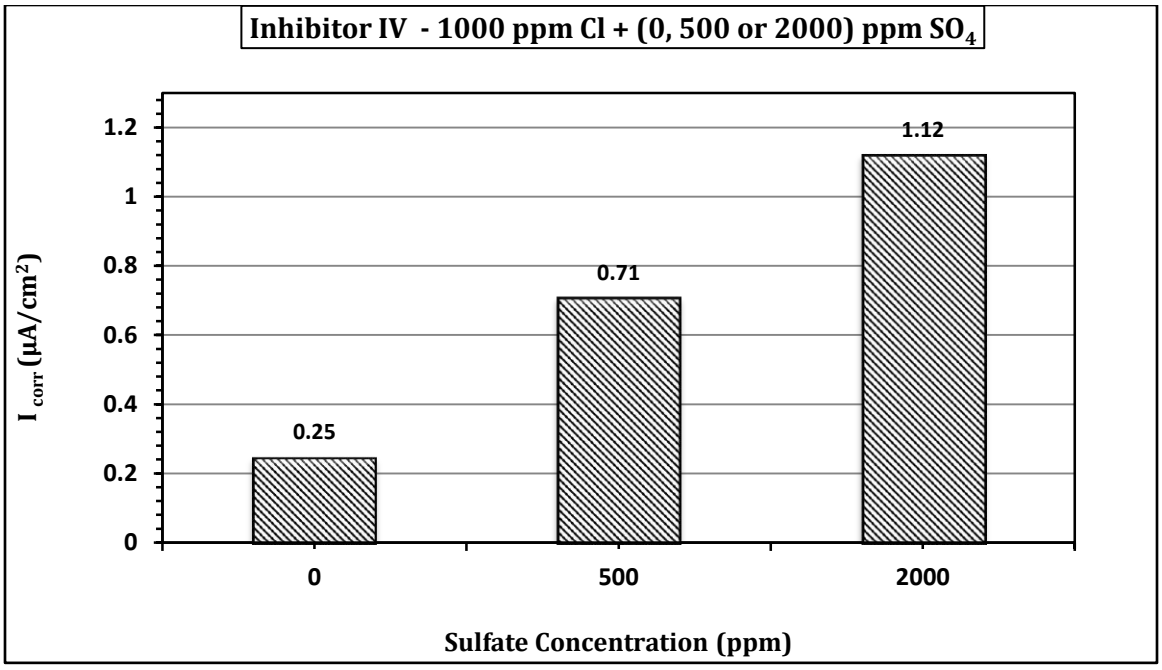


Figure 4.42: Combined Effect of Chloride, Sulfate and Temperature on Corrosion Current Density (40 °C)

### 4.5.3 Scanning Electron Microscopy of Steel Specimens Immersed in SCPS Incorporating Inhibitor IV

The scanning electron micrographs of the mild steel specimen exposed to SCPS incorporating Inhibitor IV and contaminated with sulfate and/or chloride ions are shown in Figures 4.43 through 4.45. There was general corrosion in all the specimens. The SEM in Figure 4.43 (Cl: 1,500; temperature: 25 ºC) exhibits general corrosion and a good protective adsorbed film was formed on the surface of the specimen, which decreased the corrosion current density and corrosion rate of steel in the alkaline environment. The micrograph also shows that the steel surface was better in the presence of Inhibitor IV compared to the surface of the control specimen (Figure 4.7) which was rough and covered with the corrosion product.

Figure 4.44 shows the SEM of the surface of mild steel specimen immersed in SCPS incorporating Inhibitor IV and contaminated with 1500 ppm Cl and at a temperature of 55 ºC. General corrosion was noted in this specimen also. However, there was slight damage on steel specimen surface. This might be due to the effect of chloride and elevated exposure temperature.

Figure 4.45 is a SEM micrograph of the steel immersed in SCPS incorporating Inhibitor IV and contaminated with 1000 ppm Cl and 2000 ppm sulfate at an exposure temperature of 40 ºC. General corrosion and a good protective adsorbed film is noted on the surface of the specimen. The SEM in Figures 4.43 through 4.45 indicates that Inhibitor IV can minimize corrosion of steel bars.

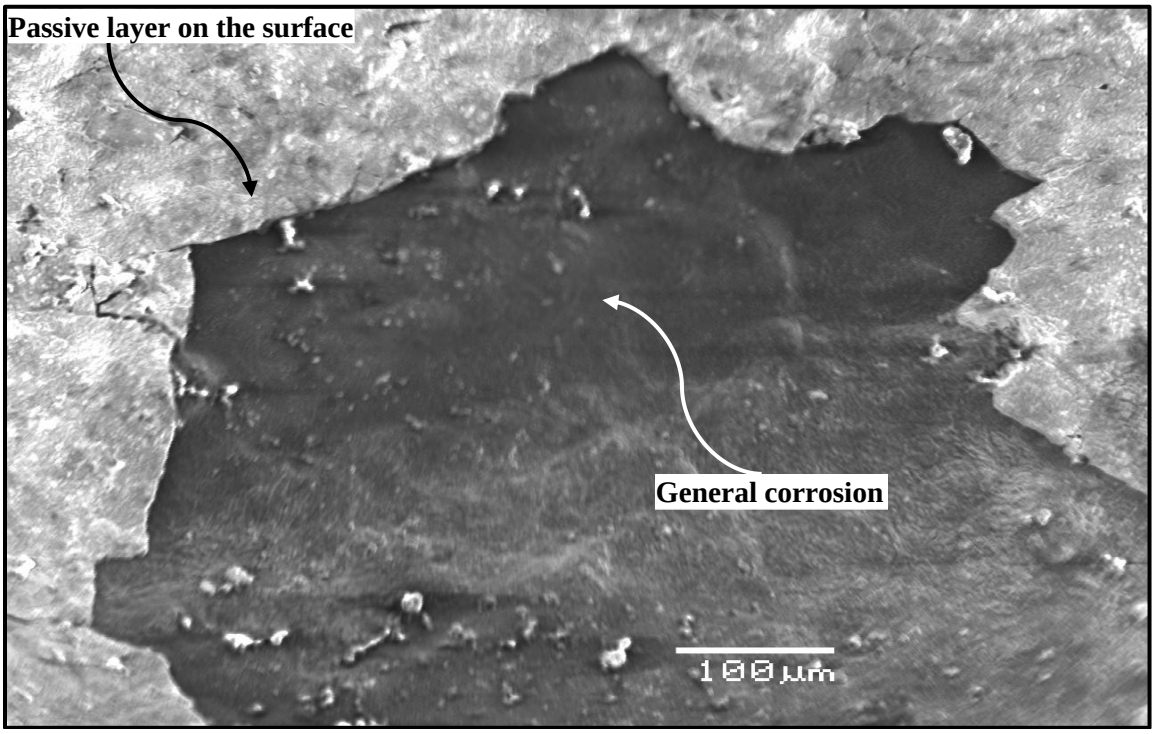


Figure 4.43: SEM (180X) for Steel Specimen in SCPS Incorporating Inhibitor IV and Contaminated with 1500 ppm Cl at 25 ºC.

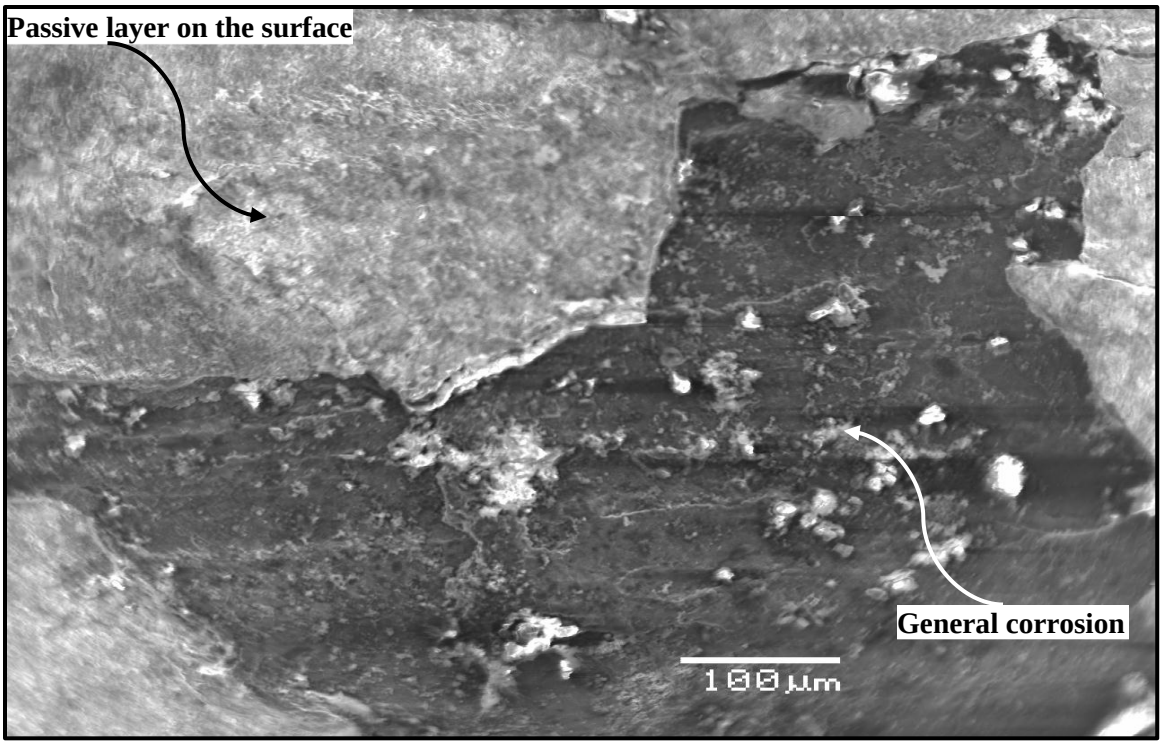


Figure 4.44: SEM (180X) for Steel Specimen in SCPS Incorporating Inhibitor IV and Contaminated with 1500 ppm Cl at 55 ºC.

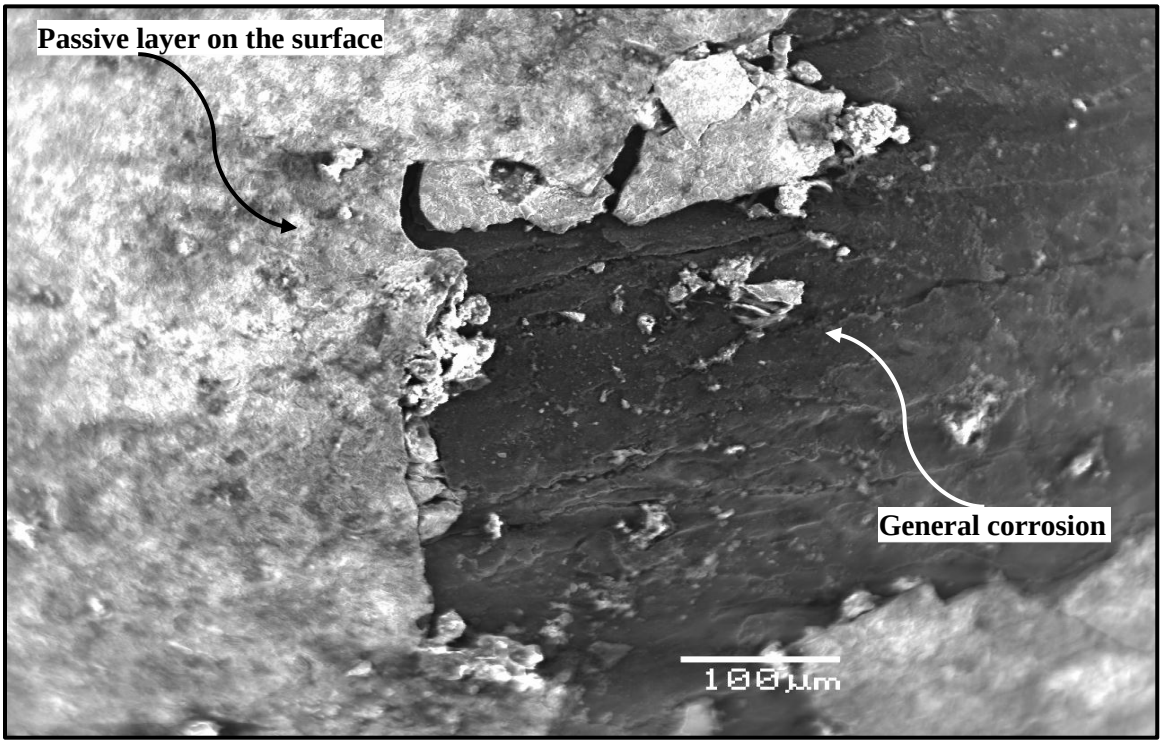


Figure 4.45: SEM (180X) for Steel Specimen in SCPS Incorporating Inhibitor IV and Contaminated with 1000 ppm Cl + 2000 ppm Sulfate at 40 ºC

## 4.6 Performance of Steel Specimens in Presence of Inhibitor V

Although many studied carried out on the performance of Inhibitor V as a corrosion inhibitor in reducing the general corrosion at 25 ºC, no previous studies were conducted on the performance of Inhibitor V at high temperature. Hence, the performance of Inhibitor V for different alkaline environments and temperature was evaluated. The results of these tests are summarized and discussed in the following sub-sections.

### 4.6.1 Effect of Chloride and Temperature on Corrosion Mechanism

The PDP curves for mild steel specimens placed in SCPS incorporating Inhibitor V are depicted in Figures 4.46 through 4.48. These curves are for the specimens immersed in SCPS contaminated with 1000, 1500 and 2000 ppm chloride and temperatures of 25, 40 and 5 5ºC.

The PDP curves for steel specimens exposed to chloride concentration of 1000 at 25, 40 and 55º C exhibits general corrosion (Figure 4.46). The current required for transition from cathodic to anodic polarization did not vary with the temperature about 0.0518 μA. As expected, the rate of corrosion increased with an increase in the temperature.

Figure 4.47 shows the PDP curves for steel specimens exposed to chloride concentration of 1500 ppm at different temperatures. The data therein exhibit general corrosion. The polarizing potential in this group of specimen is also around -420 mV and the polarization curve is also similar as in the other group of specimens (1000 ppm $Cl^-$).

The PDP drifted towards anodic region with increasing the temperature of the pore solution. While there was no significant difference in the anodic behavior of steel

specimen exposed to 25 or 40º C, the PDP for 55 ºC tends to be more than the other two curves. Figure 4.48 shows the PDPs for steel specimens placed in SCPS with 2000 ppm chloride. General corrosion was noted in all the specimens and the polarizing potential is around -328 mV for the exposure temperatures of 25 ºC and decreased to around -433 mV when the exposure temperature was increased to 55 ºC. However, the transition curve varies from a round 0.0344 to 0.0254 μA with increasing the temperature from 25 to 55 °C. This is the result of conjoint effect of temperature and increased chloride concentration.

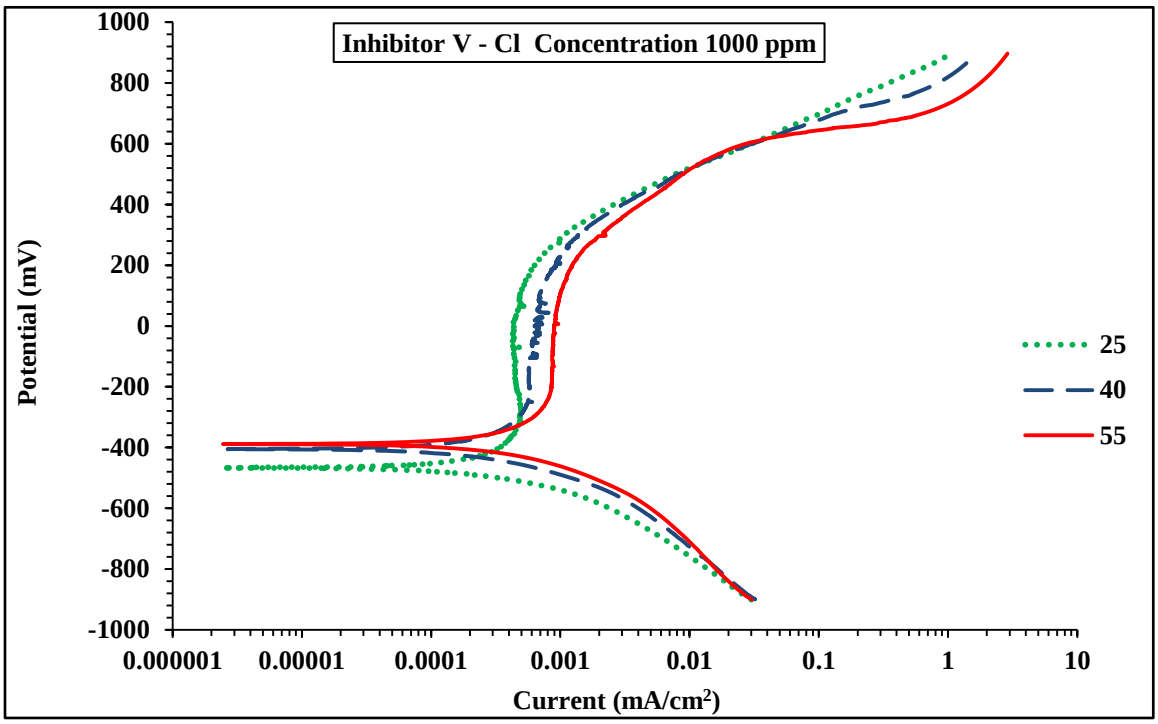


Figure 4.46: Potentio-Dynamic Polarization Curves for Mild Steel in SCPS Incorporated Inhibitor V and 1000 ppm of Cl

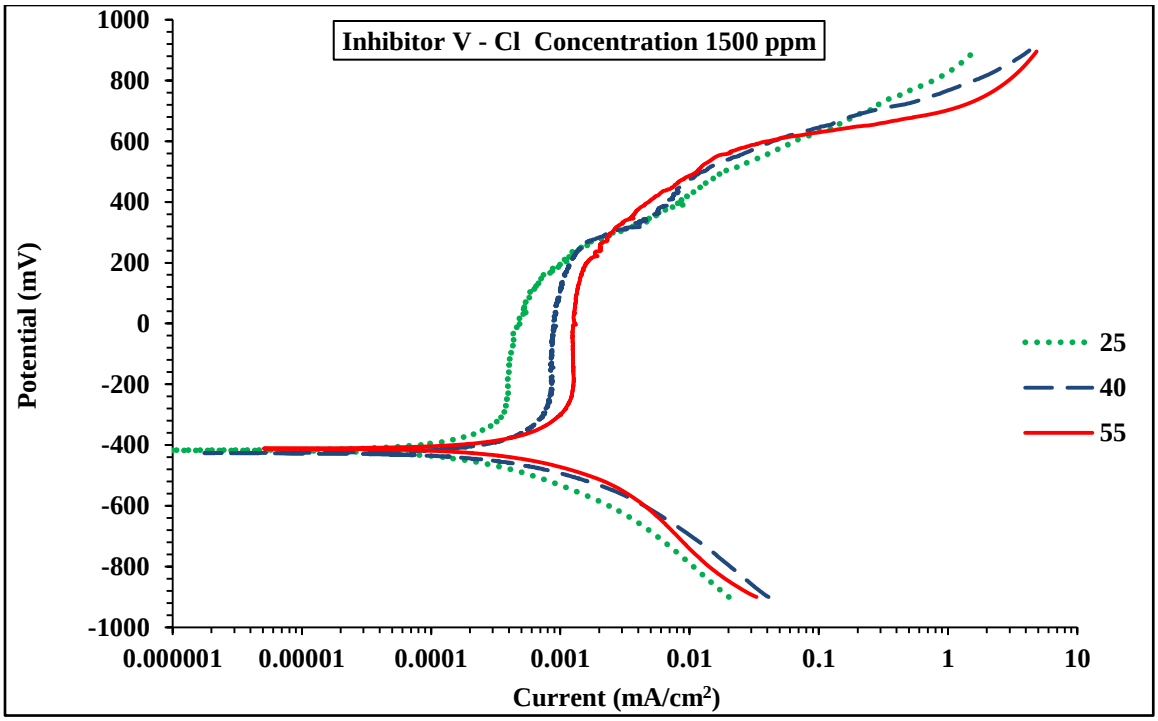


Figure 4.47: Potentio-Dynamic Polarization Curves for Mild Steel in SCPS Incorporated Inhibitor V and 1500 ppm of Cl

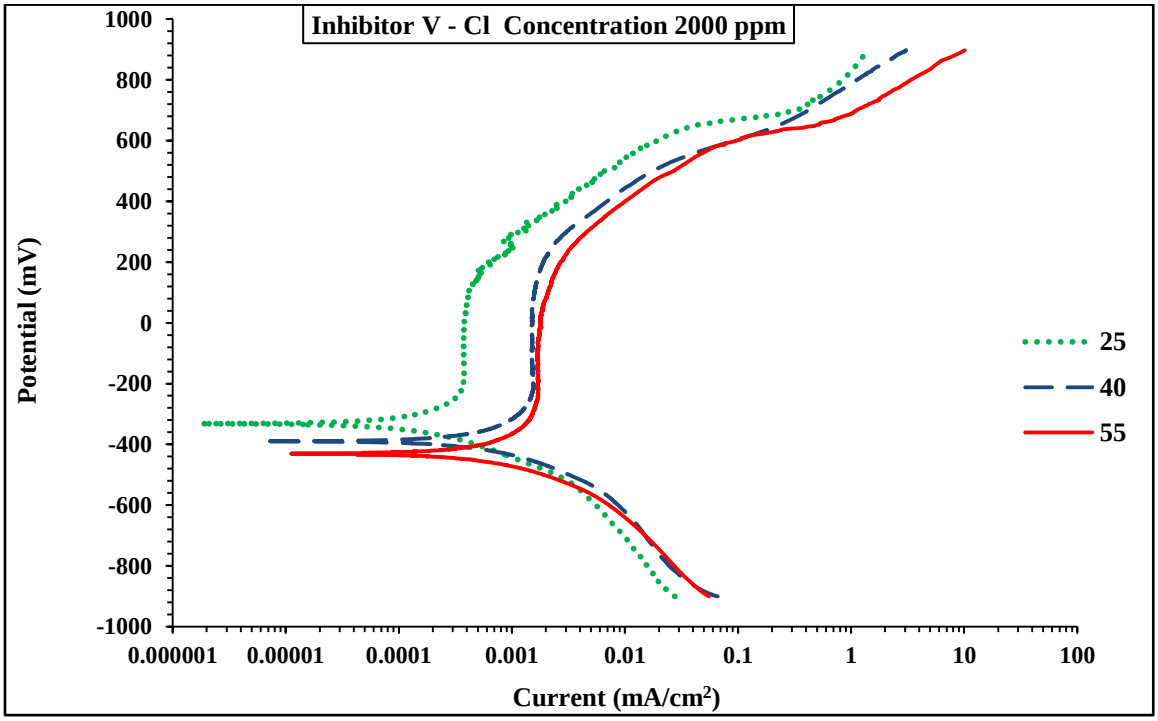


Figure 4.48: Potentio-Dynamic Polarization Curves for Mild Steel in SCPS Incorporated Inhibitor V and 2000 ppm of Cl

Figure 4.47 through 4.49 were utilized to determine the corrosion polarization parameters for specimens exposed SCPS incorporating Inhibitor V. These data are summarized in Table 4.11 and revealed that an increase in temperature increases the corrosion current density. This can be explained by the fact that an increase in temperature usually accelerates the corrosive processes

The effect of chloride content and temperature on $I_{corr}$ determined by PDP technique is plotted in Figure 4.49. The increase in $I_{corr}$ with chloride concentration and temperature is visible in these data.

Table 4.11: Potentio-Dynamic Polarization Results for Steel Specimens Immersed In SCPS Incorporating Inhibitor V

| Temperature (°C) | Chloride Concentration (ppm) | $E_{corr}$ (mV) | $R_p$ (Ohm.cm$^2$) | $I_{corr}$ (µA/cm$^2$) | Corrosion Rate (mm/year) | Inhibitor Efficiency in Reducing $I_{corr}$ % |
|---|---|---|---|---|---|---|
| 25 | 1000 | -467.73 | 198472.40 | 0.1314 | 0.0016 | 85.92 |
| | 1500 | -418.98 | 142452.20 | 0.1831 | 0.0021 | 83.21 |
| | 2000 | -328.48 | 113971.98 | 0.2289 | 0.0027 | 82.70 |
| 40 | 1000 | -404.94 | 166148.00 | 0.1570 | 0.0018 | 85.65 |
| | 1500 | -425.9 | 119439.68 | 0.2184 | 0.0025 | 84.43 |
| | 2000 | -387.74 | 47042.66 | 0.5545 | 0.0064 | 77.64 |
| 55 | 1000 | -387.69 | 38325.00 | 0.6807 | 0.0079 | 90.07 |
| | 1500 | -411.92 | 26480.02 | 0.9851 | 0.0114 | 86.89 |
| | 2000 | -433 | 14801.48 | 1.7623 | 0.0204 | 77.08 |

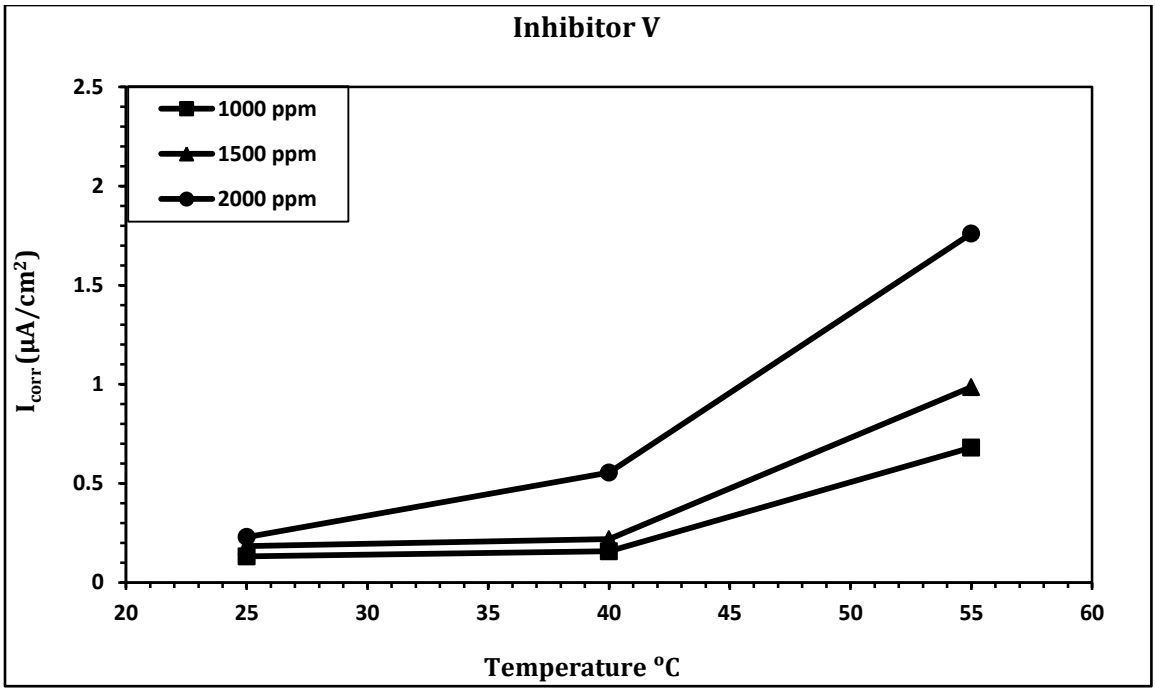


Figure 4.49: Effect of Chloride Concentration on Corrosion Current Density for Various Temperatures

### 4.6.2 Effect of Sulfate and/or Chloride and Temperature on Corrosion Mechanism

Figure 4.50 is a PDP for steel corrosion immersed in SCPS contaminated with 1000 Cl and various sulfate concentrations of 0, 500 or 2000 ppm at 40 ºC. The polarization potentials for 0, 500 and 2000 ppm $SO_4$ are -404.94, -446.76 and -540.53 mV, respectively. The PDP curves for all of the specimens are almost the same. Furthermore, corrosion current density and corrosion rate were increased around two times with increase sulfate concentration from 0 to 2000 ppm. This indicates that sulfate has effect on the mechanism of steel immersed in SCPS incorporating Inhibitor V. The polarization data are summarized in Table 4.12 which shows the increase in $I_{corr}$ from 0.157 to 0.329 μA/cm$^2$ for increase in $SO_4$ from 0 to 2000 ppm. The increase in $I_{corr}$ due to incorporation of $SO_4$ is depicted in Figure 4.51.

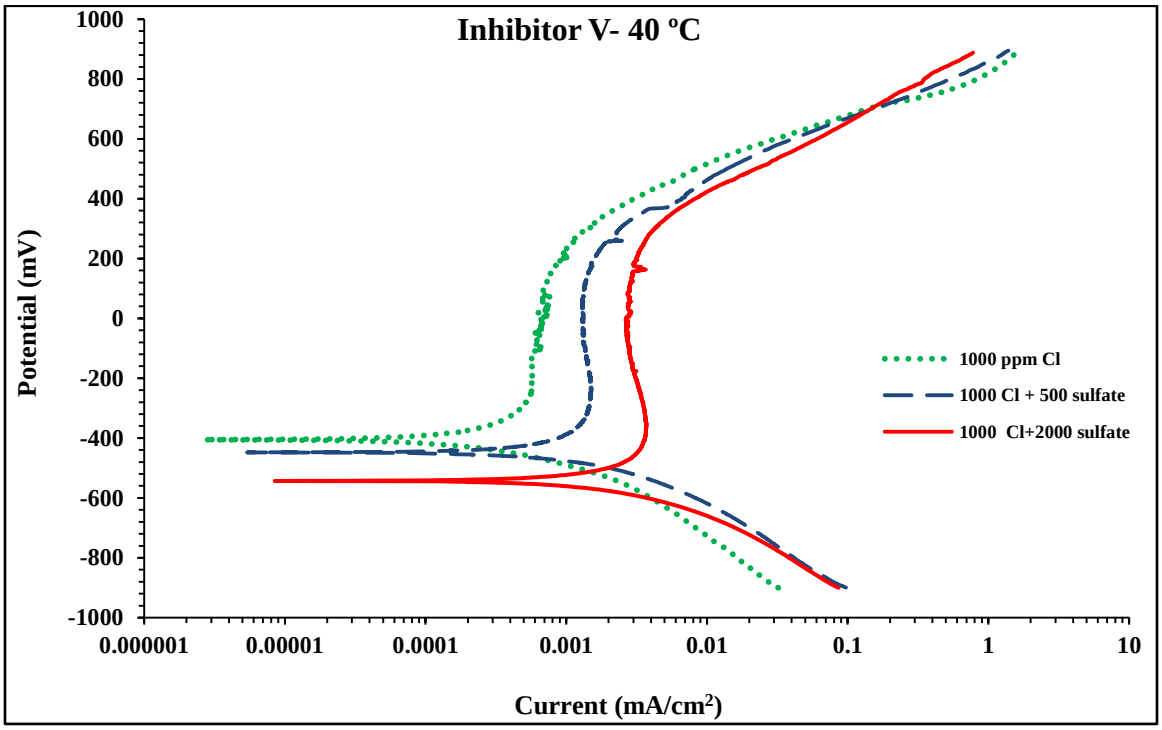


Figure 4.50: Potentio-Dynaimic Polarization Curves for Specimens Immersed in SCPS Incorporating Inhibitor V and 1000 ppm Cl plus (0, 500 and 2000) ppm $SO_4$

Table 4.12 : Potentio-Dynamic Polarization Results of Steel Specimens Immersed in SCPS Incorporating Inhibitor V at 40 ºC.

| Chloride + Sulfate Concentration (ppm) | $E_{corr}$ (mV) | $R_p$ (Ohm.cm$^2$) | $I_{corr}$ (µA/cm$^2$) | Corrosion rate (mm/year) | Inhibitor Efficiency in Reducing $I_{corr}$ % |
|---|---|---|---|---|---|
| 1000 + 0 | -404.94 | 166148.00 | 0.1570 | 0.0018 | 85.65 |
| 1000 + 500 | -446.76 | 118754.94 | 0.2197 | 0.0025 | 80.58 |
| 1000 + 2000 | -540.53 | 79305.74 | 0.3290 | 0.0038 | 78.75 |

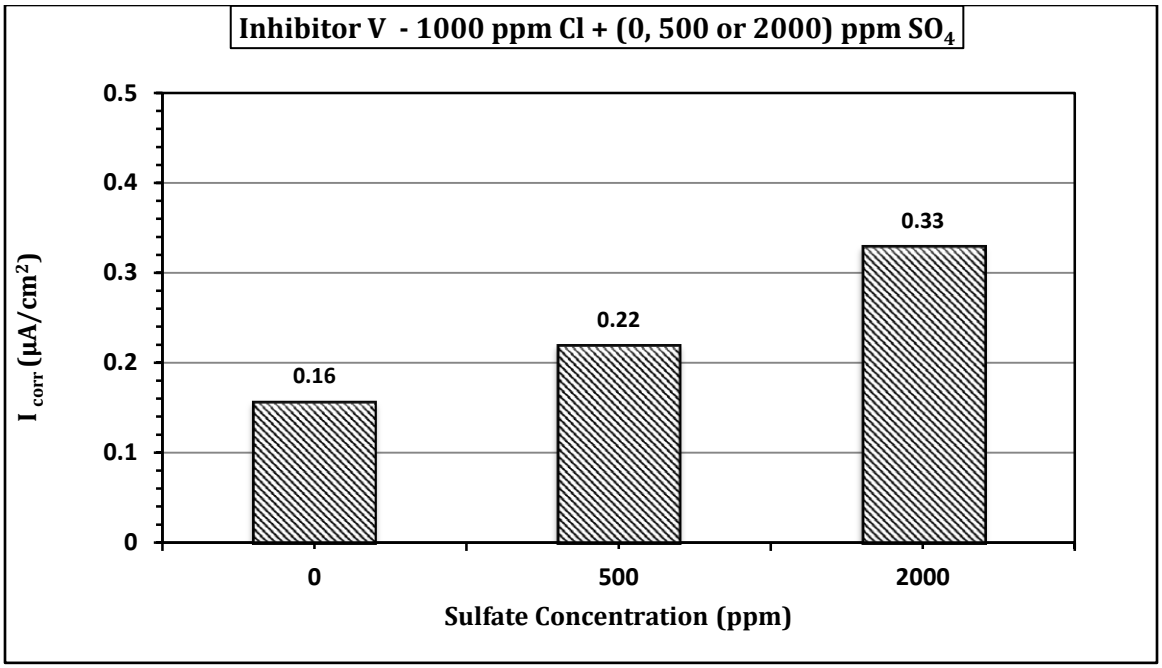


Figure 4.51: Combined Effect of Chloride, Sulfate and Temperature on Corrosion Current Density (40 °C)

### 4.6.3 Scanning Electron Microscopy of Steel Specimens Immersed in SCPS Incorporating Inhibitor V

The scanning electron micrographs of the mild steel specimen exposed to SCPS incorporating Inhibitor V and contaminated with sulfate and/or chloride ions are shown in Figures 4.52 through 4.54. There was general corrosion in all the specimens. The SEM in Figure 4.52 (Cl: 1,500; temperature: 25 ºC) exhibits general corrosion and a good protective adsorbed film was formed on the surface of the specimen, which decreased the corrosion current density and corrosion rate of steel in the alkaline environment. The micrograph also shows that the steel surface was better in the presence of Inhibitor V compared to the surface of control specimen (Figure 4.7) which was rough and covered with the corrosion product. Further, there was no corrosion product on the surface of steel

specimen comparing to the other groups of steel specimens immersed in SCPS incorporation one of the selected corrosion inhibitors.

Figure 4.53 shows the SEM of the mild steel specimen immersed in SCPS incorporating Inhibitor V and contaminated with 1500 ppm Cl and exposed to a temperature of 55 ºC. General corrosion was noted in this specimen also.

Figure 4.54 is a SEM of the steel immersed in SCPS incorporating Inhibitor V and contaminated with 1000 ppm Cl and 2000 ppm sulfate at an exposure temperature of 40 ºC. General corrosion and a good protective adsorbed film were noted on the surface of the specimen. The SEM in Figures 4.52 through 4.54 indicates that Inhibitor V can minimize corrosion of steel bars.

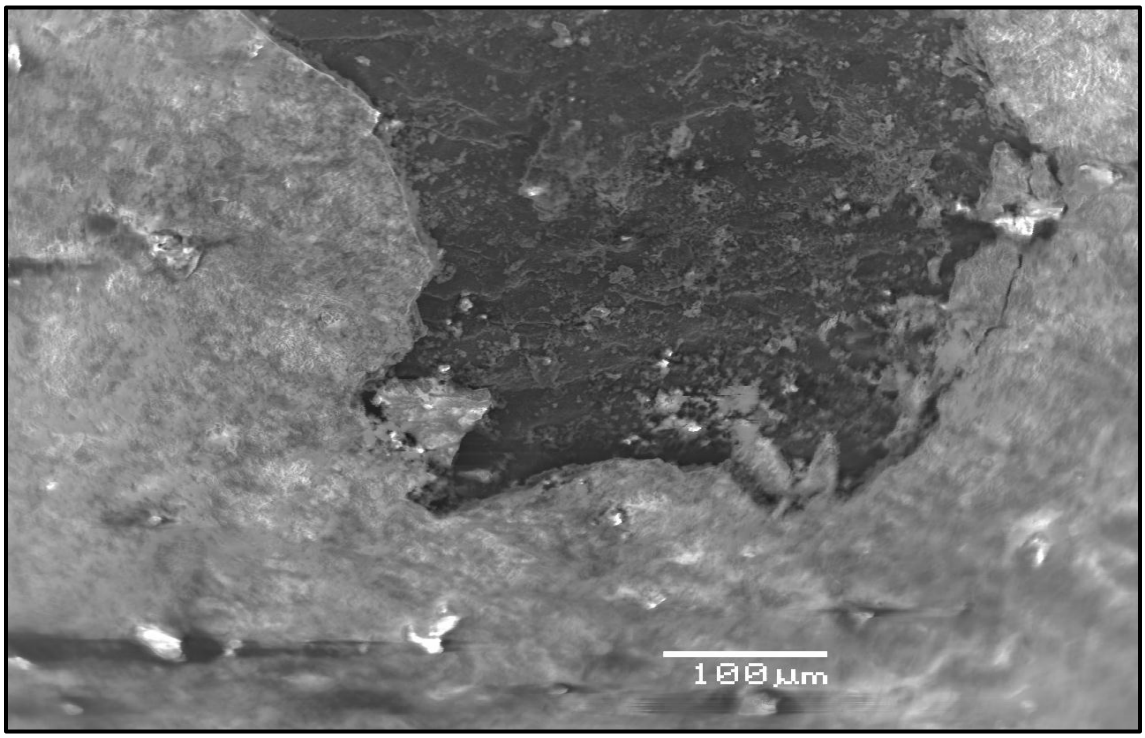


Figure 4.52: SEM (180X) for Steel Specimen in SCPS Incorporating Inhibitor V and Contaminated with 1500 ppm Cl at 25 ºC.

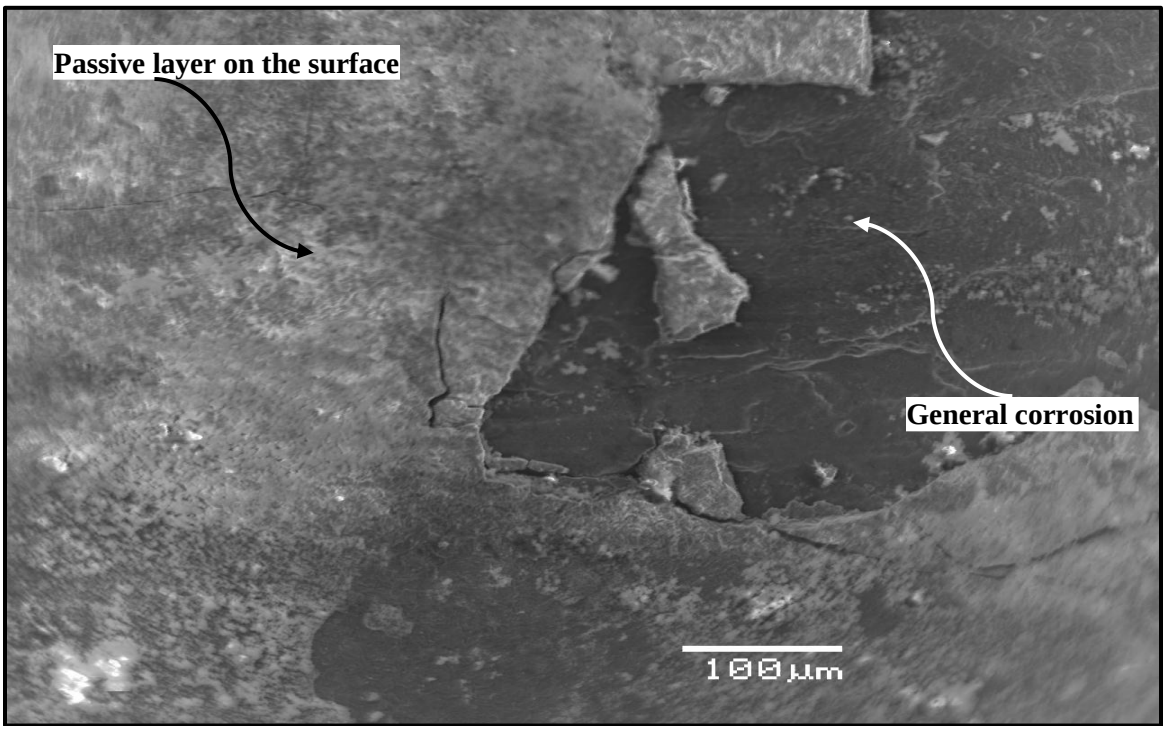


Figure 4.53: SEM (180X) for Steel Specimen in SCPS Incorporating Inhibitor V and Contaminated with 1500 ppm Cl at 55 ºC.

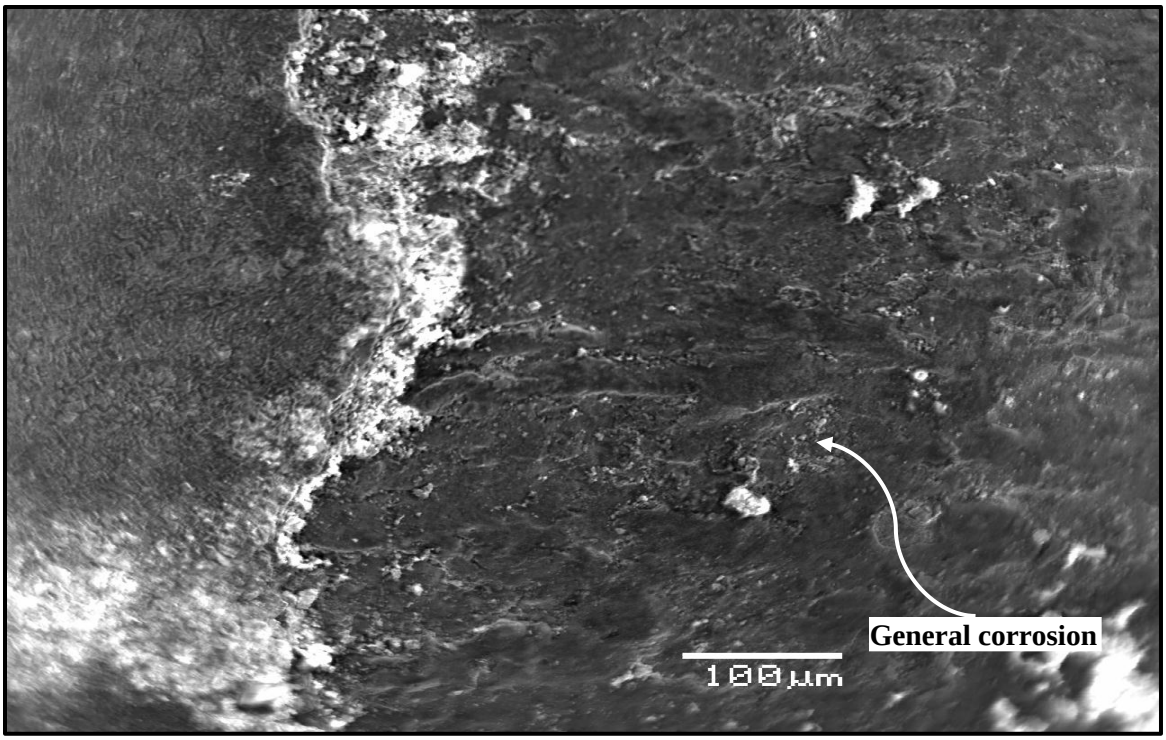


Figure 4.54: SEM (180X) for Steel Specimen in SCPS Incorporating Inhibitor V and Contaminated with 1000 ppm Cl + 2000 ppm Sulfate at 40 ºC.

## 4.7 Comparison of Corrosion Inhibiting Admixtures using PDP Technique

The performance evaluation of the selected corrosion inhibiting admixtures using potentio-dynamic polarization technique is compared in Figures 4.55 through Figure 4.73.

Figures 4.55 through 4.57 depict the PDP curves for mild steel specimens immersed in simulated concrete pore solution contaminated with 1000 ppm chloride and exposure to 25, 40 and 55 ºC, respectively. The PDP curves for steel specimens exposed to chloride concentration of 1000 at 25, 40 and 55 ºC exhibit general corrosion. The data in of polarization curves (Table 4.13) showed a reduction of the corrosion rate and corrosion current density due to the addition of corrosion inhibitors as compared with the control. The PDP drift was towards cathodic region due to addition of a corrosion inhibitor for the SCPS.

The data in Figures 4.55 through 4.57 are summarized in Table 4.13. An increase in temperature and chloride concentration tends to increase the corrosion current density. While there was a slight increase in $I_{corr}$ when the temperature was increased from 25 to 40 ºC, there was an increase in $I_{corr}$ of two to seven times when the temperature was increased from 40 to 55 ºC depending on the type of corrosion inhibitor (Table 4.13). The data in table 4.13 depicted that all inhibitors are effective in reducing $I_{corr}$ of steel specimens with 1000 ppm Cl and exposure temperature of 25°C by six to seven times. Further, Inhibitor I, Inhibitor II, Inhibitor III, Inhibitor V were effective in reducing $I_{corr}$ when exposure temperatures to 40 and 55 °C. However, when the exposure temperature

was increased from 40 to 55 °C Inhibitor IV was effective in reducing $I_{corr}$ of steel specimens by around three times.

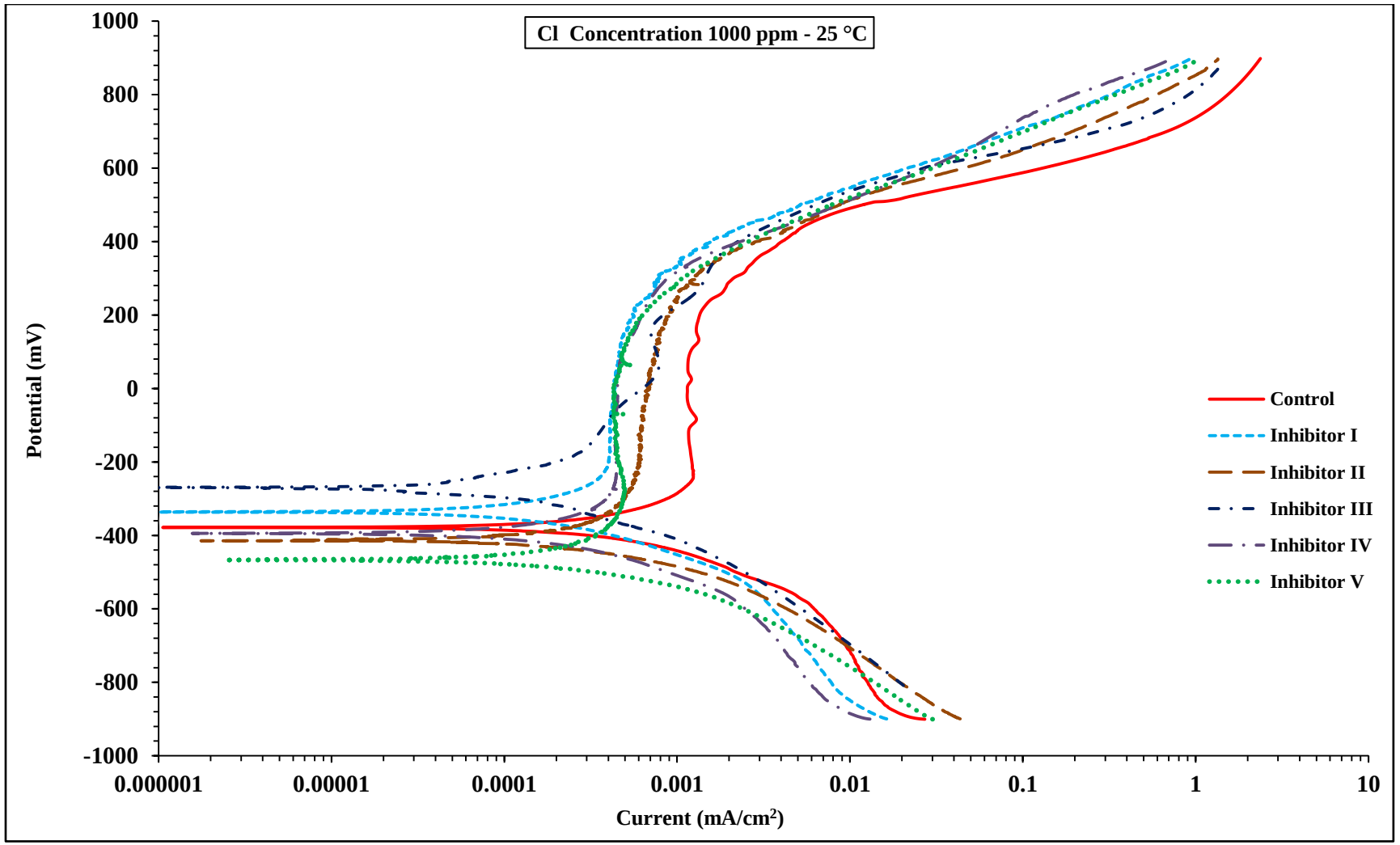


Figure 4.55: PDP Curves for Steel in SCPS with 1000 ppm Cl at 25 ºC

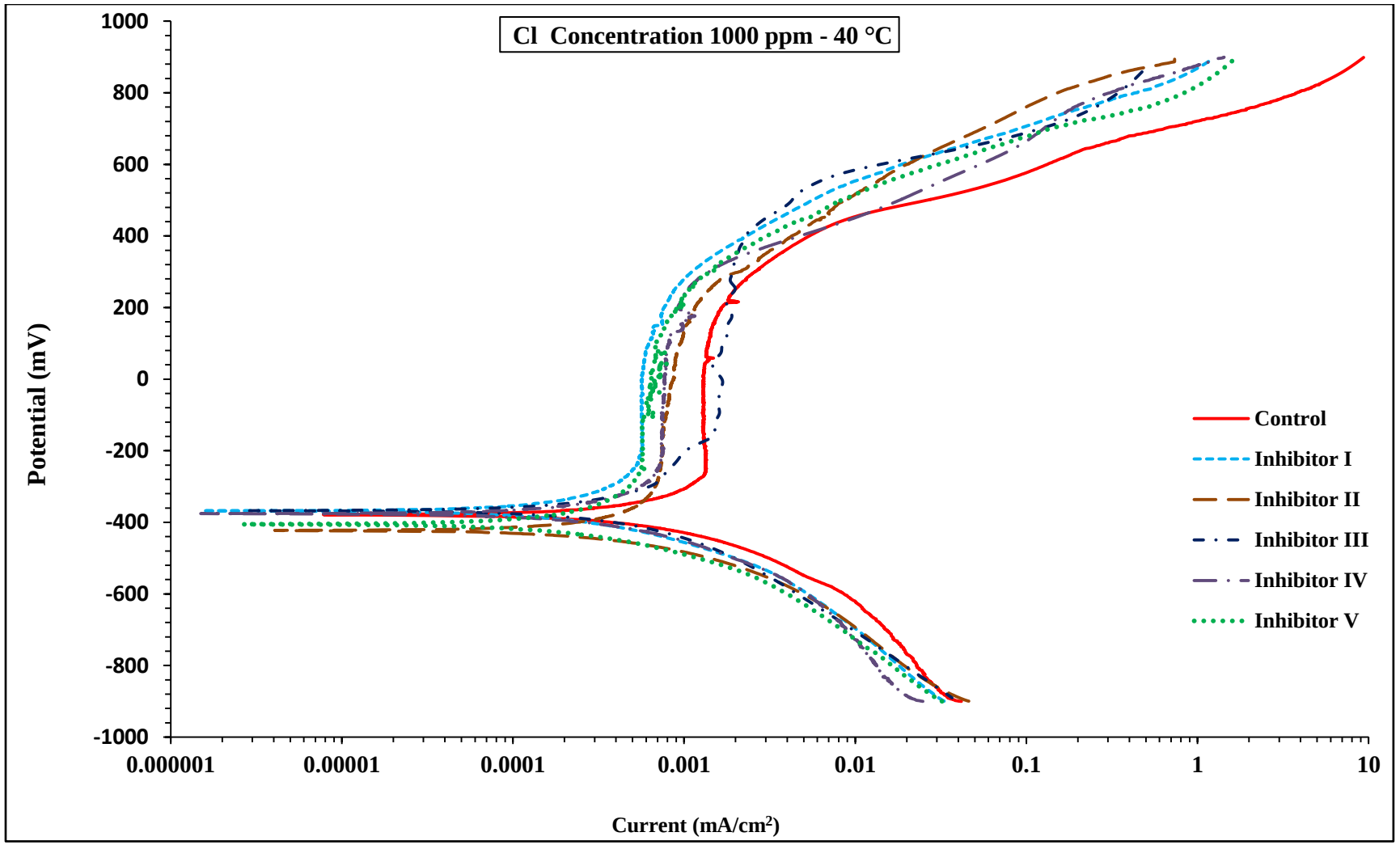


Figure 4.56: PDP Curves for Steel in SCPS with 1000 ppm Cl at 40 ºC

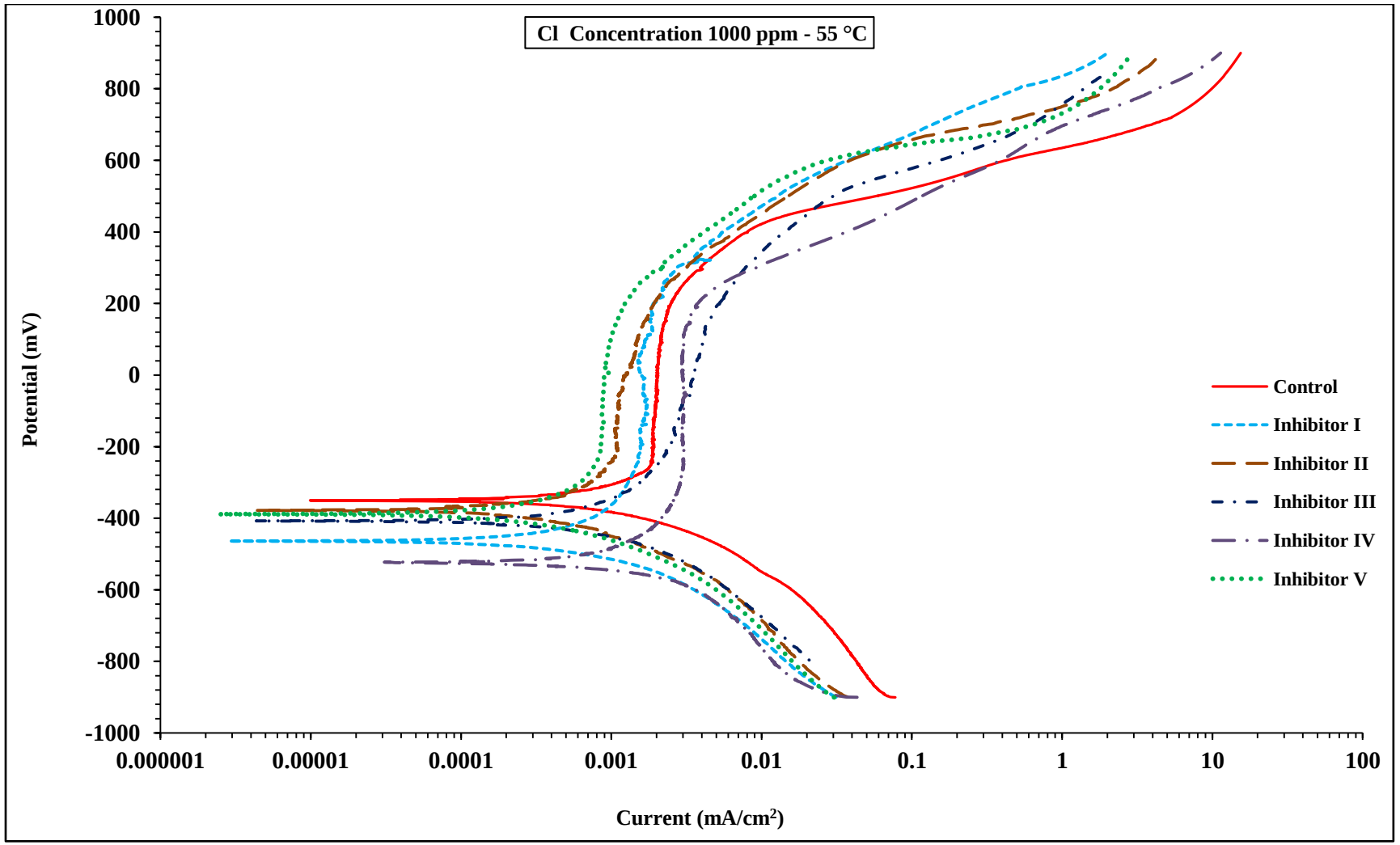


Figure 4.57: PDP Curves for Steel in SCPS with 1000 ppm Cl at 55 ºC

Table 4.13: Summary of PDP Results for Steel Specimens Immersed in SCPS Contaminated with 1000 ppm Cl Exposed to Various Temperatures

| Inhibitor | Temperature (°C) | $E_{corr}$ (mV) | $R_p$ Ohm.cm$^2$ | $I_{corr}$ (µA/cm$^2$) | Corrosion Rate (mm/year) |
|---|---|---|---|---|---|
| None (Control) | 25 | -377.17 | 27937.10 | 0.9336 | 0.0108 |
| | 40 | -377.12 | 23843.26 | 1.0938 | 0.0127 |
| | 55 | -346.03 | 3801.99 | 6.8562 | 0.0795 |
| Inhibitor I | 25 | -335.40 | 197625.60 | 0.1320 | 0.0015 |
| | 40 | -366.69 | 193552.20 | 0.1348 | 0.0016 |
| | 55 | -460.64 | 57969.30 | 0.4500 | 0.0052 |
| Inhibitor II | 25 | -412.05 | 179069.00 | 0.1457 | 0.0017 |
| | 40 | -419.12 | 155314.80 | 0.1680 | 0.0019 |
| | 55 | -373.80 | 47495.26 | 0.5492 | 0.0064 |
| Inhibitor III | 25 | -270.00 | 180748.00 | 0.1443 | 0.0017 |
| | 40 | -360.00 | 155271.00 | 0.1680 | 0.0019 |
| | 55 | -400.00 | 68579.12 | 0.3804 | 0.0044 |
| Inhibitor IV | 25 | -394.42 | 188004.20 | 0.1387 | 0.0016 |
| | 40 | -376.46 | 106247.12 | 0.2455 | 0.0028 |
| | 55 | -523.22 | 14490.79 | 1.8002 | 0.0209 |
| Inhibitor V | 25 | -467.73 | 198472.40 | 0.1314 | 0.0016 |
| | 40 | -404.94 | 166148.00 | 0.1570 | 0.0018 |
| | 55 | -387.69 | 38325.00 | 0.6807 | 0.0079 |

Figures 4.58 through 4.60 depict the PDP curves for steel specimens exposed to chloride concentration of 1500 ppm and temperature of 25, 40 and 55 ºC. These curves also exhibit general corrosion. There is a significant jump in some of the PDP curves at the exposure temperature of 55 ºC, which may be due to the acceleration of corrosion process at this temperature. The current required for transition from cathodic to anodic polarization varied depending on the type of inhibitor. The PDP drift in Figures 4.58 through 4.60 was towards the cathodic region with the addition of the selected corrosion inhibitor to the SCPS which indicates. This indicates that the selected inhibitors are effective in reducing anodic dissolution of steel specimens hence reducing corrosion rate and corrosion current density (Table 4.14).

The PDP curves in Figures 4.58 through 4.60 were utilized to determine the corrosion polarization parameters for the specimens exposed to SCPS in the presence or absence of inhibitor. These data are summarized in Table 4.14. The data in this table also revealed that an increase in the temperature and chloride concentration tends to increase the corrosion current density. The increase in $I_{corr}$ when the temperature was increased from 25 to 40 ºC was relatively marginal. However, the increase in $I_{corr}$ was significant around two to six times when the temperature was increased from 40 to 55 ºC.

The PDP curves for steel specimens exposed to chloride concentration of 2000 ppm and temperature of 25, 40 and 55 ºC (Figures 4.61 through 4.63) also exhibited general corrosion. However, the control specimen exposed to a temperature of 55 ºC showed pitting corrosion. The pitting potential was noted around 160 mV. Furthermore, the $I_{corr}$ and corrosion rate (Crate) values of 7.685 $\mu A/cm^2$ and 0.0891 mm/year, respectively, were high compared to the tested specimens with inhibitors. After the addition of the

corrosion inhibitors to the SCPS, it can be seen that the data of polarization curves in Table 4.15 showed reduction in the corrosion rate, corrosion current density and minimizing the pitting corrosion. The data in Table 4.15 revealed that an increase in the temperature and chloride concentration tends to increase the corrosion current density. Whereby the increase in $I_{corr}$ was around two times when the temperature was increased from 25 to 40 °C. However, the increase in $I_{corr}$ was significant (from two to five times), when the temperature was increased from 40 to 55 ºC.

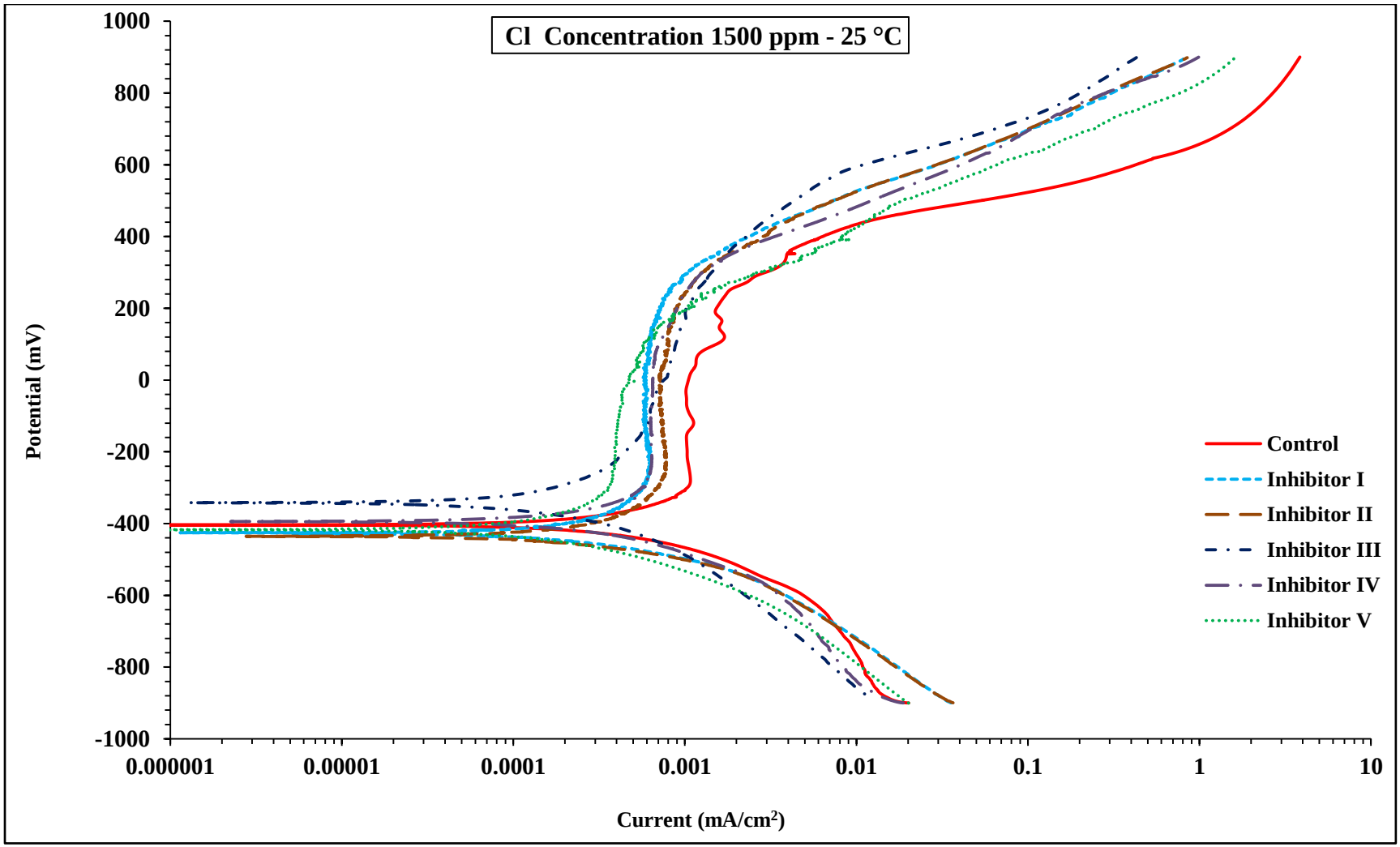


Figure 4.58: PDP Curves for Steel in SCPS with 1500 ppm Cl at 25 ºC

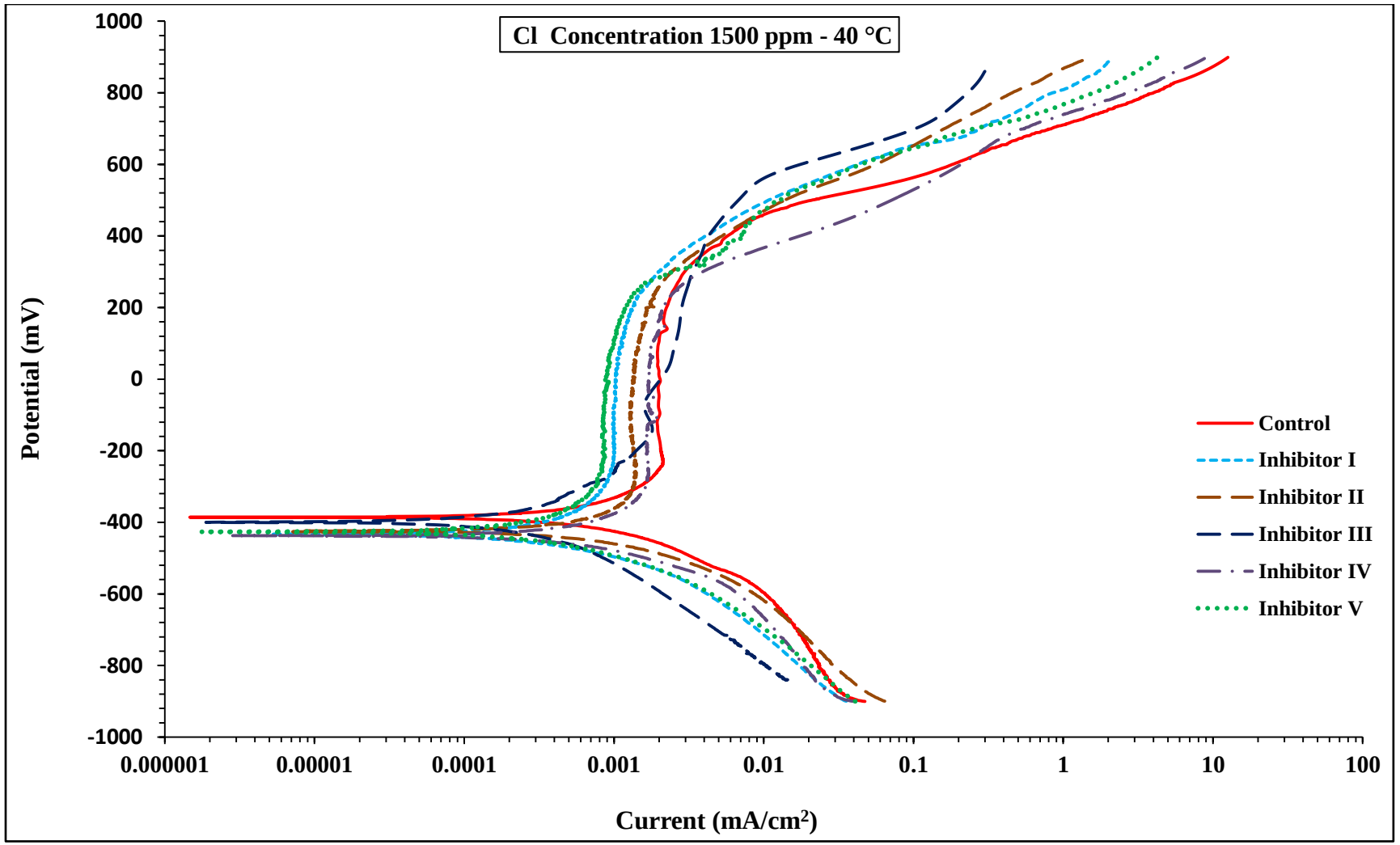


Figure 4.59: PDP Curves for Steel in SCPS with 1500 ppm Cl at 40 ºC

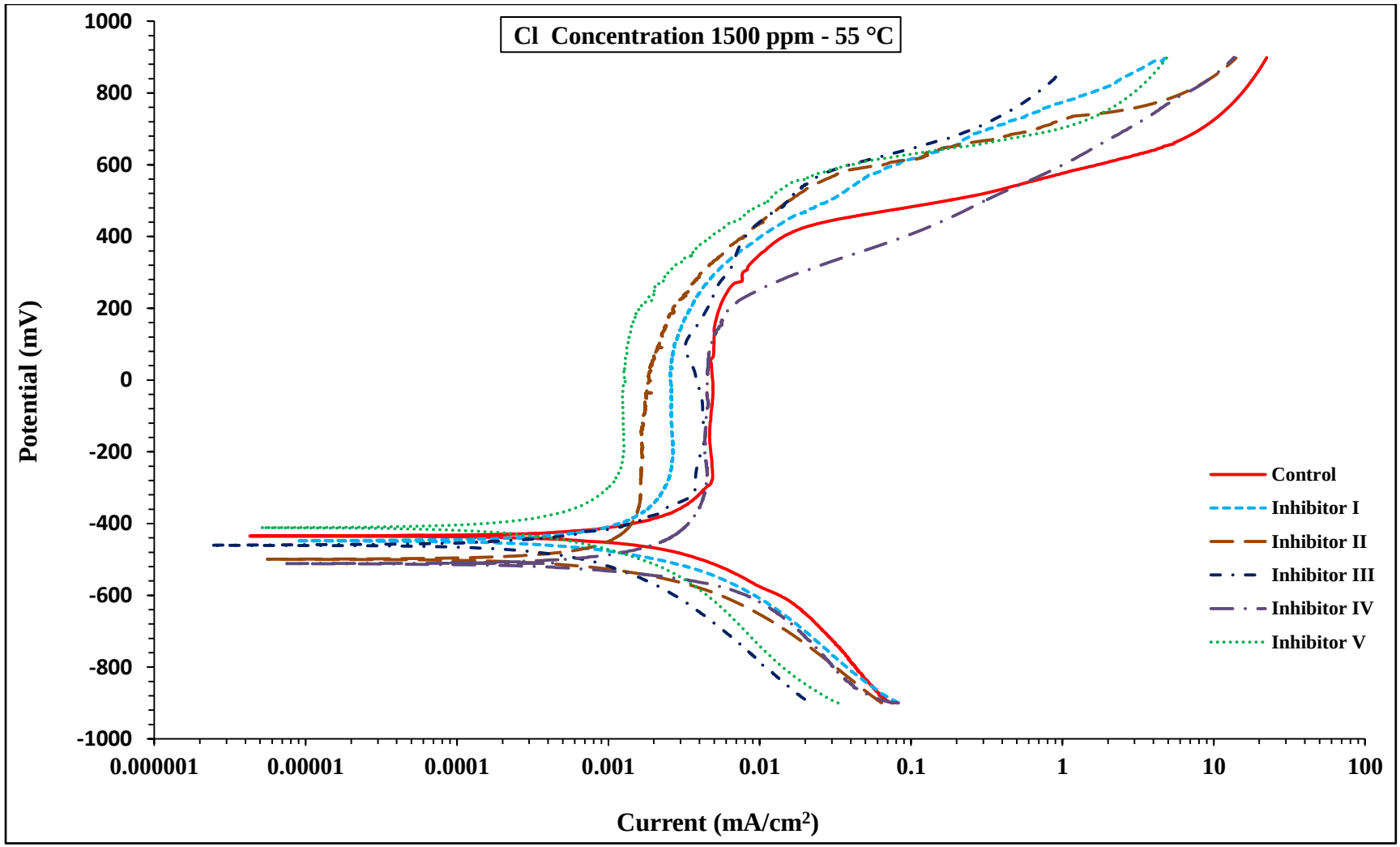


Figure 4.60: PDP Curves for Steel in SCPS with 1500 ppm Cl at 55 ºC

Table 4.14: Summary of PDP Results for Steel Specimens Immersed in SCPS Contaminated with 1500 ppm Cl Exposed to Various Temperatures

| Inhibitor | Temperature (°C) | $E_{corr}$ (mV) | $R_p$ Ohm.cm$^2$ | $I_{corr}$ (µA/cm$^2$) | Corrosion Rate (mm/year) |
|---|---|---|---|---|---|
| None (Control) | 25 | -404.83 | 23913.34 | 1.0904 | 0.0126 |
| | 40 | -384.30 | 18596.02 | 1.4027 | 0.0163 |
| | 55 | -432.79 | 3472.76 | 7.5119 | 0.0871 |
| Inhibitor I | 25 | -425.98 | 164994.60 | 0.1581 | 0.0018 |
| | 40 | -432.96 | 130272.88 | 0.2002 | 0.0023 |
| | 55 | -446.75 | 52247.56 | 0.4993 | 0.0058 |
| Inhibitor II | 25 | -432.30 | 108199.14 | 0.2411 | 0.0028 |
| | 40 | -429.61 | 86118.10 | 0.3029 | 0.0035 |
| | 55 | -502.70 | 40392.36 | 0.6458 | 0.0075 |
| Inhibitor III | 25 | -340.00 | 118792.90 | 0.2196 | 0.0025 |
| | 40 | -401.00 | 97430.18 | 0.2678 | 0.0031 |
| | 55 | -450.00 | 20847.34 | 1.2513 | 0.0145 |
| Inhibitor IV | 25 | -394.52 | 116957.68 | 0.2230 | 0.0026 |
| | 40 | -450.27 | 81865.12 | 0.3187 | 0.0037 |
| | 55 | -512.87 | 12511.32 | 2.0849 | 0.0242 |
| Inhibitor V | 25 | -418.98 | 142452.20 | 0.1831 | 0.0021 |
| | 40 | -425.90 | 119439.68 | 0.2184 | 0.0025 |
| | 55 | -411.92 | 26480.02 | 0.9851 | 0.0114 |

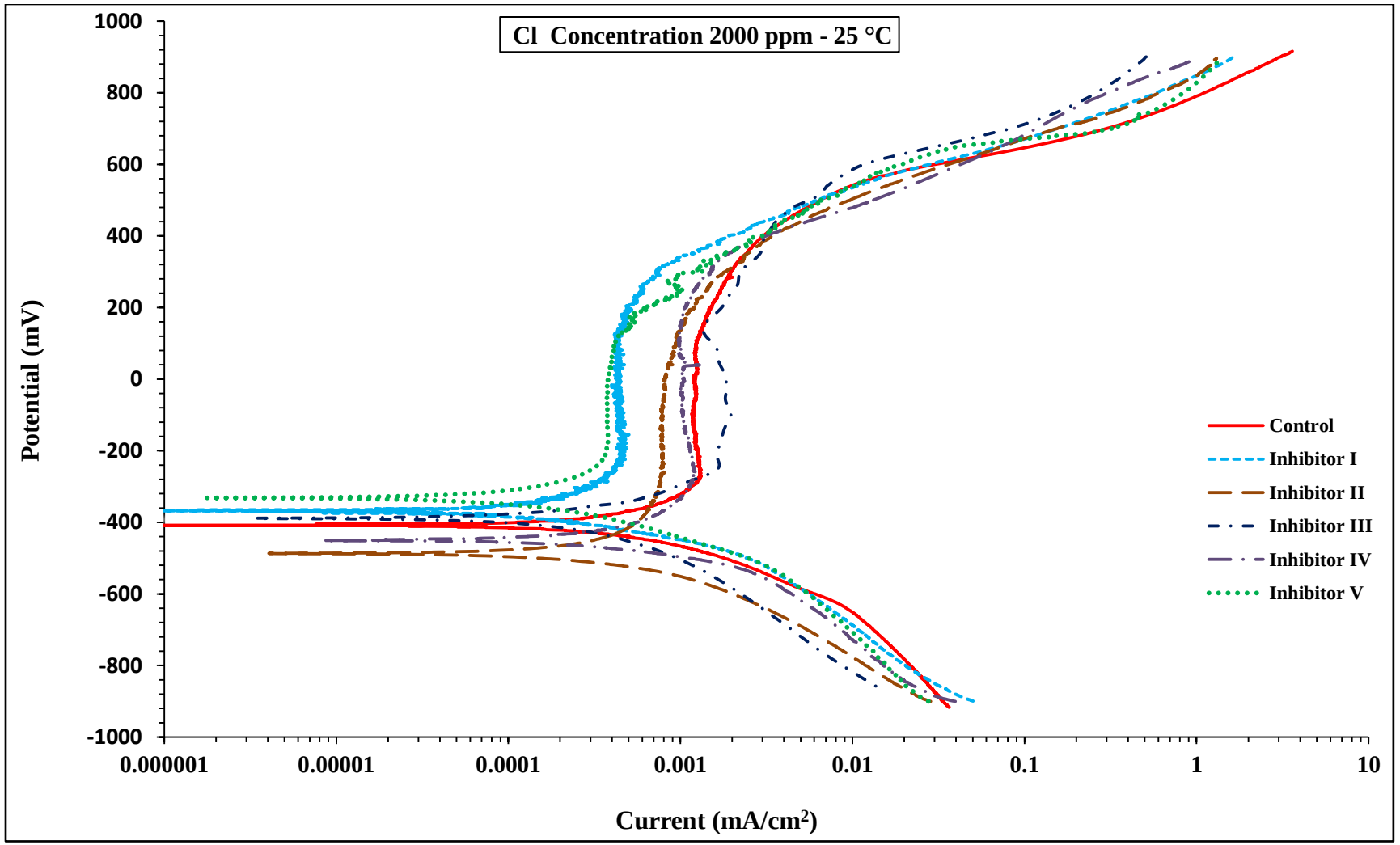


Figure 4.61: PDP Curves for Steel in SCPS with 2000 ppm Cl at 25 ºC

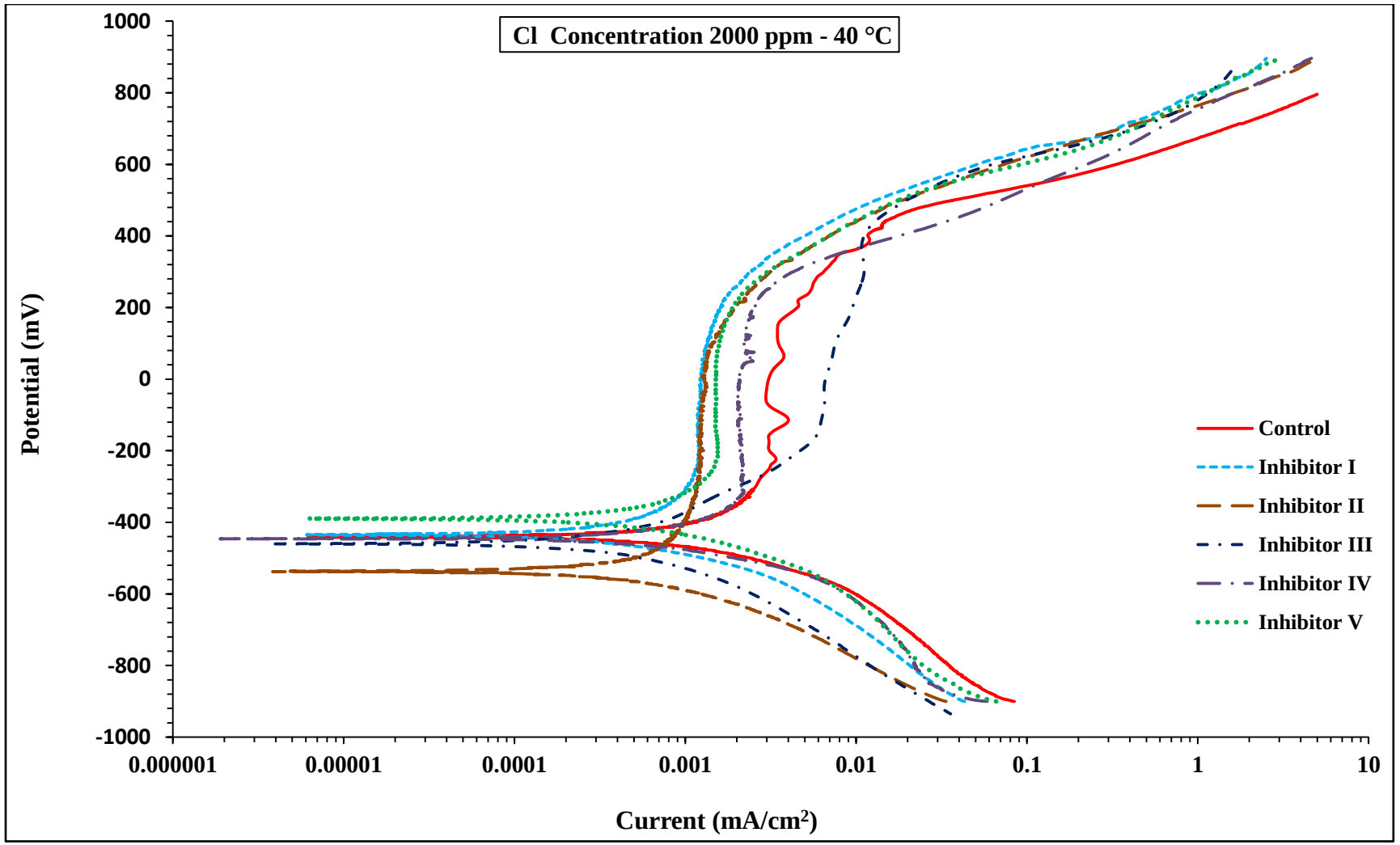


Figure 4.62: PDP Curves for Steel in SCPS with 2000 ppm Cl at 40 ºC

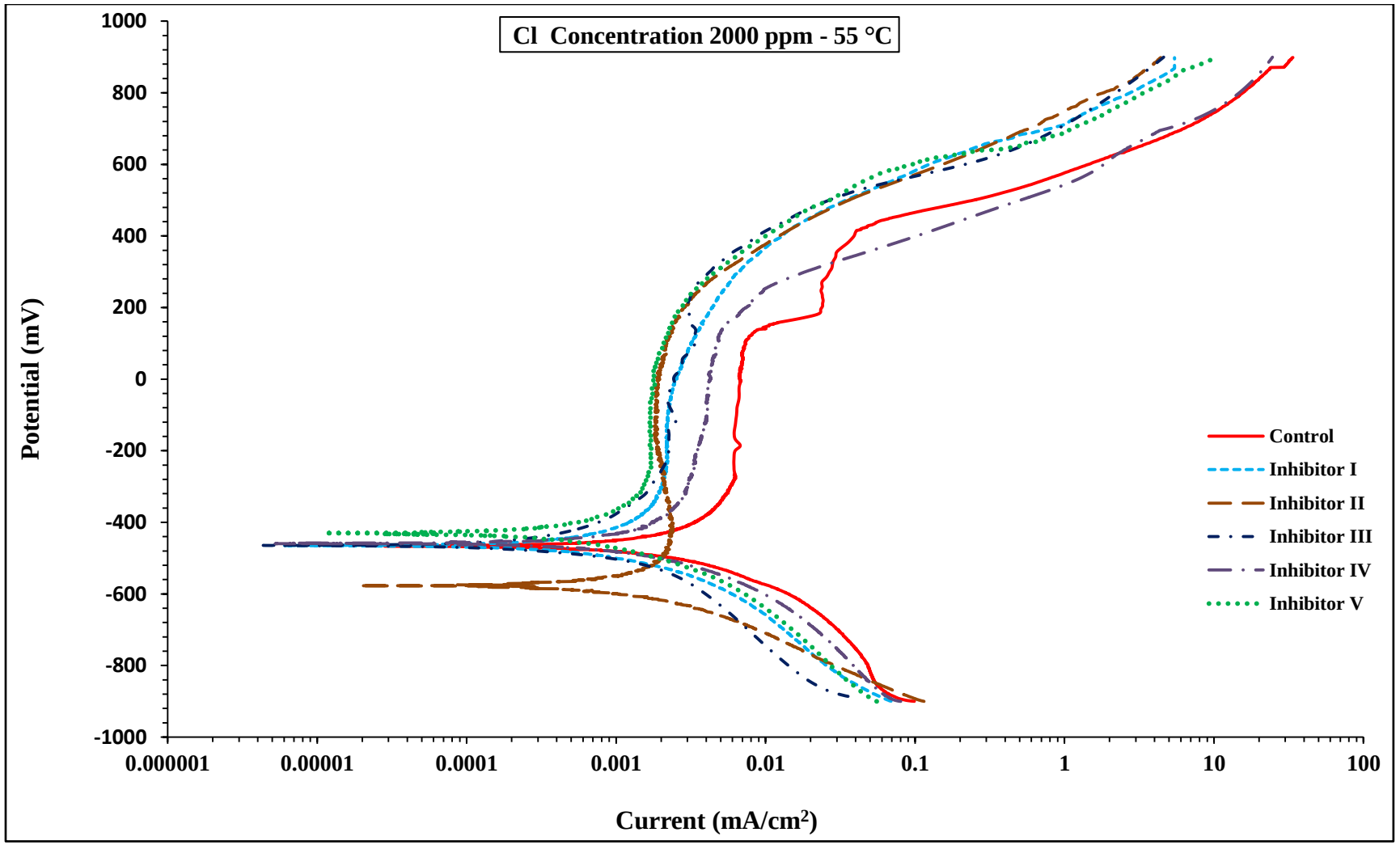


Figure 4.63: PDP Curves for Steel in SCPS with 2000 ppm Cl at 55 ºC

Table 4.15: Summary of PDP Results for Steel Specimens Immersed in SCPS Contaminated with 2000 ppm Cl Exposed to Various Temperatures

| Inhibitor | Temperature (°C) | $E_{corr}$ (mV) | $R_p$ Ohm.cm$^2$ | $I_{corr}$ (µA/cm$^2$) | Corrosion Rate (mm/year) |
|---|---|---|---|---|---|
| None | 25 | -405.36 | 19704.16 | 1.3233 | 0.0153 |
| | 40 | -439.89 | 10517.26 | 2.4801 | 0.0287 |
| | 55 | -436.38 | 3392.46 | 7.6849 | 0.0891 |
| Inhibitor I | 25 | -366.75 | 105633.92 | 0.2470 | 0.0029 |
| | 40 | -429.53 | 56386.66 | 0.4626 | 0.0054 |
| | 55 | -464.03 | 19728.98 | 1.3219 | 0.0153 |
| Inhibitor II | 25 | -485.13 | 84998.28 | 0.3069 | 0.0036 |
| | 40 | -537.27 | 47261.66 | 0.5520 | 0.0064 |
| | 55 | -579.40 | 25352.90 | 1.0289 | 0.0119 |
| Inhibitor III | 25 | -390.00 | 68579.12 | 0.3804 | 0.0044 |
| | 40 | -471.00 | 53856.48 | 0.4844 | 0.0056 |
| | 55 | -479.00 | 14836.52 | 1.7583 | 0.0204 |
| Inhibitor IV | 25 | -446.82 | 89585.60 | 0.2912 | 0.0034 |
| | 40 | -446.88 | 29305.12 | 0.8902 | 0.0103 |
| | 55 | -457.26 | 6226.32 | 4.1897 | 0.0486 |
| Inhibitor V | 25 | -328.48 | 113971.98 | 0.2289 | 0.0027 |
| | 40 | -387.74 | 47042.66 | 0.5545 | 0.0064 |
| | 55 | -433.00 | 14801.48 | 1.7623 | 0.0204 |

Figures 4.64 through Figure 4.66 show the efficiency of corrosion inhibitors in reducing the corrosion current density with respect to control reinforcing steel at various temperatures and chloride concentrations. These figures show that the efficiency is very high (between 84.40 to 85.92%) of the selected corrosion inhibitors of steel specimens immersed in SCPS incorporating corrosion inhibitors and contaminated with chloride concentrations of 1000 and exposure temperature of 25 °C (Figure 4.64). However, the efficiency of these inhibitors decreased to (between 71.26 to 82.70%) with an increase in the chloride concentration from 1000 to 2000 ppm for the same exposure temperatures.

Figure 4.65 shows a slight variation (77 to 87%) in the efficiency of the selected corrosion inhibitors in reducing corrosion current density of steel specimens immersed in SCPS incorporating corrosion inhibitors and contaminated with chloride concentrations of 1000 and 1500 and exposure temperature of 40 °C. However, the efficiency of these inhibitors indicates high variation (64 to 81%) with an increase in the chloride concentration from 1500 to 2000 ppm for the same exposure temperatures.

Figure 4.66 shows a minor variation in the efficiency of the selected corrosion inhibitors in reducing corrosion current density of steel specimens immersed in SCPS incorporating corrosion inhibitors and contaminated with chloride concentrations of 1000, 1500 and 2000 ppm and exposure temperature of 55 °C. However, the efficiency of Inhibitor IV sharply decreased from 73 to 45 % with increase chloride concentration from 1000 to 2000 ppm for the same exposure temperature. This indicates that the efficiency of Inhibitor IV was significantly affected at high exposure temperatures. That is might be Inhibitor IV was designed for aggressive environments with low exposure temperature.

It is clear that all the selected corrosion inhibitors were efficient in decreasing the corrosion current density for all the chloride exposures. However, the efficiency of Inhibitor IV in reducing corrosion current density was sharply reduced with an increase in the temperature.

Figure 4.67 displays the combined effect of chloride, sulfate and temperature on the efficiency of the selected corrosion inhibitors in decreasing the corrosion current density. The data in Figure 4.67 shows the variation in the efficiency of the selected corrosion inhibitors of steel specimens immersed in SCPS incorporating corrosion inhibitors and contaminated with 1000 ppm chloride and 500 or 2000 ppm sulfate at a temperature of 40 ºC. It is clear that Inhibitor V and Inhibitor I provided the highest corrosion efficiency (around 80 to 85 %) and Inhibitor IV provided the lowest corrosion efficiency (about 37 to 27%) in decreasing the corrosion current densities as compared with control steel specimens.

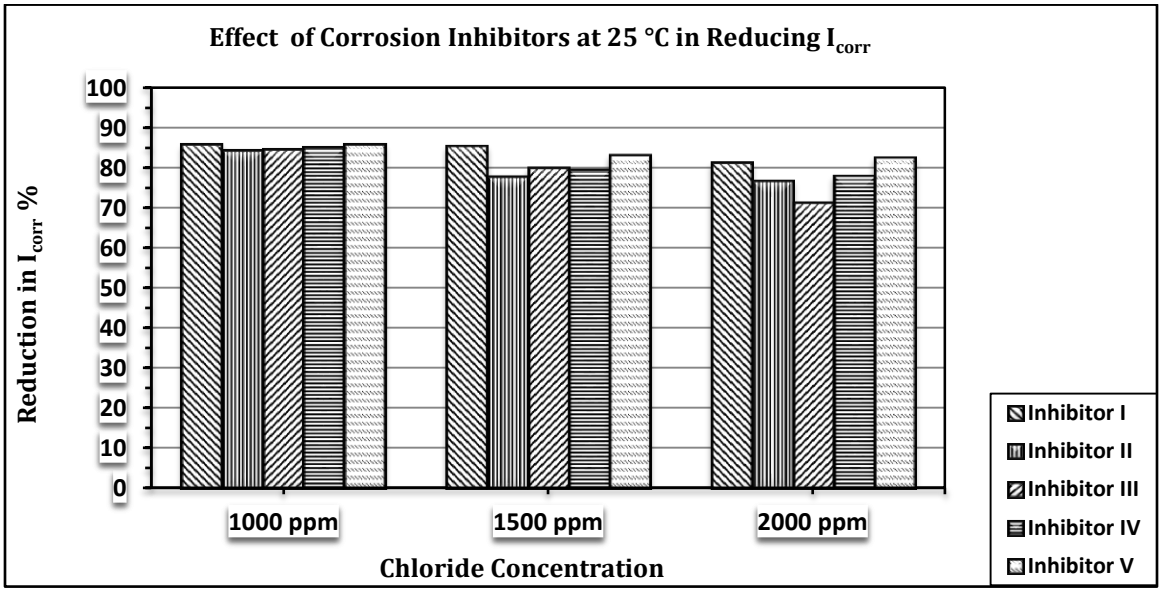


Figure 4.64: Effect of Corrosion Inhibitors in Reducing $I_{corr}$ at 25 ºC and Various Chloride Concentrations

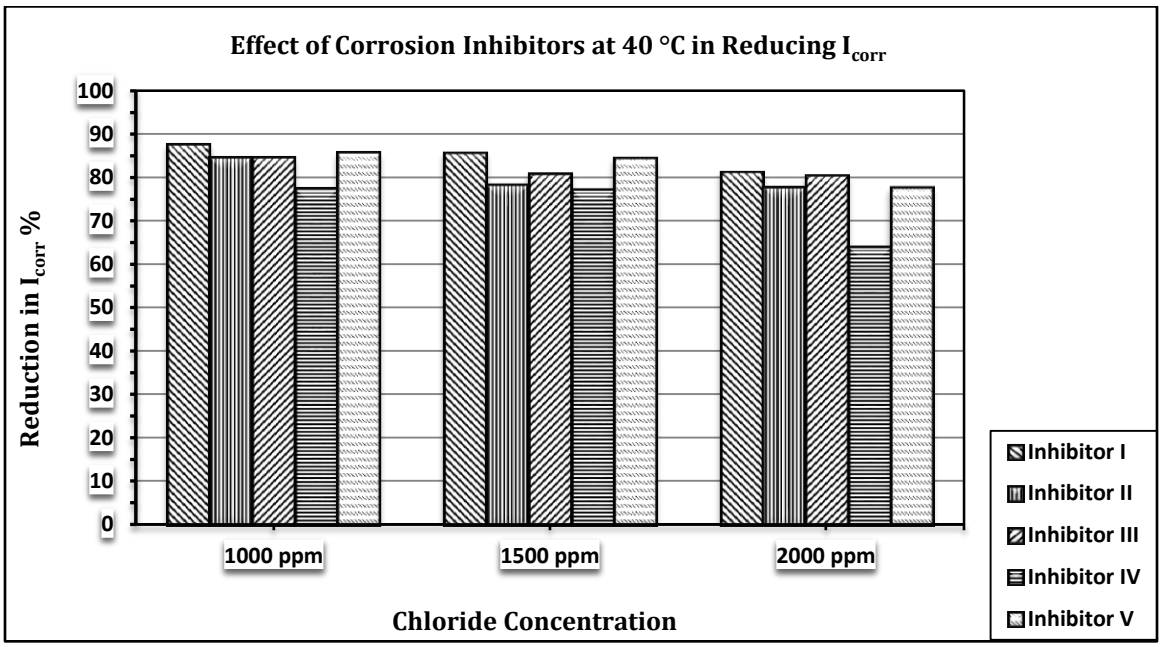


Figure 4.65: Effect of Corrosion Inhibitors in Reducing $I_{corr}$ at 40 ºC and Various Chloride Concentrations

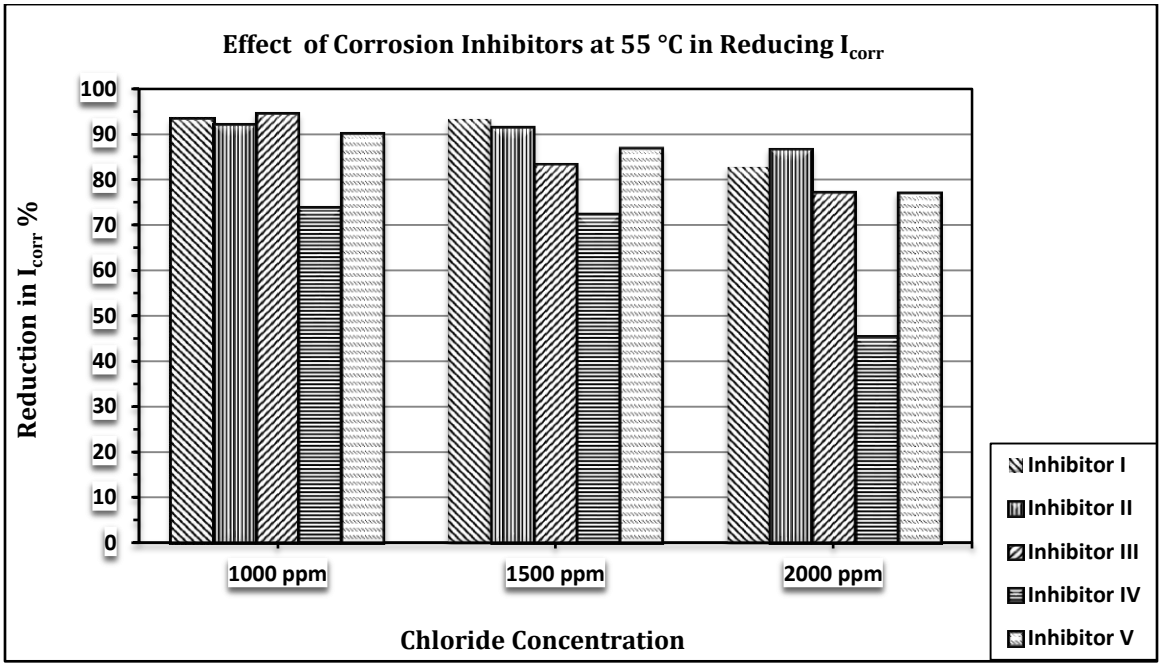


Figure 4.66: Effect of corrosion inhibitors in reducing $I_{corr}$ at 55 ºC and various chloride concentrations.

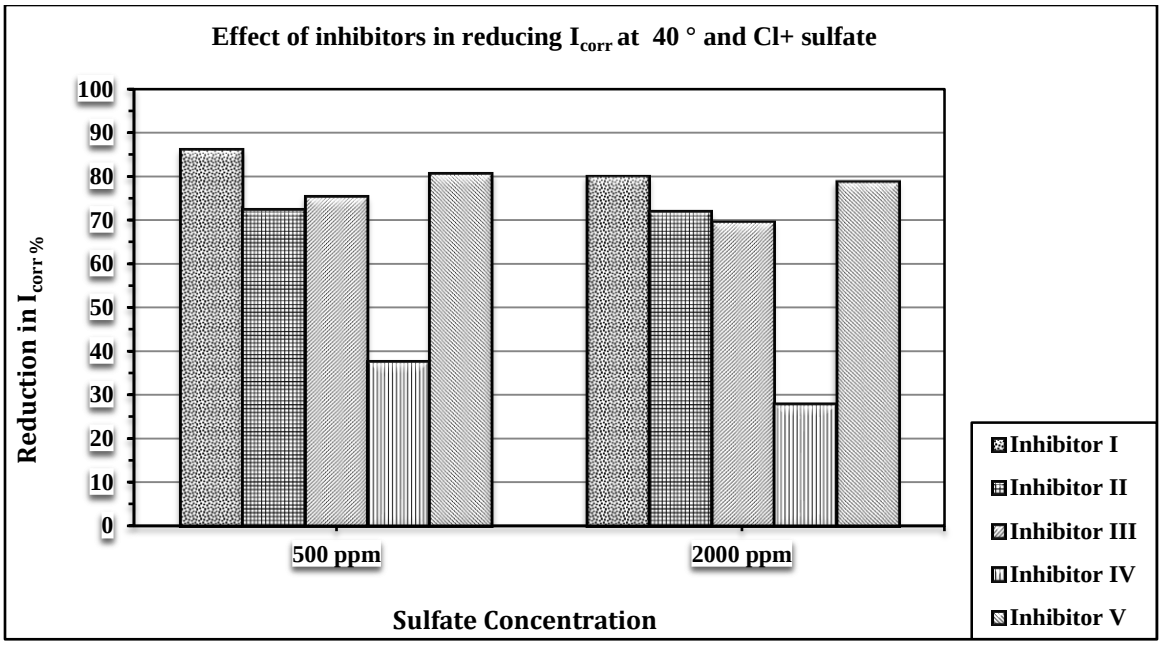


Figure 4.67: Effect of Corrosion Inhibitors in Reducing $I_{corr}$ at 40 °c and 1000 Cl and (500 or 2000) ppm Sulfate

Overall, the selected corrosion inhibitors were effective in decreasing the corrosion current density, corrosion rate and minimizing pitting corrosion compared with the control specimens. This may be due to their ability to reduce anodic dissolution by forming a protective layer on the surface of steel.

Table 4.16 summarizes the effectiveness of the selected inhibitors in reducing the corrosion current density of steel specimens immersed in SCPS during the course of this research program. From these data, the recommended corrosion inhibitor for different chloride concentrations and various exposure temperatures are displayed in priority in Table 4.17.

Table 4.16 : Effect of Inhibitors in Reducing $I_{corr}$ at Various Chlorides and Temperatures

| Chloride Con. | Temperature ( °C ) | Reduction in $I_{corr}$ % | | | | |
|---|---|---|---|---|---|---|
| | | Inhibitor I | Inhibitor II | Inhibitor III | Inhibitor IV | Inhibitor V |
| 1000 ppm | 25 | 85.86 | 84.40 | 84.54 | 85.14 | 85.92 |
| 1500 ppm | | 85.50 | 77.89 | 79.86 | 79.54 | 83.21 |
| 2000 ppm | | 81.34 | 76.82 | 71.26 | 78.00 | 82.70 |
| 1000 ppm | 40 | 87.68 | 84.65 | 84.64 | 77.55 | 85.65 |
| 1500 ppm | | 85.72 | 78.40 | 80.91 | 77.28 | 84.43 |
| 2000 ppm | | 81.35 | 77.75 | 80.47 | 64.11 | 77.64 |
| 1000 ppm | 55 | 93.44 | 91.99 | 94.46 | 73.76 | 90.07 |
| 1500 ppm | | 93.35 | 91.41 | 83.34 | 72.24 | 86.89 |
| 2000 ppm | | 82.81 | 86.62 | 77.13 | 45.51 | 77.08 |

Table 4.17: Recommended Corrosion Inhibitor in Priority for Different Exposures

| Chloride Concentration | 25 ºC | 40 ºC | 55 ºC |
|---|---|---|---|
| 2000 ppm | Inhibitor V, Inhibitor I , Inhibitor IV, Inhibitor II and Inhibitor III | Inhibitor I, Inhibitor III, Inhibitor II, Inhibitor V and Inhibitor IV | Inhibitor II, Inhibitor I, Inhibitor III, Inhibitor V and Inhibitor IV |
| 1500 ppm | Inhibitor I , Inhibitor V, Inhibitor III Inhibitor IV and Inhibitor II | Inhibitor I, Inhibitor V, Inhibitor III, Inhibitor II and Inhibitor IV | Inhibitor I, Inhibitor II, Inhibitor V, Inhibitor III and Inhibitor IV |
| 1000 ppm | Inhibitor V, Inhibitor I, Inhibitor IV, Inhibitor III and Inhibitor II | Inhibitor I, Inhibitor V, Inhibitor II, Inhibitor III and Inhibitor IV | Inhibitor III, Inhibitor I , Inhibitor II, Inhibitor V and Inhibitor IV |

Temperature

## 4.8 Effect of Inhibitors on Reinforcement Corrosion using ASTM G 109

The effect of the selected inhibitors in minimizing reinforcement corrosion in concrete was evaluated using two types of concrete specimens. The first type of concrete specimens was designed according to ASTM G 109 while the second type was designed according to ASTM G 109 but with adding artificial a crack. Macro-cell current and corrosion potentials were measured at regular intervals (every four weeks). The corrosion potentials were measured using high impedance voltmeter in conjunction with a SCE, while the macro-cell current was measured using macro-cell set-up [68]. Furthermore, visual inspection of the top bar and determination of the chloride concentration at the top bar level were also evaluated. The details of these tests were discussed in Chapter 3.

### 4.8.1 Macro-Cell Current

The macro-cell current was measured at regular intervals (once at the start of the second week of wetting cycle) for a period of 25 weeks (twelve wetting cycles) for each specimen. The macro-cell current was measured for both uncracked and cracked specimens. The average macro-cell current for the control specimens as well as the specimens made with the selected corrosion inhibitors (both uncracked and cracked specimens) is shown in Tables 4.18 through 4.29. Further, Figures 4.68 through 4.82 show the average macro-cell current values plotted versus time. However, the individual macro-cell current verses time plots for each specimen of each group and type are presented in Appendices B and C.

Figure 4.68 shows the average macro-cell current in the control uncracked specimens. From the data in this figure, it is noted that a steady rise in the average measured macro-

cell current was recorded till it reached 2.247 μA after the 25th week. Whereas Figures 4.69 displays the average macro-cell current in the uncracked concrete specimens made with the Inhibitor I. The maximum average macro-cell current was 0.223 μA which is much less than that in the control specimens (Figure 4.68).

The maximum average macro-cell current for the concrete specimens made with Inhibitor II (Figure 4.70) was 0.219 μA by the end of 13th wetting cycle, which is much less than the limit value 10 μA [68]. Figures 4.71 through 4.73 shows the average macro-cell current in the uncracked concrete specimens incorporating Inhibitor III, Inhibitor IV and Inhibitor V. The maximum average macro-cell current values were 0.260, 0.267 and 0.213 μA, respectively, which are much lower than that in the control specimens.

Figure 4.74 shows the comparison of average macro-cell current for uncracked specimens. Control specimens displayed high values compared to the other specimens made with the selected corrosion inhibitors. All the uncracked specimens prepared with the corrosion inhibitors almost have the same values of macro-cell current during all exposure period. Figure 4.75 compares the average macro-cell current of uncracked specimens made with the corrosion inhibitors only in order to illustrate the variation in macro-cell current during exposure period.

Figure 4.76 shows the average macro-cell current in the control cracked specimens. From this figure, it is noted that a steady rise in the average measured macro-cell current was recorded till it reach 31.27 μA after 9th wetting cycle.

The measured macro-cell current, shown in Figures 4.77 through 4.79, for cracked concrete specimens made with Inhibitor I, Inhibitor II and Inhibitor III was more than

10 μA. However, the macro-cell current in the concrete specimen prepared with Inhibitor IV or Inhibitor V was less than 10 μA, as shown in Figures 4.80 and 4.81, respectively.

Figure 4.82 presents a comparison of the average macro-cell current for cracked specimens. Cracked concrete specimens displayed high value of 31.27 μA after $9^{th}$ wetting cycle compared to the other specimens made with the selected inhibitors. The maximum macro-cell current values for the specimens made with Inhibitor I, Inhibitor II and Inhibitor III were 15.2, 19.56 and 13.48 μA, respectively. However, the maximum macro-cell current values for the specimens prepared with Inhibitor IV and Inhibitor V were 2.891 and 0.853 μA, respectively. This may be due to their ability to affect the shrinkage property of concrete and close the crack. Further, they form a protective layer on the surface of steel.

Many fluctuations can be noted in the trends contained in most of the above mentioned figures. In the laboratory tests, it has been reported that temperature and other ambient conditions significantly affect the readings as well as the moisture content of the concrete from wetting-drying cycles affect the results [69]. These factors that exist in the laboratory can be neglected due to the fact that at the time of testing all the specimens are under the same conditions. Therefore, for evaluation purposes, the error due to ambient conditions can be ignored.

Table 4.18: Macro-Cell Current for Uncracked Control Specimens

| Date | Cycle No. | Macrocell Current (μA) | | | Average |
|---|---|---|---|---|---|
| | | Specimen 1 | Specimen 2 | Specimen 3 | |
| 27/04/2013 | Starting wetting cycles | | | | |
| 04/05/2013 | 1 | 0.08 | 0.08 | 0.05 | 0.070 |
| 01/06/2013 | 3 | 0.12 | 0.21 | 0.18 | 0.170 |
| 29/06/2013 | 5 | 0.1 | 0.13 | 0.17 | 0.133 |
| 27/07/2013 | 7 | 0.1 | 0.28 | 0.6 | 0.327 |
| 25/08/2013 | 9 | 0.12 | 1.87 | 0.1 | 0.697 |
| 22/09/2013 | 11 | 0.13 | 2.38 | 0.16 | 0.890 |
| 22/10/2013 | 13 | 1.85 | 2.001 | 2.89 | 2.247 |

Table 4.19: Macro-Cell Current for Uncracked Concrete Specimens Made with Inhibitor I

| Date | Cycle No. | Macrocell Current (μA) | | | Average |
|---|---|---|---|---|---|
| | | Specimen 1 | Specimen 2 | Specimen 3 | |
| 27/04/2013 | Starting wetting cycles | | | | |
| 04/05/2013 | 1 | 0 | 0 | 0 | 0.000 |
| 01/06/2013 | 3 | 0.101 | 0.141 | 0.131 | 0.124 |
| 29/06/2013 | 5 | 0.202 | 0.172 | 0.162 | 0.179 |
| 27/07/2013 | 7 | 0.105 | 0.121 | 0.106 | 0.111 |
| 25/08/2013 | 9 | 0.202 | 0.212 | 0.182 | 0.199 |
| 22/09/2013 | 11 | 0.182 | 0.242 | 0.213 | 0.212 |
| 22/10/2013 | 13 | 0.192 | 0.253 | 0.223 | 0.223 |

Table 4.20: Macro-Cell Current for Uncracked Concrete Specimens Made with Inhibitor II

| Date | Cycle No. | Macrocell Current (μA) | | | Average |
|---|---|---|---|---|---|
| | | Specimen 1 | Specimen 2 | Specimen 3 | |
| 27/04/2013 | Starting wetting cycles | | | | |
| 04/05/2013 | 1 | 0 | 0 | 0 | 0.000 |
| 01/06/2013 | 3 | 0.142 | 0.162 | 0.142 | 0.148 |
| 29/06/2013 | 5 | 0.202 | 0.233 | 0.162 | 0.199 |
| 27/07/2013 | 7 | 0.162 | 0.121 | 0.071 | 0.118 |
| 25/08/2013 | 9 | 0.263 | 0.243 | 0.243 | 0.250 |
| 22/09/2013 | 11 | 0.182 | 0.233 | 0.233 | 0.216 |
| 22/10/2013 | 13 | 0.192 | 0.222 | 0.243 | 0.219 |

Table 4.21: Macro-Cell Current for Uncracked Concrete Specimens Made with Inhibitor III

| Date | Cycle No. | Macrocell Current (μA) | | | Average |
|---|---|---|---|---|---|
| | | Specimen 1 | Specimen 2 | Specimen 3 | |
| 27/04/2013 | Starting wetting cycles | | | | |
| 04/05/2013 | 1 | 0 | 0 | 0 | 0 |
| 01/06/2013 | 3 | 0.152 | 0.152 | 0.152 | 0.152 |
| 29/06/2013 | 5 | 0.163 | 0.182 | 0.142 | 0.162 |
| 27/07/2013 | 7 | 0.163 | 0.122 | 0.121 | 0.135 |
| 25/08/2013 | 9 | 0.183 | 0.193 | 0.172 | 0.182 |
| 22/09/2013 | 11 | 0.224 | 0.263 | 0.283 | 0.257 |
| 22/10/2013 | 13 | 0.234 | 0.254 | 0.294 | 0.260 |

Table 4.22: Macro-Cell Current for Uncracked Concrete Specimens Made with Inhibitor IV

| Date | Cycle No. | Macrocell Current (µA) | | | Average |
|---|---|---|---|---|---|
| | | Specimen 1 | Specimen 2 | Specimen 3 | |
| 27/04/2013 | Starting wetting cycles | | | | |
| 04/05/2013 | 1 | 0 | 0 | 0 | 0.000 |
| 01/06/2013 | 3 | 0.121 | 0.101 | 0.082 | 0.101 |
| 29/06/2013 | 5 | 0.202 | 0.162 | 0.112 | 0.159 |
| 27/07/2013 | 7 | 0.152 | 0.101 | 0.102 | 0.118 |
| 25/08/2013 | 9 | 0.202 | 0.233 | 0.276 | 0.237 |
| 22/09/2013 | 11 | 0.294 | 0.283 | 0.224 | 0.267 |
| 22/10/2013 | 13 | 0.283 | 0.294 | 0.204 | 0.260 |

Table 4.23: Macro-Cell Current for Uncracked Concrete Specimens Made with Inhibitor V

| Date | Cycle No. | Macrocell Current (µA) | | | Average |
|---|---|---|---|---|---|
| | | Specimen 1 | Specimen 2 | Specimen 3 | |
| 27/04/2013 | Starting wetting cycles | | | | |
| 04/05/2013 | 1 | 0 | 0 | 0 | 0.000 |
| 01/06/2013 | 3 | 0.0652 | 0.0837 | 0.0911 | 0.0802 |
| 29/06/2013 | 5 | 0.112 | 0.112 | 0.101 | 0.108 |
| 27/07/2013 | 7 | 0.101 | 0.102 | 0.121 | 0.108 |
| 25/08/2013 | 9 | 0.203 | 0.224 | 0.213 | 0.213 |
| 22/09/2013 | 11 | 0.152 | 0.122 | 0.142 | 0.139 |
| 22/10/2013 | 13 | 0.162 | 0.143 | 0.152 | 0.152 |

Table 4.24: Macro-Cell Current for Control Cracked Concrete Specimens

| Date | Cycle No. | Macrocell Current (µA) | | | Average |
|---|---|---|---|---|---|
| | | Specimen 1 | Specimen 2 | Specimen 3 | |
| 27/04/2013 | Starting wetting cycles | | | | |
| 04/05/2013 | 1 | 17.7 | 15.3 | 22.1 | 18.37 |
| 01/06/2013 | 3 | 25.2 | 24.4 | 28.4 | 26.00 |
| 29/06/2013 | 5 | 28.9 | 26.5 | 31.1 | 28.83 |
| 27/07/2013 | 7 | 31.4 | 27.5 | 32.5 | 30.47 |
| 25/08/2013 | 9 | 31.9 | 28.4 | 33.5 | 31.27 |

Table 4.25: Macro-Cell Current for Cracked Concrete Specimens Made with Inhibitor I

| Date | Cycle No. | Macrocell Current (µA) | | | Average |
|---|---|---|---|---|---|
| | | Specimen 1 | Specimen 2 | Specimen 3 | |
| 27/04/2013 | Starting wetting cycles | | | | |
| 04/05/2013 | 1 | 13.20 | 9.23 | 6.71 | 9.712 |
| 01/06/2013 | 3 | 12.90 | 11.88 | 5.85 | 10.211 |
| 29/06/2013 | 5 | 16.55 | 12.77 | 7.64 | 12.318 |
| 27/07/2013 | 7 | 17.36 | 14.29 | 9.60 | 13.748 |
| 25/08/2013 | 9 | 22.23 | 12.11 | 11.37 | 15.240 |

Table 4.26: Macro-Cell Current for Cracked Concrete Specimens Made with Inhibitor II

| Date | Cycle No. | Macrocell Current (µA) | | | Average |
|---|---|---|---|---|---|
| | | Specimen 1 | Specimen 2 | Specimen 3 | |
| 27/04/2013 | Starting wetting cycles | | | | |
| 04/05/2013 | 1 | 16.18 | 24.27 | 5.07 | 15.17 |
| 01/06/2013 | 3 | 27.71 | 25.99 | 14.47 | 22.72 |
| 29/06/2013 | 5 | 27.40 | 23.21 | 13.68 | 21.43 |
| 27/07/2013 | 7 | 25.38 | 23.46 | 10.16 | 19.67 |
| 25/08/2013 | 9 | 21.23 | 27.00 | 10.46 | 19.56 |

Table 4.27: Macro-Cell Current for Cracked Concrete Specimens Made with Inhibitor III

| Date | Cycle No. | Macrocell Current (μA) | | | Average |
|---|---|---|---|---|---|
| | | Specimen 1 | Specimen 2 | Specimen 3 | |
| 27/04/2013 | Starting wetting cycles | | | | |
| 04/05/2013 | 1 | 3.05 | 4.78 | 12.18 | 6.673 |
| 01/06/2013 | 3 | 8.59 | 11.78 | 17.93 | 12.767 |
| 29/06/2013 | 5 | 13.24 | 12.59 | 13.27 | 13.032 |
| 27/07/2013 | 7 | 12.51 | 11.37 | 19.09 | 14.321 |
| 25/08/2013 | 9 | 12.96 | 10.40 | 17.086 | 13.482 |

Table 4.28: Macro-Cell Current for Cracked Concrete Specimens Made with Inhibitor IV

| Date | Cycle No. | Macrocell Current (μA) | | | Average |
|---|---|---|---|---|---|
| | | Specimen 1 | Specimen 2 | Specimen 3 | |
| 27/04/2013 | Starting wetting cycles | | | | |
| 04/05/2013 | 1 | 0 | 1.90 | 0 | 0.633 |
| 01/06/2013 | 3 | 1.63 | 2.15 | 2.03 | 1.936 |
| 29/06/2013 | 5 | 1.73 | 2.60 | 1.93 | 2.086 |
| 27/07/2013 | 7 | 1.02 | 3.06 | 1.18 | 1.731 |
| 25/08/2013 | 9 | 2.54 | 4.10 | 2.03 | 2.891 |

Table 4.29: Macro-Cell Current for Cracked Concrete Specimens Made with Inhibitor V

| Date | Cycle No. | Macrocell Current (μA) | | | Average |
|---|---|---|---|---|---|
| | | Specimen 1 | Specimen 2 | Specimen 3 | |
| 27/04/2013 | Starting wetting cycles | | | | |
| 04/05/2013 | 1 | 0 | 0 | 0 | 0.000 |
| 01/06/2013 | 3 | 0.244 | 1.32 | 0.152 | 0.573 |
| 29/06/2013 | 5 | 3.37 | 0.234 | 0.266 | 1.290 |
| 27/07/2013 | 7 | 2.89 | 0.183 | 0.558 | 1.211 |
| 25/08/2013 | 9 | 1.85 | 0.356 | 0.355 | 0.853 |

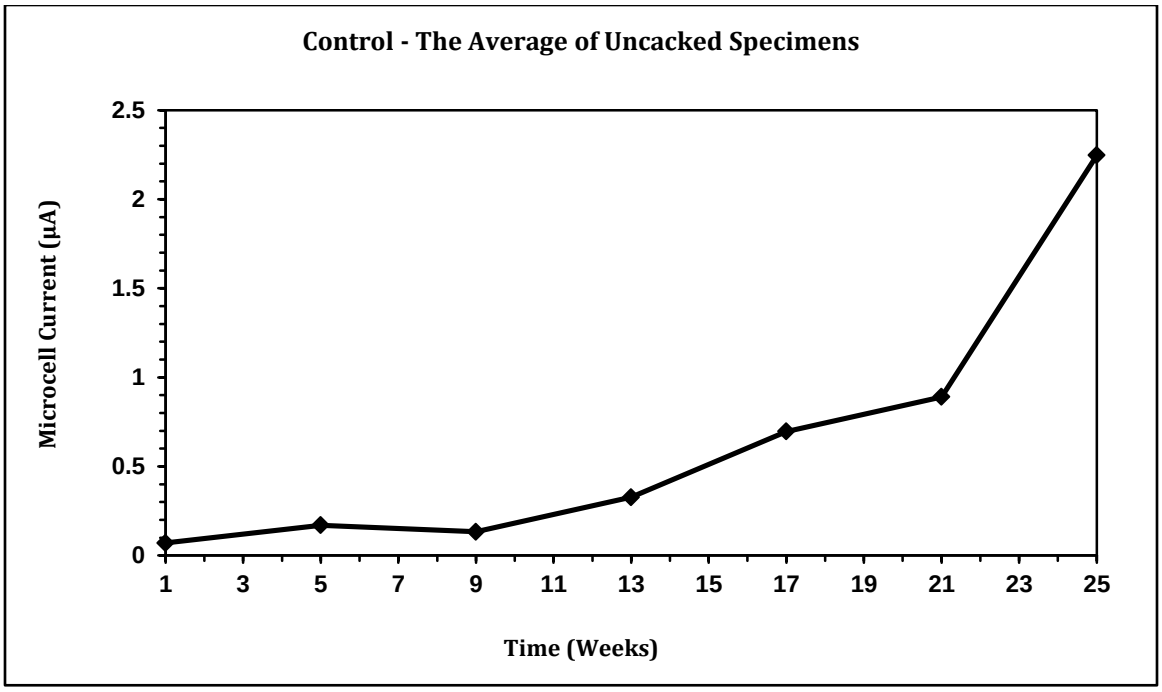


Figure 4.68: Average Macro-Cell Current for Steel in Control Uncracked Concrete Specimens

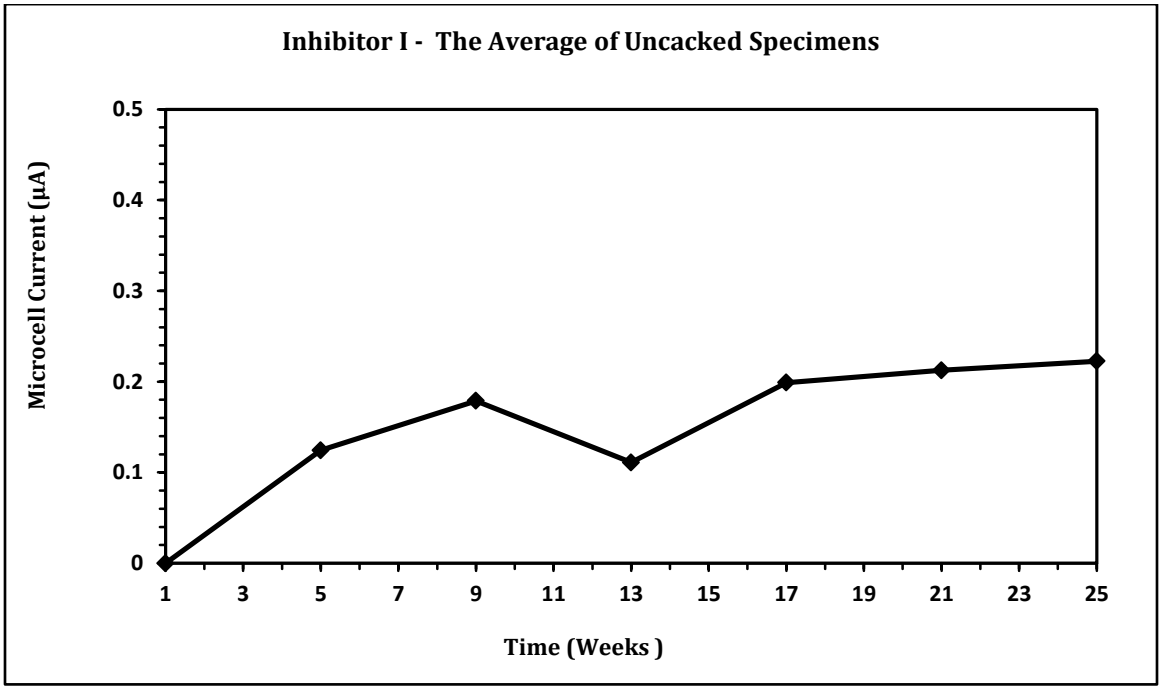


Figure 4.69: Average Macro-Cell Current for Steel in Uncracked Concrete Specimens Made with Inhibitor I

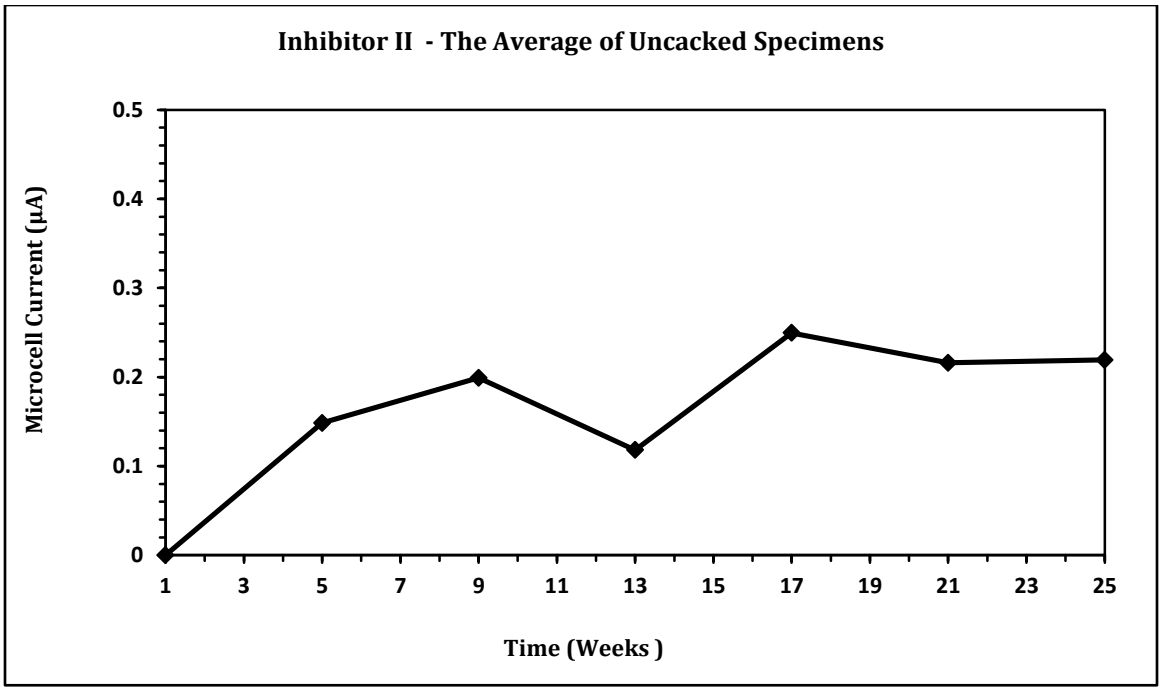


Figure 4.70: Average Macro-Cell Current for Steel in Uncracked Concrete Specimens Made with Inhibitor II

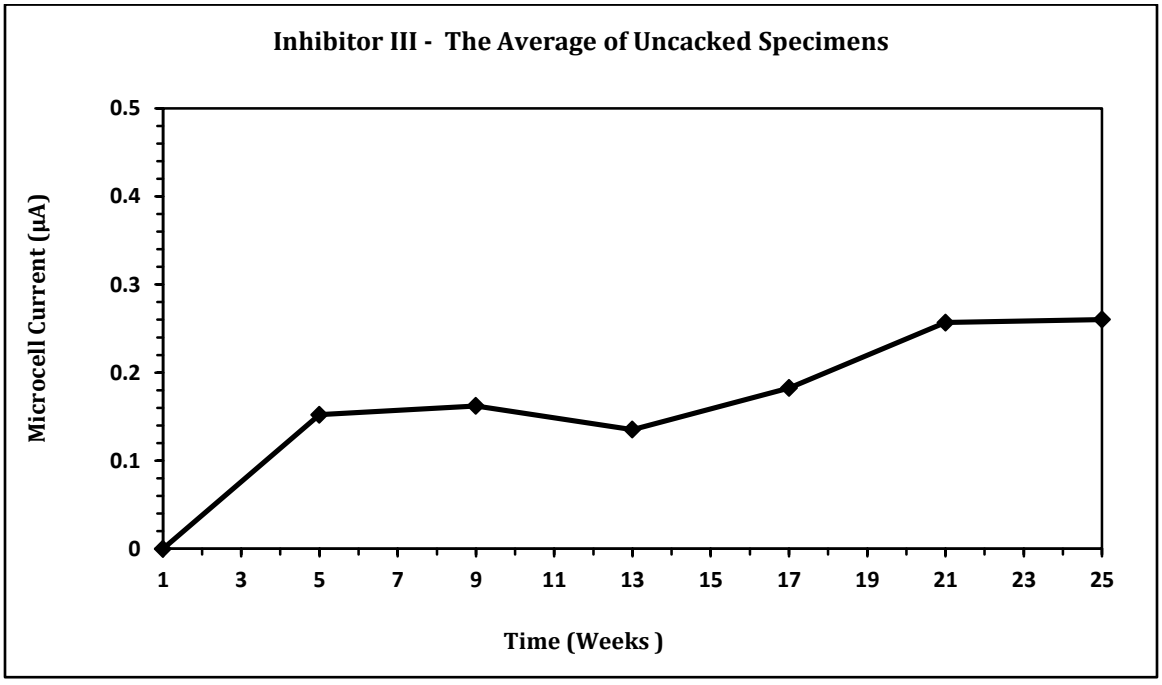


Figure 4.71: Average Macro-Cell Current for Steel in Uncracked Concrete Specimens Made with Inhibitor III

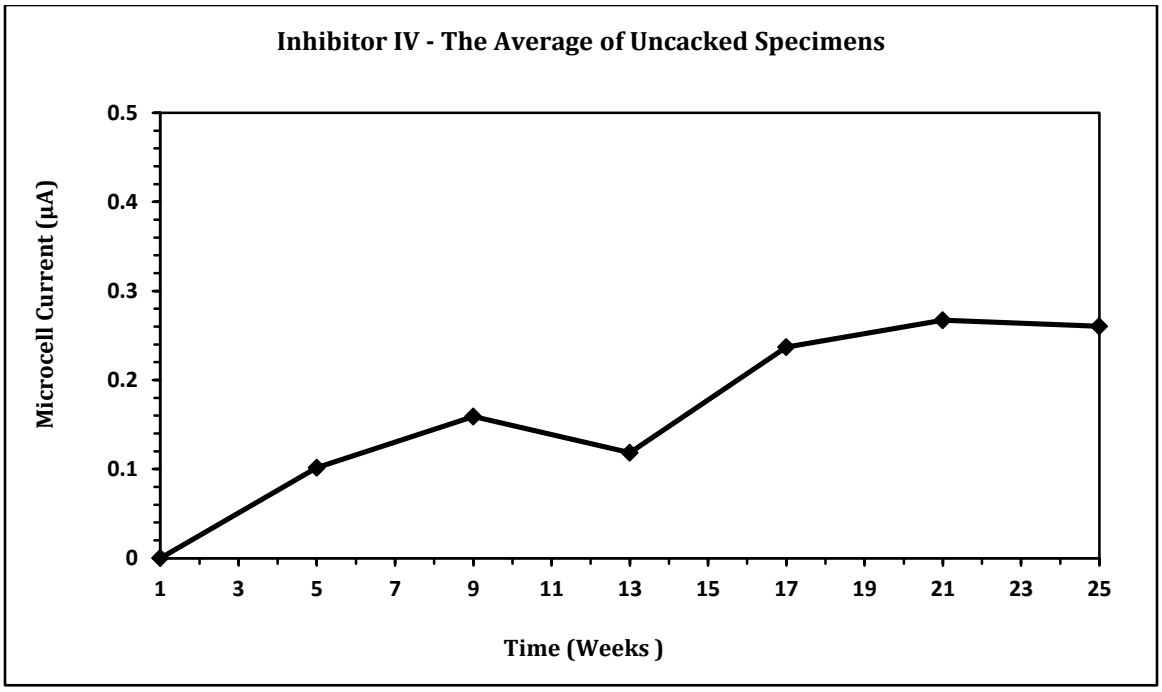


Figure 4.72: Average Macro-Cell Current for Steel in Uncracked Concrete Specimens Made with Inhibitor IV

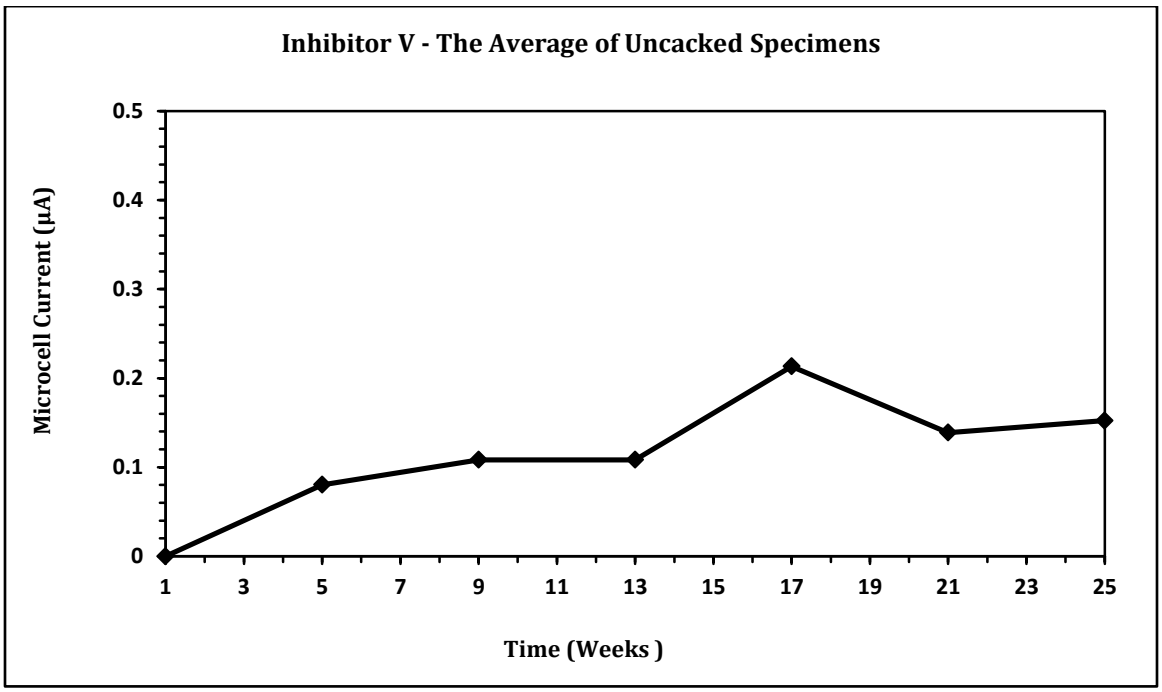


Figure 4.73: Average Macro-Cell Current for Steel in Uncracked Concrete Specimens Made with Inhibitor V

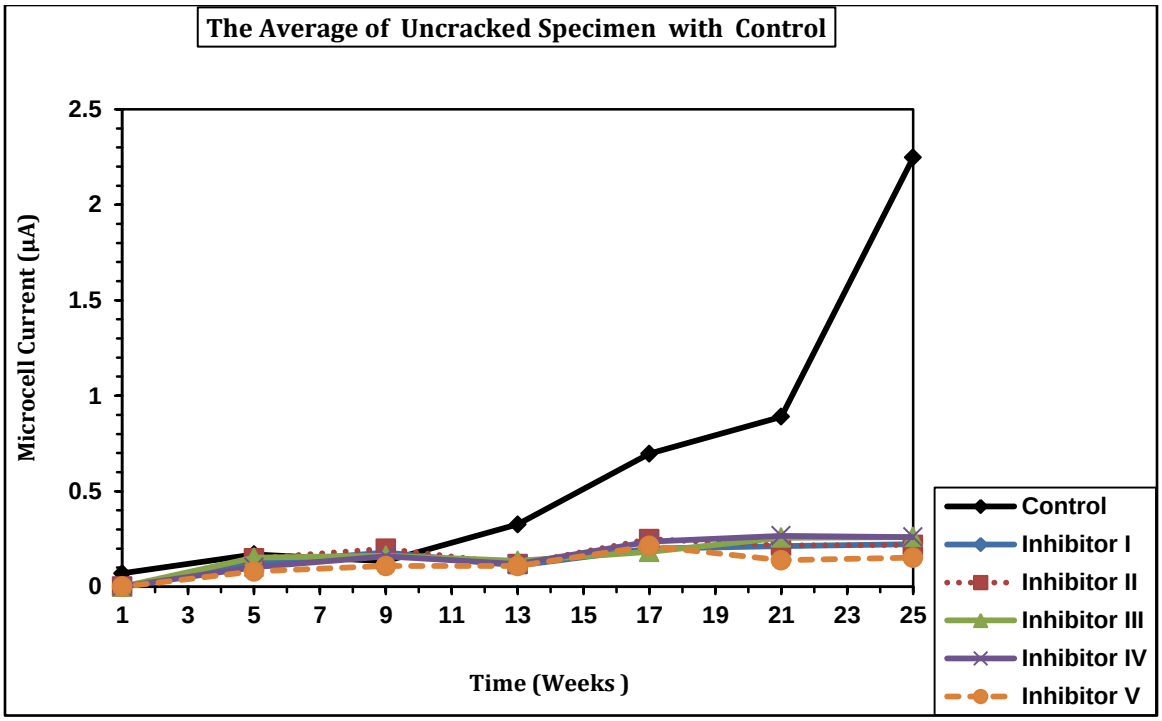


Figure 4.74: Comparison of the Average Macro-Cell Current of Uncracked Specimens Made with Corrosion Inhibitor and Control Specimens

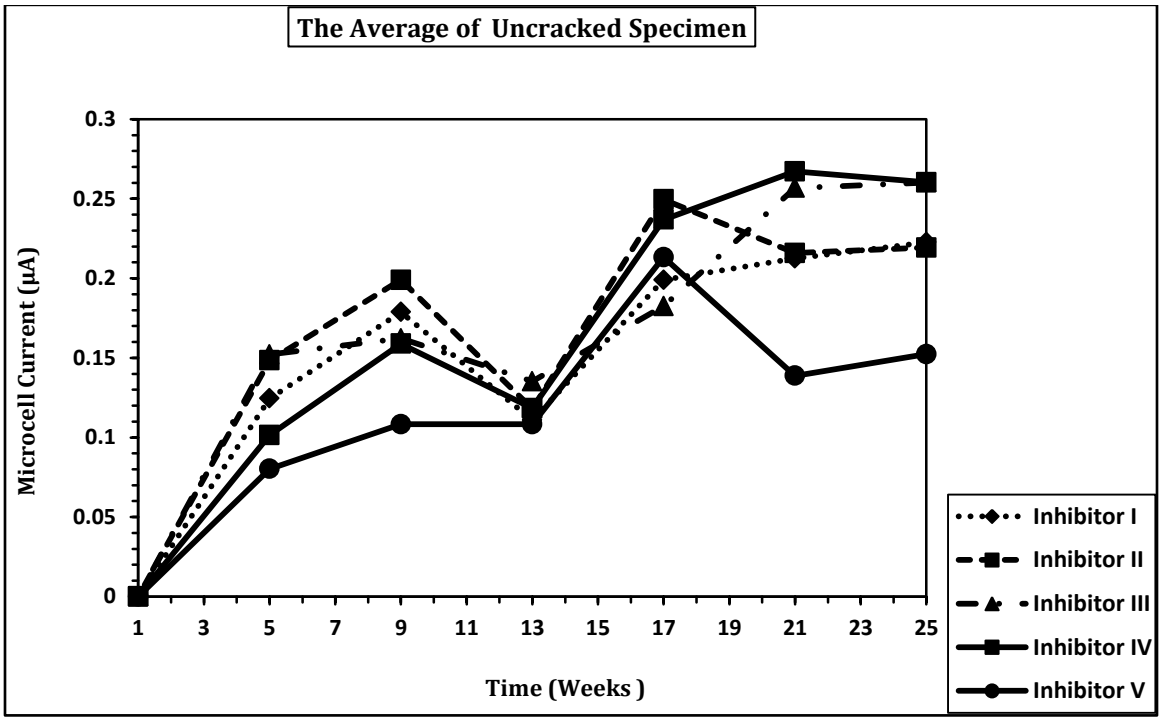


Figure 4.75: Comparison of the Average Macro-Cell Current of Uncracked Specimens Made with Corrosion Inhibitors

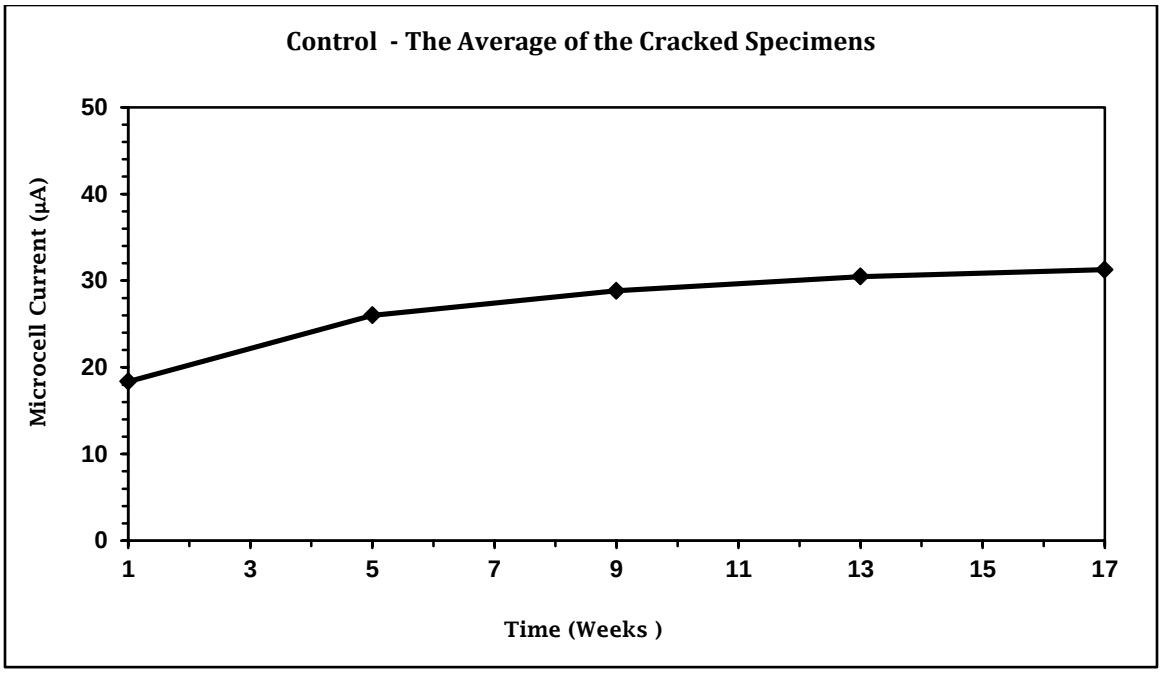


Figure 4.76: Average Macro-Cell Current for Steel in Control Cracked Concrete Specimens

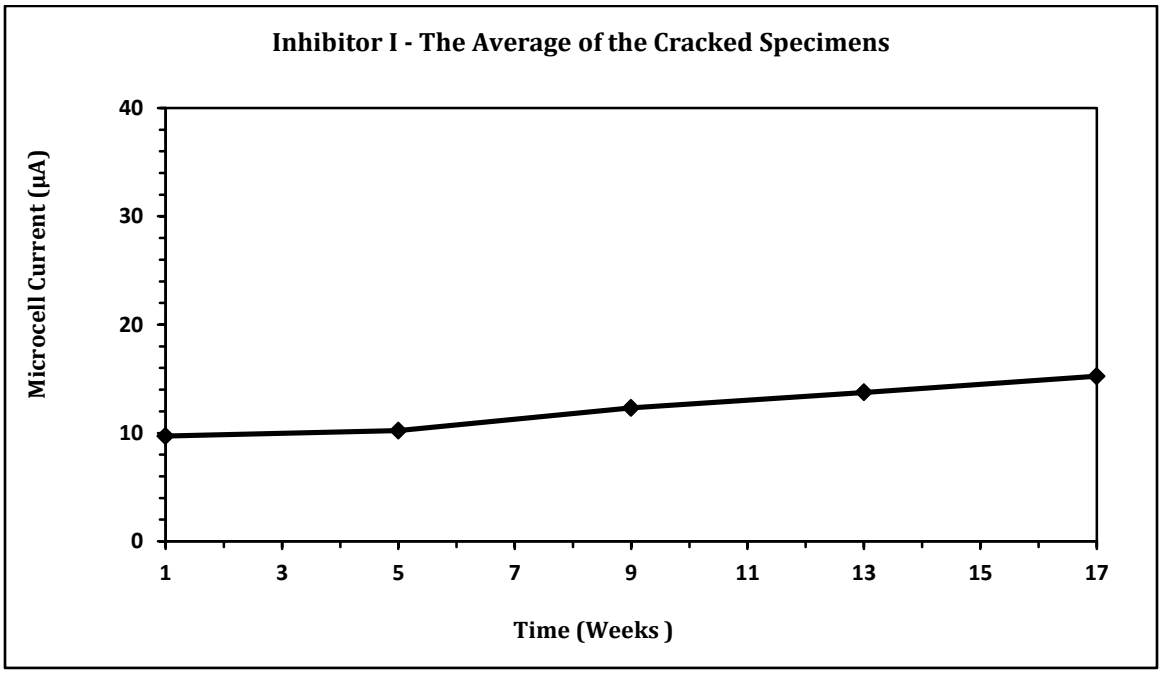


Figure 4.77: Average Macro-Cell Current for Steel in Cracked Concrete Specimens Made with Inhibitor I

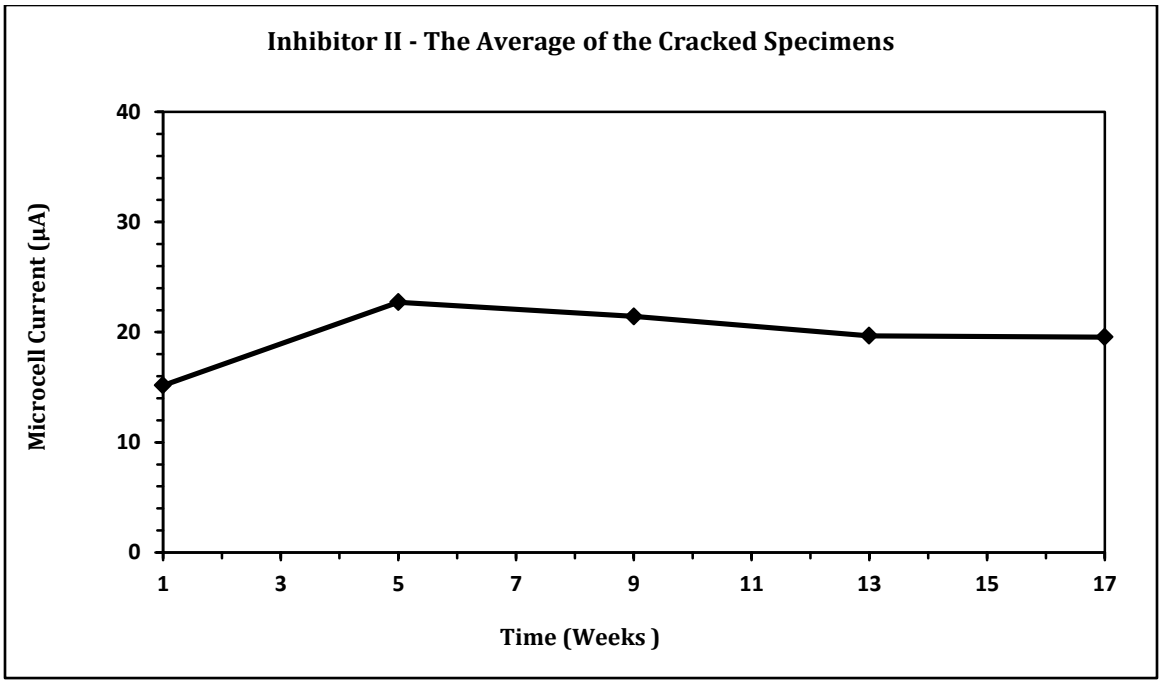


Figure 4.78: Average Macro-Cell Current for Steel in Cracked Concrete Specimens Made with Inhibitor II

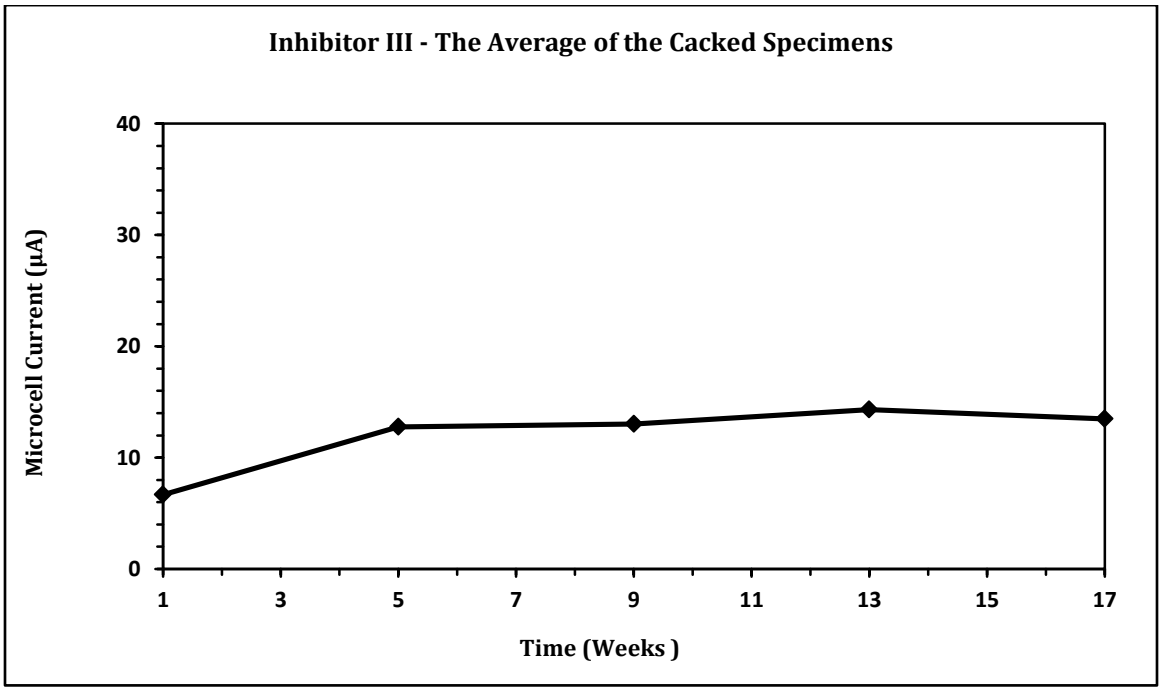


Figure 4.79: Average Macro-Cell Current Exposure for Steel in Cracked Concrete Specimens Made with Inhibitor III

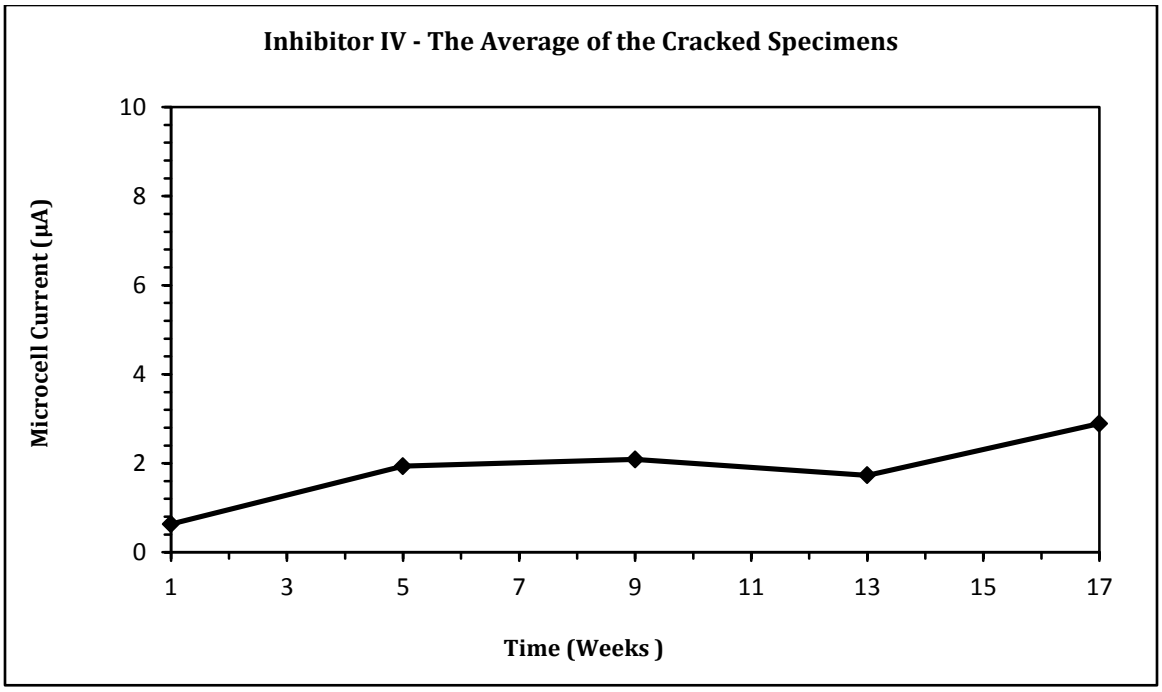


Figure4.80: Average Macro-Cell for Steel in Cracked Concrete Specimens Made with Inhibitor IV

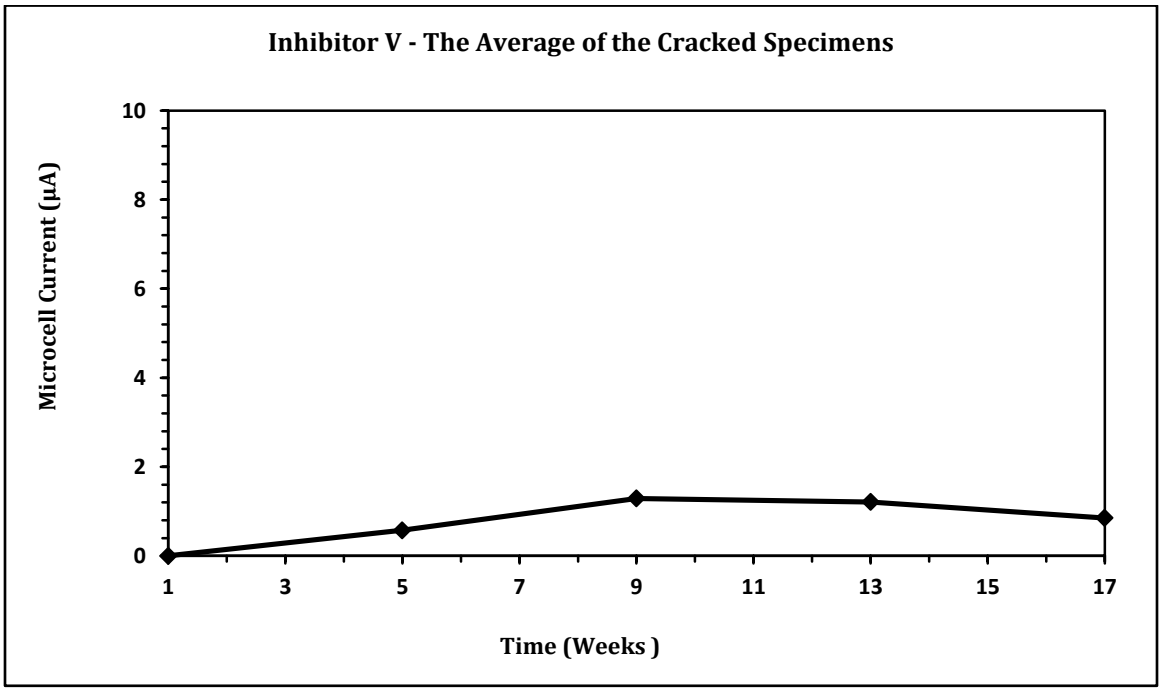


Figure 4.81: Average Macro-Cell Current for Steel in Cracked Concrete Specimens Made with Inhibitor V

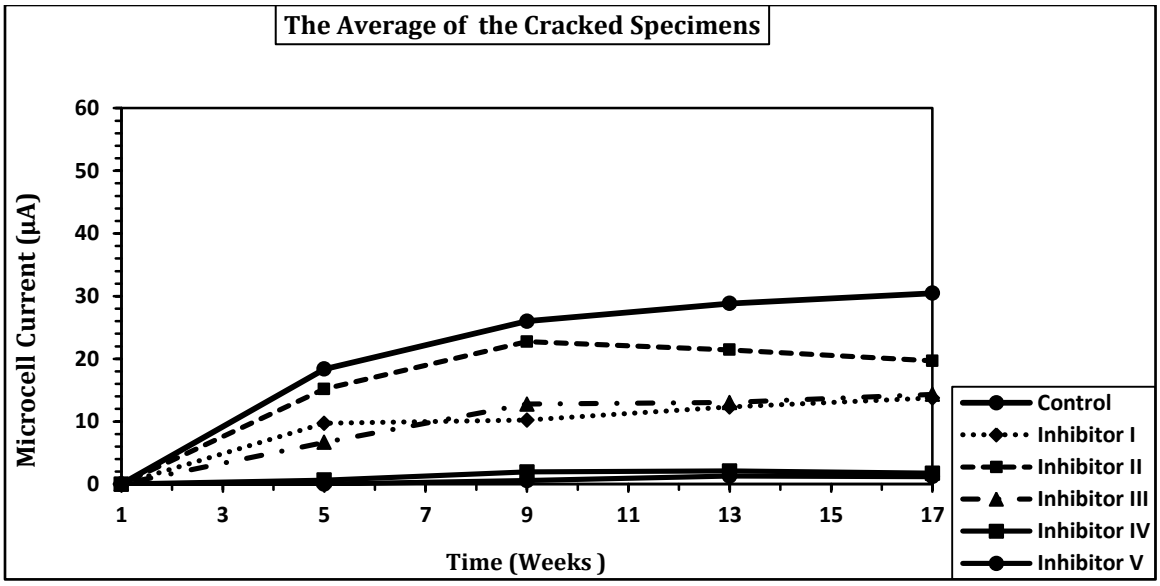


Figure 4.82: Comparison of the Average Macro-Cell Current of Cracked Specimens Made with Corrosion Inhibitors

Overall, no significant macro-cell corrosion current could be noted in any of uncracked concrete specimens incorporating inhibitors, based on ASTM G 109 test, through the end of the 6- month evaluation. Therefore, from the available data of macro-cell current, the time required for these specimens to reach 10 μA was calculated by extrapolation. Table 4.30 shows the estimated time in years for all uncracked concrete specimens.

Table 4.30: Estimated Time for Uncracked Concrete Specimens to Fail

| Inhibitor | Equation | Time (years) | Improvement % |
|---|---|---|---|
| None (Control) | y=0.006x - .0795 | 4.62 | - |
| Inhibitor I | y = 0.001x + 0.058 | 27.31 | 491.13 |
| Inhibitor II | y = 0.0011x + 0.0673 | 24.81 | 437.01 |
| Inhibitor III | y = 0.0013x + 0.0478 | 21.03 | 355.19 |
| Inhibitor IV | y = 0.0015x + 0.0262 | 18.27 | 295.45 |
| Inhibitor V | y = 0.0009x + 0.0363 | 30.41 | 558.23 |

Table 4.31 shows the estimated cost per year depending on the estimated time for uncracked concrete specimens to reach 10 μA (Table 4.30) and the cost of the used inhibitors.

However, the macro-cell current in all the cracked specimens was more than 10 μA, except in the specimens prepared with Inhibitor V and Inhibitor IV. This might be due to the effect of Inhibitor V and Inhibitor IV on shrinkage property of the cracked specimens and their ability to close the cracks. Further, Inhibitor V and Inhibitor IV might be forming protective layer on the surface of reinforcing steel.

### 4.8.2 Total Current

ASTM G 109 requires the period of testing to continue till the average macro-cell current reaches 10 μA or greater, and at least half of the specimens show integrated macro-cell currents equal to or greater than 150 Coulombs. In those cases, where the admixtures being tested are corrosive, the tests are to be completed within three full cycles after an average integrated macro-cell current of 75 Coulombs is measured [68]. The total corrosion current which is the integration of the macro-cell current over time of each specimen was calculated using the following equation (as per ASTM G 109):

$$TC_j = TC_{j-1} + [(t_j - t_{j-1}) \times (i + i_{j-1})/2] \quad 4.1$$

Where:

TC: the total corrosion in Coulombs,

$t_j$: the time in seconds when the macro-cell current was measured, and

$i_j$: the macro-cell current in Amperes at time, $t_j$.

The total current of the cracked and uncracked specimens is shown in Table 4.31. The current measured for individual specimens are shown in Appendices B and C.

Table 4.31: Total Current of the Cracked and Uncracked Specimens

| Specimen Type | Inhibitor Name | Total Current (Coulombs) | | | |
|---|---|---|---|---|---|
| | | Specimen 1 | Specimen 2 | Specimen 3 | Average |
| Uncracked | Control | 3.92 | 14.79 | 6.79 | 8.50 |
| Uncracked | Inhibitor I | 2.20 | 2.51 | 2.24 | 2.32 |
| Uncracked | Inhibitor II | 2.58 | 2.72 | 2.41 | 2.57 |
| Uncracked | Inhibitor III | 2.48 | 2.57 | 2.52 | 2.52 |
| Uncracked | Inhibitor IV | 2.76 | 2.55 | 2.23 | 2.51 |
| Uncracked | Inhibitor V | 1.77 | 1.77 | 1.84 | 1.79 |
| Cracked | Control | 274.92 | 249.57 | 299.35 | 274.62 |
| Cracked | Inhibitor I | 161.81 | 123.94 | 80.65 | 122.13 |
| Cracked | Inhibitor II | 246.89 | 247.28 | 113.87 | 202.68 |
| Cracked | Inhibitor III | 104.47 | 107.20 | 162.30 | 124.66 |
| Cracked | Inhibitor IV | 13.80 | 27.04 | 14.89 | 18.57 |
| Cracked | Inhibitor V | 18.18 | 4.66 | 2.83 | 8.56 |

The average total current in the uncracked concrete specimens with inhibitors is plotted in Figure 4.83. It can be noted that the total current in the uncracked control specimens (8.5 Coulombs) was more than that in the uncracked specimens with inhibitors (1.79 to 2.57 Coulombs). The least total current was measured in the concrete specimens prepared with Inhibitor V and Inhibitor II.

Overall, the total current of uncracked specimens was very low (less than 2.6 Coulombs). This is due to the fact that most of these specimens did not produce a measurable macro-cell current from the beginning of the test.

From the data in Figure 4.84, it is clear that the average total current of all the cracked concrete specimens except those with Inhibitor IV and Inhibitor V have shown total macro-cell current of more than 75 Coulombs. This might be due to the effect of Inhibitor V and Inhibitor IV on shrinkage property of the cracked specimens and their ability to close the cracks. Further, Inhibitor V and Inhibitor IV might be forming protective layer on the surface of reinforcing steel.

Overall, in cracked concrete specimens containing Inhibitor I, Inhibitor II and Inhibitor III, it has been observed that these inhibitors could not provide or they provide limited protection to reinforcing steel. However, the specimens containing Inhibitor IV and Inhibitor V succeeded to provide good protection to reinforcing steel.

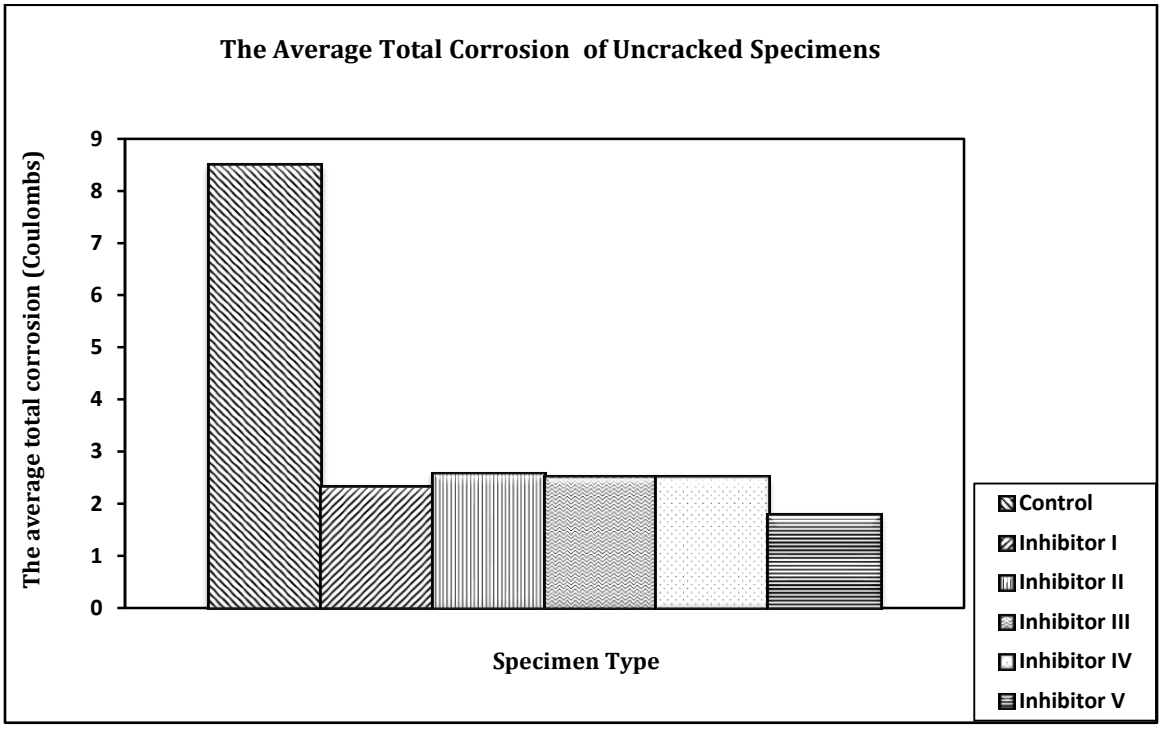


Figure 4.83: Total Current in Uncracked Concrete Specimens

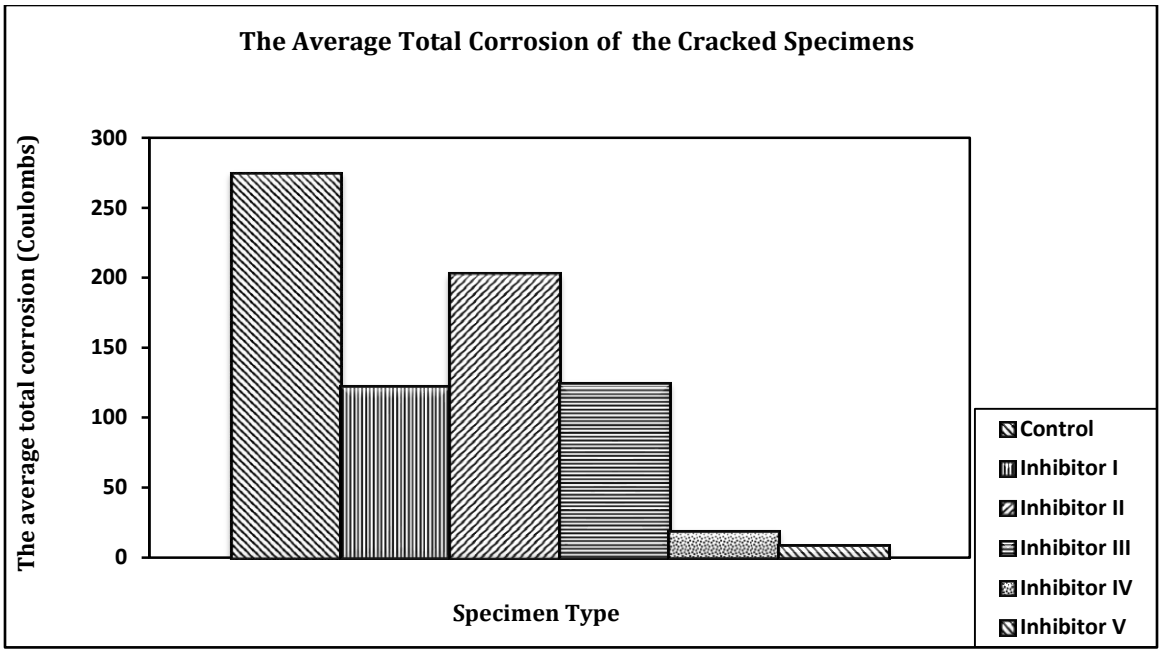


Figure 4.84: Total Current in the Cracked Concrete Specimens

### 4.8.3 Macro-Cell Corrosion Potential

The average time-corrosion potential curves for steel in ASTM G 109 concrete specimens made with one type of the selected corrosion inhibitors and exposed to 3% of NaCl solution are shown in Figures 4.85 through 4.96. The individual time-corrosion potential curve for each specimen is shown in Appendices B and C. Furthermore, Tables 4.32 through 4.43 summarize the average data of corrosion potential measurements for the control specimens as well as for the specimens made with the selected corrosion inhibitors (both uncracked and cracked).

The average corrosion potentials in the uncracked control concrete specimens was more than the ASTM C 876 threshold value of -270 mV SCE after 25 weeks of drying and wetting (Figure 4.85). However, the corrosion potentials in the uncracked concrete

specimens with inhibitors (Figs. 4.86 through 4.90) were less negative than the ASTM C 876 threshold value of -270 mV SCE after 25 weeks of drying and wetting. The maximum readings were in the range of -113 to -126 mV, which indicate less than 10% probability of corrosion.

The average corrosion potential for cracked control specimens and specimens incorporating Inhibitor II (Figures 4.91 and 4.93) was more negative than the ASTM C 876 threshold value of -426 mV SCE after 17 weeks of drying and wetting which indicate sever corrosion. However, the average corrosion potentials for the cracked concrete specimens incorporating Inhibitor I and Inhibitor III was more negative than – 270 mV SCE, which indicates more than 90% probability of corrosion (Figs. 4.92 and 4.94) were more negative than the ASTM C 876 threshold value of -270 mV SCE after 17 weeks of drying and wetting which indicate more than 90% probability of corrosion (active corrosion). The corrosion potential for cracked specimens incorporating Inhibitor V and Inhibitor IV was in the range of uncertain corrosion.

Overall, cracked specimens made with Inhibitor II had the most negative readings of -466 mV SCE which indicates that Inhibitor II to be the worst among the tested inhibitors in terms of corrosion initiation of reinforcing steel in cracked concrete specimens, whereas Inhibitor IV and Inhibitor V had the lowest negative readings for the same type of concrete specimens. This indicates that Inhibitor IV and Inhibitor V to be the best in terms of corrosion initiation in cracked concrete specimens.

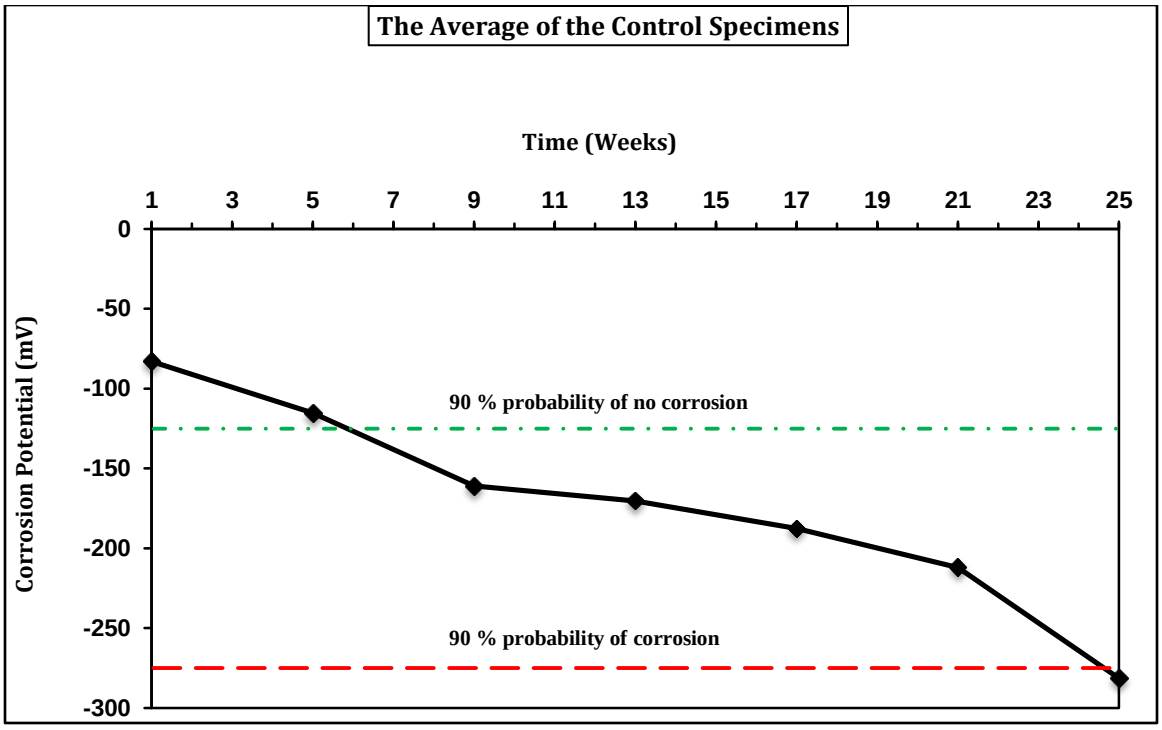


Figure 4.85: Corrosion Potential for Steel in Uncracked Control Concrete Specimens

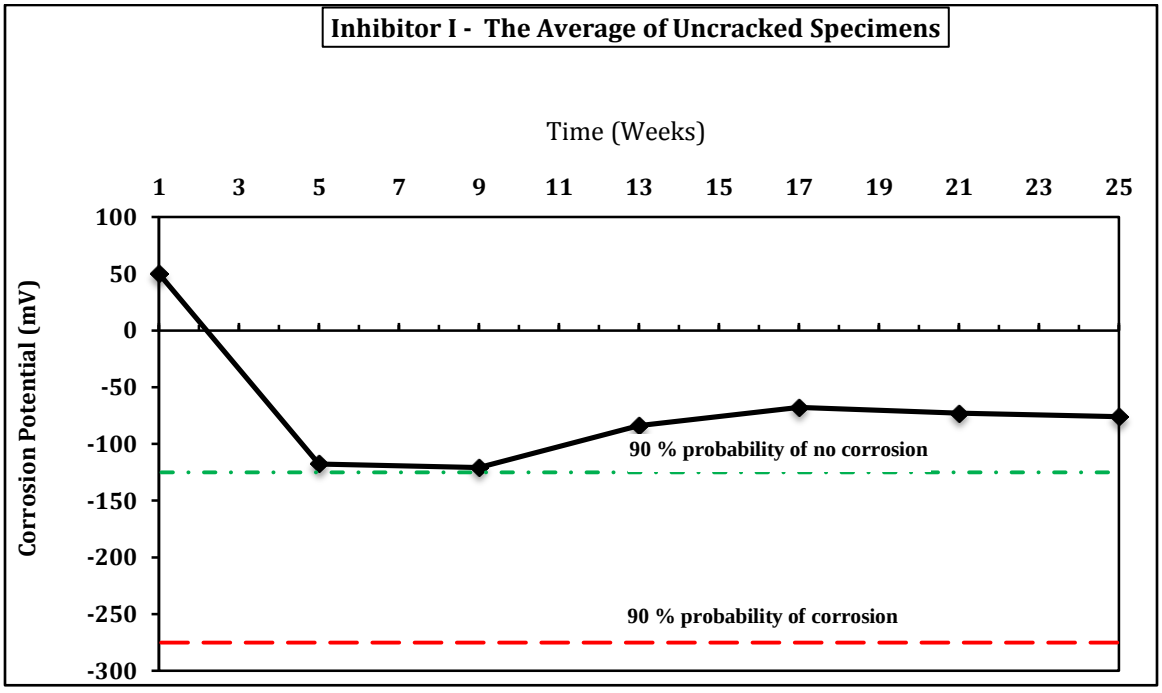


Figure 4.86: Corrosion Potential for Steel in Uncracked Concrete Specimens Made with Inhibitor I

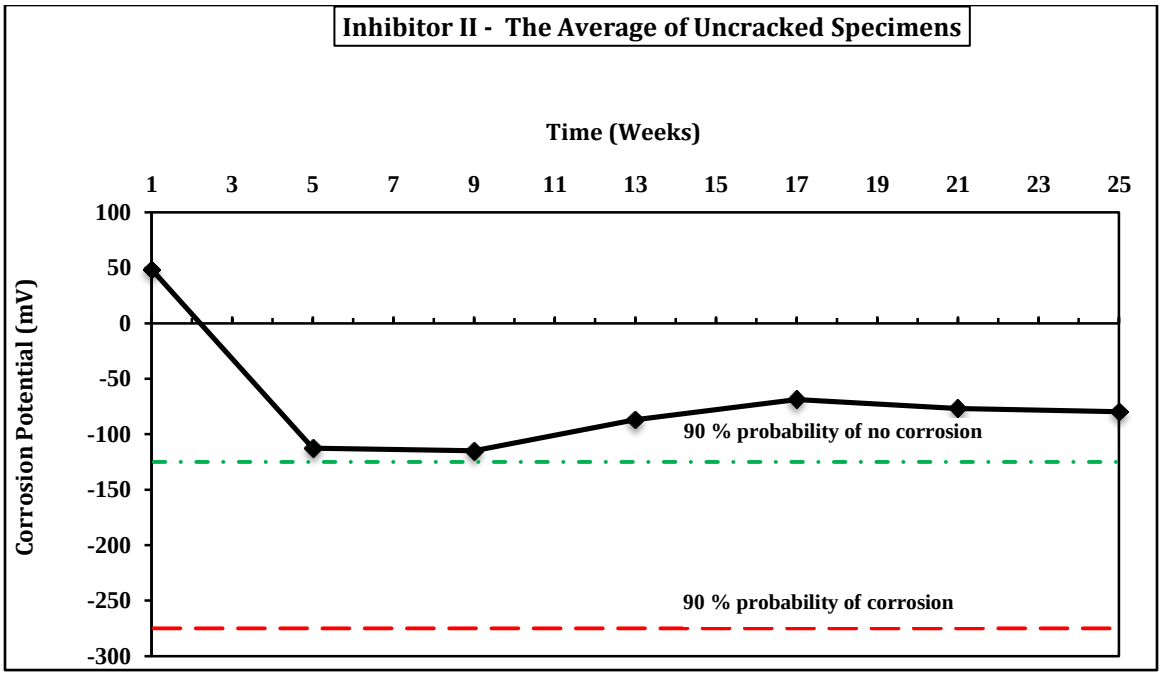


Figure 4.87: Corrosion Potential for Steel in Uncracked Concrete Specimens Made with Inhibitor II

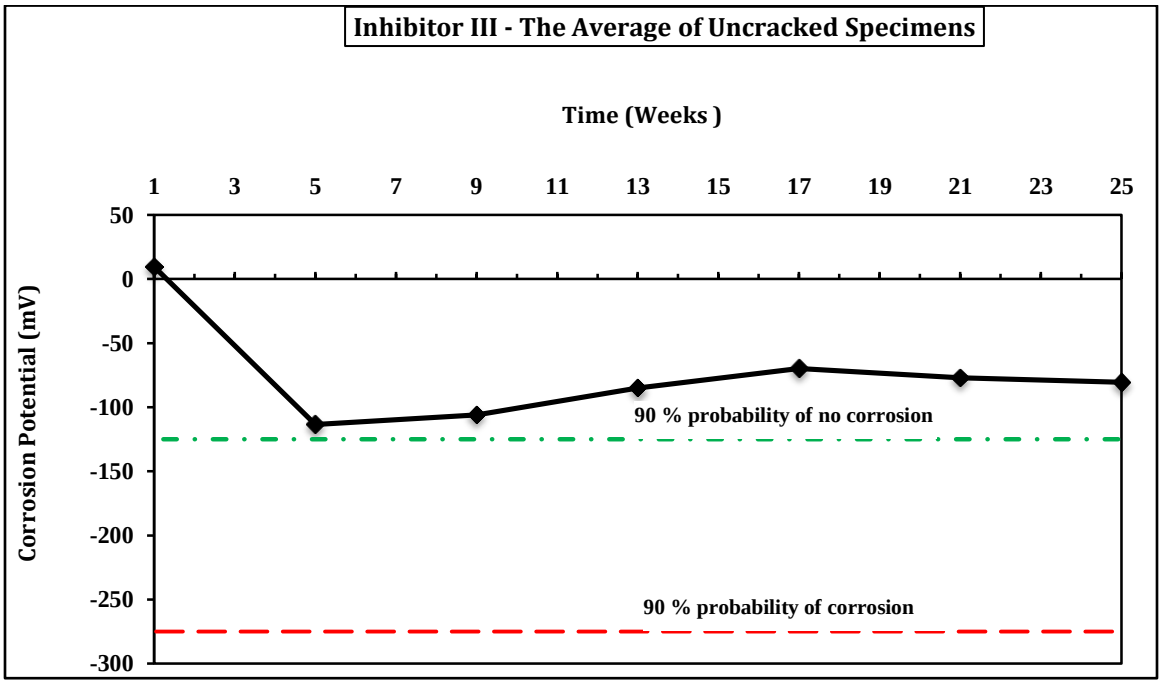


Figure 4.88: Corrosion Potential for Steel in Uncracked Concrete Specimens Made with Inhibitor III

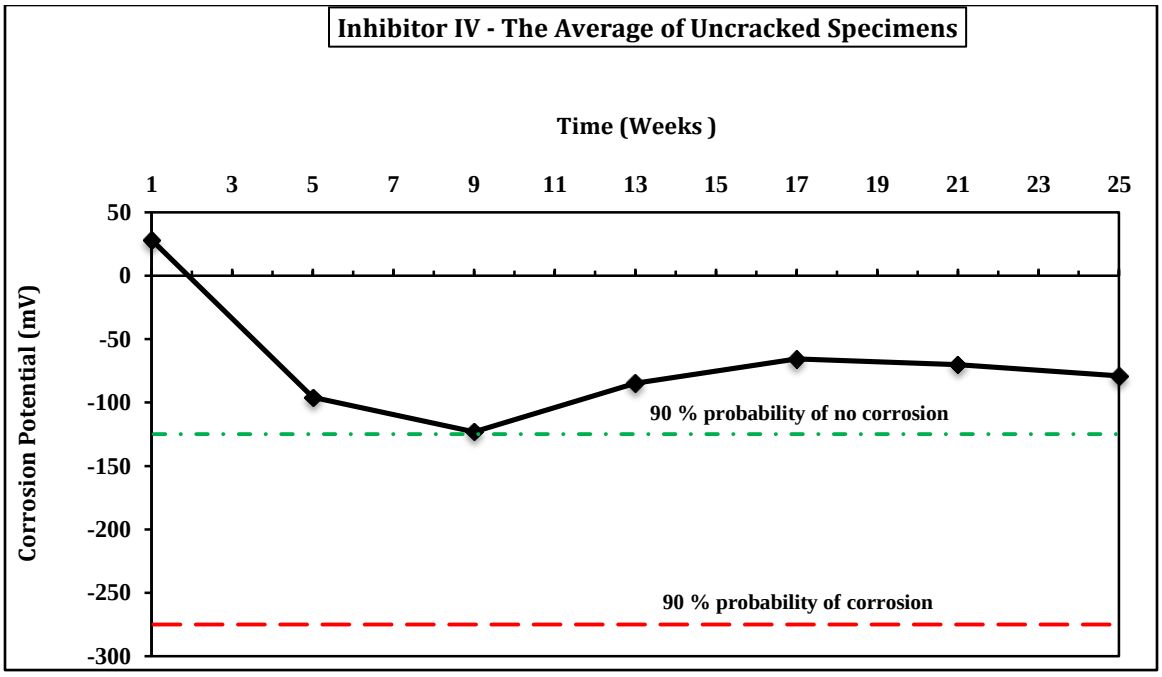


Figure 4.89: Corrosion Potential for Steel in Uncracked Concrete Specimens Made with Inhibitor IV

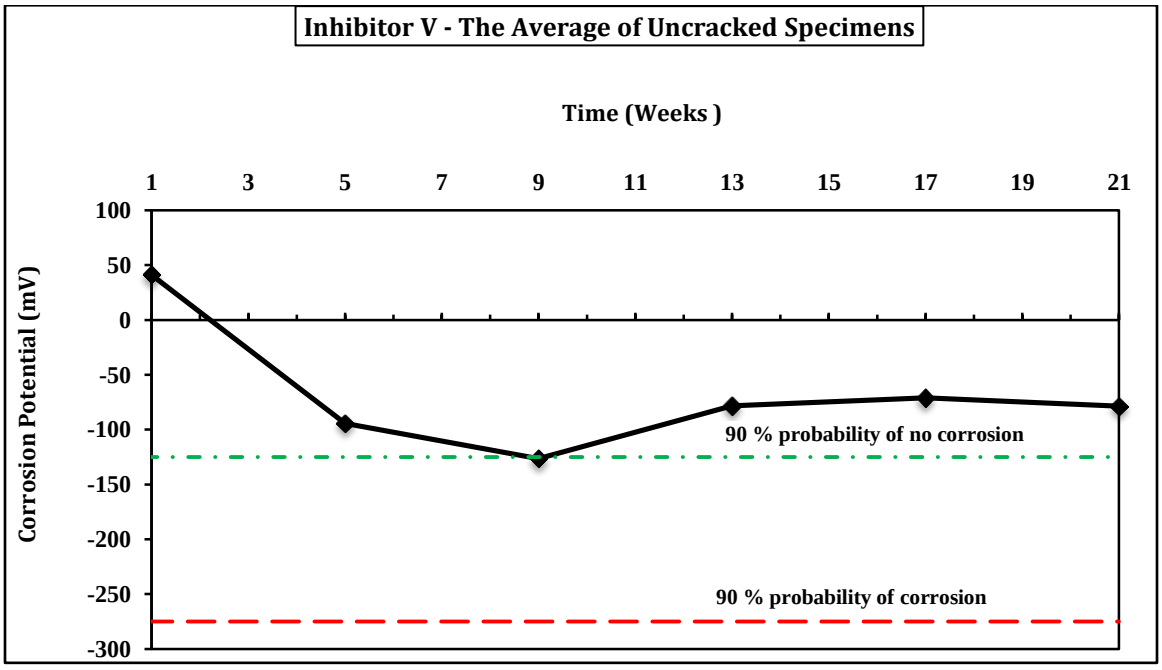


Figure 4.90: Corrosion Potential for Steel in Uncracked Concrete Specimens Made with Inhibitor V.

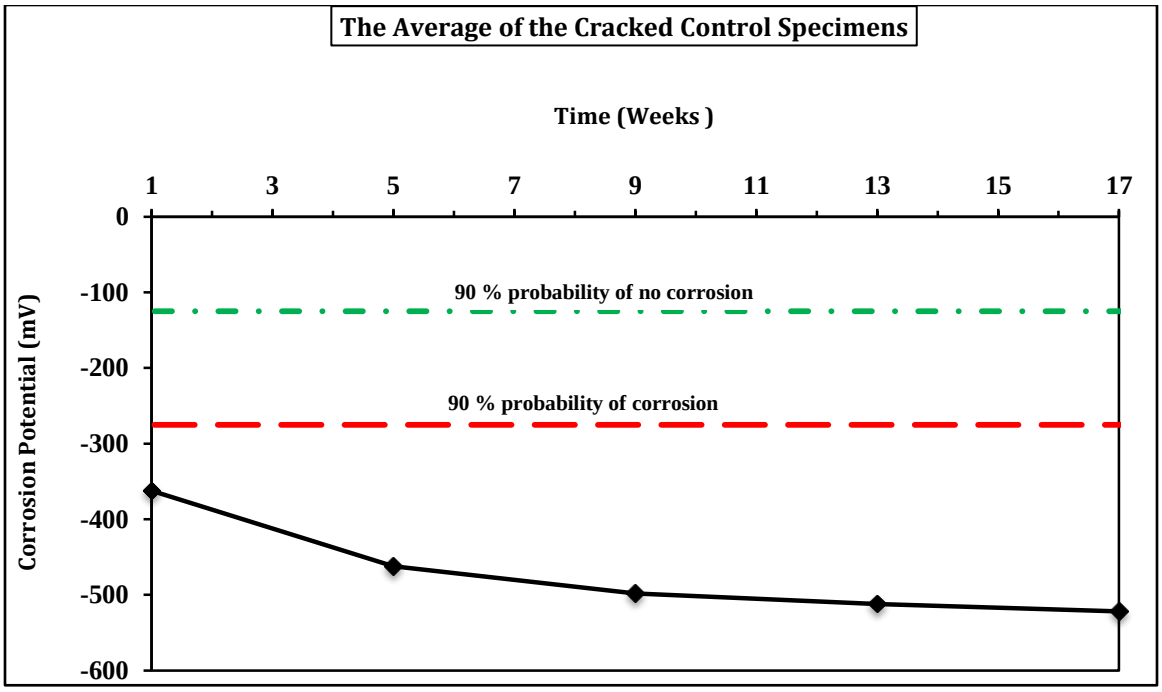


Figure 4.91: Corrosion Potential for Steel in Control Cracked Concrete Specimens

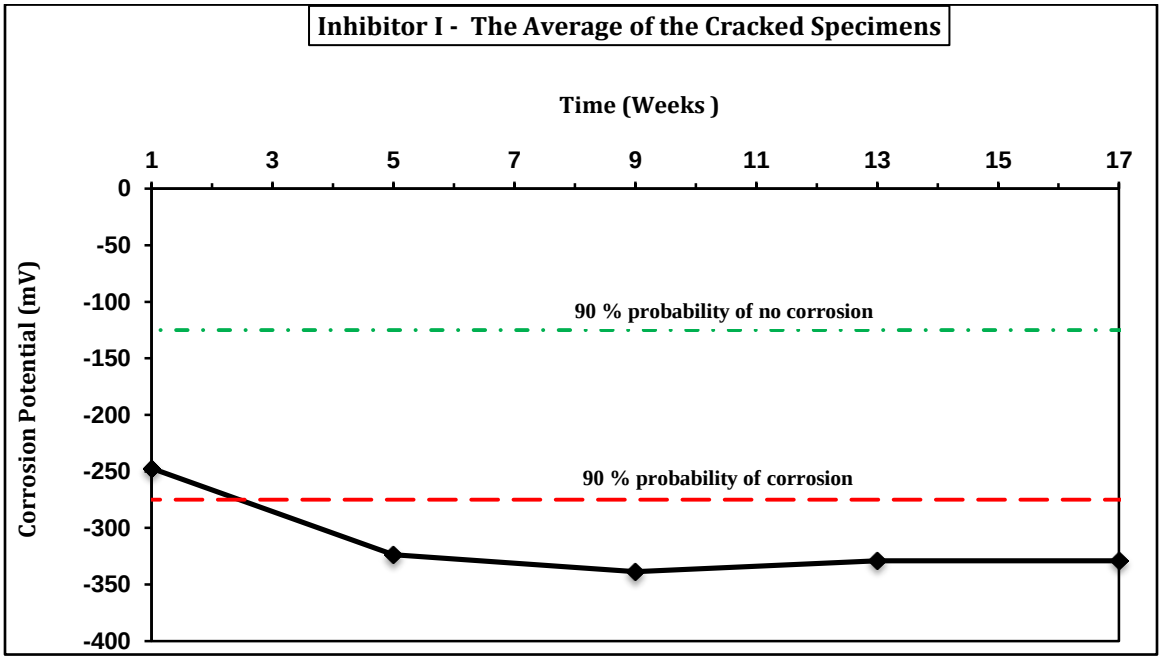


Figure 4.92: Corrosion Potential for Steel in Cracked Concrete Specimens Made with Inhibitor I

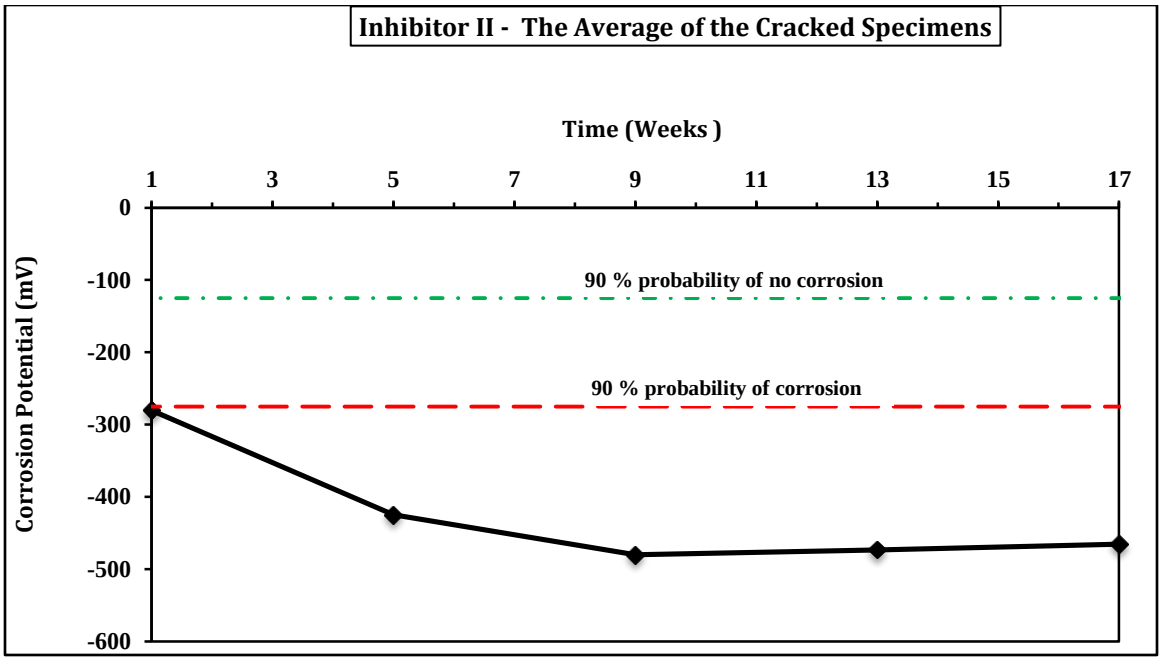


Figure 4.93: Corrosion potential for steel in cracked concrete specimens made with Inhibitor II.

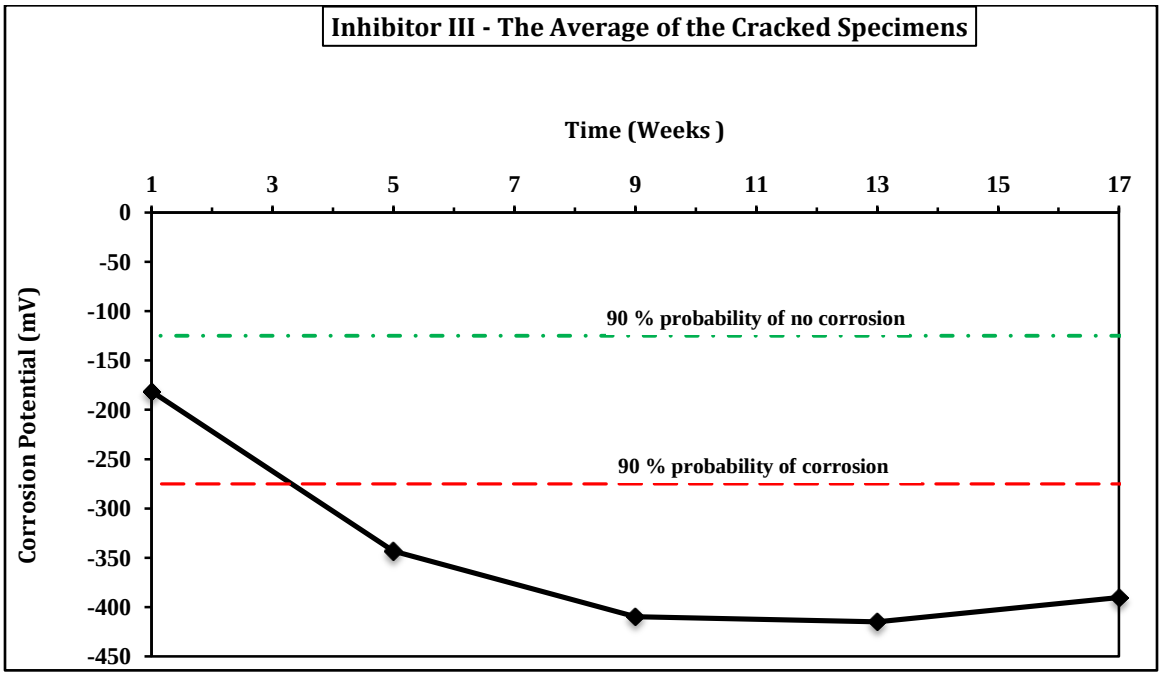


Figure 4.94: Corrosion Potential for Steel in Cracked Concrete Specimens Made with Inhibitor III

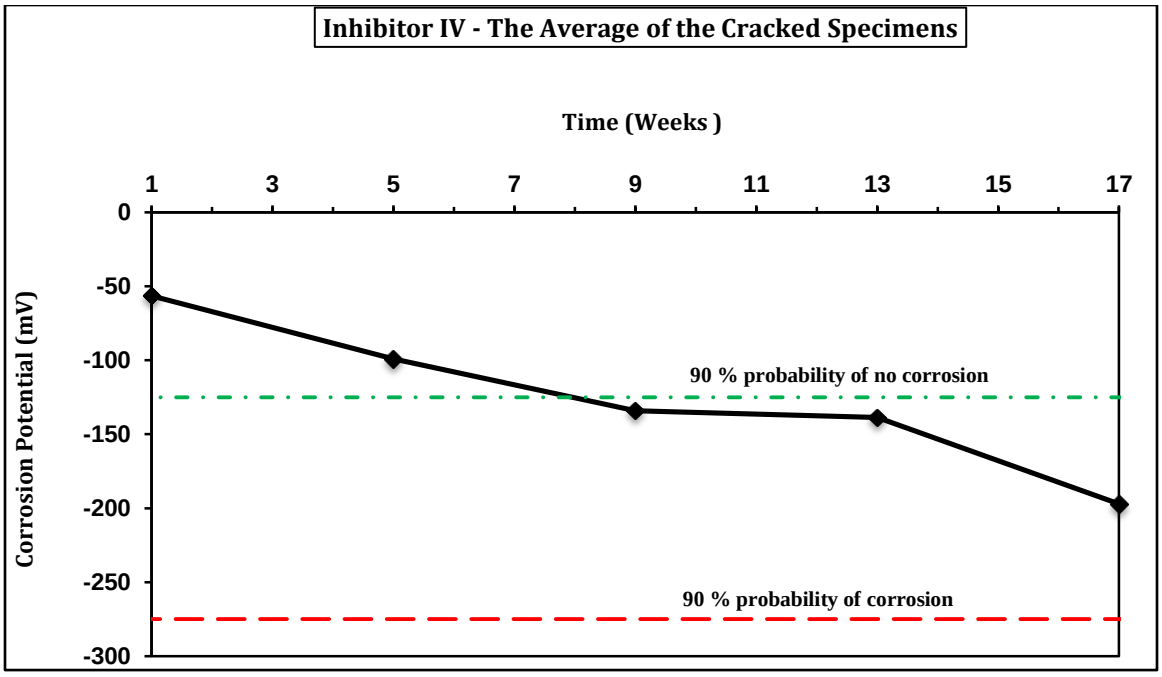


Figure 4.95: Corrosion Potential for Steel in Cracked Concrete Specimens Made with Inhibitor IV

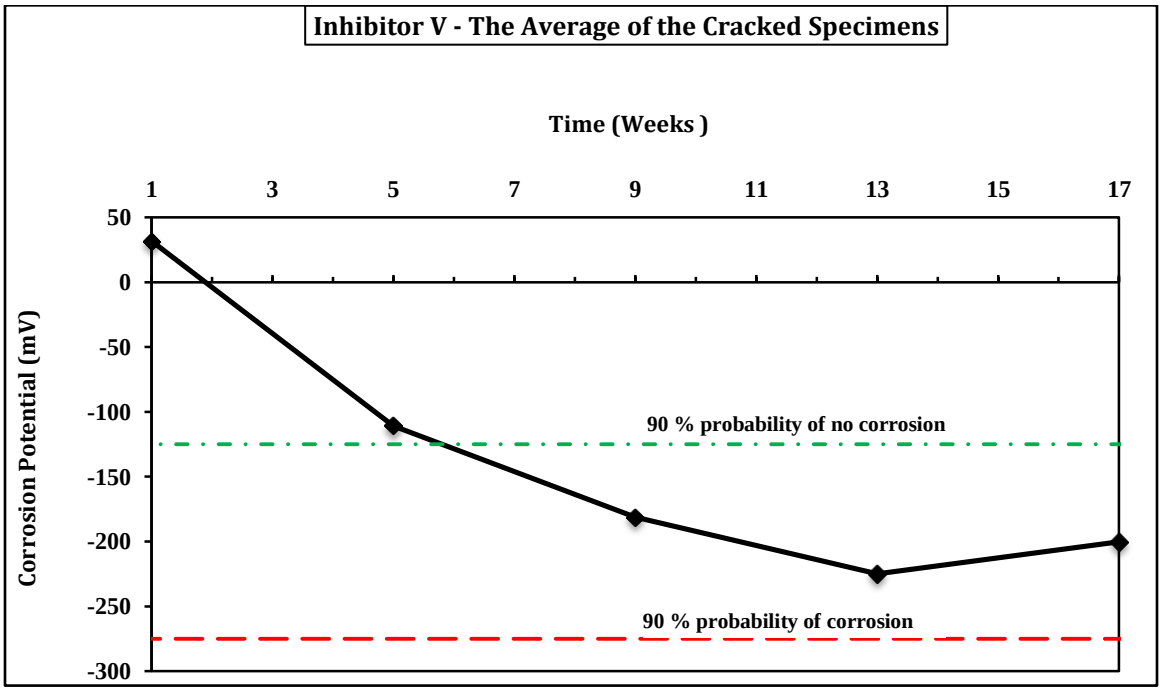


Figure 4.96: Corrosion Potential for Steel in Cracked Concrete Specimens Made with Inhibitor V

Figure 4.97 illustrates the comparison of average corrosion potential for uncracked concrete specimens. The data in this Figure show that only uncracked control concrete specimens pass the limit value of -270 mV after 12 cycles of wetting and drying. However, specimens made with inhibitors showed corrosion potential values less negative than -126 mV which indicate 10 % probability of corrosion [62].

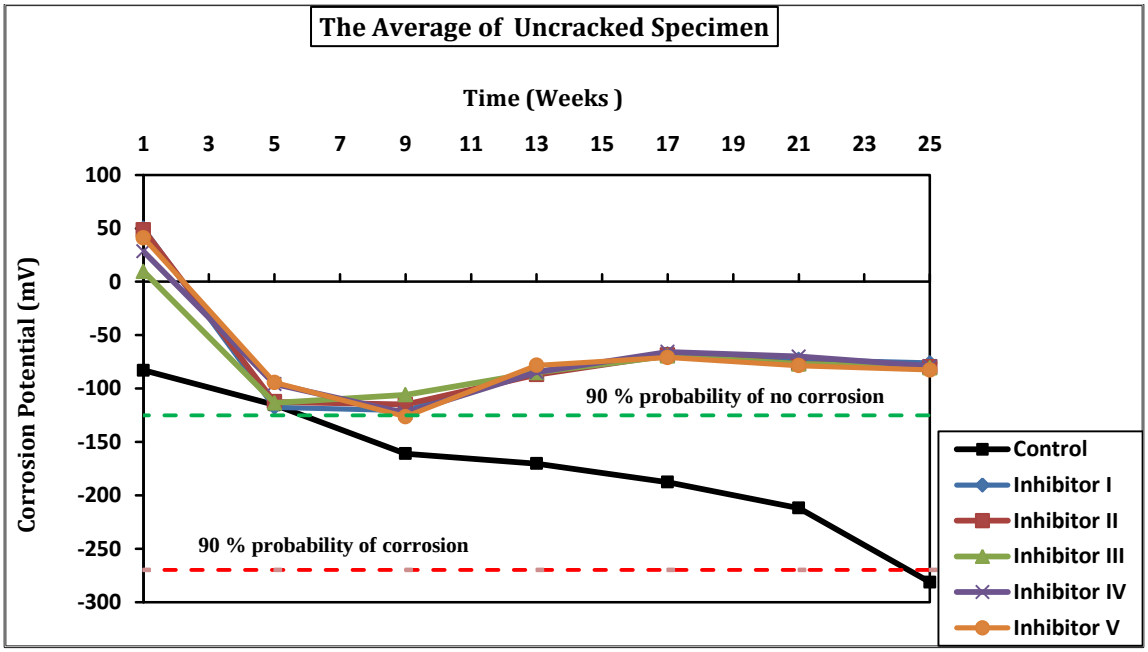


Figure 4.97: Comparison of the Average Corrosion Potential of Uncracked Specimens Made with Corrosion Inhibitors and Control Specimens

Figure 4.98 illustrates the average corrosion potential for cracked concrete specimens. It is to be noted that the specimens made with Inhibitor I, Inhibitor II and Inhibitor III showed high corrosion potential values after about nine weeks of wetting cycles while the concrete specimens made with Inhibitor V and Inhibitor IV did not reach the threshold value even 9$^{th}$ wetting cycle. This may be due to the fact that Inhibitor V and Inhibitor IV were forming a protective layer on the steel surface.

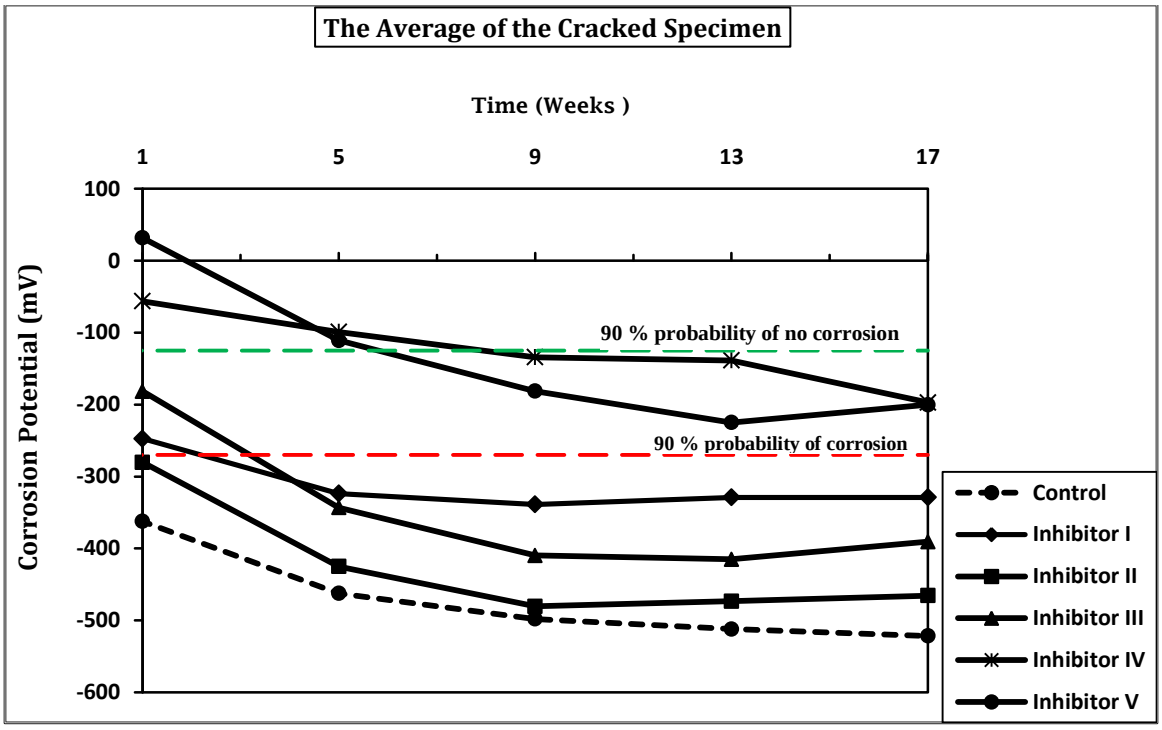


Figure 4.98: Comparison of Average Corrosion Potential of Cracked Specimens Made with Corrosion Inhibitors

Table 4.32: Corrosion Potential Data for Uncracked Control Specimens

| Date | Cycle No. | Corrosion potential (mV) SCE | | | |
|---|---|---|---|---|---|
| | | Specimen 1 | Specimen 2 | Specimen 3 | Average |
| 27/04/2013 | Starting wetting cycles | | | | |
| 04/05/2013 | one | -79 | -92 | -78 | -83.0 |
| 01/06/2013 | three | -96 | -156 | -94 | -115.3 |
| 29/06/2013 | five | -156 | -160 | -167 | -161.0 |
| 27/07/2013 | seven | -160 | -183 | -168 | -170.3 |
| 25/08/2013 | nine | -174 | -198 | -191 | -187.7 |
| 22/09/2013 | eleven | -204 | -224 | -208 | -212.0 |
| 22/10/2013 | twelve | -263 | -296 | -285 | -281.3 |

Table 4.33: Corrosion Potential Data for Uncracked Concrete Specimens Made with Inhibitor I

| Date | Cycle No. | Corrosion potential (mV) SCE | | | |
|---|---|---|---|---|---|
| | | Specimen 1 | Specimen 2 | Specimen 3 | Average |
| 27/04/2013 | Starting wetting cycles | | | | |
| 04/05/2013 | one | 59 | 43 | 48 | 50 |
| 01/06/2013 | three | -113 | -119 | -120 | -118 |
| 29/06/2013 | five | -117 | -121 | -124 | -121 |
| 27/07/2013 | seven | -86 | -92 | -74 | -84 |
| 25/08/2013 | nine | -65 | -70 | -68 | -68 |
| 22/09/2013 | eleven | -69 | -73 | -77 | -73 |
| 22/10/2013 | twelve | -72 | -77 | -79 | -76 |

Table 4.34: Corrosion Potential Data for Uncracked Concrete Specimens Made with Inhibitor II

| Date | Cycle No. | Corrosion potential (mV) SCE | | | |
|---|---|---|---|---|---|
| | | Specimen 1 | Specimen 2 | Specimen 3 | Average |
| 27/04/2013 | Starting wetting cycles | | | | |
| 04/05/2013 | one | 51 | 38 | 57 | 49 |
| 01/06/2013 | three | -119 | -113 | -105 | -113 |
| 29/06/2013 | five | -121 | -116 | -108 | -115 |
| 27/07/2013 | seven | -94 | -87 | -80 | -87 |
| 25/08/2013 | nine | -77 | -69 | -60 | -69 |
| 22/09/2013 | eleven | -87 | -74 | -69 | -77 |
| 22/10/2013 | twelve | -91 | -75 | -73 | -80 |

Table 4.35: Corrosion Potential Data for Uncracked Concrete Specimens Made with Inhibitor III

| Date | Cycle No. | Corrosion potential (mV) SCE | | | |
|---|---|---|---|---|---|
| | | Specimen 1 | Specimen 2 | Specimen 3 | Average |
| 27/04/2013 | Starting wetting cycles | | | | |
| 04/05/2013 | one | 22 | 2 | 5 | 10 |
| 01/06/2013 | three | -107 | -116 | -117 | -113 |
| 29/06/2013 | five | -109 | -106 | -103 | -106 |
| 27/07/2013 | seven | -76 | -89 | -90 | -85 |
| 25/08/2013 | nine | -62 | -70 | -77 | -70 |
| 22/09/2013 | eleven | -72 | -79 | -79 | -77 |
| 22/10/2013 | twelve | -77 | -82 | -82 | -81 |

Table 4.36: Corrosion Potential Data for Uncracked Concrete Specimens Made with Inhibitor IV

| Date | Cycle No. | Corrosion potential (mV) SCE | | | |
|---|---|---|---|---|---|
| | | Specimen 1 | Specimen 2 | Specimen 3 | Average |
| 27/04/2013 | Starting wetting cycles | | | | |
| 04/05/2013 | one | 20 | 31 | 34 | 28 |
| 01/06/2013 | three | -101 | -90 | -97 | -96 |
| 29/06/2013 | five | -125 | -123 | -121 | -123 |
| 27/07/2013 | seven | -92 | -78 | -84 | -85 |
| 25/08/2013 | nine | -71 | -66 | -60 | -66 |
| 22/09/2013 | eleven | -76 | -71 | -64 | -70 |
| 22/10/2013 | twelve | -85 | -79 | -73 | -79 |

Table 4.37: Corrosion Potential Data for Uncracked Concrete Specimens Made with Inhibitor V

| Date | Cycle No. | Corrosion potential (mV) SCE | | | |
|---|---|---|---|---|---|
| | | Specimen 1 | Specimen 2 | Specimen 3 | Average |
| 27/04/2013 | Starting wetting cycles | | | | |
| 04/05/2013 | one | 41 | 50 | 32 | 41 |
| 01/06/2013 | three | -91 | -88 | -104 | -94 |
| 29/06/2013 | five | -124 | -120 | -135 | -126 |
| 27/07/2013 | seven | -74 | -81 | -80 | -78 |
| 25/08/2013 | nine | -70 | -62 | -82 | -71 |
| 22/09/2013 | eleven | -77 | -69 | -89 | -79 |
| 22/10/2013 | twelve | -81 | -73 | -94 | -83 |

Table 4.38: Corrosion Potential Data for Cracked Control Specimens

| Date | Cycle No. | Corrosion potential (mV) SCE | | | |
|---|---|---|---|---|---|
| | | Specimen 1 | Specimen 2 | Specimen 3 | Average |
| 27/04/2013 | Starting wetting cycles | | | | |
| 04/05/2013 | one | -345 | -317 | -425 | -362.33 |
| 01/06/2013 | three | -498 | -394 | -495 | -462.33 |
| 29/06/2013 | five | -504.2 | -477 | -513 | -498.07 |
| 27/07/2013 | seven | -512 | -503 | -521 | -512 |
| 25/08/2013 | nine | -521 | -515 | -529 | -521.67 |

Table 4.39: Corrosion Potential Data for Cracked Concrete Specimens Made with Inhibitor I

| Date | Cycle No. | Corrosion potential (mV) SCE | | | |
|---|---|---|---|---|---|
| | | Specimen 1 | Specimen 2 | Specimen 3 | Average |
| 27/04/2013 | Starting wetting cycles | | | | |
| 04/05/2013 | one | -308 | -250 | -184 | -247 |
| 01/06/2013 | three | -389 | -336 | -246 | -324 |
| 29/06/2013 | five | -366 | -385 | -266 | -339 |
| 27/07/2013 | seven | -388 | -308 | -291 | -329 |
| 25/08/2013 | nine | -420 | -256 | -311 | -329 |

Table 4.40: Corrosion Potential Data for Cracked Concrete Specimens Made with Inhibitor II

| Date | Cycle No. | Corrosion potential (mV) SCE | | | |
|---|---|---|---|---|---|
| | | Specimen 1 | Specimen 2 | Specimen 3 | Average |
| 27/04/2013 | Starting wetting cycles | | | | |
| 04/05/2013 | one | -259 | -322 | -260 | -185 |
| 01/06/2013 | three | -430 | -417 | -428 | -425 |
| 29/06/2013 | five | -491 | -517 | -433 | -480 |
| 27/07/2013 | seven | -479 | -525 | -416 | -473 |
| 25/08/2013 | nine | -502 | -495 | -400 | -466 |

Table 4.41: Corrosion Potential Data for Cracked Concrete Specimens Made with Inhibitor III

| Date | Cycle No. | Corrosion potential (mV) SCE | | | |
|---|---|---|---|---|---|
| | | Specimen 1 | Specimen 2 | Specimen 3 | Average |
| 27/04/2013 | Starting wetting cycles | | | | |
| 04/05/2013 | one | -161 | -123 | -260 | -181 |
| 01/06/2013 | three | -349 | -239 | -441 | -343 |
| 29/06/2013 | five | -435 | -324 | -471 | -410 |
| 27/07/2013 | seven | -403 | -384 | -458 | -415 |
| 25/08/2013 | nine | -406 | -367 | -399 | -391 |

Table 4.42: Corrosion Potential Data for Cracked Concrete Specimens Made with Inhibitor IV

| Date | Cycle No. | Corrosion potential (mV) SCE | | | |
|---|---|---|---|---|---|
| | | Specimen 1 | Specimen 2 | Specimen 3 | Average |
| 27/04/2013 | Starting wetting cycles | | | | |
| 04/05/2013 | one | -49 | -85 | -35 | -56 |
| 01/06/2013 | three | -78 | -127 | -92 | -99 |
| 29/06/2013 | five | -114 | -182 | -106 | -134 |
| 27/07/2013 | seven | -104 | -214 | -98 | -139 |
| 25/08/2013 | nine | -153 | -288 | -151 | -197 |

Table 4.43: Corrosion Potential Data for Cracked Concrete Specimens Made with Inhibitor V

| Date | Cycle No. | Corrosion potential (mV) SCE | | | |
|---|---|---|---|---|---|
| | | Specimen 1 | Specimen 2 | Specimen 3 | Average |
| 27/04/2013 | Starting wetting cycles | | | | |
| 04/05/2013 | one | 35 | 38 | 22 | 32 |
| 01/06/2013 | three | -107 | -122 | -103 | -111 |
| 29/06/2013 | five | -219 | -176 | -149 | -181 |
| 27/07/2013 | seven | -285 | -162 | -228 | -225 |
| 25/08/2013 | nine | -251 | -194 | -156 | -200 |

### 4.8.4 Chemical Analysis for Free Chloride Contents

After 12 cyclic exposures to 3% NaCl solution, the chloride content at the steel level in ASTM G 109 cracked and uncracked specimens was measured. Table 4.44 summarizes the chloride content at the bar level for all ASTM G 109 specimens. The control concrete specimen had the highest diffused chloride, based on water-soluble chloride content at the

bar level (25 mm depth) of 0.75% by weight of cement. The chloride content for the control specimens as well as the specimens which were made with corrosion inhibitors was more than the minimum threshold value of 0.15%. However, the chloride concentration in the concrete specimens with Inhibitor V was less than 0.15% by weight of cement. That is might be due to Inhibitor V ability to reduce the permeability of the concrete. Furthermore, the chloride concentration in the concrete specimens with all the inhibitors was less than that in the control concrete specimens. This indicates that the investigated inhibitors were effective in binding the chlorides.

Table 4.44: Chloride Content at the Bar Level

| Specimen Type | Inhibitor | Chloride Concentration (% by Weight of Cement) |
|---|---|---|
| Uncracked | Control | 0.747 |
| Uncracked | Inhibitor I | 0.1996 |
| Uncracked | Inhibitor II | 0.293 |
| Uncracked | Inhibitor III | 0.261 |
| Uncracked | Inhibitor IV | 0.230 |
| Uncracked | Inhibitor V | 0.1096 |
| Cracked | Control | 1.330 |
| Cracked | Inhibitor I | 1.017 |
| Cracked | Inhibitor II | 1.258 |
| Cracked | Inhibitor III | 1.052 |
| Cracked | Inhibitor IV | 0.983 |
| Cracked | Inhibitor V | 0.814 |

### 4.8.5 Visual Examination of Steel

At the end of the exposure period, the concrete specimens were broken and the anodic steel was visually inspected and photographed.

#### 4.4.5.1 Uncracked Control Specimen

The inspection of the top bar of the steel bar in the uncracked control specimen (photo 4.1) shows extensive corrosion at the ends of the bar. Also, marginal general corrosion was noted at the middle of the bar. The maximum average macro-cell current reading was 2.247 µA which indicates that the specimens has not yet reached the failure threshold of 10 µA and the half-cell potential readings were in the range of 90% probability of corrosion.

Photo 4.1: Steel in Uncracked Control Specimen

#### 4.4.5.2 Uncracked Concrete Specimen incorporating Inhibitor I

The condition of this specimen is shown in Photo 4.2. Small areas of corrosion on the top ribs and at the ends of the exposure area of the anodic bar (the top bar) were noted. This specimen revealed initiation of corrosion but not yet at a critical point. This specimen was removed after six months (12 cycles) and both the maximum average macro-cell and potential readings fell into the lower ranges 0.223 µA and -121 mV respectively. The

measured macro-cell current was less than 2 μA and the half-cell potential values indicated a 10% probability of corrosion.

Photo 4.2: Steel in Uncracked Concrete Specimen with Inhibitor I

#### 4.4.5.3 Uncracked Concrete Specimen Incorporating Inhibitor II

The condition of the steel bar in the concrete specimen incorporating Inhibitor II is shown in Photo 4.3. Corrosion spots and pits on the edges of the top of the anodic bar were noted. This specimen revealed initiation of corrosion but not yet at a critical point. This specimen was removed after six months (12 cycles) and both the maximum average macro-cell and potential readings fell into the lower ranges 0.250 μA and -115 mV respectively. The measured macro-cell current was less than 2 μA and the half-cell potential values indicated a 10% probability of corrosion.

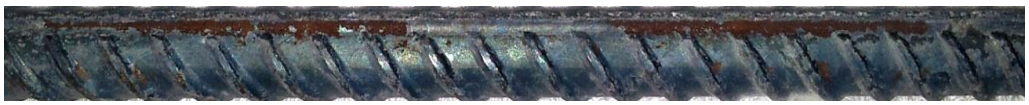

Photo 4.3: Steel Bar in Uncracked Specimen Incorporating Inhibitor II

#### 4.4.5.4 Uncracked Concrete Specimen Incorporating Inhibitor III

The steel in concrete with Inhibitor III is shown in Photo 4.4. The top side of the anodic bar showed marginal general corrosion on the top side of the bar as well as tiny spots of corrosion were noted on the top ribs. This specimen revealed marginal initiation of corrosion on the ribs but it has not yet been in a critical point. This specimen was

removed after six months (12 cycles) and both the maximum average macro-cell and potential readings fell into the lower ranges 0.260 μA and -113 mV respectively. The measured macro-cell current was less than 2 μA and the half-cell potential values indicated a 10% probability of corrosion.

Photo 4.4: Steel Bar in Uncracked Specimen Incorporating Inhibitor III

#### 4.4.5.5 Uncracked Concrete Specimen Incorporating Inhibitor IV

The steel bar in the concrete incorporating Inhibitor IV is shown in Photo 4.5. Localized corrosion at one end of the bar was noted. The specimen revealed initiation of corrosion but it has not yet been at a critical point. This specimen was removed after six months (12 cycles) and both the maximum average macro-cell and potential readings fell into the lower ranges 0.267 μA and -123 mV respectively. The measured macro-cell current was less than 2 μA and the half-cell potential values indicated a 10% probability of corrosion.

Photo 4.5: Steel Bar in Uncracked Specimen Incorporating Inhibitor IV

#### 4.4.5.6 Uncracked Concrete Specimen Incorporating Inhibitor V

The steel bar in the concrete incorporating Inhibitor V is shown in Photo 4.6. Tiny spots of corrosion were noted on the top ribs. This specimen was removed after six months (12 cycles) and both the maximum average macro-cell and potential readings fell into the lower ranges 0.152 μA and -126 mV respectively. The measured macro-cell current was less than 2 μA and the half-cell potential values indicated a 10% probability of corrosion.

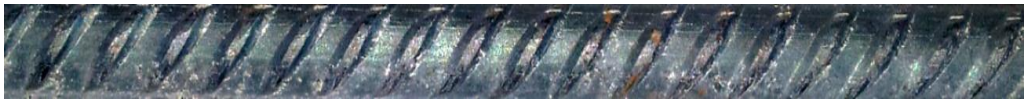

Photo 4.6: Steel Bar in Uncracked Specimen Incorporating Inhibitor V

#### 4.4.5.7 Crcked Control Specimen

The steel in cracked control specimen had extensive corrosion along the top side of the anodic bar (the top bar). The inspection of the top bar (photo 4.7) shows multiple pits distributed along the top side of the anodic bar. Also, the top bar was almost completely covered in corrosion for the full length of the bar. The average macro-cell current readings revealed the specimens passed the threshold and the half-cell potential readings were in the range of severe corrosion.

Photo 4.7: Steel in Cracked Control Specimen

#### 4.4.5.8 Cracked Concrete Specimen Incorporating Inhibitor I

The steel bar in the concrete incorporating Inhibitor I is shown in Photo 4.8. Extensive corrosion at the ends of the bar was noted. Also, slight general corrosion was noted at the middle of the bar. The maximum average current was 15.24 μA which is more than 10 μA and the maximum half-cell potential reading was -339 mV which fells into the 90% probability of corrosion.

Photo 4.8: Steel Bar in Cracked Specimen Incorporating Inhibitor I

#### 4.4.5.9 Cracked Concrete Specimen Incorporating Inhibitor II

The steel bar in the concrete incorporating Inhibitor II is shown in Photo 4.9. Extensive corrosion at the ends of the exposure area of the top bar is noted. Also, slight general corrosion was observed at the middle of the bar. The maximum average current was 22.72 μA which is more than 10 μA and the maximum half-cell potential reading was -480 mV which indicates sever corrosion.

Photo 4.9: Steel Bar in Cracked Specimen Incorporating Inhibitor II

#### 4.4.5.10 Cracked Concrete Specimen Incorporating Inhibitor III

The steel bar in the concrete incorporating Inhibitor III is shown in Photo 4.10. The top side of the anodic bar was almost completely covered with slight general corrosion. This specimen revealed initiation of corrosion. The maximum average current was 14.32 µA which is more than 10 µA and the maximum half-cell potential reading was -415 mV which fells into the 90% probability of corrosion.

Photo 4.10: Steel Bar in Cracked Specimen Incorporating Inhibitor III

#### 4.4.5.11 Cracked Concrete Specimen Incorporating Inhibitor IV

The steel bar in the concrete incorporating Inhibitor IV is shown in Photo 4.11. Localized corrosion at different points of the bar was noted. The maximum average current was 2.89 µA which is less than 10 µA and the maximum half-cell potential reading was -197 mV which fells into corrosion activity uncertain.

Photo 4.11: Steel Bar in Cracked Specimen Incorporating Inhibitor IV

#### 4.4.5.12 Cracked Concrete Specimen Incorporating Inhibitor V

The steel bar in the concrete incorporating Inhibitor V is shown in Photo 4.12. Tiny spots of corrosion were noted on the top ribs. This specimen was removed after six months

(12 cycles) and both the macro-cell and potential fell into the lower range. The maximum average current was 1.29 μA which is less than 10 μA and the maximum half-cell potential reading was -225 mV which fells into corrosion activity uncertain.

Photo 4.12: Steel Bar in Cracked Specimen Incorporating Inhibitor V

From the data in Table 4.45 and 4.46, it can be seen that Inhibitor V and Inhibitor I are the best performers in uncracked specimens whereas Inhibitor V and Inhibitor IV are the best in cracked specimens, though the differences in the overall performance of the used corrosion inhibitors in uncracked specimens are not that significant.

Table 4.45: Summery Results of Evaluation for Uncracked Specimens

| **Test Method (ASTM G 109)** | **Inhibitor I** | **Inhibitor II** | **Inhibitor III** | **Inhibitor IV** | **Inhibitor V** | **Control** |
|---|---|---|---|---|---|---|
| Average Total Integrated Current (Coulombs) | 2.32 | 2.57 | 2.52 | 2.51 | 1.79 | 8.50 |
| Corrosion Potential (maximum value) mV | -121 | -115 | -113 | -123 | -126 | -281.3 |
| Chloride Concentration (%by weight of cement) | 0.1996 | 0.293 | 0.261 | 0.230 | 0.1096 | 0.747 |
| (Corroded area %) by Visual Inspection | 5 | 8 | 5 | 5 | 5 | 45 |

Table 4.46: Summery Results of Evaluation for Cracked Specimens

| Test Method (ASTM G 109) | Inhibitor I | Inhibitor II | Inhibitor III | Inhibitor IV | Inhibitor V | Control |
|---|---|---|---|---|---|---|
| Average Total Integrated Current (Coulombs) | 122.13 | 202.68 | 124.66 | 18.57 | 8.56 | 274.62 |
| Corrosion Potential (maximum value) mV | -339 | -480 | -415 | -197 | -224 | -521 |
| Chloride Concentration (%by weight of cement) | 1.017 | 1.258 | 1.052 | 0.983 | 0.814 | 1.330 |
| (corroded area %) by Visual Inspection | 40 | 50 | 30 | 20 | 15 | 90 |

Macro-cell current readings are used to determine the total integrated current passed during the whole period of testing whereas corrosion potential readings are used to predict the susceptibility of corrosion initiation. Further, chloride concentration at the bar level gives indication about the permeability of concrete specimens. Visual inspection of steel bars can be used to determine the corroded area and type of the corrosion (general or pitting corrosion).

### 4.8.6 Cost Evaluation

Table 4.47 shows the cost comparison of all the selected corrosion inhibitors, the costs of theses inhibitors are calculated considering the costs of corrosion inhibitors in Saudi Arabia for the years 2013 through 2014. These costs do not include delivery, fabrication

and placement in the concrete mix. All costs are expressed in Saudi riyal per cubic meter of concrete.

The cost per cubic meter of concrete per year based on the time to reach 10 µA is summarized in Table 4.47. From these data (Table 4.47) it is clear that inhibitor V has the lowest cost of 9 SR/$m^3$ of concrete, followed by Inhibitor II, inhibitor I and Inhibitor III whereas inhibitor IV has the highest cost of 15.7 SR/ $m^3$. However, the cost of concrete with Inhibitor IV is still less than that of control specimens which is SR 43.3.

Table 4.47: The Estimated Cost for One Cubic Meter of Concrete per Year

| **Inhibitor** | **Dosage ($l/m^3$)** | **Cost per Litter (SR)** | **Cost/$m^3$ of concrete (SR)** | **Estimated time to reach 10 µA(years)** | **Cost per year (SR)** |
|---|---|---|---|---|---|
| None (control) | - | - | 200 | 4.62 | 43.3 |
| Inhibitor I | 15 | 5 | 275 | 27.31 | 10.1 |
| Inhibitor II | 15 | 3.1 | 246.5 | 24.81 | 9.9 |
| Inhibitor III | 0.6 | 55 | 233 | 21.03 | 11.1 |
| Inhibitor IV | 15 | 12.5 | 287.5 | 18.27 | 15.7 |
| Inhibitor V | 15 | 5 | 275 | 30.41 | 9.0 |

# CHAPTER 5

# CONCLUSIONS AND RECOMMENDATIONS

## 5.1 Conclusions

This investigation was conduct to evaluate the performance of different types of corrosion inhibitors in retarding reinforcement corrosion. Based on the experimental results developed in this investigation, the following conclusions could be drawn:

1. Potentio-dynamic curves (PDCs) for mild steel specimens placed in simulated concrete pore solution (SCPS) without any corrosion inhibitor and contaminated with 1000 or 1500 ppm exhibited general corrosion for all exposure temperatures. Steel specimens exposed to chloride concentration of 2000 ppm and temperatures of 25, 40 °C also exhibited general corrosion. However, when the temperature of the SCPS increased to 55 °C, pitting corrosion was observed.
2. PDCs for steel in all the investigated corrosion inhibitors indicated general corrosion and they were efficient in minimizing pitting corrosion and decreasing the rate of corrosion. The efficiency of the selected inhibitors in reducing corrosion current ranges from 45 to 94 % depending on inhibitor type, chloride concentration and exposure temperature.
3. An increase in temperature and/or chloride concentration increased the corrosion current density as well as the corrosion rate. This increase was low for exposure temperatures of 25 and 40 °C. However, this increase was significant when the exposure temperature was increased to 55 °C.

4. The presence of chloride and sulfate at elevated temperature conditions, simulation the exposure conditions in Saudi Arabia, can significantly accelerate the steel corrosion in alkaline media, as in concrete.
5. Corrosion current density and corrosion rate of steel specimens immersed in SCPS incorporating selected inhibitors were increased by two to three times with the increase in the sulfate concentration from 0 to 2,000 ppm.
6. The PDP curves showed that an increase in the sulfate concentration from 0 to 2000 ppm significantly increased the anodic dissolution at low potential levels.
7. The efficiency of all the selected corrosion inhibitors decreased with an increase in the sulfate concentration from 0 to 2000 ppm.
8. Among the inhibitors investigated, the performance of Inhibitor I, Inhibitor V, Inhibitor II and Inhibitor III was better than that of Inhibitor IVwhen exposed to high temperature.
9. PDP curves showed that the current required for transition from cathodic to anodic polarization decreased with an increase in the temperature. This indicates a decrease in the polarization resistance of the solution and acceleration in the corrosion process.
10. The total corrosion current in an uncracked concrete specimens with the selected corrosion inhibitors was three to four times less than that in the control concrete specimens.
11. Inhibitor I, Inhibitor II and Inhibitor III provided limited protection to reinforcing steel in cracked concrete specimens. However, Inhibitor IV and Inhibitor V provided better protection to reinforcing steel in the cracked specimens.

12. The measured corrosion potential of all the uncracked concrete specimens incorporating the selected inhibitors was approximately the same, less negative than –126 mV SCE, which indicates less than 10% probability of corrosion. However, the corrosion potential of uncracked control specimens was more negative than -270 mV SCE, which indicates 90% probability of corrosion.
13. The corrosion potential for cracked concrete specimens incorporating Inhibitor I and Inhibitor III was more negative than -270 mV SCE, which indicates more than 90% probability of corrosion. However, the corrosion potential of cracked control specimens and specimens incorporating Inhibitor II was more negative than -426 mV SCE, which indicates severe corrosion. The corrosion potential for cracked specimens incorporating Inhibitor V and Inhibitor IV was in the range of uncertain corrosion.
14. The chloride content at the level of the top bar for both uncracked and cracked specimens was more the threshold limits. However, it was less than the threshold limits in the uncracked concrete specimens incorporating Inhibitor V.
15. The chloride content at the level of the top bar level did not show a strong correlation with the corrosion observed in the uncracked specimens.

## 5.2 Recommendations

Many specific recommendations have been noticed during the course of this study. Recommendations are divided into two parts: The first part of the recommendation is for the continuation of the existing study; while the second one identifies the specific ideas for future applications (i.e. studies).

### 5.2.1 Recommendations

1. The recommended corrosion inhibitor for varying chloride and sulfate concentrations and exposure temperatures in order of priority are provided in the following table:

| Chloride Concentration (ppm) | Sulfate Concentration (ppm) | Temperature (°C) | | |
|---|---|---|---|---|
| | | 25 | 40 | 55 |
| **1000 (Low)** | 0 | All | All | All except IV |
| | 500 | | Inhibitor I, Inhibitor V , Inhibitor III, and Inhibitor II | |
| | 2000 | | Inhibitor I, Inhibitor V, Inhibitor II and Inhibitor III | |
| **1500 (moderate)** | 0 | All | All | Inhibitor I, Inhibitor II, Inhibitor V |
| | 500 | | | |
| | 2000 | | | |
| **2000 (sever)** | 0 | All | All except IV | Inhibitor II, Inhibitor I |
| | 500 | | | |
| | 2000 | | | |

2. All corrosion inhibitors performed well in the uncracked concrete specimens. However, the recommended corrosion inhibitors depending on the cost per cubic meter of concrete per year in order of priority are Inhibitor V followed by Inhibitor II, inhibitor I, Inhibitor III and Inhibitor IV.

### 5.2.2 Future Works

1. In addition to laboratory ASTM G 109 test specimens' results, it is clear that the evaluation of field applications with the five selected inhibiting admixtures would be required. The results of both the laboratory study and the field study can then be compared to determine how well they correlate and determine whether the laboratory procedure effectively simulates the field performance.
2. It may be useful to evaluate the performance of corrosion inhibitors when used in conjunction with other concrete admixtures, such as slag cement, fiber reinforcement, and pozzolans which are becoming more common these days.
3. The effect of crack width and type on the performance of corrosion inhibitor should be investigated. Cracks in concrete are not of the same size, and not all types of corrosion inhibitor necessarily work well to minimize corrosion in reinforcement. Previous researches in this area are limited. Different crack types and widths were not included in this study due to the number of other variables considered. Hence, a more extensive investigation of these variables should be performed.

# APPENDICES

## APPENDIX (A)

## A. Data Interpretation Tables

Table 0A.1: Interpretation of Half-Cell (Corrosion) Potential Readings (ASTM C 876)

| Half-cell Potential (mV) | Corrosion Activity |
|---|---|
| < -426 | Sever Corrosion |
| > -270 | 90% Probability of Corrosion Occurring |
| -126 to –270 | Corrosion Activity Uncertain |
| < -125 | 90% Probability of No Corrosion Occurring |

Table A.2: Interpretation of Corrosion Rate Data (Scannell, 1997)

| $I_{corr}$ $\mu A/cm^2$ | Corrosion Condition |
|---|---|
| Less than 0.1 | Passive Condition |
| 0.1 to 0.5 | Low to Moderate Corrosion |
| 0.5 to 1.0 | Moderate to High Corrosion |
| Greater than 1.0 | High Corrosion |

Table A.3: Water-Soluble Chloride-Ion Limits in ACI 318-9

| Type of member | Maximum water-soluble chloride ion ($Cl^-$) content in concrete, percent by weight of cement |
|---|---|
| Prestressed concrete | 0.06 |
| Reinforced concrete exposed to chloride in service | 0.15 |
| Reinforced concrete that will be dry or protected from moisture in service | 1 |
| Other reinforced concrete construction | 0.3 |

# APPENDIX (B)

## RECORD OF ALL READINGS FOR ASTM G109

### B. 1 Macro-cell Readings for Uncracked ASTM G109 Specimens

Table B.1: Macro-Cell Current for Uncracked Control Specimen (1)

| Date | Cycle No. | Condition Wet/Dry | Specimen 1 | | | |
|---|---|---|---|---|---|---|
| | | | Resistor (Ohms) | Voltage (mV) | Current (µA) | Total Corrosion (Coulombs) |
| 27/04/2013 | Starting of wetting cycles | | | | | |
| 04/05/2013 | 1 | wet | 100 | 0.008 | 0.08 | 0.02 |
| 01/06/2013 | 3 | wet | 100 | 0.012 | 0.12 | 0.27 |
| 29/06/2013 | 5 | wet | 100 | 0.010 | 0.10 | 0.53 |
| 27/07/2013 | 7 | wet | 100 | 0.010 | 0.10 | 0.77 |
| 25/08/2013 | 9 | wet | 100 | 0.012 | 0.12 | 1.05 |
| 22/09/2013 | 11 | wet | 100 | 0.013 | 0.13 | 1.35 |
| 22/10/2013 | 13 | wet | 100 | 0.185 | 1.85 | 3.92 |

Table B.2: Macro-Cell Current for Uncracked Control Specimen (2)

| Date | Cycle No. | Condition Wet/Dry | Specimen 2 | | | |
|---|---|---|---|---|---|---|
| | | | Resistor (Ohms) | Voltage (mV) | Current (µA) | Total Corrosion (Coulombs) |
| 27/04/2013 | Starting of wetting cycles | | | | | |
| 04/05/2013 | 1 | wet | 100 | 0.008 | 0.08 | 0.02 |
| 01/06/2013 | 3 | wet | 100 | 0.021 | 0.21 | 0.37 |
| 29/06/2013 | 5 | wet | 100 | 0.013 | 0.13 | 0.79 |
| 27/07/2013 | 7 | wet | 100 | 0.028 | 0.28 | 1.28 |
| 25/08/2013 | 9 | wet | 100 | 0.187 | 1.87 | 3.98 |
| 22/09/2013 | 11 | wet | 100 | 0.238 | 2.38 | 9.12 |
| 22/10/2013 | 13 | wet | 100 | 0.200 | 2.00 | 14.79 |

Table B.3: Macro-Cell Current for Uncracked Control Specimen (3)

| Date | Cycle No. | Condition Wet/Dry | Specimen 3 | | | |
|---|---|---|---|---|---|---|
| | | | Resistor (Ohms) | Voltage (mV) | Current (µA) | Total Corrosion (Coulombs) |
| 27/04/2013 | Starting of wetting cycles | | | | | |
| 04/05/2013 | 1 | wet | 100 | 0.005 | 0.05 | 0.02 |
| 01/06/2013 | 3 | wet | 100 | 0.018 | 0.18 | 0.29 |
| 29/06/2013 | 5 | wet | 100 | 0.017 | 0.17 | 0.72 |
| 27/07/2013 | 7 | wet | 100 | 0.060 | 0.60 | 1.65 |
| 25/08/2013 | 9 | wet | 100 | 0.010 | 0.10 | 2.53 |
| 22/09/2013 | 11 | wet | 100 | 0.016 | 0.16 | 2.84 |
| 22/10/2013 | 13 | wet | 100 | 0.289 | 2.89 | 6.79 |

Table B.4: Macro-Cell Current for Uncracked Concrete Specimen (1) Made with Inhibitor I

| Date | Cycle No. | Condition Wet/Dry | Specimen 1 | | | |
|---|---|---|---|---|---|---|
| | | | Resistor (Ohms) | Voltage (mV) | Current (µA) | Total Corrosion (Coulombs) |
| 27/04/2013 | Starting of wetting cycles | | | | | |
| 04/05/2013 | 1 | wet | 98.8 | 0.000 | 0.00 | 0.00 |
| 01/06/2013 | 3 | wet | 98.8 | 0.010 | 0.10 | 0.12 |
| 29/06/2013 | 5 | wet | 98.8 | 0.020 | 0.20 | 0.49 |
| 27/07/2013 | 7 | wet | 98.8 | -0.010 | 0.11 | 0.86 |
| 25/08/2013 | 9 | wet | 98.8 | -0.020 | 0.20 | 1.25 |
| 22/09/2013 | 11 | wet | 98.8 | -0.018 | 0.18 | 1.71 |
| 22/10/2013 | 13 | wet | 98.8 | -0.019 | 0.19 | 2.20 |

Table B.5: Macro-Cell Current for Uncracked Concrete Specimen (2) Made with Inhibitor I

| Date | Cycle No. | Condition Wet/Dry | Specimen 2 | | | |
|---|---|---|---|---|---|---|
| | | | Resistor (Ohms) | Voltage (mV) | Current (µA) | Total Corrosion (Coulombs) |
| 27/04/2013 | Starting of wetting cycles | | | | | 0.00 |
| 04/05/2013 | 1 | wet | 99 | 0.000 | 0.00 | 0.00 |
| 01/06/2013 | 3 | wet | 99 | 0.014 | 0.14 | 0.17 |
| 29/06/2013 | 5 | wet | 99 | 0.017 | 0.17 | 0.55 |
| 27/07/2013 | 7 | wet | 99 | -0.012 | 0.12 | 0.90 |
| 25/08/2013 | 9 | wet | 99 | -0.021 | 0.21 | 1.32 |
| 22/09/2013 | 11 | wet | 99 | -0.024 | 0.24 | 1.87 |
| 22/10/2013 | 13 | wet | 99 | -0.025 | 0.25 | 2.51 |

Table B.6: Macro-Cell Current for Uncracked Concrete Specimen (3) Made with Inhibitor I

| Date | Cycle No. | Condition Wet/Dry | Specimen 3 | | | |
|---|---|---|---|---|---|---|
| | | | Resistor (Ohms) | Voltage (mV) | Current (µA) | Total Corrosion (Coulombs) |
| 27/04/2013 | Starting of wetting cycles | | | | | 0.00 |
| 04/05/2013 | 1 | wet | 98.7 | 0.000 | 0.00 | 0.00 |
| 01/06/2013 | 3 | wet | 98.7 | 0.013 | 0.13 | 0.16 |
| 29/06/2013 | 5 | wet | 98.7 | 0.016 | 0.16 | 0.51 |
| 27/07/2013 | 7 | wet | 98.7 | -0.011 | 0.11 | 0.84 |
| 25/08/2013 | 9 | wet | 98.7 | -0.018 | 0.18 | 1.20 |
| 22/09/2013 | 11 | wet | 98.7 | -0.021 | 0.21 | 1.68 |
| 22/10/2013 | 13 | wet | 98.7 | -0.022 | 0.22 | 2.24 |

Table B.7: Macro-Cell Current for Uncracked Concrete Specimen (1) Made with Inhibitor II

| Date | Cycle No. | Condition Wet/Dry | Specimen 1 | | | |
|---|---|---|---|---|---|---|
| | | | Resistor (Ohms) | Voltage (mV) | Current (μA) | Total Corrosion (Coulombs) |
| 27/04/2013 | Starting of wetting cycles | | | | | 0.00 |
| 04/05/2013 | 1 | wet | 98.8 | 0.000 | 0.00 | 0.00 |
| 01/06/2013 | 3 | wet | 98.8 | 0.014 | 0.14 | 0.17 |
| 29/06/2013 | 5 | wet | 98.8 | 0.020 | 0.20 | 0.59 |
| 27/07/2013 | 7 | wet | 98.8 | -0.016 | 0.16 | 1.03 |
| 25/08/2013 | 9 | wet | 98.8 | -0.026 | 0.26 | 1.56 |
| 22/09/2013 | 11 | wet | 98.8 | -0.018 | 0.18 | 2.10 |
| 22/10/2013 | 13 | wet | 98.8 | -0.019 | 0.19 | 2.58 |

Table B.8: Macro-Cell Current for Uncracked Concrete Specimen (2) Made with Inhibitor II

| Date | Cycle No. | Condition Wet/Dry | Specimen 2 | | | |
|---|---|---|---|---|---|---|
| | | | Resistor (Ohms) | Voltage (mV) | Current (μA) | Total Corrosion (Coulombs) |
| 27/04/2013 | Starting of wetting cycles | | | | | 0.00 |
| 04/05/2013 | 1 | wet | 99 | 0.000 | 0.00 | 0.00 |
| 01/06/2013 | 3 | wet | 99 | 0.016 | 0.16 | 0.20 |
| 29/06/2013 | 5 | wet | 99 | 0.023 | 0.23 | 0.67 |
| 27/07/2013 | 7 | wet | 99 | -0.012 | 0.12 | 1.10 |
| 25/08/2013 | 9 | wet | 99 | -0.024 | 0.24 | 1.56 |
| 22/09/2013 | 11 | wet | 99 | -0.023 | 0.23 | 2.13 |
| 22/10/2013 | 13 | wet | 99 | -0.022 | 0.22 | 2.72 |

Table B.9: Macro-Cell Current for Uncracked Concrete Specimen (3) Made with Inhibitor II

| Date | Cycle No. | Condition Wet/Dry | Specimen 3 | | | |
|---|---|---|---|---|---|---|
| | | | Resistor (Ohms) | Voltage (mV) | Current (μA) | Total Corrosion (Coulombs) |
| 27/04/2013 | Starting of wetting cycles | | | | | 0.00 |
| 04/05/2013 | 1 | wet | 98.7 | 0.000 | 0.00 | 0.00 |
| 01/06/2013 | 3 | wet | 98.7 | 0.014 | 0.14 | 0.17 |
| 29/06/2013 | 5 | wet | 98.7 | 0.016 | 0.16 | 0.54 |
| 27/07/2013 | 7 | wet | 98.7 | -0.007 | 0.07 | 0.82 |
| 25/08/2013 | 9 | wet | 98.7 | -0.024 | 0.24 | 1.21 |
| 22/09/2013 | 11 | wet | 98.7 | -0.023 | 0.23 | 1.79 |
| 22/10/2013 | 13 | wet | 98.7 | -0.024 | 0.24 | 2.41 |

Table B.10: Macro-Cell Current for Uncracked Concrete Specimen (1) Made with Inhibitor III

| Date | Cycle No. | Condition Wet/Dry | Specimen 1 | | | |
|---|---|---|---|---|---|---|
| | | | Resistor (Ohms) | Voltage (mV) | Current (μA) | Total Corrosion (Coulombs) |
| 27/04/2013 | Starting of wetting cycles | | | | | 0.00 |
| 04/05/2013 | 1 | wet | 98.4 | 0.000 | 0.00 | 0.00 |
| 01/06/2013 | 3 | wet | 98.8 | 0.015 | 0.15 | 0.18 |
| 29/06/2013 | 5 | wet | 98.8 | -0.016 | 0.16 | 0.57 |
| 27/07/2013 | 7 | wet | 98.8 | -0.016 | 0.16 | 0.96 |
| 25/08/2013 | 9 | wet | 98.8 | -0.018 | 0.18 | 1.39 |
| 22/09/2013 | 11 | wet | 98.8 | -0.022 | 0.22 | 1.88 |
| 22/10/2013 | 13 | wet | 98.8 | -0.023 | 0.23 | 2.48 |

Table B.11: Macro-Cell Current for Uncracked Concrete Specimen (2) Made with Inhibitor III

| Date | Cycle No. | Condition Wet/Dry | Specimen 2 | | | |
|---|---|---|---|---|---|---|
| | | | Resistor (Ohms) | Voltage (mV) | Current (μA) | Total Corrosion (Coulombs) |
| 27/04/2013 | Starting of wetting cycles | | | | | 0.00 |
| 04/05/2013 | 1 | wet | 98.7 | 0.000 | 0.00 | 0.00 |
| 01/06/2013 | 3 | wet | 98.7 | 0.015 | 0.15 | 0.18 |
| 29/06/2013 | 5 | wet | 98.7 | -0.018 | 0.18 | 0.59 |
| 27/07/2013 | 7 | wet | 98.7 | -0.012 | 0.12 | 0.96 |
| 25/08/2013 | 9 | wet | 98.7 | -0.019 | 0.19 | 1.35 |
| 22/09/2013 | 11 | wet | 98.7 | -0.026 | 0.26 | 1.90 |
| 22/10/2013 | 13 | wet | 98.7 | -0.025 | 0.25 | 2.57 |

Table B.12: Macro-Cell Current for Uncracked Concrete Specimen (3) Made with Inhibitor III

| Date | Cycle No. | Condition Wet/Dry | Specimen 3 | | | |
|---|---|---|---|---|---|---|
| | | | Resistor (Ohms) | Voltage (mV) | Current (μA) | Total Corrosion (Coulombs) |
| 27/04/2013 | Starting of wetting cycles | | | | | 0.00 |
| 04/05/2013 | 1 | wet | 98.8 | 0.000 | 0.00 | 0.00 |
| 01/06/2013 | 3 | wet | 98.8 | 0.015 | 0.15 | 0.18 |
| 29/06/2013 | 5 | wet | 98.8 | -0.014 | 0.14 | 0.54 |
| 27/07/2013 | 7 | wet | 98.8 | -0.012 | 0.12 | 0.86 |
| 25/08/2013 | 9 | wet | 98.8 | -0.017 | 0.17 | 1.22 |
| 22/09/2013 | 11 | wet | 98.8 | -0.028 | 0.28 | 1.78 |
| 22/10/2013 | 13 | wet | 98.8 | -0.029 | 0.29 | 2.52 |

Table B.13: Macro-Cell Current for Uncracked Concrete Specimen (1) Made with Inhibitor IV

| Date | Cycle No. | Condition Wet/Dry | Specimen 1 | | | |
|---|---|---|---|---|---|---|
| | | | Resistor (Ohms) | Voltage (mV) | Current (µA) | Total Corrosion (Coulombs) |
| 27/04/2013 | Starting of wetting cycles | | | | | 0.00 |
| 04/05/2013 | 1 | wet | 98.8 | 0.000 | 0.00 | 0.00 |
| 01/06/2013 | 3 | wet | 98.8 | -0.012 | 0.12 | 0.15 |
| 29/06/2013 | 5 | wet | 98.8 | -0.020 | 0.20 | 0.54 |
| 27/07/2013 | 7 | wet | 98.8 | -0.015 | 0.15 | 0.97 |
| 25/08/2013 | 9 | wet | 98.8 | -0.020 | 0.20 | 1.41 |
| 22/09/2013 | 11 | wet | 98.8 | -0.029 | 0.29 | 2.01 |
| 22/10/2013 | 13 | wet | 98.8 | -0.028 | 0.28 | 2.76 |

Table B.14: Macro-Cell Current for Uncracked Concrete Specimen (2) Made with Inhibitor IV

| Date | Cycle No. | Condition Wet/Dry | Specimen 2 | | | |
|---|---|---|---|---|---|---|
| | | | Resistor (Ohms) | Voltage (mV) | Current (µA) | Total Corrosion (Coulombs) |
| 27/04/2013 | Starting of wetting cycles | | | | | 0.00 |
| 04/05/2013 | 1 | wet | 98.8 | 0.000 | 0.00 | 0.00 |
| 01/06/2013 | 3 | wet | 98.8 | 0.010 | 0.10 | 0.12 |
| 29/06/2013 | 5 | wet | 98.8 | -0.016 | 0.16 | 0.44 |
| 27/07/2013 | 7 | wet | 98.8 | -0.010 | 0.10 | 0.76 |
| 25/08/2013 | 9 | wet | 98.8 | -0.023 | 0.23 | 1.18 |
| 22/09/2013 | 11 | wet | 98.8 | -0.028 | 0.28 | 1.80 |
| 22/10/2013 | 13 | wet | 98.8 | -0.029 | 0.29 | 2.55 |

Table B.15: Macro-Cell Current for Uncracked Concrete Specimen (3) Made with Inhibitor IV

| Date | Cycle No. | Condition Wet/Dry | Specimen 3 | | | |
|---|---|---|---|---|---|---|
| | | | Resistor (Ohms) | Voltage (mV) | Current (µA) | Total Corrosion (Coulombs) |
| 27/04/2013 | Starting of wetting cycles | | | | | 0.00 |
| 04/05/2013 | 1 | wet | 98 | 0.000 | 0.00 | 0.00 |
| 01/06/2013 | 3 | wet | 98 | 0.008 | 0.08 | 0.10 |
| 29/06/2013 | 5 | wet | 98 | -0.011 | 0.11 | 0.33 |
| 27/07/2013 | 7 | wet | 98 | -0.010 | 0.10 | 0.59 |
| 25/08/2013 | 9 | wet | 98 | -0.027 | 0.28 | 1.07 |
| 22/09/2013 | 11 | wet | 98 | -0.022 | 0.22 | 1.67 |
| 22/10/2013 | 13 | wet | 98 | -0.020 | 0.20 | 2.23 |

Table B.16: Macro-Cell Current for Uncracked Concrete Specimen (1) Made with Inhibitor V

| Date | Cycle No. | Condition Wet/Dry | Specimen 1 | | | |
|---|---|---|---|---|---|---|
| | | | Resistor (Ohms) | Voltage (mV) | Current (µA) | Total Corrosion (Coulombs) |
| 27/04/2013 | Starting of wetting cycles | | | | | 0.00 |
| 04/05/2013 | 1 | wet | 98.6 | 0.000 | 0.00 | 0.00 |
| 01/06/2013 | 3 | wet | 98.6 | -0.007 | 0.07 | 0.08 |
| 29/06/2013 | 5 | wet | 98.6 | -0.011 | 0.11 | 0.29 |
| 27/07/2013 | 7 | wet | 98.6 | -0.010 | 0.10 | 0.55 |
| 25/08/2013 | 9 | wet | 98.6 | -0.020 | 0.20 | 0.93 |
| 22/09/2013 | 11 | wet | 98.6 | -0.015 | 0.15 | 1.36 |
| 22/10/2013 | 13 | wet | 98.6 | -0.016 | 0.16 | 1.77 |

Table B.17: Macro-Cell Current for Uncracked Concrete Specimen (2) Made with Inhibitor V

| Date | Cycle No. | Condition Wet/Dry | Specimen 2 | | | |
|---|---|---|---|---|---|---|
| | | | Resistor (Ohms) | Voltage (mV) | Current (μA) | Total Corrosion (Coulombs) |
| 27/04/2013 | Starting of wetting cycles | | | | | 0.00 |
| 04/05/2013 | 1 | wet | 98 | 0.000 | 0.00 | 0.00 |
| 01/06/2013 | 3 | wet | 98 | 0.008 | 0.08 | 0.10 |
| 29/06/2013 | 5 | wet | 98 | -0.011 | 0.11 | 0.34 |
| 27/07/2013 | 7 | wet | 98 | -0.010 | 0.10 | 0.60 |
| 25/08/2013 | 9 | wet | 98 | -0.022 | 0.22 | 1.01 |
| 22/09/2013 | 11 | wet | 98 | -0.012 | 0.12 | 1.43 |
| 22/10/2013 | 13 | wet | 98 | -0.014 | 0.14 | 1.77 |

Table B.18: Macro-Cell Current for Uncracked Concrete Specimen (3) Made with Inhibitor V

| Date | Cycle No. | Condition Wet/Dry | Specimen 3 | | | |
|---|---|---|---|---|---|---|
| | | | Resistor (Ohms) | Voltage (mV) | Current (μA) | Total Corrosion (Coulombs) |
| 27/04/2013 | Starting of wetting cycles | | | | | 0.00 |
| 04/05/2013 | 1 | wet | 98.8 | 0.000 | 0.00 | 0.00 |
| 01/06/2013 | 3 | wet | 98.8 | 0.009 | 0.09 | 0.11 |
| 29/06/2013 | 5 | wet | 98.8 | -0.010 | 0.10 | 0.34 |
| 27/07/2013 | 7 | wet | 98.8 | -0.012 | 0.12 | 0.61 |
| 25/08/2013 | 9 | wet | 98.8 | -0.021 | 0.21 | 1.03 |
| 22/09/2013 | 11 | wet | 98.8 | -0.014 | 0.14 | 1.46 |
| 22/10/2013 | 13 | wet | 98.8 | -0.015 | 0.15 | 1.84 |

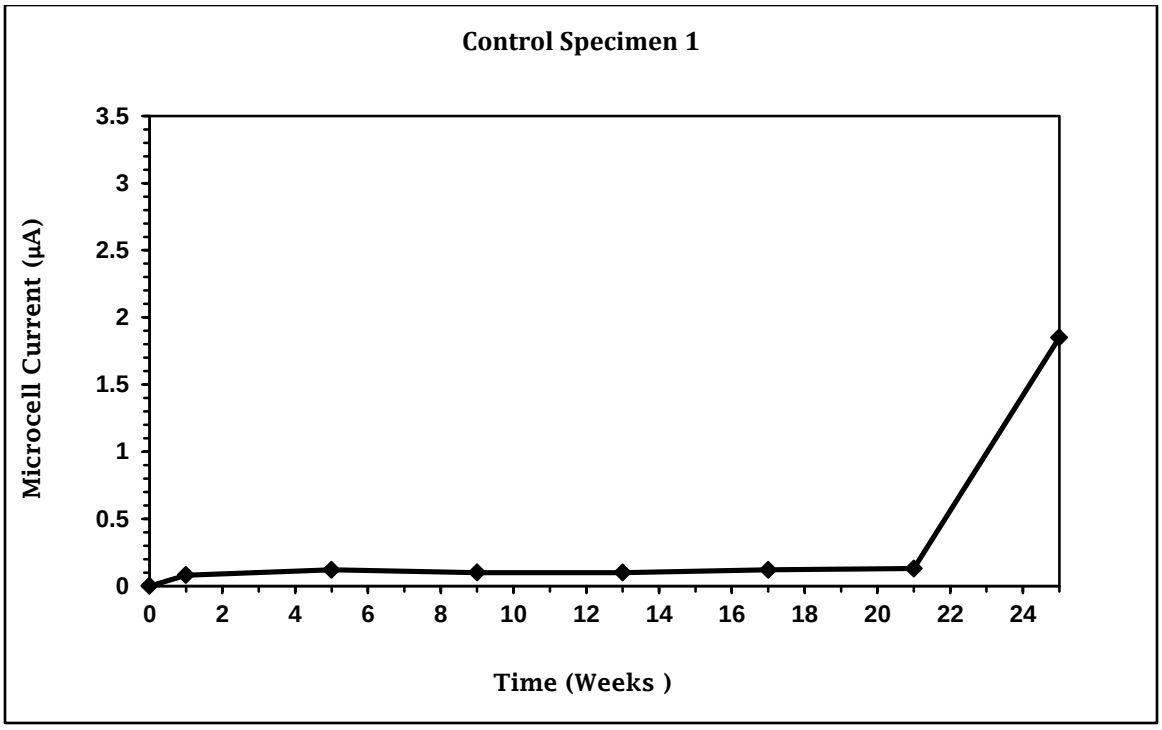


Figure B.1: Macro-Cell Current for Steel in Uncracked Control Concrete Specimen (1)

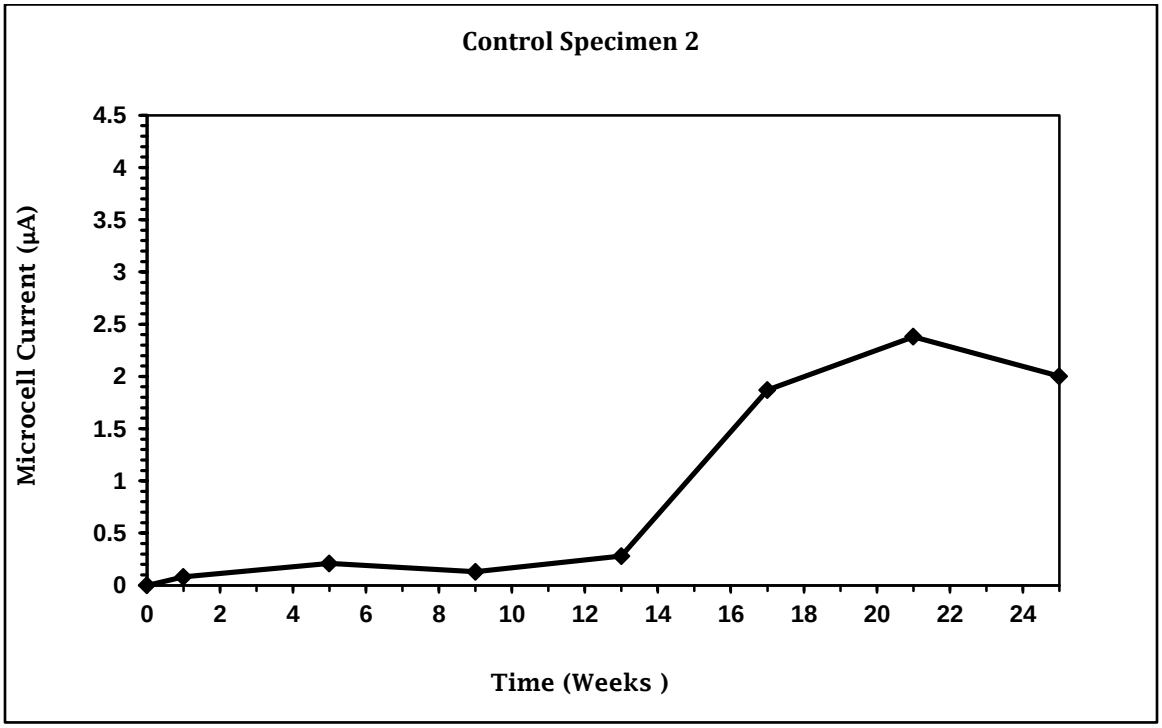


Figure B.2: Macro-Cell Current for Steel in Control Concrete Specimen (2)

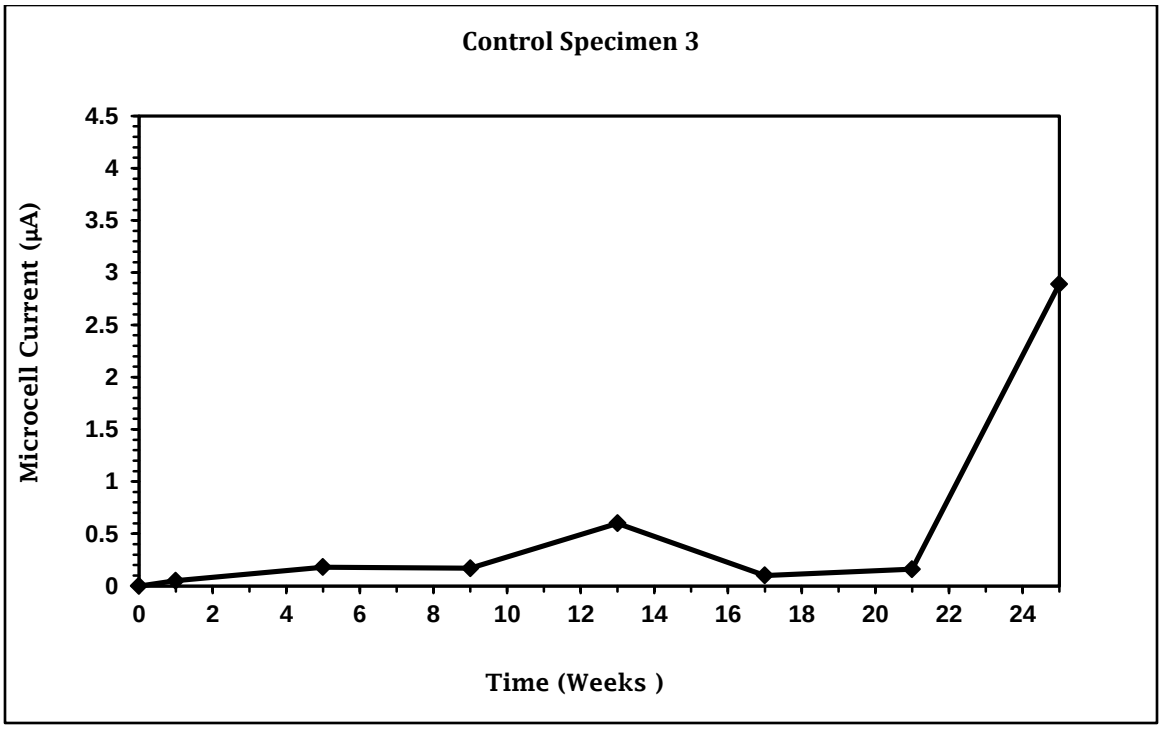


Figure B.3: Macro-Cell Current for Steel in Uncracked Control Concrete Specimen (3).

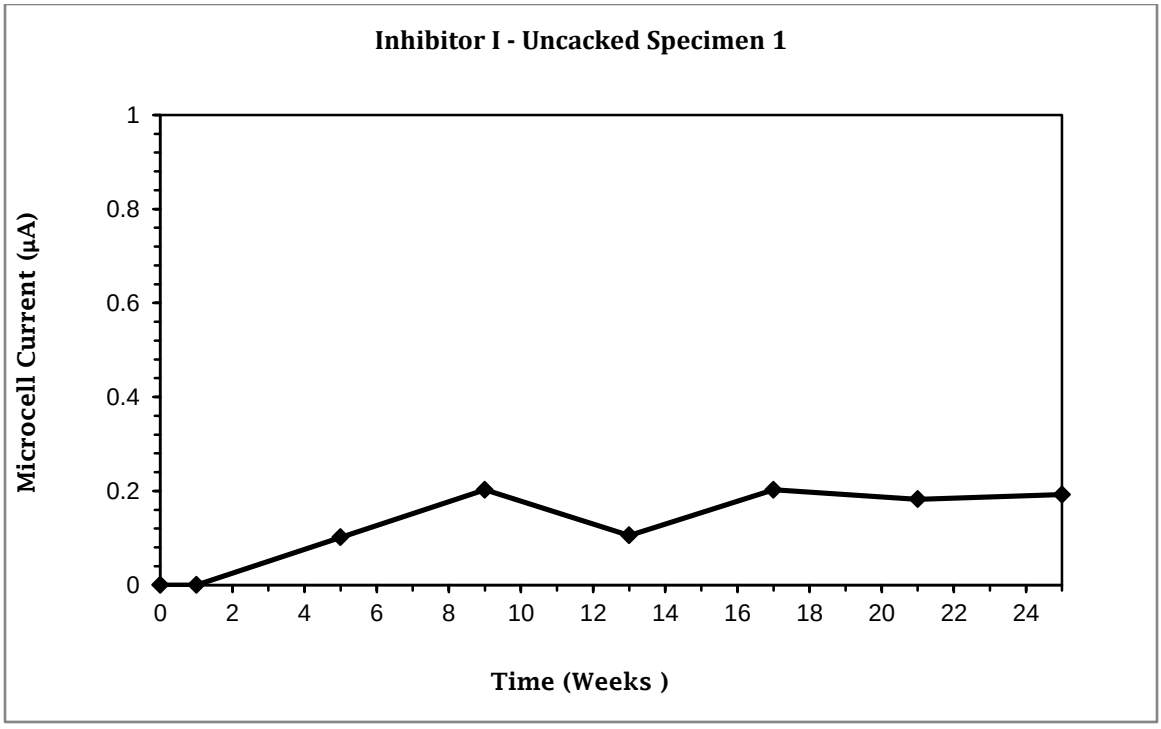


Figure B.4: Macro-Cell Current for Steel in Uncracked Concrete Specimen (1) Made with Inhibitor I

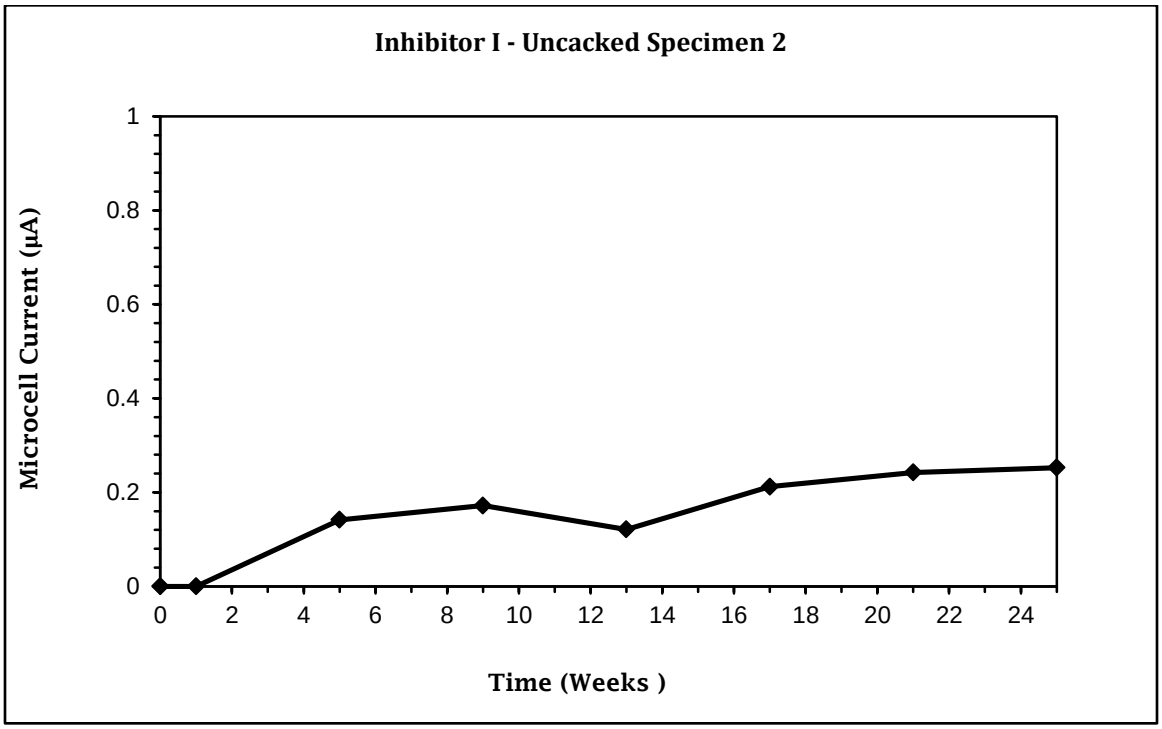


Figure B.5: Macro-Cell Current for Steel in Uncracked Concrete Specimen (2) Made with Inhibitor I

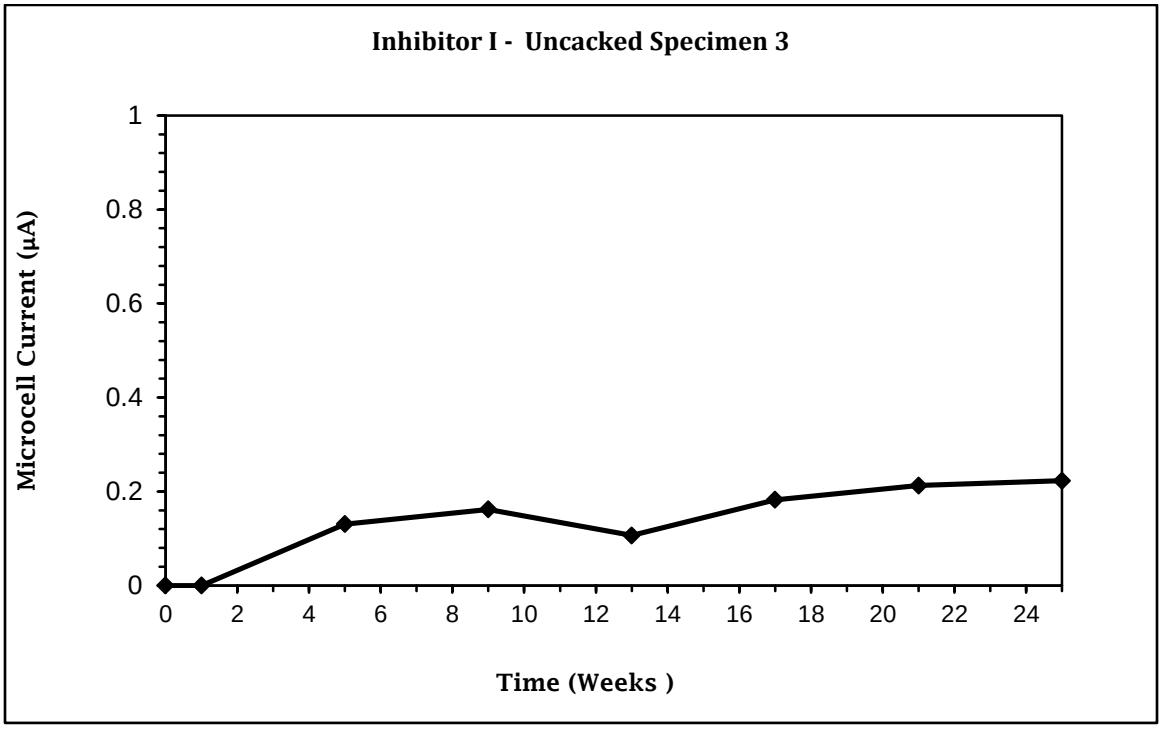


Figure B.6: Macro-Cell Current for Steel in Uncracked Concrete Specimen (3) Made with Inhibitor I

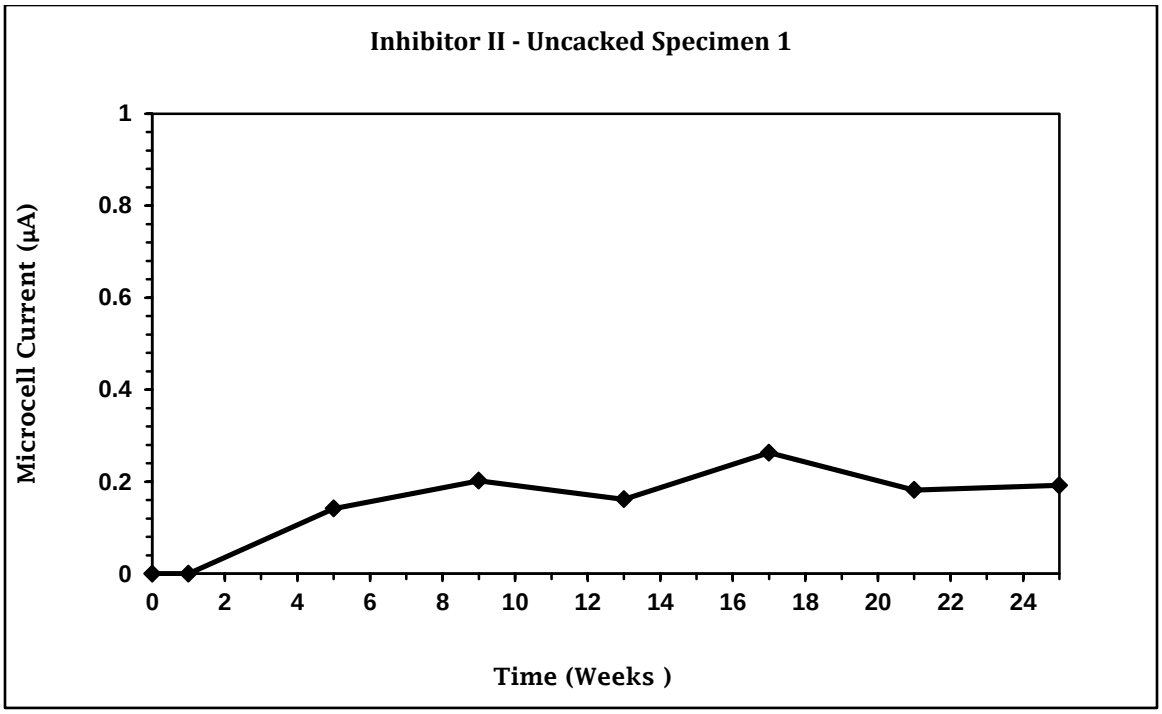


Figure B.7: Macro-Cell Current for Steel in Uncracked Concrete Specimen (1) Made with Inhibitor II

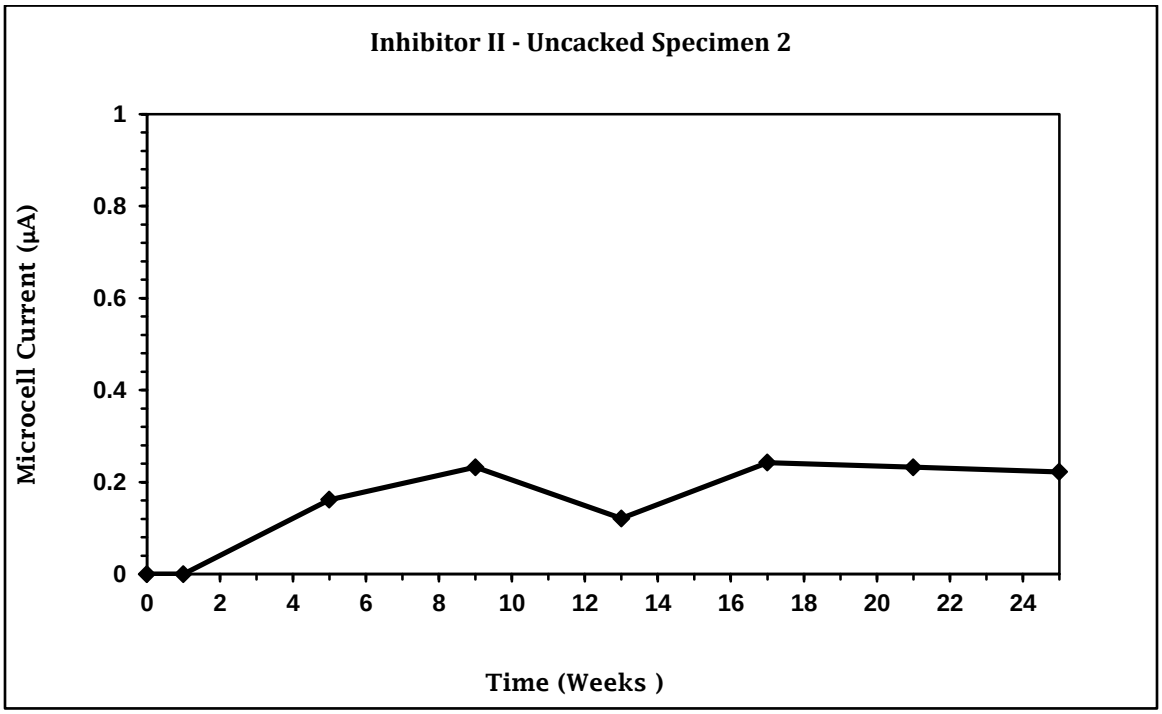


Figure B.8: Macro-Cell Current for Steel in Uncracked Concrete Specimen (2) Made with Inhibitor II

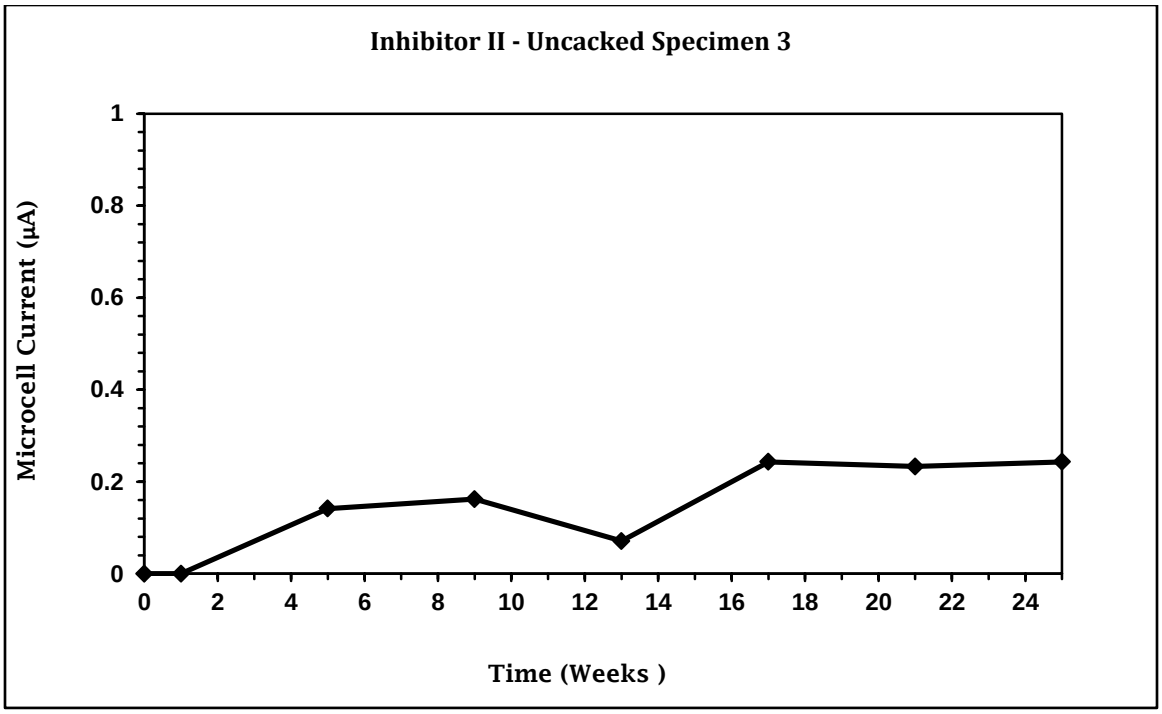


Figure B.9: Macro-Cell Current for Steel in Uncracked Concrete Specimen (3) Made with Inhibitor II

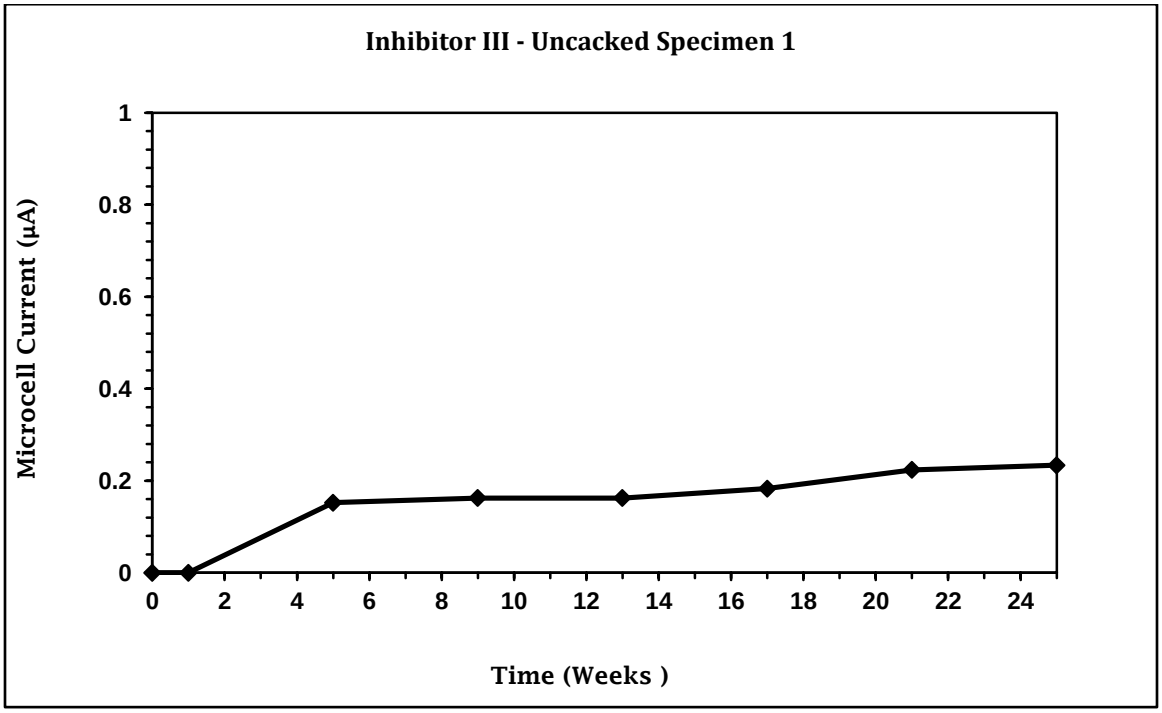


Figure B.10: Macro-Cell Current for Steel in Uncracked Concrete Specimen (1) Made with Inhibitor III

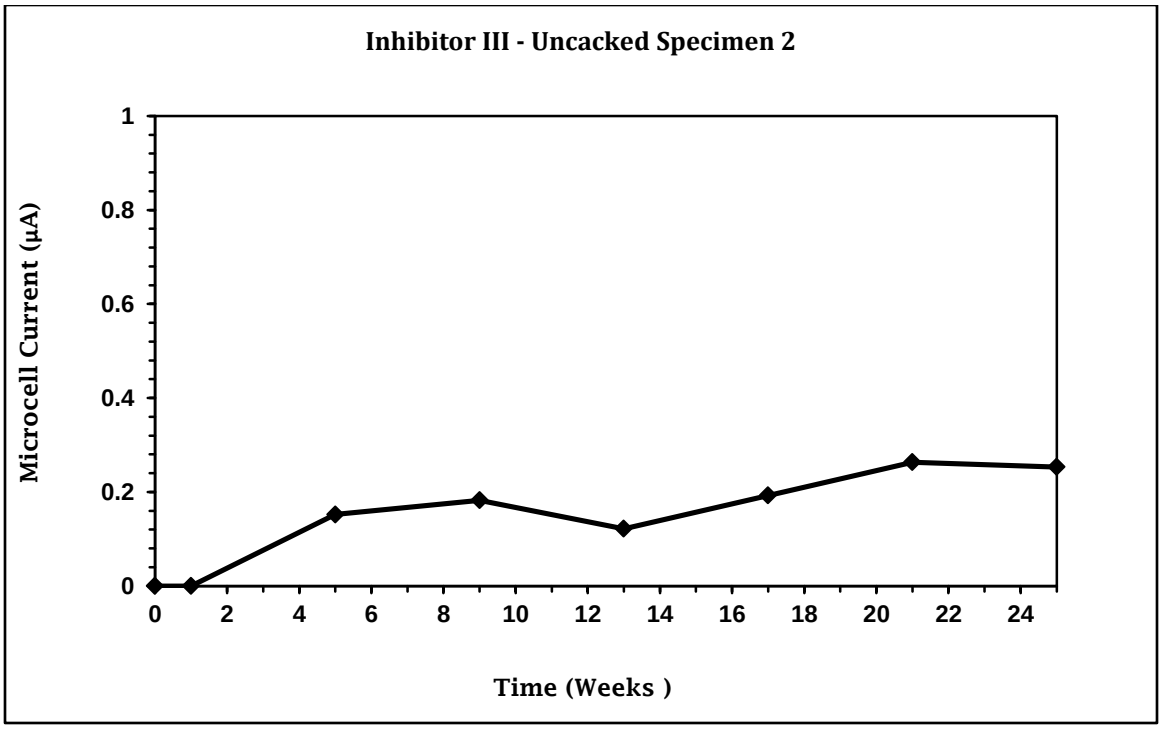


Figure B.11: Macro-Cell Current for Steel in Uncracked Concrete Specimen (2) Made with Inhibitor III

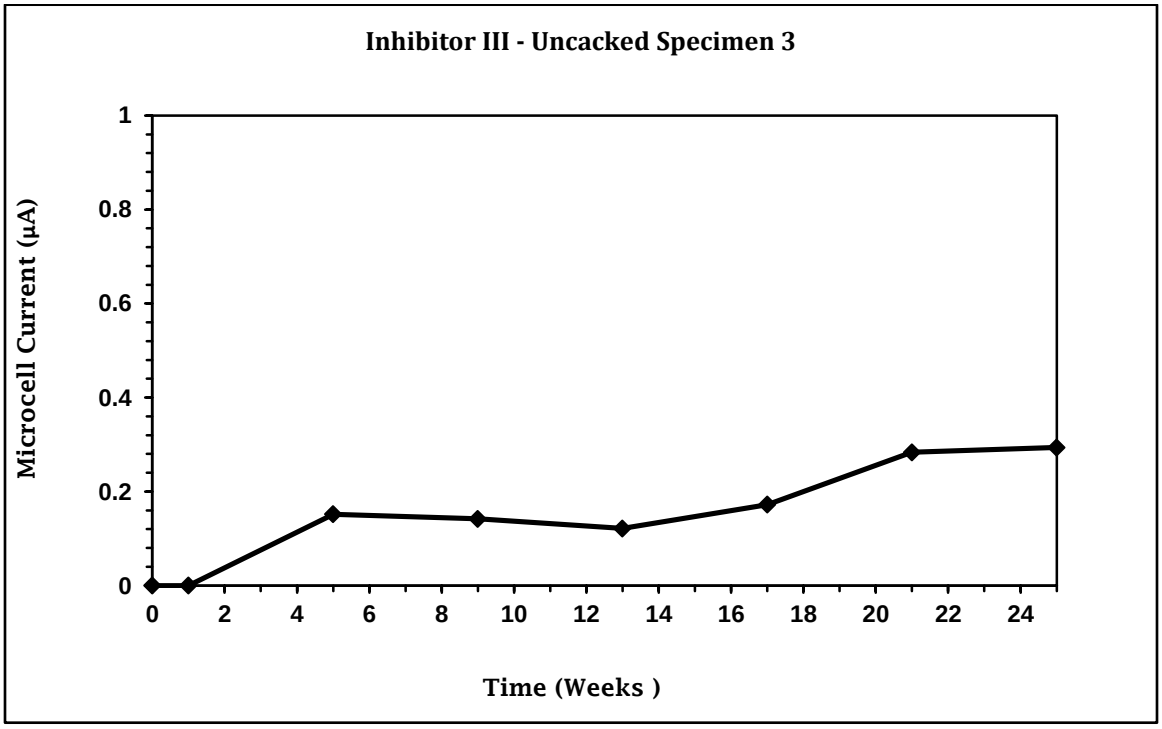


Figure B.12: Macro-Cell Current for Steel in Uncracked Concrete Specimen (3) Made with Inhibitor III.

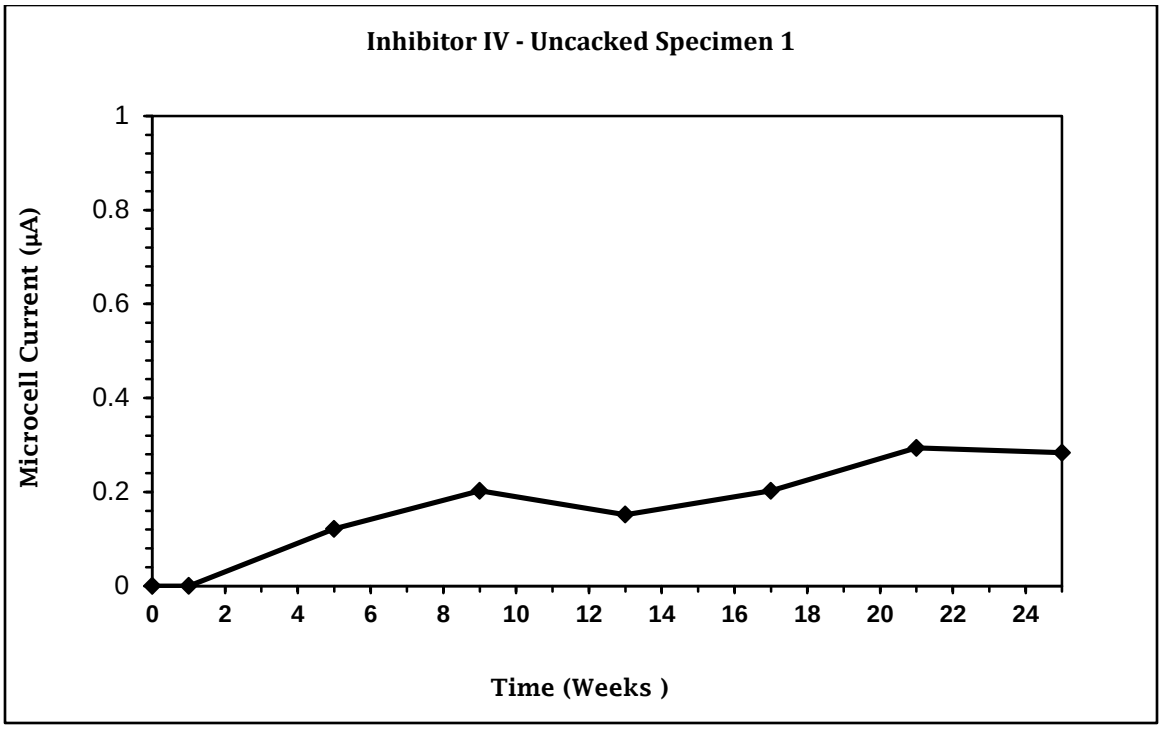


Figure B.13: Macro-Cell Current for Steel in Uncracked Concrete Specimen (1) Made with Inhibitor IV

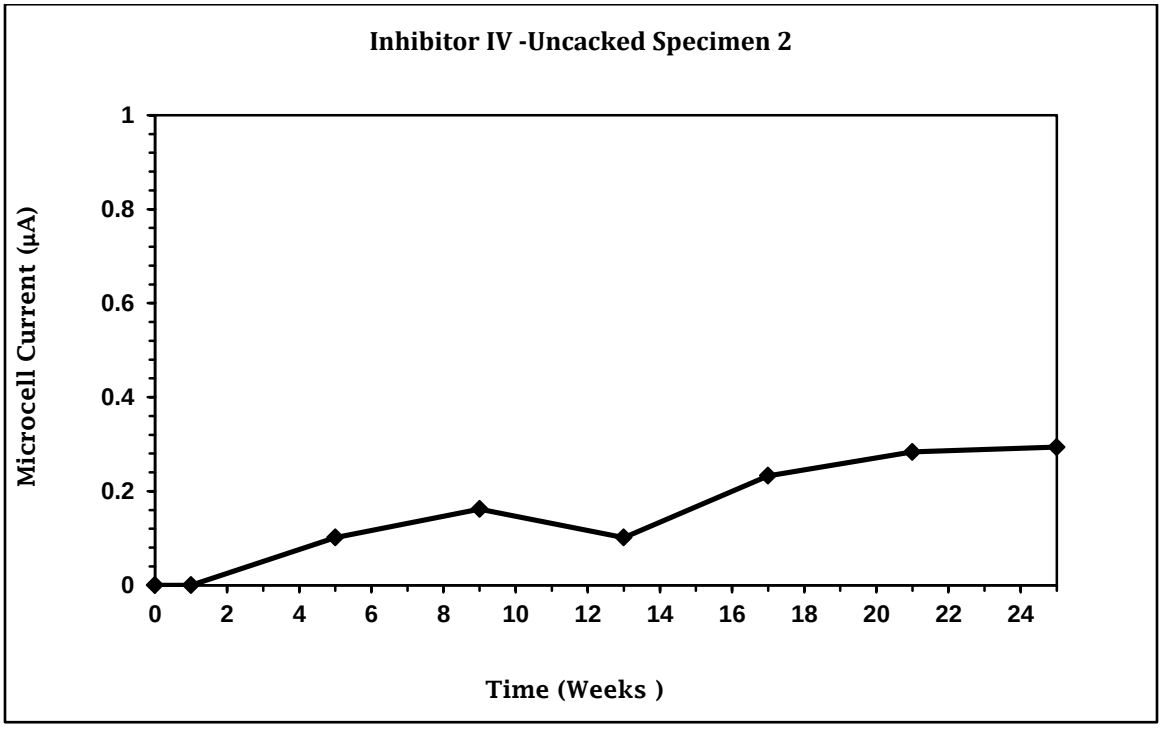


Figure B.14: Macro-Cell Current for Steel in Uncracked Concrete Specimen (2) Made with Inhibitor IV

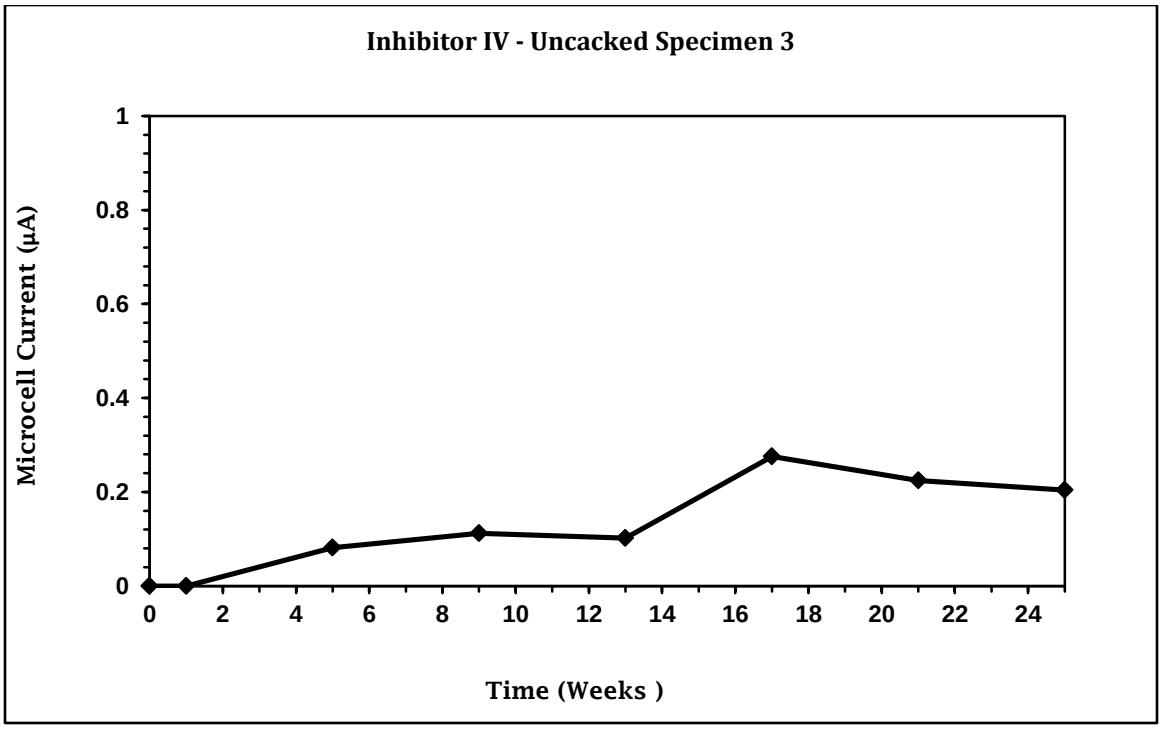


Figure B.15: Macro-Cell Current for Steel in Uncracked Concrete Specimen (3) Made with Inhibitor IV

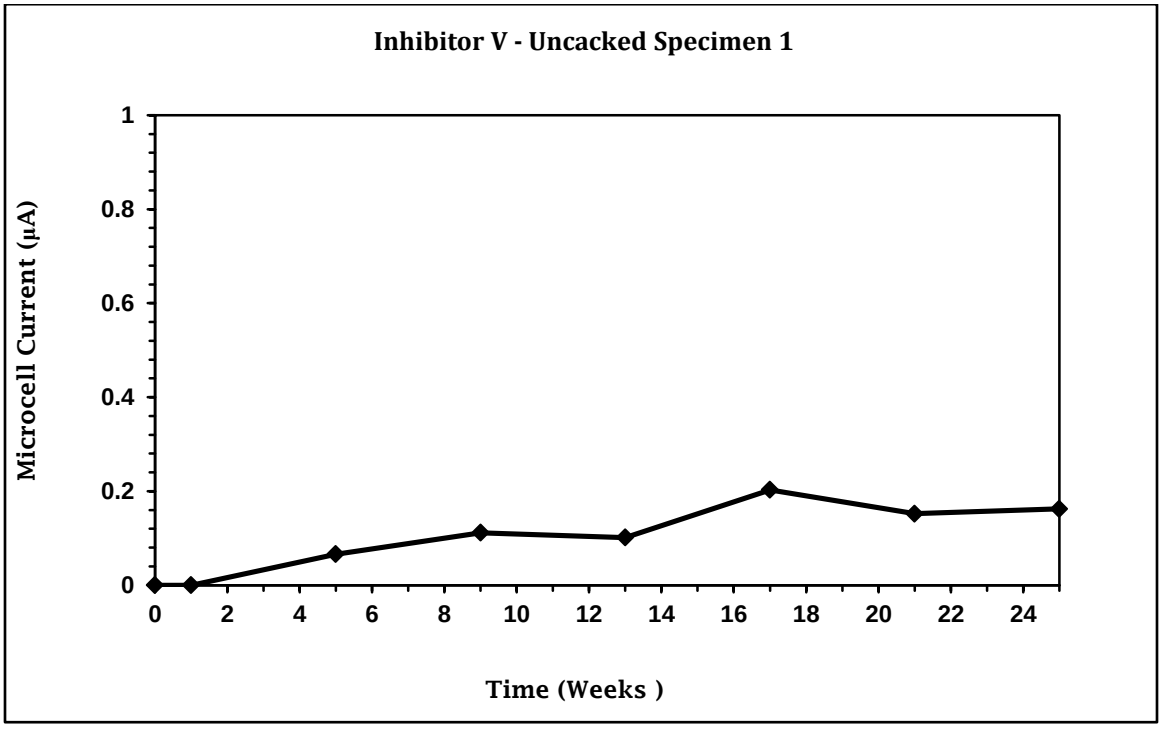


Figure B.16: Macro Cell Current for Steel in Uncracked Concrete Specimen (1) Made with Inhibitor V

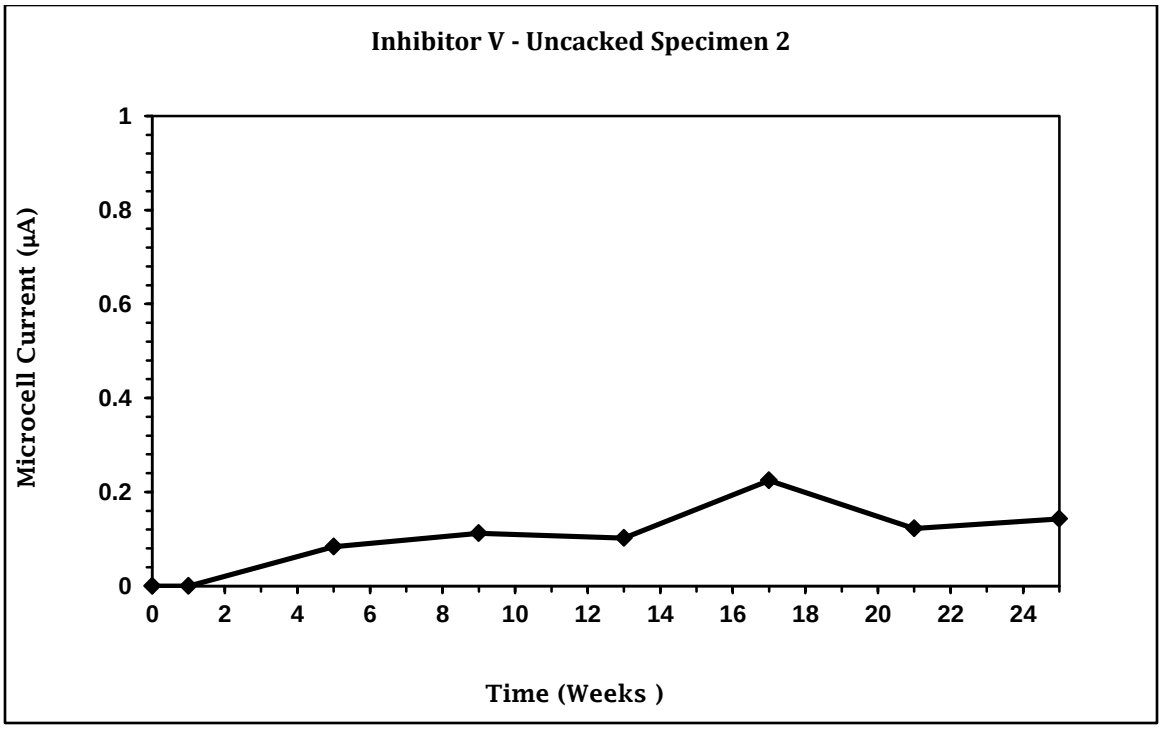


Figure B.17: Macro-Cell Current for Steel in Uncracked Concrete Specimen (2) Made with Inhibitor V

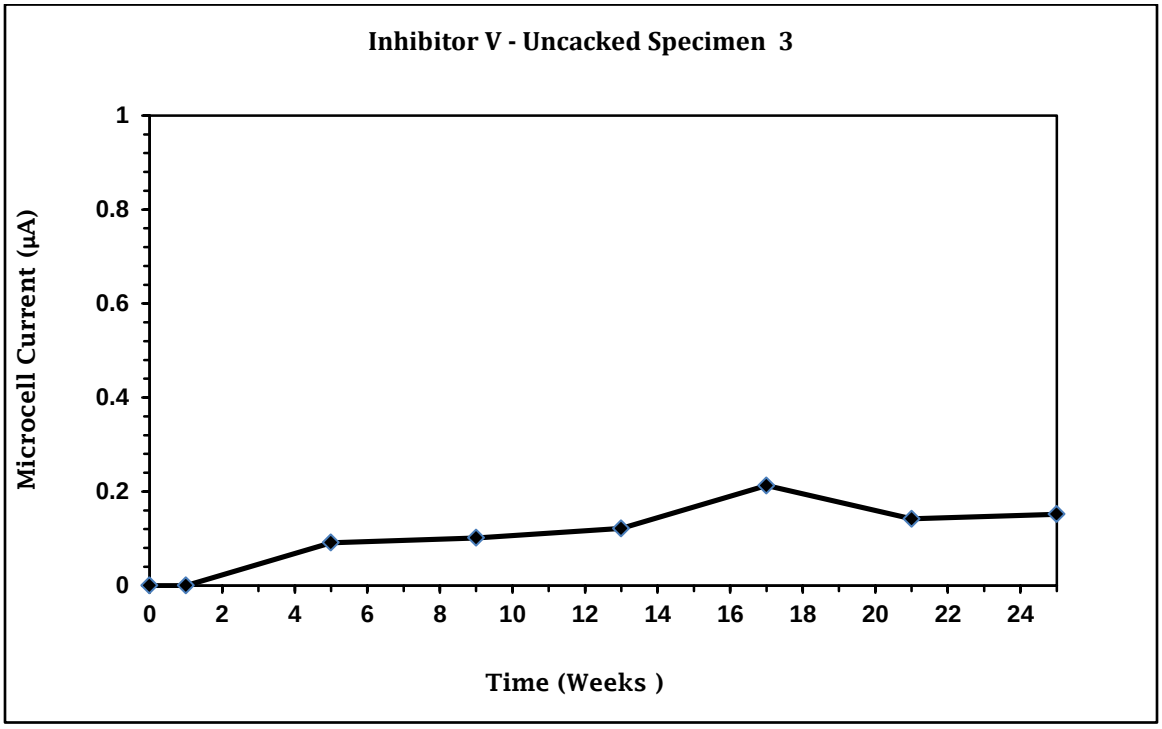


Figure B.18: Macro-Cell Current for Steel in Uncracked Concrete Specimen (3) Made with Inhibitor V

## B.2 Corrosion Potential Readings for Uncracked ASTM G109 Specimens

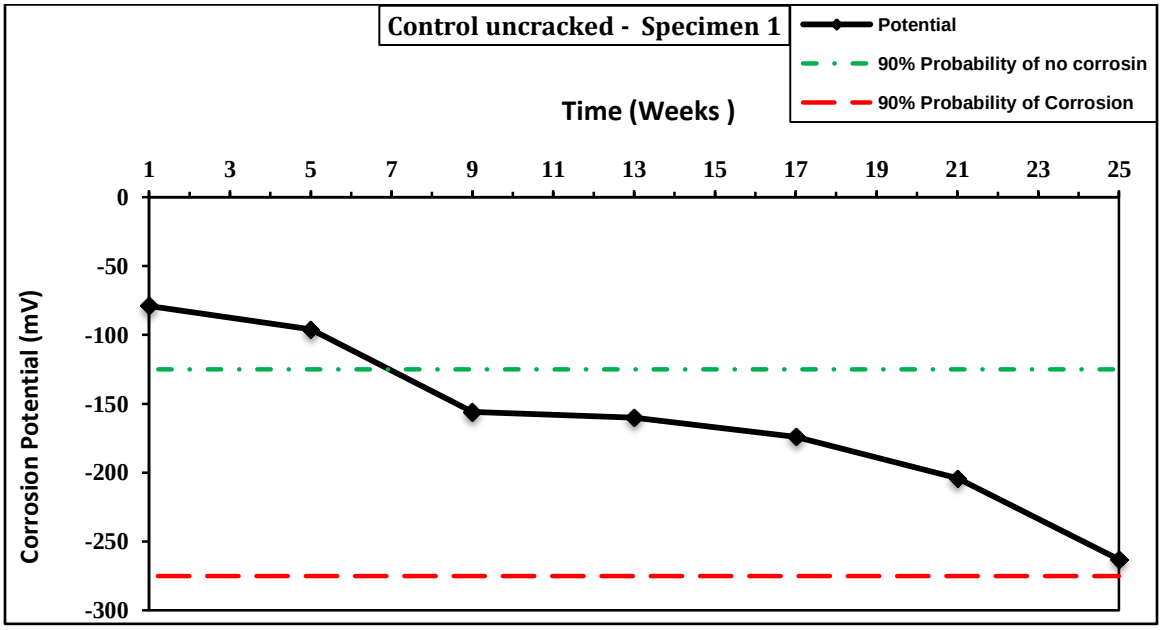


Figure B.19: Corrosion Potential for Steel in Control Concrete Specimen (1)

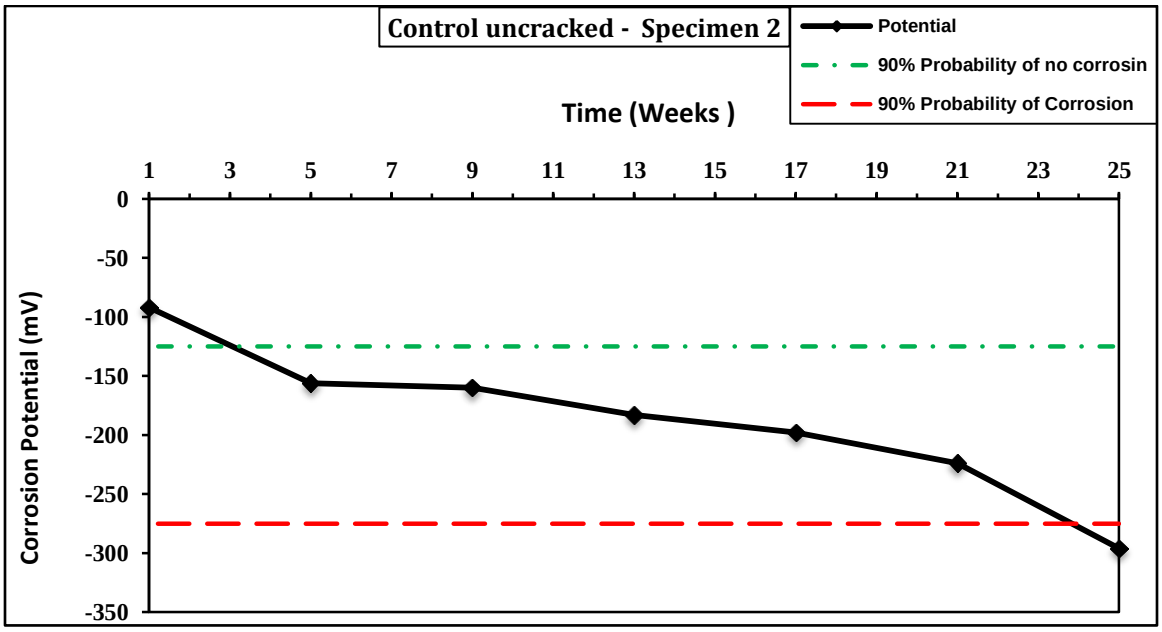


Figure B.20: Corrosion Potential for Steel in Control Concrete Specimen (2)

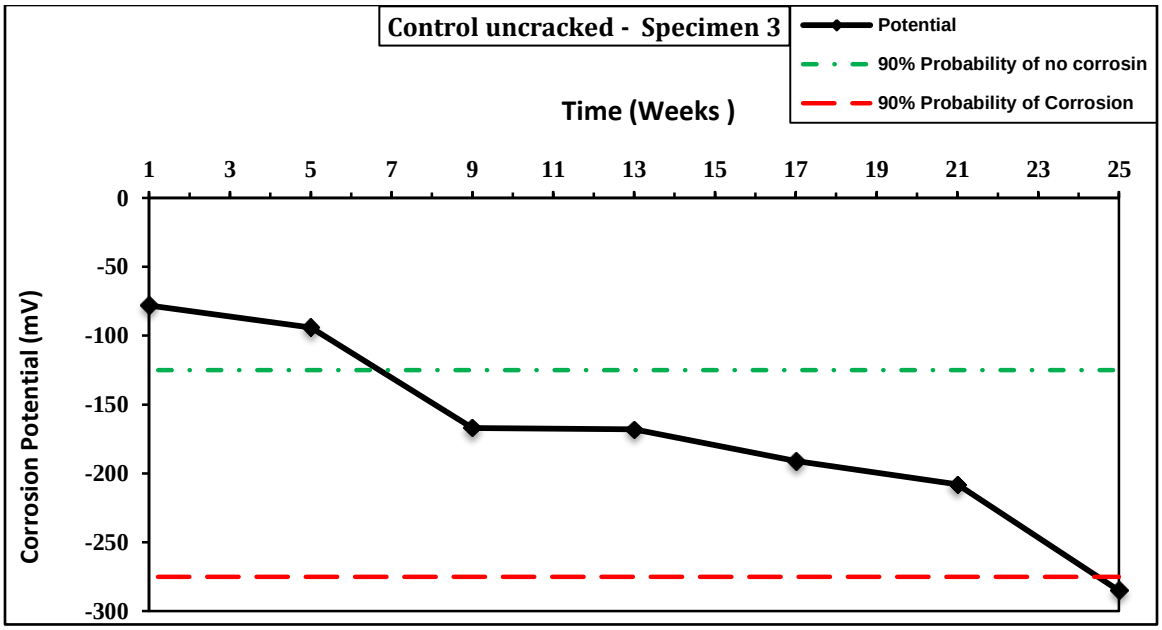


Figure B.21: Corrosion Potential for Steel in Control Concrete Specimen (3)

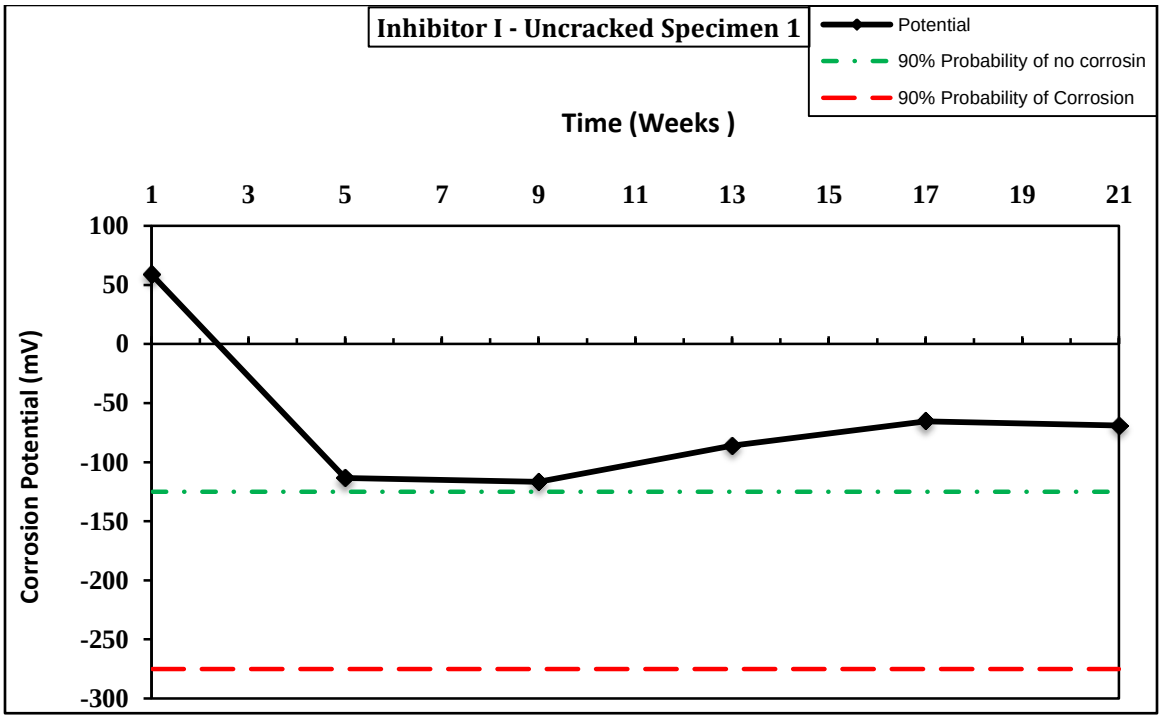


Figure B.22: Corrosion Potential for Steel in Uncracked Concrete Specimen (1) Made with Inhibitor I

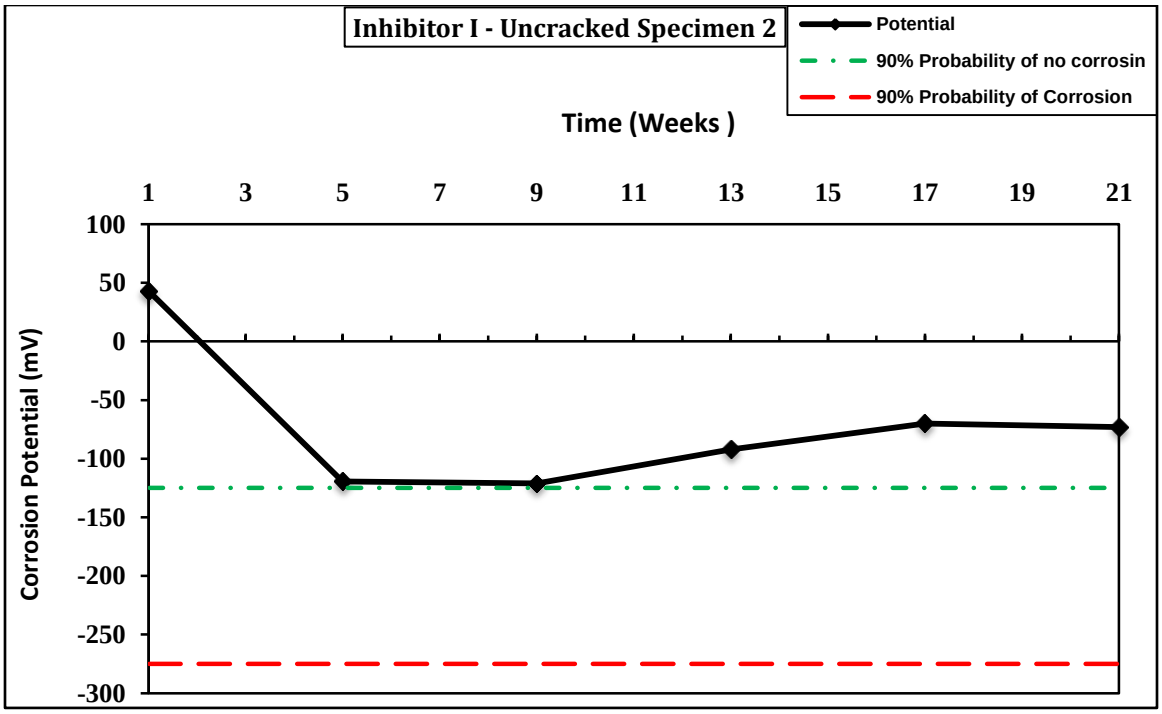


Figure B.23: Corrosion Potential for Steel in Uncracked Concrete Specimen (2) Made with Inhibitor I

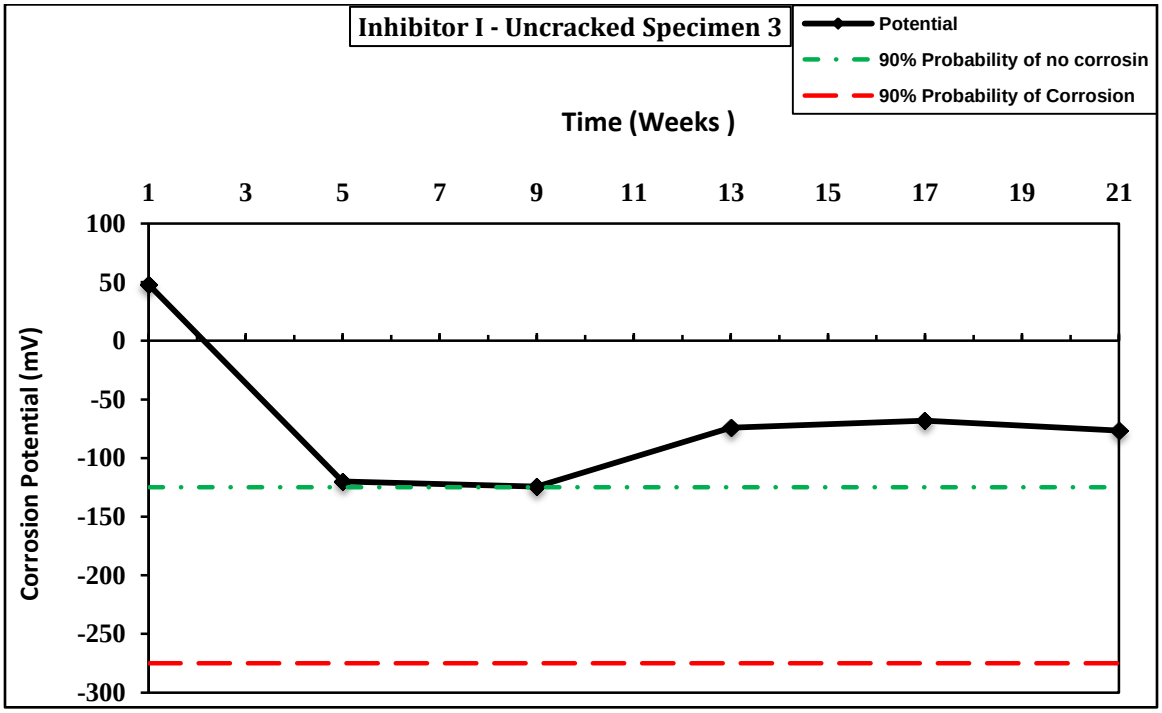


Figure B.24: Corrosion Potential for Steel in Uncracked Concrete Specimen (3) Made with Inhibitor I

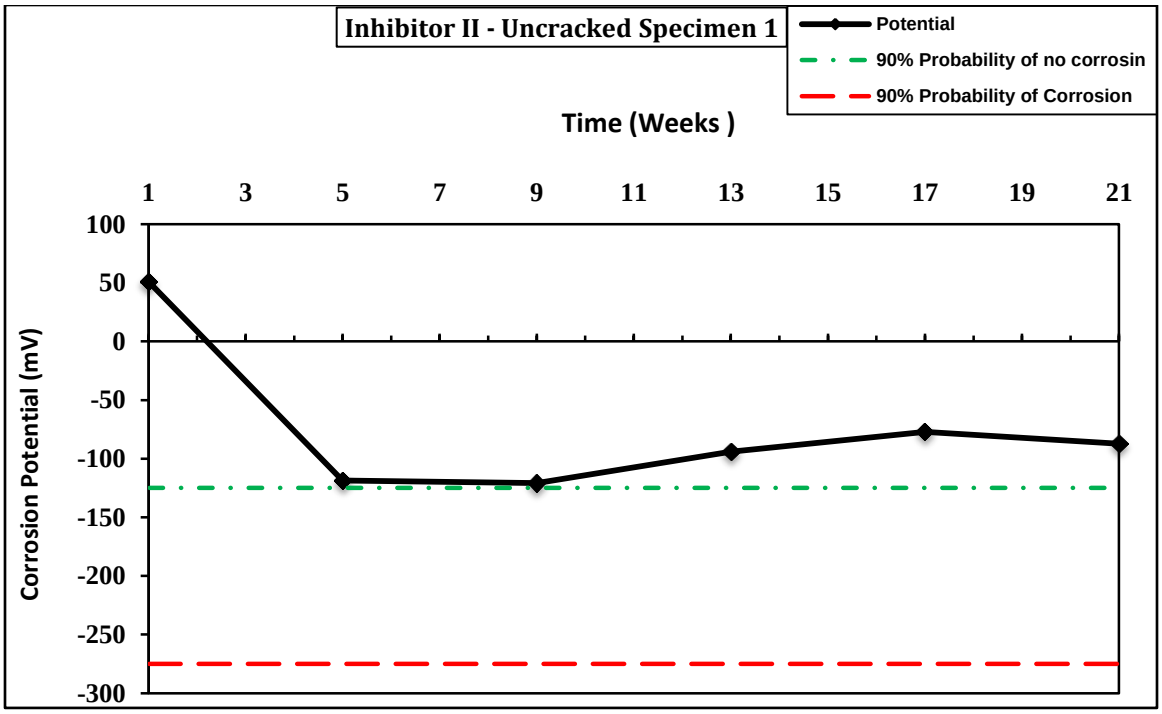


Figure B.25: Corrosion Potential for Steel in Uncracked Concrete Specimen (1) Made with Inhibitor II

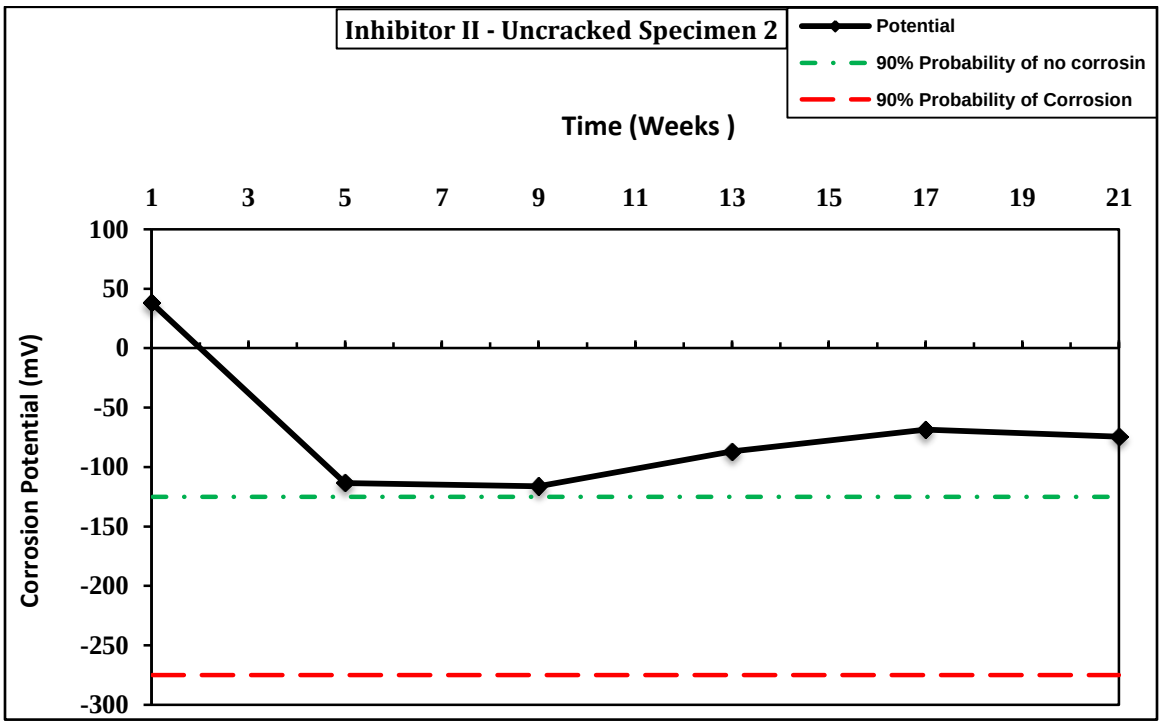


Figure B.26: Corrosion Potential for Steel in Uncracked Concrete Specimen (2) Made with Inhibitor II

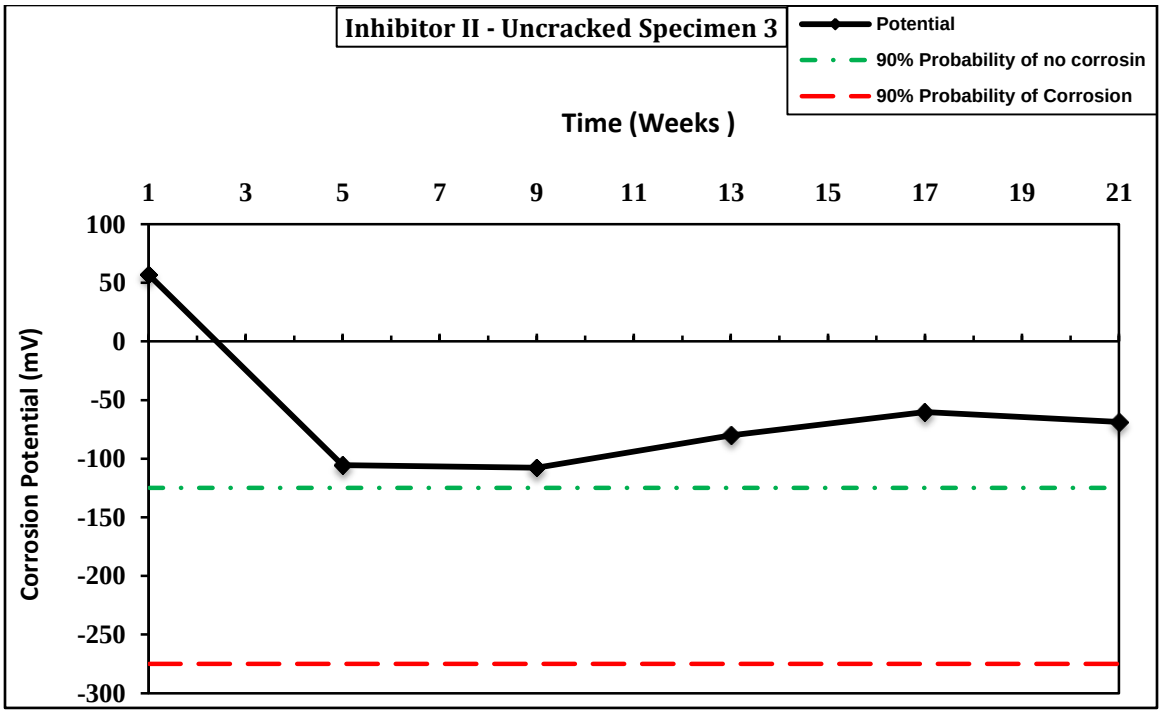


Figure B.27: Corrosion Potential for Steel in Uncracked Concrete Specimen (3) Made with Inhibitor II

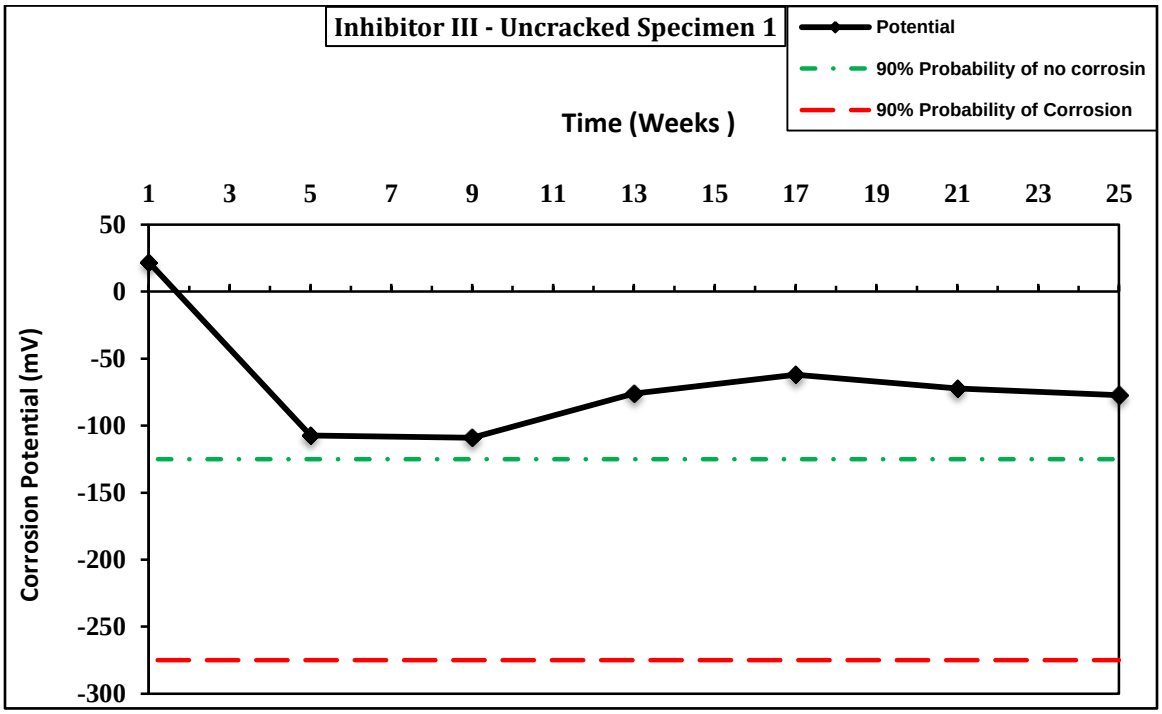


Figure B.28: Corrosion Potential for Steel in Uncracked Concrete Specimen (1) Made with Inhibitor III

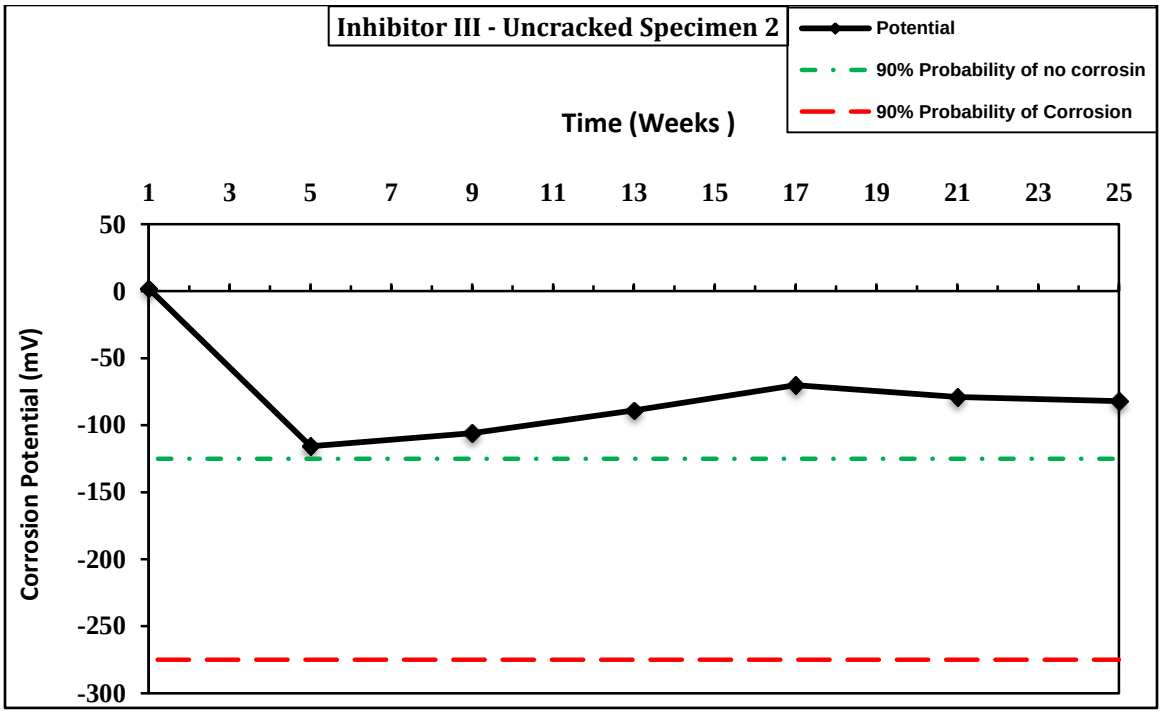


Figure B.29: Corrosion Potential for Steel in Uncracked Concrete Specimen (2) Made with Inhibitor III

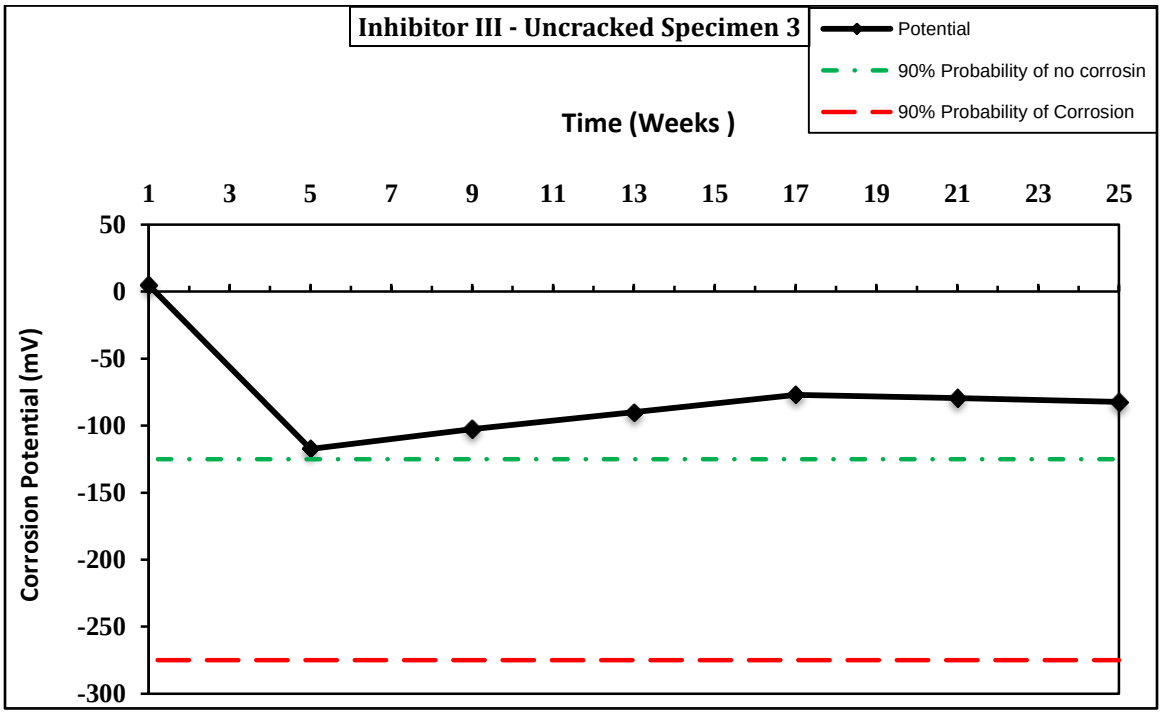


Figure B.30: Corrosion Potential for Steel in Uncracked Concrete Specimen (3) Made with Inhibitor III

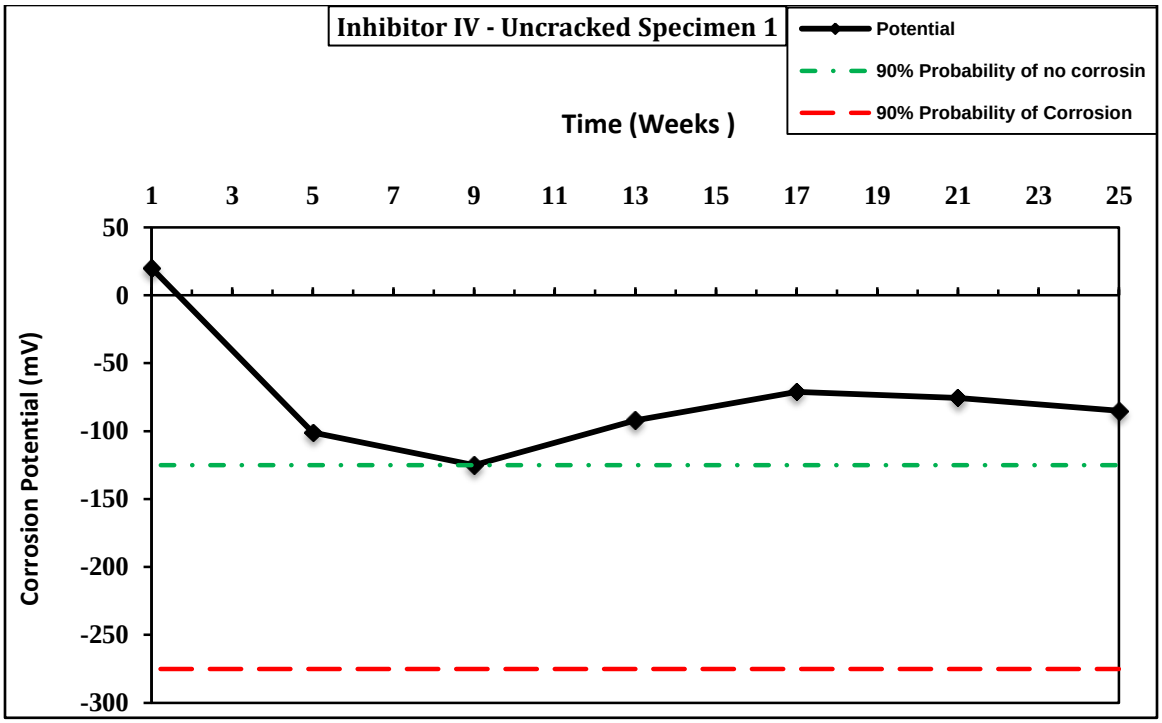


Figure B.31: Corrosion Potential for Steel in Uncracked Concrete Specimen (1) Made with Inhibitor IV

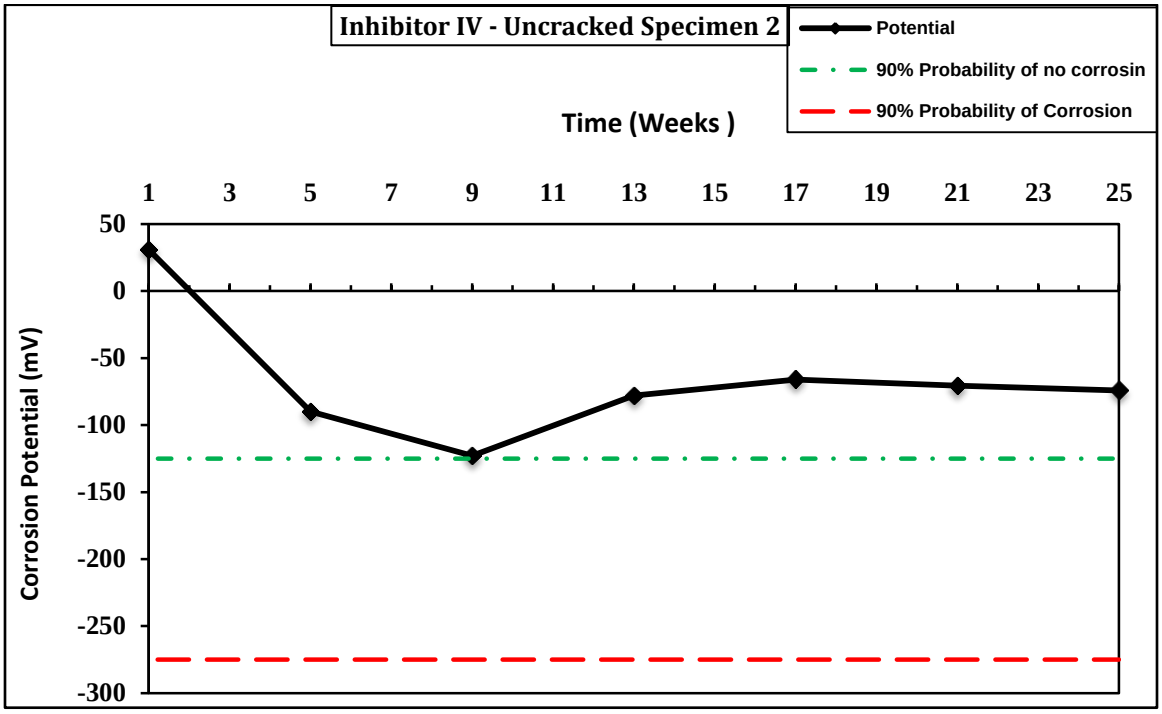


Figure B.32: Corrosion Potential for Steel in Uncracked Concrete Specimen (2) Made with Inhibitor IV

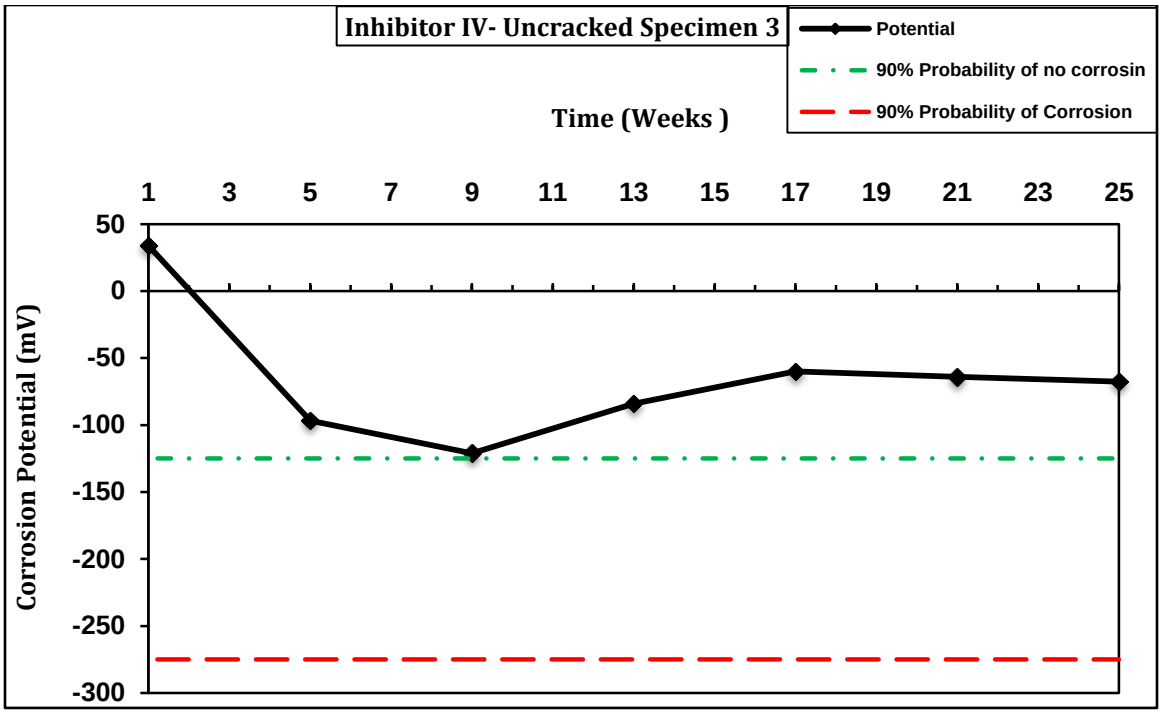


Figure B.33: Corrosion Potential for Steel In Uncracked Concrete Specimen (3) Made with Inhibitor IV

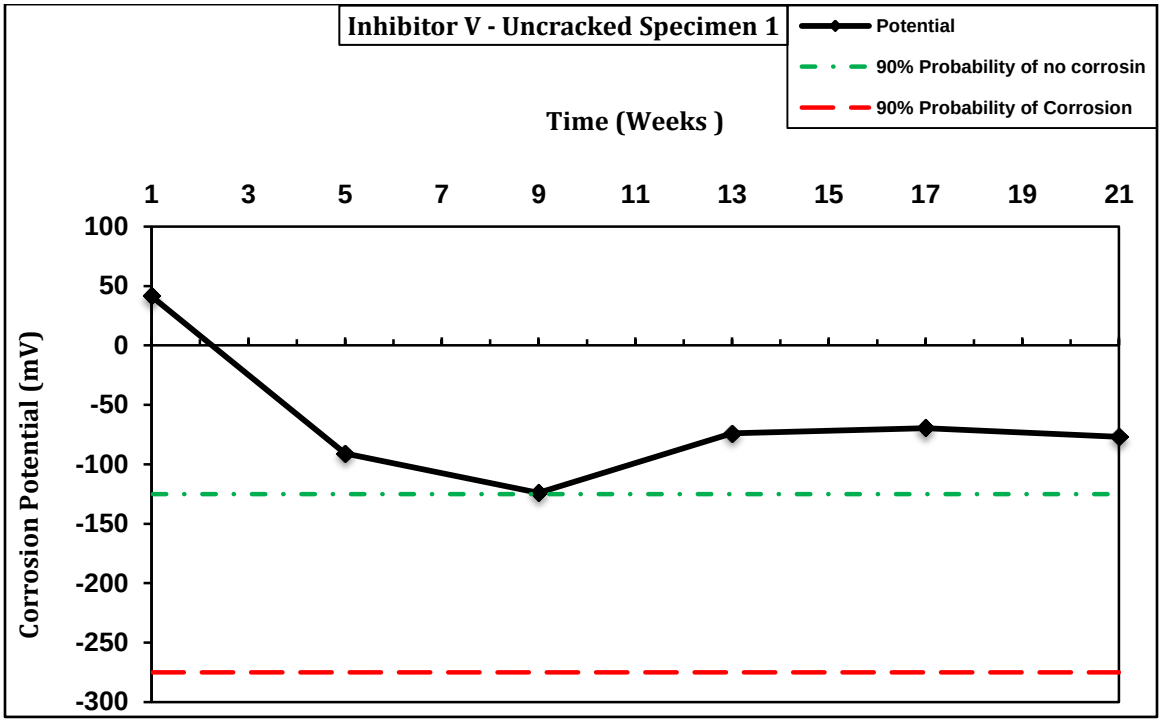


Figure B.34: Corrosion Potential for Steel in Uncracked Concrete Specimen (1) Made with Inhibitor V

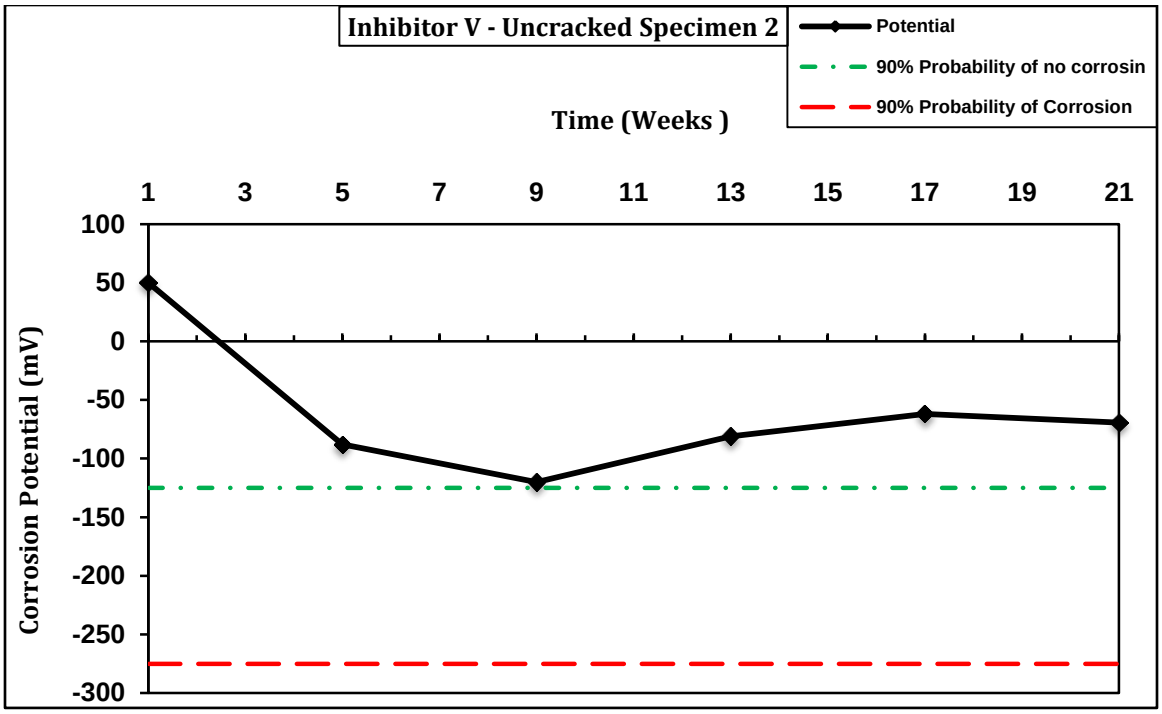


Figure B.35: Corrosion Potential for Steel in Uncracked Concrete Specimen (2) Made with Inhibitor V

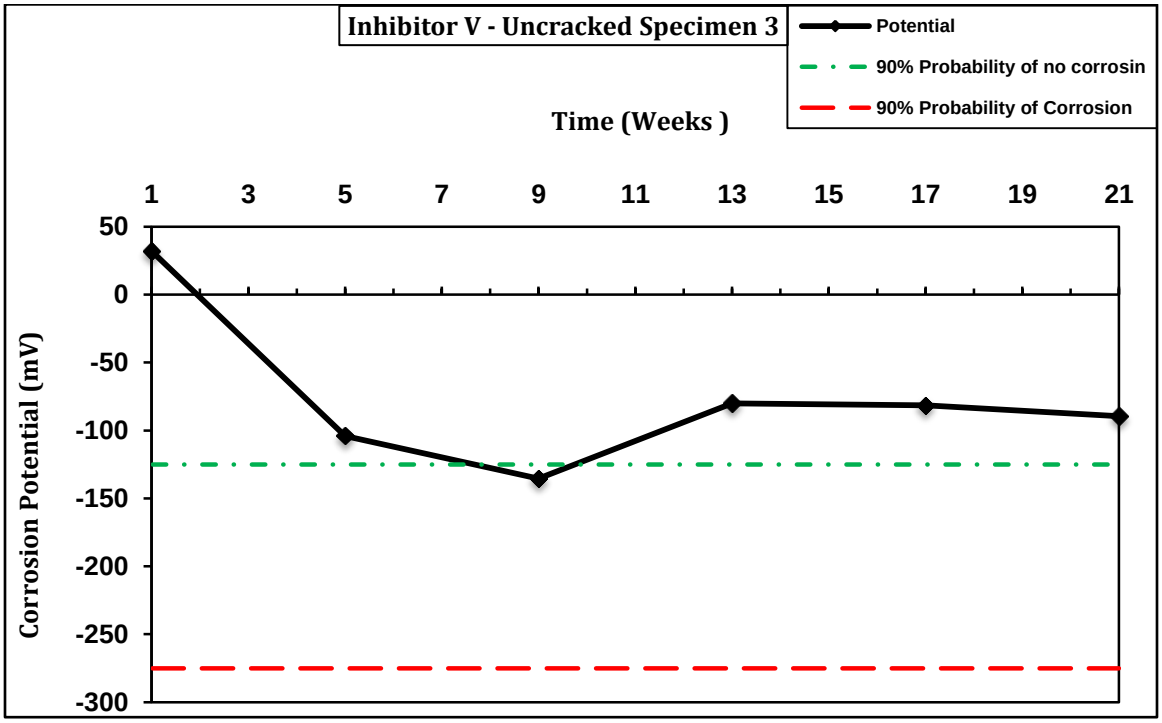


Figure B.36: Corrosion Potential for Steel in Uncracked Concrete Specimen (3) Made with Inhibitor V

# APPENDIX (C)

## C.1 Macro-cell Readings for Cracked ASTM G109 Specimens

Table C.1: Macro-Cell Current for Cracked Control Specimen (1)

| Date | Cycle No. | Condition Wet/Dry | Specimen 1 | | | |
|---|---|---|---|---|---|---|
| | | | Resistor (Ohms) | Voltage (mV) | Current (µA) | Total Corrosion (Coulombs) |
| 27/04/2013 | Starting of wetting cycles | | | | | 0.00 |
| 04/05/2013 | 1 | wet | 100 | -1.77 | 17.70 | 5.35 |
| 01/06/2013 | 3 | wet | 100 | -2.52 | 25.20 | 57.24 |
| 29/06/2013 | 5 | wet | 100 | -2.89 | 28.90 | 122.68 |
| 27/07/2013 | 7 | wet | 100 | -3.14 | 31.40 | 195.62 |
| 25/08/2013 | 9 | wet | 100 | -3.19 | 31.90 | 274.92 |

Table C.2: Macro-Cell Current for Cracked Control Specimen (2)

| Date | Cycle No. | Condition Wet/Dry | Specimen 2 | | | |
|---|---|---|---|---|---|---|
| | | | Resistor (Ohms) | Voltage (mV) | Current (µA) | Total Corrosion (Coulombs) |
| 27/04/2013 | Starting of wetting cycles | | | | | 0.00 |
| 04/05/2013 | 1 | wet | 100 | -1.53 | 15.30 | 4.63 |
| 01/06/2013 | 3 | wet | 100 | -2.44 | 24.40 | 52.65 |
| 29/06/2013 | 5 | wet | 100 | -2.65 | 26.50 | 114.22 |
| 27/07/2013 | 7 | wet | 100 | -2.75 | 27.50 | 179.53 |
| 25/08/2013 | 9 | wet | 100 | -2.84 | 28.40 | 249.57 |

Table C.3: Macro-Cell Current for Cracked Control Specimen (3)

| Date | Cycle No. | Condition Wet/Dry | Specimen 3 | | | |
|---|---|---|---|---|---|---|
| | | | Resistor (Ohms) | Voltage (mV) | Current (µA) | Total Corrosion (Coulombs) |
| 27/04/2013 | Starting of wetting cycles | | | | | 0.00 |
| 04/05/2013 | 1 | wet | 100 | -2.21 | 22.10 | 6.68 |
| 01/06/2013 | 3 | wet | 100 | -2.84 | 28.40 | 67.77 |
| 29/06/2013 | 5 | wet | 100 | -3.11 | 31.10 | 139.74 |
| 27/07/2013 | 7 | wet | 100 | -3.25 | 32.50 | 216.67 |
| 25/08/2013 | 9 | wet | 100 | -3.35 | 33.50 | 299.35 |

Table C.4: Macro-Cell Current for Cracked Concrete Specimen (1) Made with Inhibitor I

| Date | Cycle No. | Condition Wet/Dry | Specimen 1 | | | |
|---|---|---|---|---|---|---|
| | | | Resistor (Ohms) | Voltage (mV) | Current (µA) | Total Corrosion (Coulombs) |
| 27/04/2013 | Starting of wetting cycles | | | | | 0.00 |
| 04/05/2013 | 1 | wet | 98.5 | -1.300 | 13.20 | 3.99 |
| 01/06/2013 | 3 | wet | 98.5 | -1.271 | 12.90 | 35.56 |
| 29/06/2013 | 5 | wet | 98.5 | -1.630 | 16.55 | 71.19 |
| 27/07/2013 | 7 | wet | 98.5 | -1.710 | 17.36 | 112.20 |
| 25/08/2013 | 9 | wet | 98.5 | -2.190 | 22.23 | 161.81 |

Table C.5: Macro-Cell Current for Cracked Concrete Specimen (2) Made with Inhibitor I

| Date | Cycle No. | Condition Wet/Dry | Specimen 2 | | | |
|---|---|---|---|---|---|---|
| | | | Resistor (Ohms) | Voltage (mV) | Current (µA) | Total Corrosion (Coulombs) |
| 27/04/2013 | Starting of wetting cycles | | | | | 0.00 |
| 04/05/2013 | 1 | wet | 97.5 | -0.900 | 9.23 | 2.79 |
| 01/06/2013 | 3 | wet | 97.5 | -1.158 | 11.88 | 28.32 |
| 29/06/2013 | 5 | wet | 97.5 | -1.245 | 12.77 | 58.14 |
| 27/07/2013 | 7 | wet | 97.5 | -1.393 | 14.29 | 90.86 |
| 25/08/2013 | 9 | wet | 97.5 | -1.181 | 12.11 | 123.94 |

Table C.6: Macro-Cell Current for Cracked Concrete Specimen (3) Made ith Inhibitor I

| Date | Cycle No. | Condition Wet/Dry | Specimen 3 | | | |
|---|---|---|---|---|---|---|
| | | | Resistor (Ohms) | Voltage (mV) | Current (µA) | Total Corrosion (Coulombs) |
| 27/04/2013 | Starting of wetting cycles | | | | | 0.00 |
| 04/05/2013 | 1 | wet | 96.9 | -0.650 | 6.71 | 2.03 |
| 01/06/2013 | 3 | wet | 96.9 | -0.567 | 5.85 | 17.22 |
| 29/06/2013 | 5 | wet | 96.9 | -0.740 | 7.64 | 33.54 |
| 27/07/2013 | 7 | wet | 96.9 | -0.930 | 9.60 | 54.38 |
| 25/08/2013 | 9 | wet | 96.9 | -1.102 | 11.37 | 80.65 |

Table C.7: Macro-Cell Current for Cracked Concrete Specimen (1) Made with Inhibitor II

| Date | Cycle No. | Condition Wet/Dry | Specimen 1 | | | |
|---|---|---|---|---|---|---|
| | | | Resistor (Ohms) | Voltage (mV) | Current (µA) | Total Corrosion (Coulombs) |
| 27/04/2013 | Starting of wetting cycles | | | | | 0.00 |
| 04/05/2013 | 1 | wet | 98.9 | -1.600 | 16.18 | 4.89 |
| 01/06/2013 | 3 | wet | 98.9 | -2.741 | 27.71 | 57.98 |
| 29/06/2013 | 5 | wet | 98.9 | -2.710 | 27.40 | 124.65 |
| 27/07/2013 | 7 | wet | 98.9 | -2.510 | 25.38 | 188.50 |
| 25/08/2013 | 9 | wet | 98.9 | -2.100 | 21.23 | 246.89 |

Table C.8: Macro-Cell Current for Cracked Concrete Specimen (2) Made with Inhibitor II

| Date | Cycle No. | Condition Wet/Dry | Specimen 2 | | | |
|---|---|---|---|---|---|---|
| | | | Resistor (Ohms) | Voltage (mV) | Current (µA) | Total Corrosion (Coulombs) |
| 27/04/2013 | Starting of wetting cycles | | | | | 0.00 |
| 04/05/2013 | 1 | wet | 94.3 | -2.400 | 25.45 | 7.34 |
| 01/06/2013 | 3 | wet | 94.3 | 2.570 | 27.25 | 68.12 |
| 29/06/2013 | 5 | wet | 94.3 | -2.295 | 24.34 | 127.63 |
| 27/07/2013 | 7 | wet | 94.3 | -2.320 | 24.60 | 184.07 |
| 25/08/2013 | 9 | wet | 94.3 | -2.670 | 28.31 | 247.28 |

Table C.9: Macro-Cell Current for Cracked Concrete Specimen (3) Made with Inhibitor II

| Date | Cycle No. | Condition Wet/Dry | Specimen 3 | | | |
|---|---|---|---|---|---|---|
| | | | Resistor (Ohms) | Voltage (mV) | Current (μA) | Total Corrosion (Coulombs) |
| 27/04/2013 | Starting of wetting cycles | | | | | 0.00 |
| 04/05/2013 | 1 | wet | 99 | 0.500 | 5.05 | 1.53 |
| 01/06/2013 | 3 | wet | 99 | 1.428 | 14.42 | 25.16 |
| 29/06/2013 | 5 | wet | 99 | -1.350 | 13.64 | 59.21 |
| 27/07/2013 | 7 | wet | 99 | -1.003 | 10.13 | 88.04 |
| 25/08/2013 | 9 | wet | 99 | -1.032 | 10.42 | 113.87 |

Table C.10: Macro-Cell Current for Cracked Concrete Specimen (1) Made with Inhibitor III

| Date | Cycle No. | Condition Wet/Dry | Specimen 1 | | | |
|---|---|---|---|---|---|---|
| | | | Resistor (Ohms) | Voltage (mV) | Current (μA) | Total Corrosion (Coulombs) |
| 27/04/2013 | Starting of wetting cycles | | | | | 0.00 |
| 04/05/2013 | 1 | wet | 98.2 | 0.300 | 3.05 | 0.92 |
| 01/06/2013 | 3 | wet | 98.2 | 0.844 | 8.59 | 15.02 |
| 29/06/2013 | 5 | wet | 98.2 | -1.300 | 13.24 | 41.42 |
| 27/07/2013 | 7 | wet | 98.2 | -1.228 | 12.51 | 72.56 |
| 25/08/2013 | 9 | wet | 98.2 | -1.273 | 12.96 | 104.47 |

Table C.11: Macro-Cell Current for Cracked Concrete Specimen (2) Made with Inhibitor III

| Date | Cycle No. | Condition Wet/Dry | Specimen 2 | | | |
|---|---|---|---|---|---|---|
| | | | Resistor (Ohms) | Voltage (mV) | Current (µA) | Total Corrosion (Coulombs) |
| 27/04/2013 | Starting of wetting cycles | | | | | 0.00 |
| 04/05/2013 | 1 | wet | 98.5 | 0.471 | 4.78 | 1.45 |
| 01/06/2013 | 3 | wet | 98.5 | 1.160 | 11.78 | 21.48 |
| 29/06/2013 | 5 | wet | 98.5 | -1.240 | 12.59 | 50.95 |
| 27/07/2013 | 7 | wet | 98.5 | -1.120 | 11.37 | 79.93 |
| 25/08/2013 | 9 | wet | 98.5 | -1.024 | 10.40 | 107.20 |

Table C.12: Macro-Cell Current for Cracked Concrete Specimen (3) Made with Inhibitor III

| Date | Cycle No. | Condition Wet/Dry | Specimen 3 | | | |
|---|---|---|---|---|---|---|
| | | | Resistor (Ohms) | Voltage (mV) | Current (µA) | Total Corrosion (Coulombs) |
| 27/04/2013 | Starting of wetting cycles | | | | | 0.00 |
| 04/05/2013 | 1 | wet | 98.5 | 1.200 | 12.18 | 3.68 |
| 01/06/2013 | 3 | wet | 98.5 | 1.766 | 17.93 | 40.11 |
| 29/06/2013 | 5 | wet | 98.5 | -1.307 | 13.27 | 77.84 |
| 27/07/2013 | 7 | wet | 98.5 | -1.880 | 19.09 | 116.98 |
| 25/08/2013 | 9 | wet | 98.5 | -1.683 | 17.09 | 162.30 |

Table C.13: Macro-Cell Current for Cracked Concrete Specimen (1) Made with Inhibitor IV

| Date | Cycle No. | Condition Wet/Dry | Specimen 1 | | | |
|---|---|---|---|---|---|---|
| | | | Resistor (Ohms) | Voltage (mV) | Current (µA) | Total Corrosion (Coulombs) |
| 27/04/2013 | Starting of wetting cycles | | | | | 0.00 |
| 04/05/2013 | 1 | wet | 98.4 | 0.000 | 0.00 | 0.00 |
| 01/06/2013 | 3 | wet | 98.4 | 0.160 | 1.63 | 1.97 |
| 29/06/2013 | 5 | wet | 98.4 | -0.170 | 1.73 | 6.02 |
| 27/07/2013 | 7 | wet | 98.4 | -0.100 | 1.02 | 9.34 |
| 25/08/2013 | 9 | wet | 98.4 | -0.250 | 2.54 | 13.80 |

Table C.14: Macro-Cell Current for Cracked Concrete Specimen (2) Made with Inhibitor IV

| Date | Cycle No. | Condition Wet/Dry | Specimen 2 | | | |
|---|---|---|---|---|---|---|
| | | | Resistor (Ohms) | Voltage (mV) | Current (µA) | Total Corrosion (Coulombs) |
| 27/04/2013 | Starting of wetting cycles | | | | | 0.00 |
| 04/05/2013 | 1 | wet | 100 | 0.190 | 1.90 | 0.57 |
| 01/06/2013 | 3 | wet | 100 | 0.215 | 2.15 | 5.47 |
| 29/06/2013 | 5 | wet | 100 | 0.260 | 2.60 | 11.22 |
| 27/07/2013 | 7 | wet | 100 | 0.306 | 3.06 | 18.07 |
| 25/08/2013 | 9 | wet | 100 | 0.410 | 4.10 | 27.04 |

Table C.15: Macro-Cell Current for Cracked Concrete Specimen (3) Made with Inhibitor IV

| Date | Cycle No. | Condition Wet/Dry | Specimen 3 | | | |
|---|---|---|---|---|---|---|
| | | | Resistor (Ohms) | Voltage (mV) | Current (µA) | Total Corrosion (Coulombs) |
| 27/04/2013 | Starting of wetting cycles | | | | | 0.00 |
| 04/05/2013 | 1 | wet | 98.4 | 0.000 | 0.00 | 0.00 |
| 01/06/2013 | 3 | wet | 98.4 | 0.200 | 2.03 | 2.46 |
| 29/06/2013 | 5 | wet | 98.4 | -0.190 | 1.93 | 7.25 |
| 27/07/2013 | 7 | wet | 98.4 | -0.110 | 1.12 | 10.94 |
| 25/08/2013 | 9 | wet | 98.4 | -0.200 | 2.03 | 14.89 |

Table C.16: Macro-Cell Current for Cracked Concrete Specimen (1) Made with Inhibitor V

| Date | Cycle No. | Condition Wet/Dry | Specimen 1 | | | |
|---|---|---|---|---|---|---|
| | | | Resistor (Ohms) | Voltage (mV) | Current (µA) | Total Corrosion (Coulombs) |
| 27/04/2013 | Starting of wetting cycles | | | | | 0.00 |
| 04/05/2013 | 1 | wet | 98.5 | 0.000 | 0.00 | 0.00 |
| 01/06/2013 | 3 | wet | 98.5 | 0.024 | 0.24 | 0.29 |
| 29/06/2013 | 5 | wet | 98.5 | -0.332 | 3.37 | 4.67 |
| 27/07/2013 | 7 | wet | 98.5 | -0.285 | 2.89 | 12.24 |
| 25/08/2013 | 9 | wet | 98.5 | -0.182 | 1.85 | 18.18 |

Table C.17: Macro-Cell Current for Cracked Concrete Specimen (2) Made with Inhibitor V

| Date | Cycle No. | Condition Wet/Dry | Specimen 2 | | | |
|---|---|---|---|---|---|---|
| | | | Resistor (Ohms) | Voltage (mV) | Current (µA) | Total Corrosion (Coulombs) |
| 27/04/2013 | Starting of wetting cycles | | | | | 0.00 |
| 04/05/2013 | 1 | wet | 98.3 | 0.000 | 0.00 | 0.00 |
| 01/06/2013 | 3 | wet | 98.3 | 0.130 | 1.32 | 1.60 |
| 29/06/2013 | 5 | wet | 98.3 | -0.023 | 0.23 | 3.48 |
| 27/07/2013 | 7 | wet | 98.3 | -0.018 | 0.18 | 3.99 |
| 25/08/2013 | 9 | wet | 98.3 | -0.035 | 0.36 | 4.66 |

Table C.18: Macro-Cell Current for Cracked Concrete Specimen (3) Made with Inhibitor V

| Date | Cycle No. | Condition Wet/Dry | Specimen 3 | | | |
|---|---|---|---|---|---|---|
| | | | Resistor (Ohms) | Voltage (mV) | Current (µA) | Total Corrosion (Coulombs) |
| 27/04/2013 | Starting of wetting cycles | | | | | 0.00 |
| 04/05/2013 | 1 | wet | 98.6 | 0.000 | 0.00 | 0.00 |
| 01/06/2013 | 3 | wet | 98.6 | 0.015 | 0.15 | 0.18 |
| 29/06/2013 | 5 | wet | 98.6 | -0.026 | 0.27 | 0.69 |
| 27/07/2013 | 7 | wet | 98.6 | -0.055 | 0.56 | 1.69 |
| 25/08/2013 | 9 | wet | 98.6 | -0.035 | 0.35 | 2.83 |

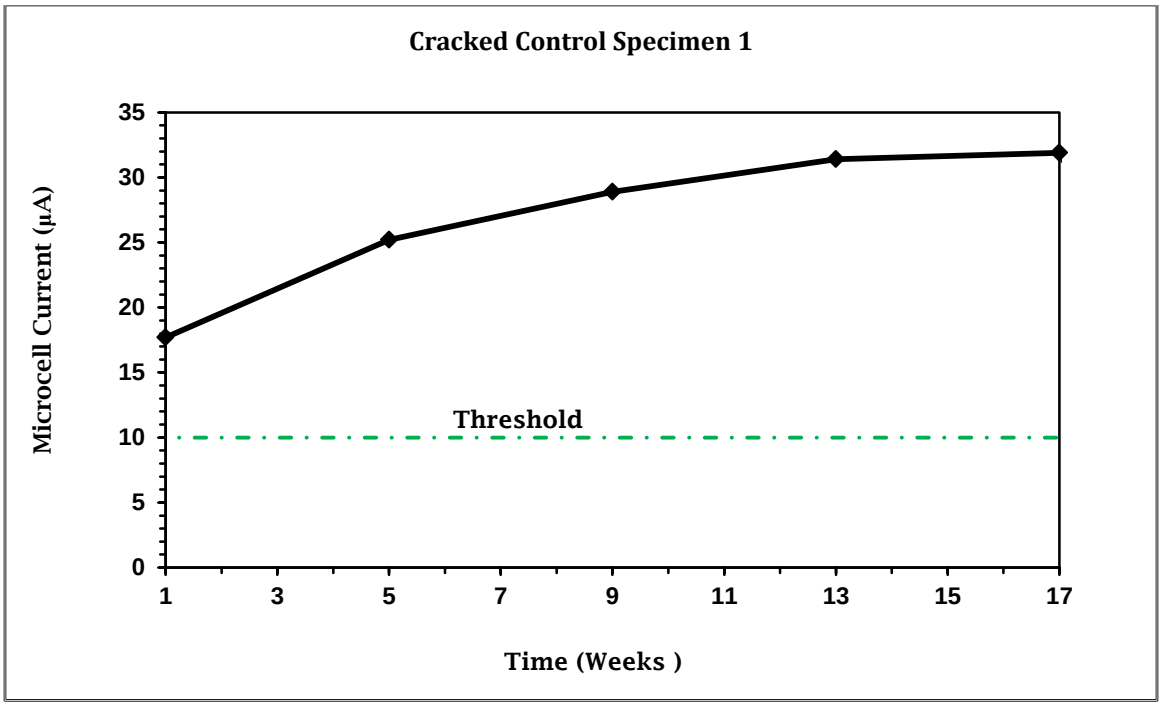


Figure C.1: Macro-Cell Current for Steel in Cracked Control Concrete Specimen (1)

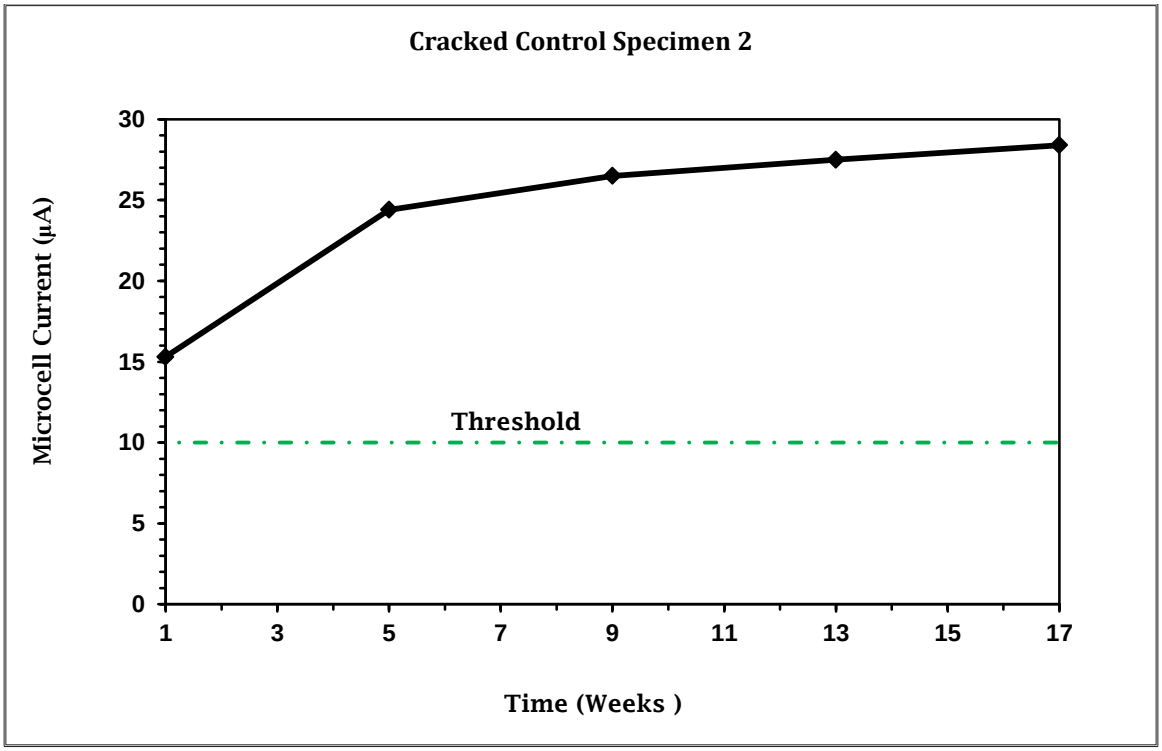


Figure C.2: Macro-Cell Current for Steel in Cracked Control Concrete Specimen (2)

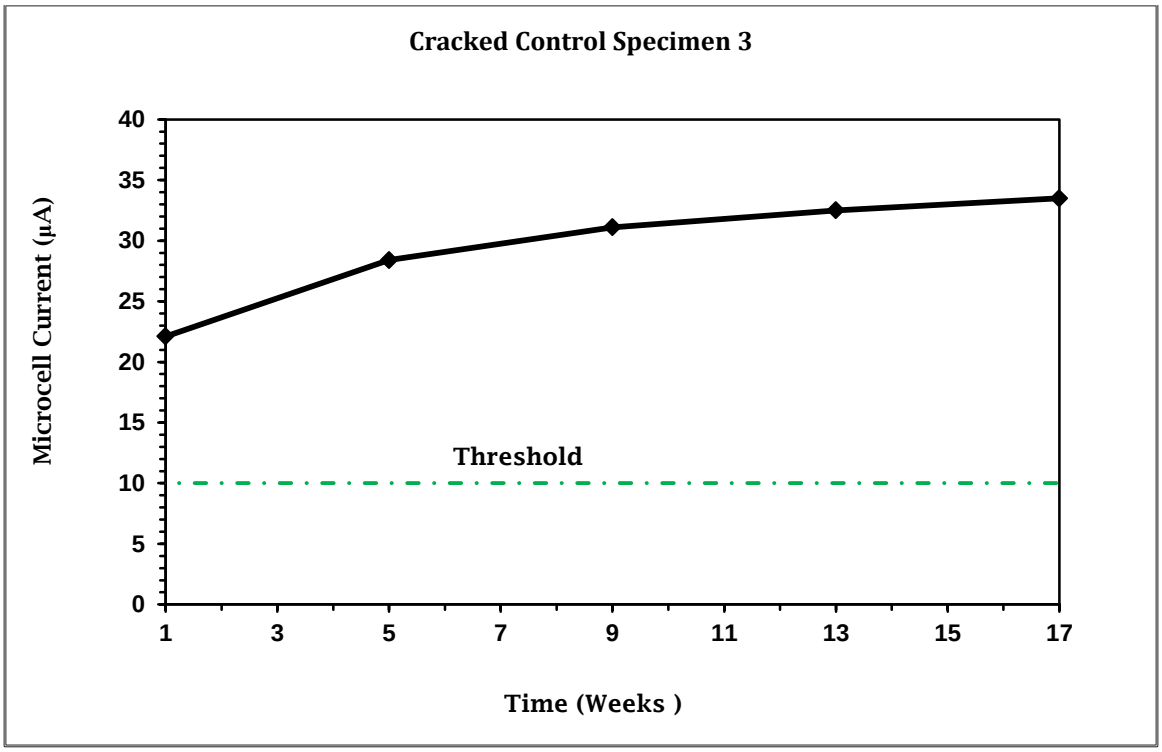


Figure C.3: Macro-Cell Current for Steel in Cracked Control Concrete Specimen (3)

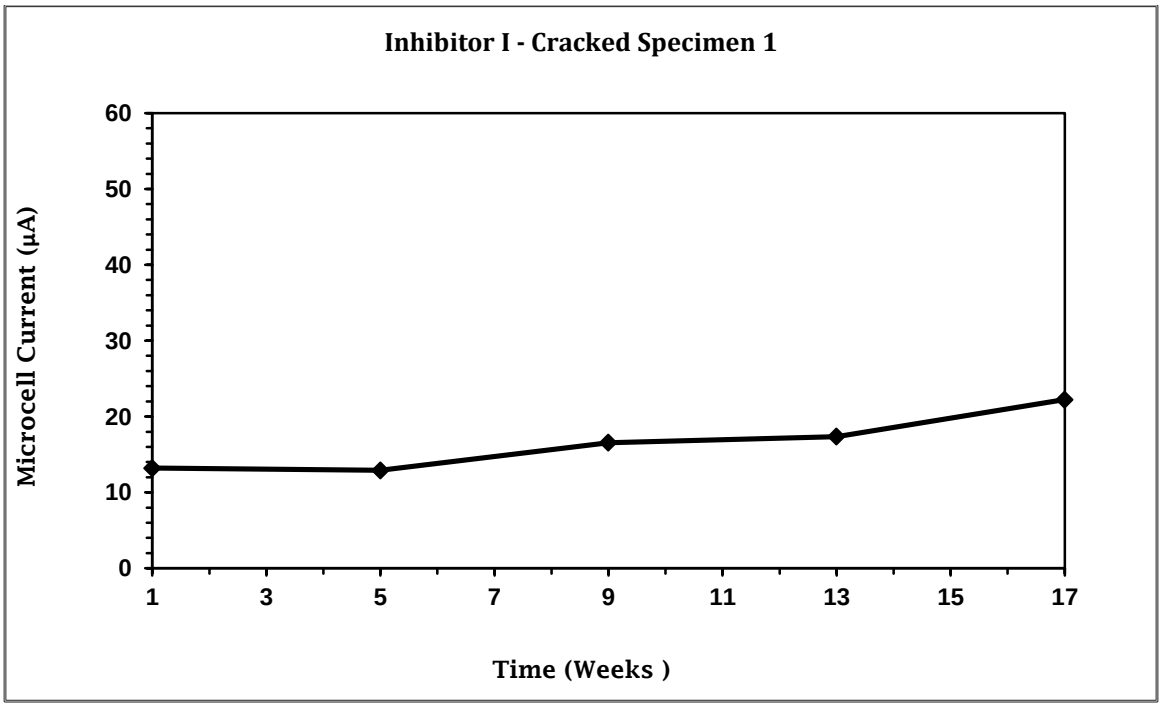


Figure C.4: Macro-Cell Current for Steel in Cracked Concrete Specimen (1) Made with Inhibitor I

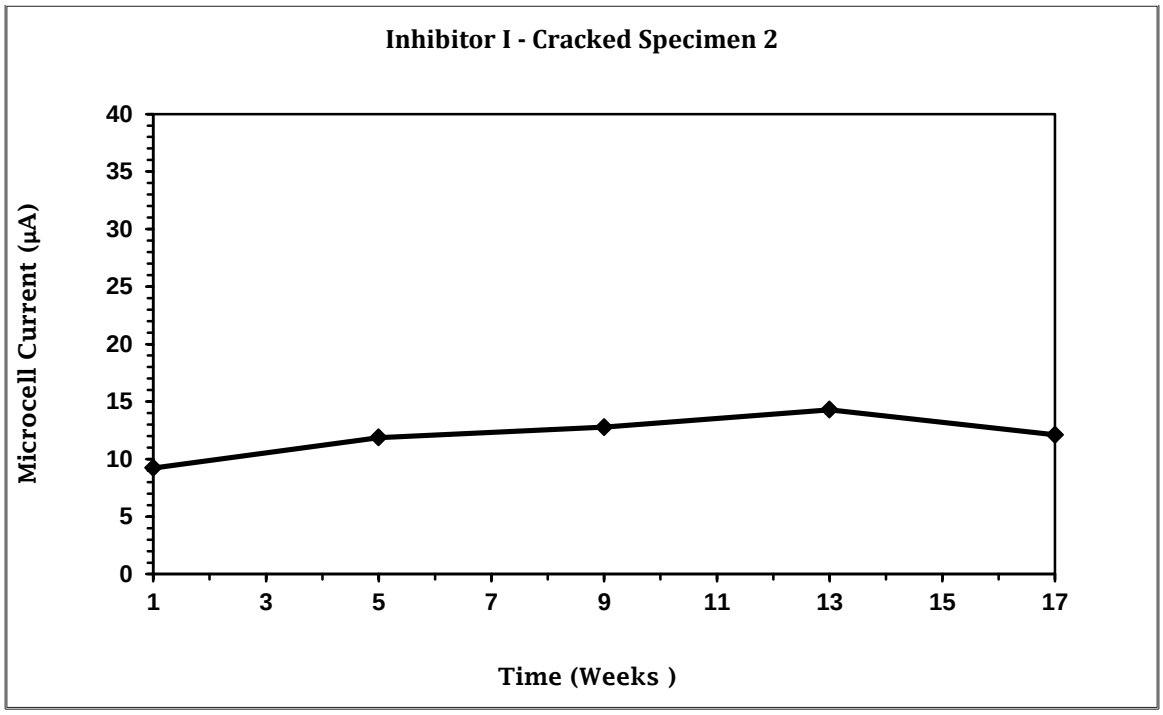


Figure C.5: Macro-Cell Current for Steel in Cracked Concrete Specimen (2) Made with Inhibitor I

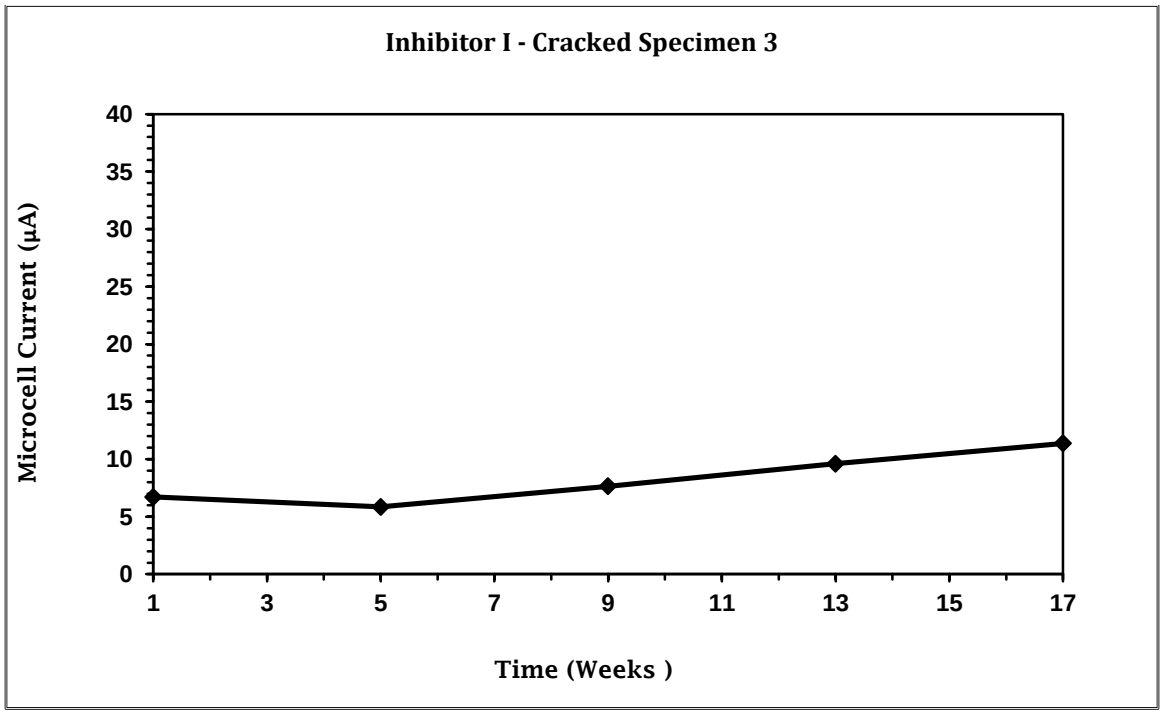


Figure C.6: Macro-Cell Current for Steel in Cracked Concrete Specimen (3) Made with Inhibitor I

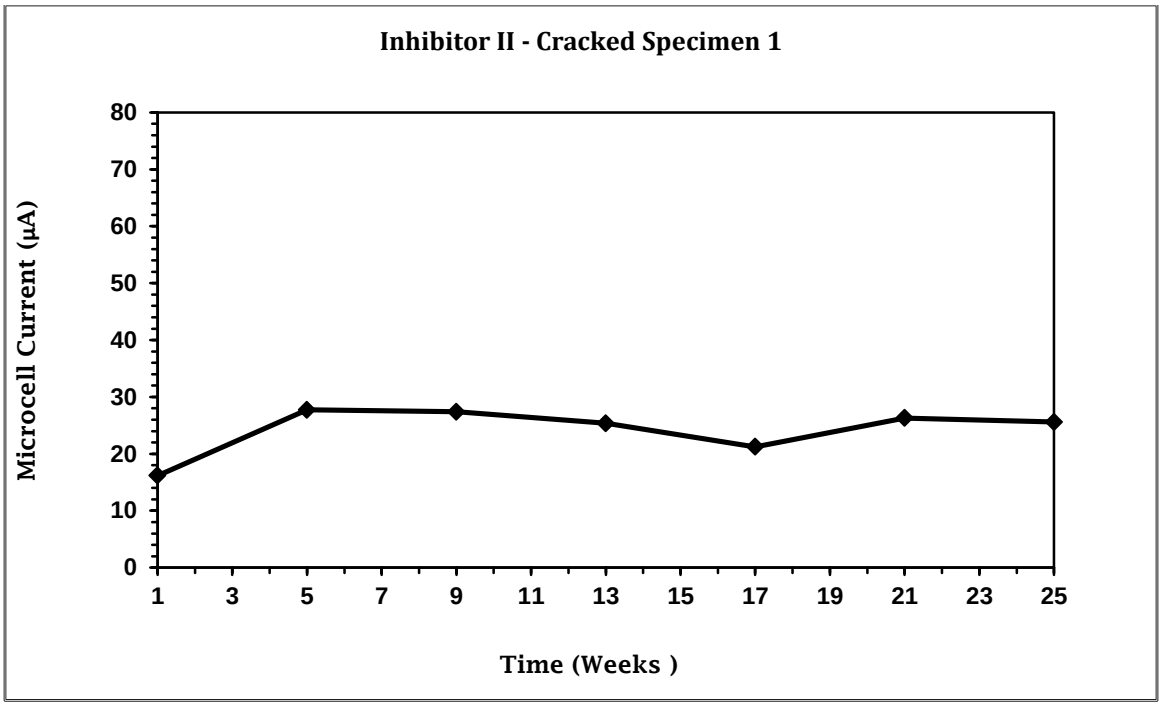


Figure C.7: Macro-Cell Current for Steel in Cracked Concrete Specimen (1) Made with Inhibitor II

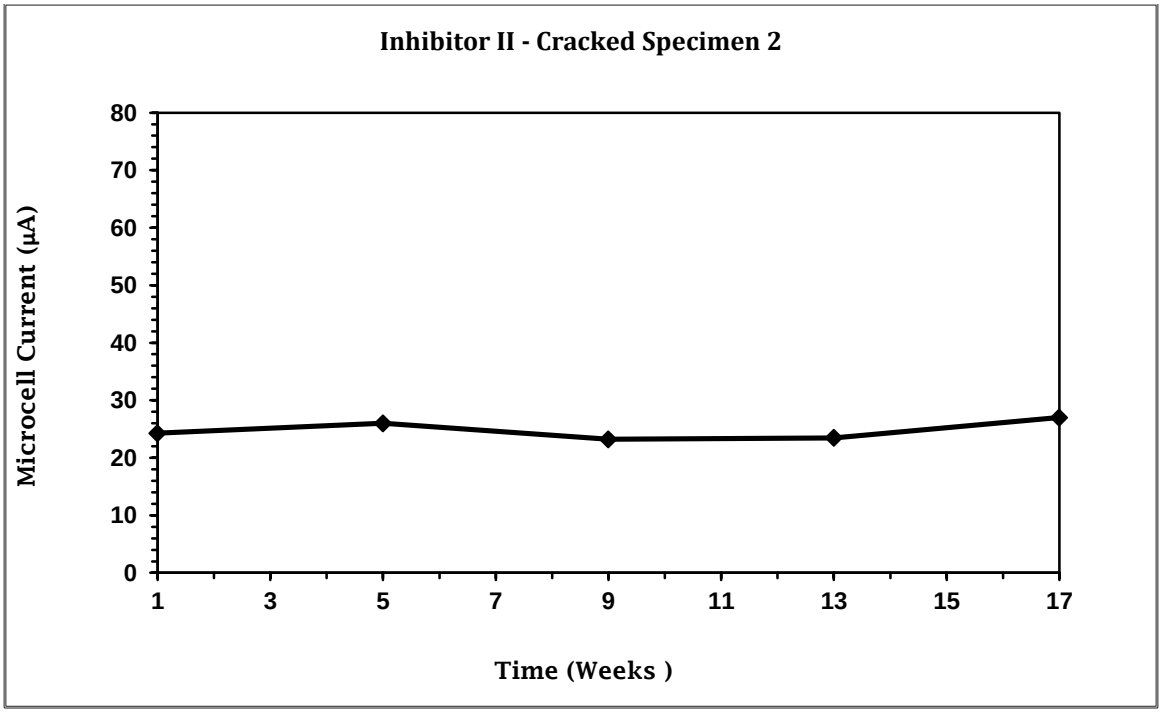


Figure C.8: Macro-Cell Current for Steel in Cracked Concrete Specimen (2) Made with Inhibitor II

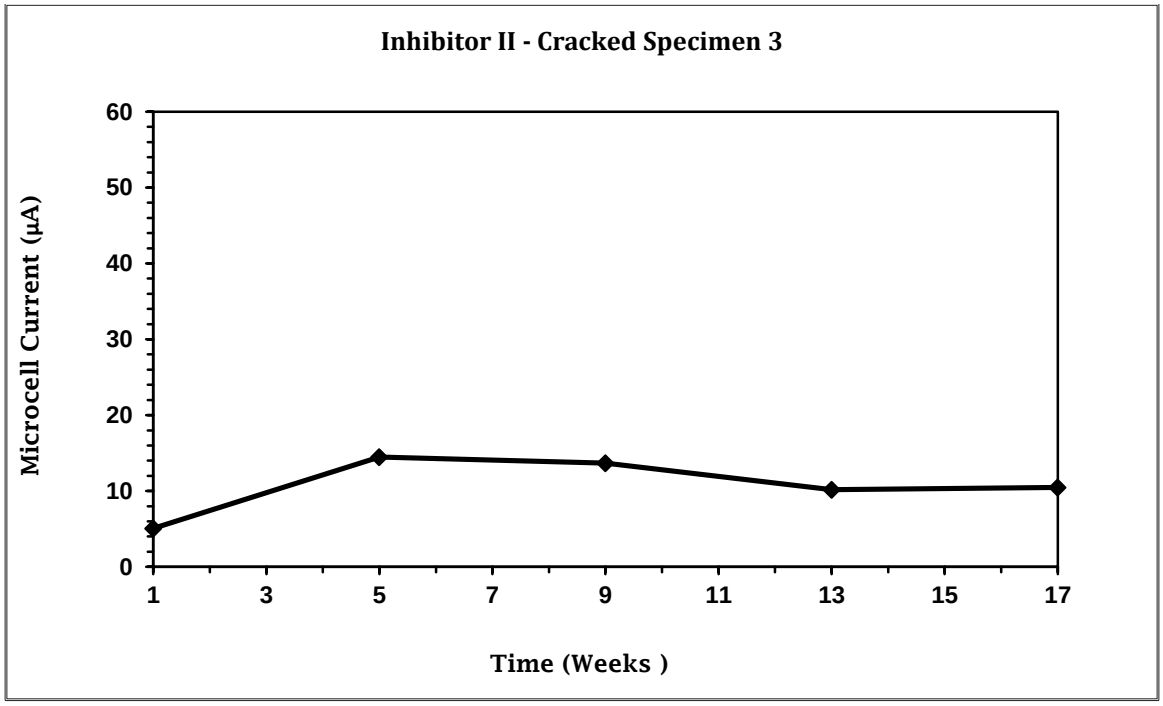


Figure C.9: Macro-Cell Current for Steel in Cracked Concrete Specimen (3) Made with Inhibitor II

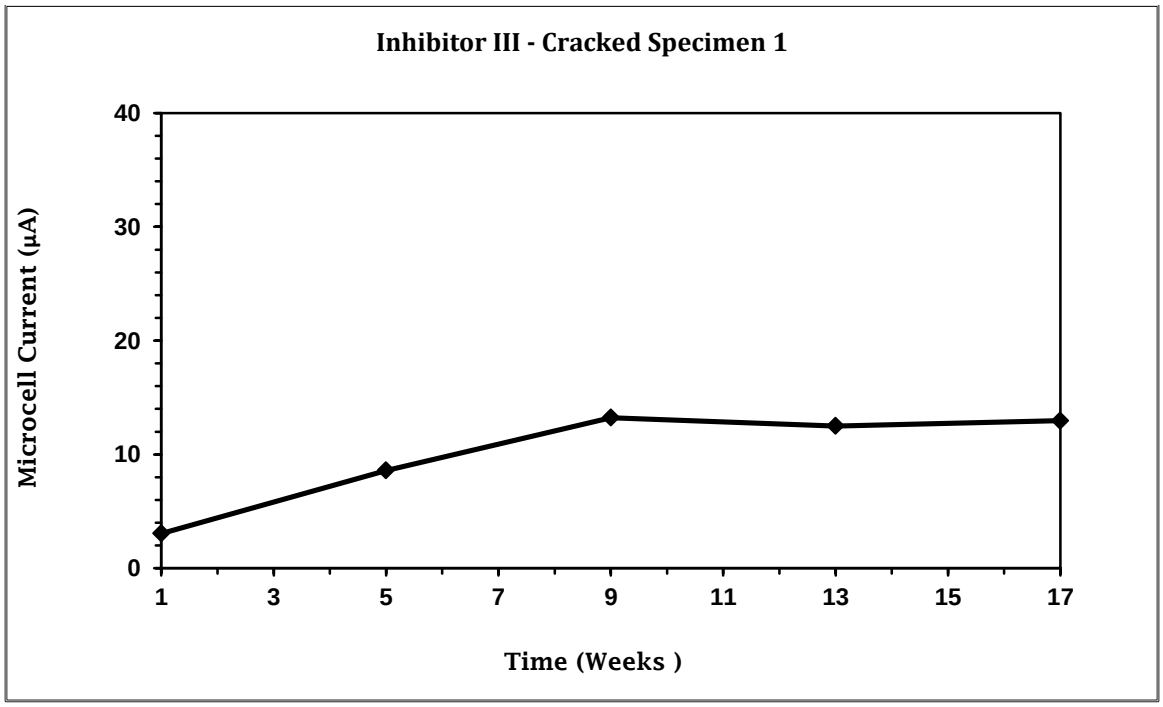


Figure C.10: Macro-Cell Current for Steel in Cracked Concrete Specimen (1) Made with Inhibitor III

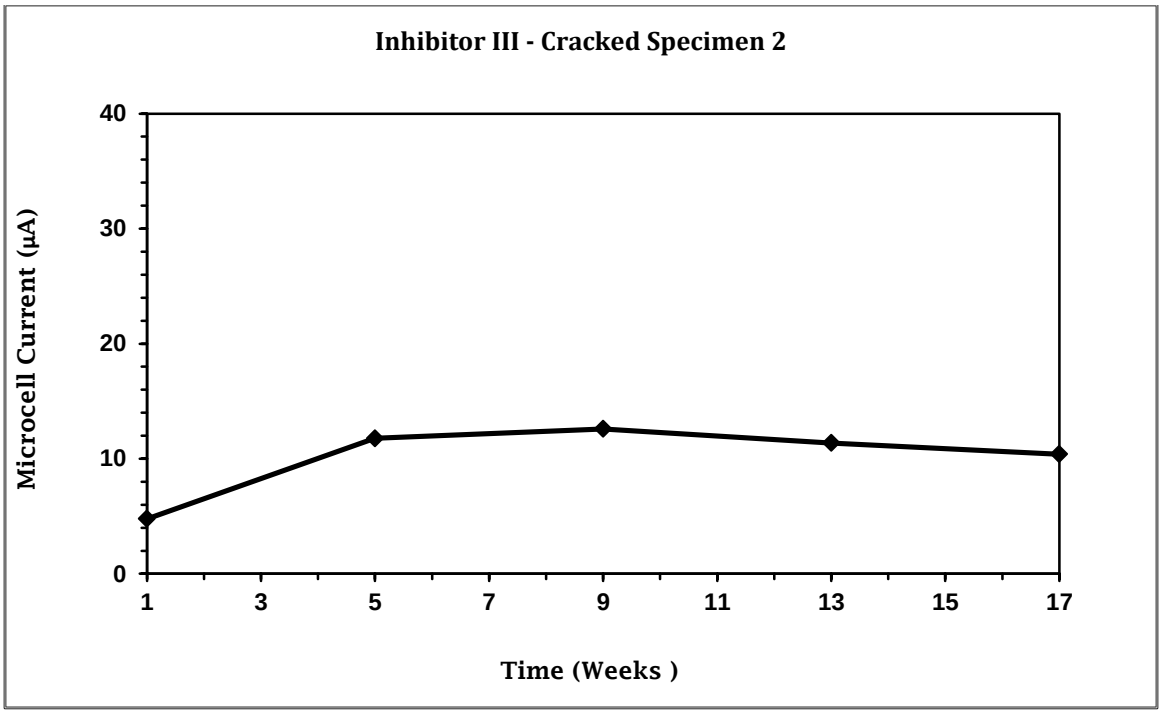


Figure C.11: Macro-Cell Current for Steel in Cracked Concrete Specimen (2) Made with Inhibitor III

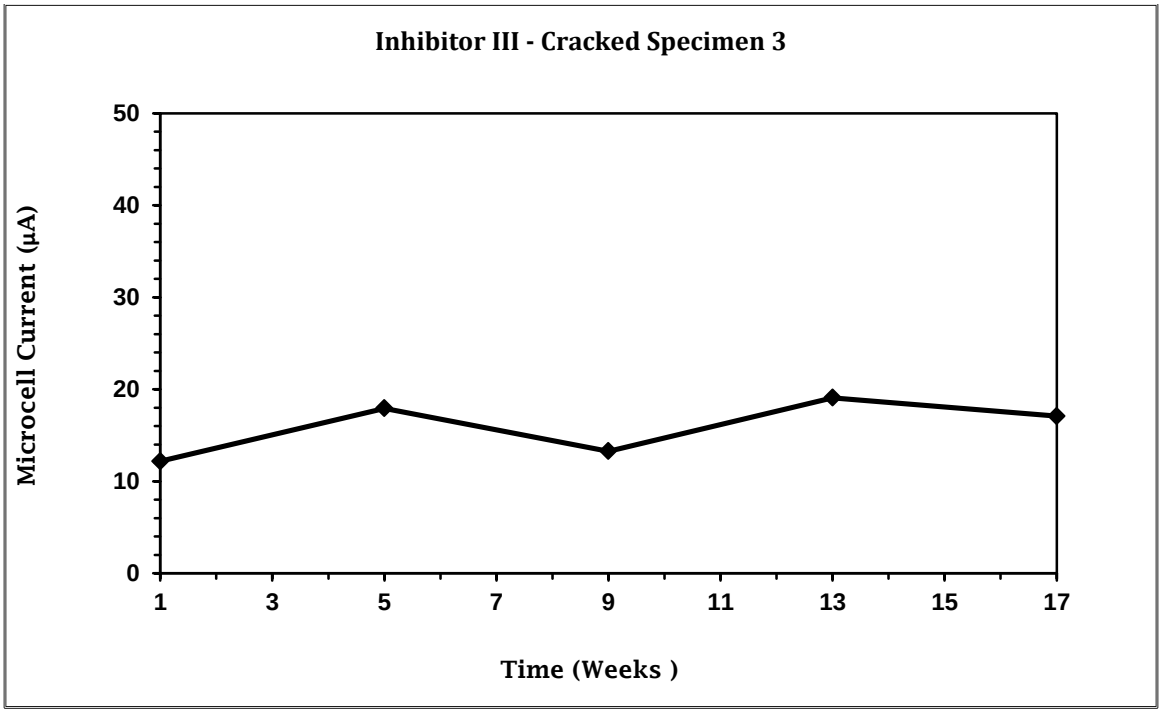


Figure C.12: Macro-Cell Current for Steel in Cracked Concrete Specimen (3) Made with Inhibitor III

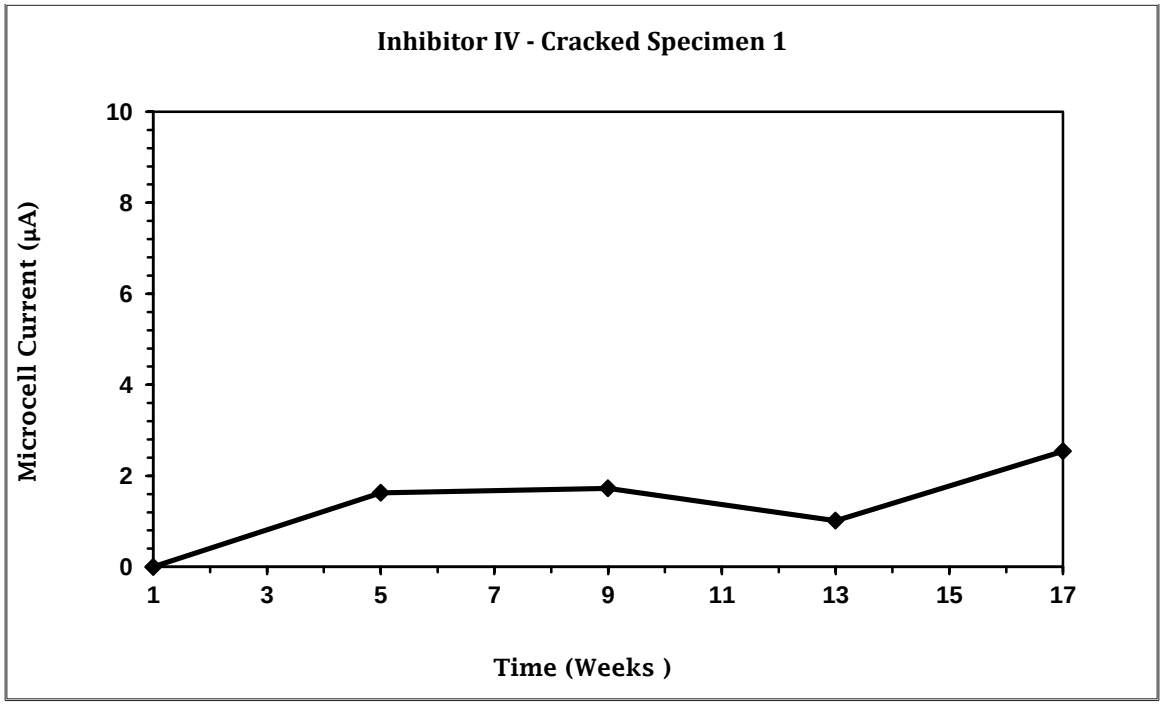


Figure C.13: Macro-Cell Current for Steel in Cracked Concrete Specimen (1) Made with Inhibitor IV

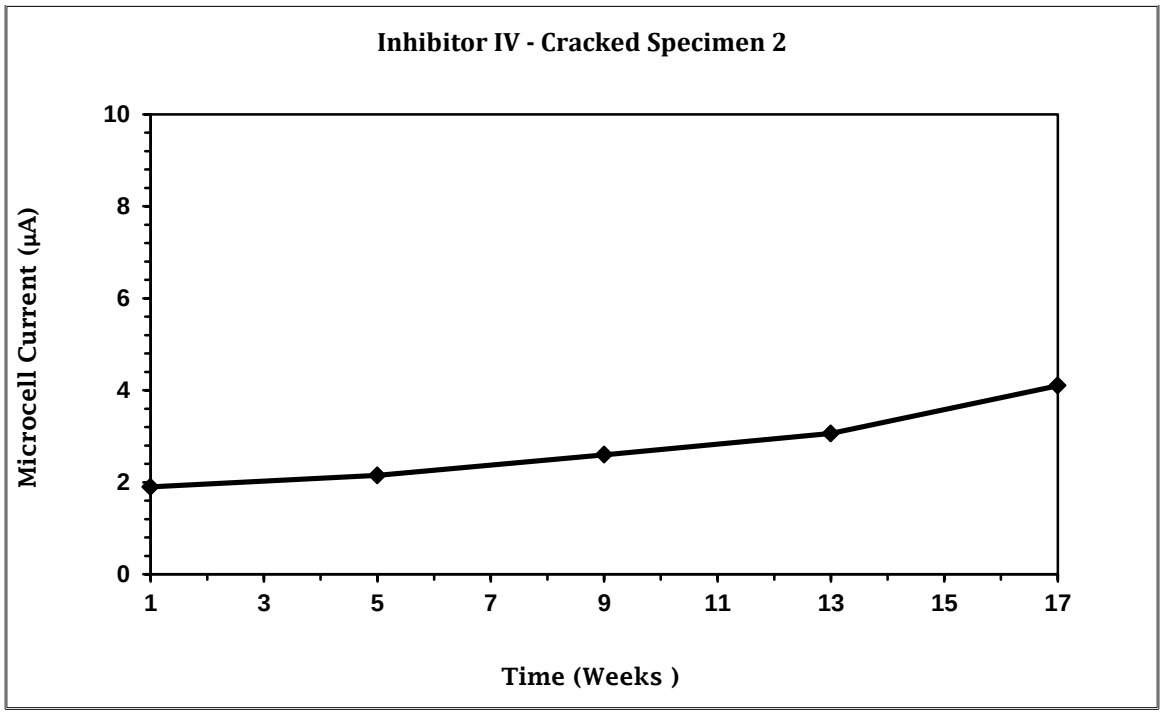


Figure C.14: Macro-Cell Current for Steel in Cracked Concrete Specimen (2) Made with Inhibitor IV

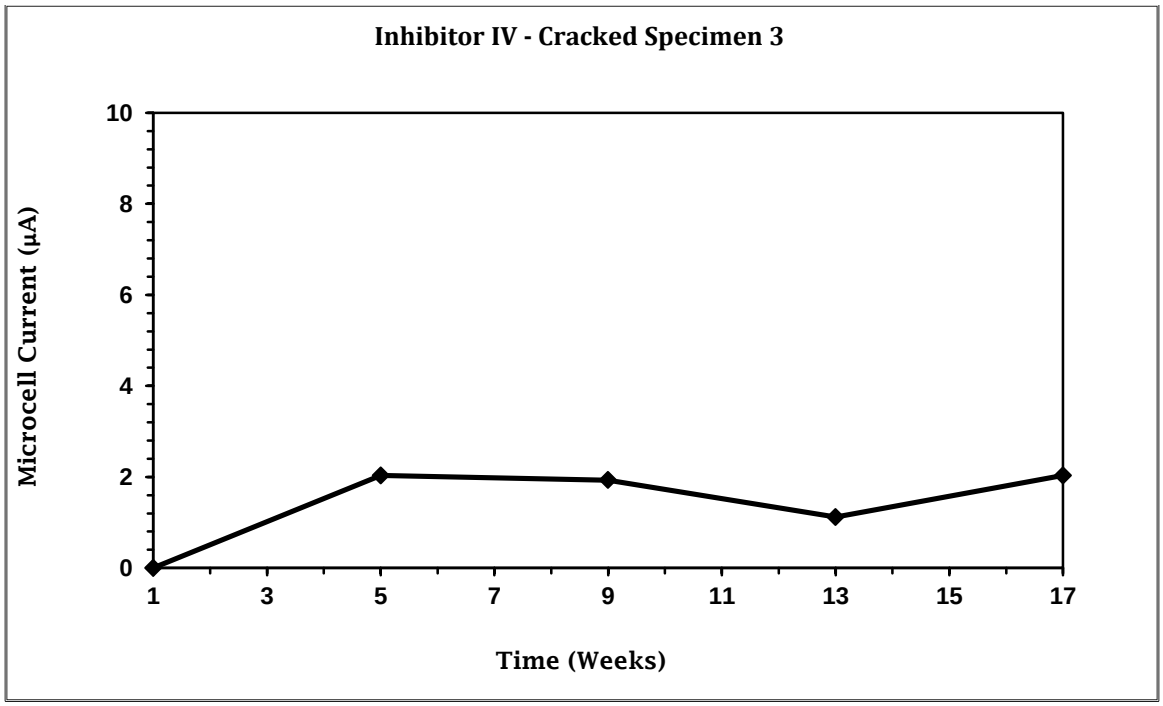


Figure C.15: Macro-Cell Current for Steel in Cracked Concrete Specimen (3) Made with Inhibitor IV

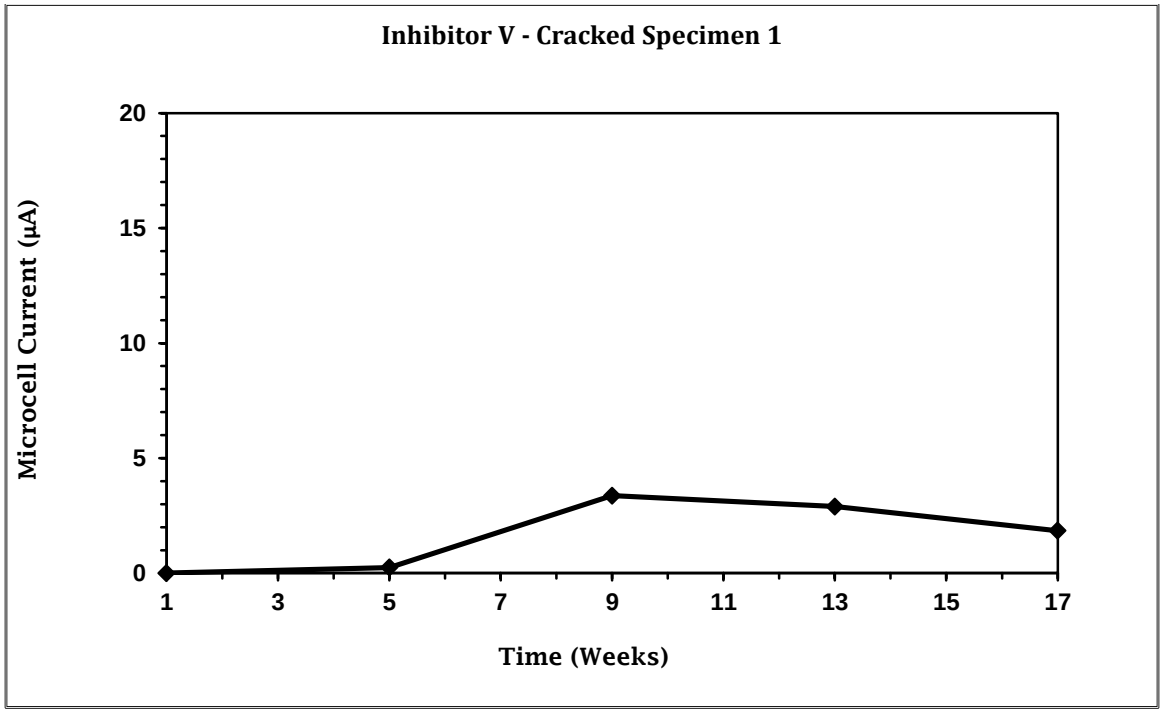


Figure C.16: Macro-Cell Current for Steel in Cracked Concrete Specimen (1) Made with Inhibitor V

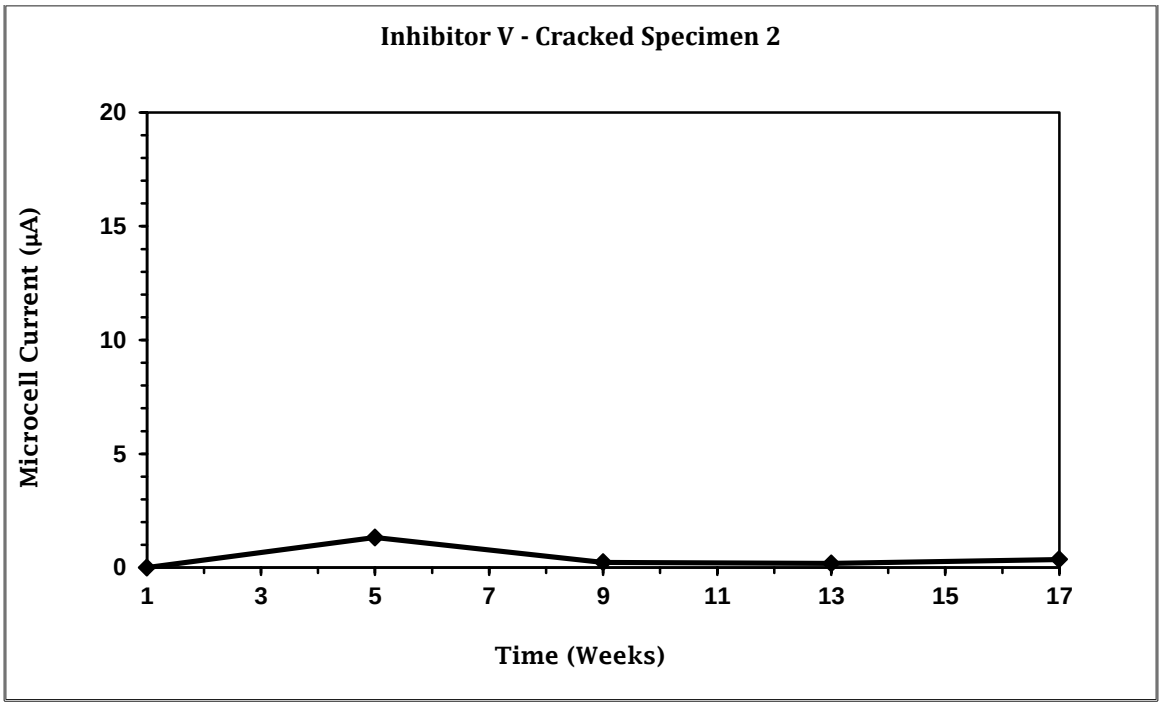


Figure C.17: Macro-Cell Current for Steel in Cracked Concrete Specimen (2) Made with Inhibitor V

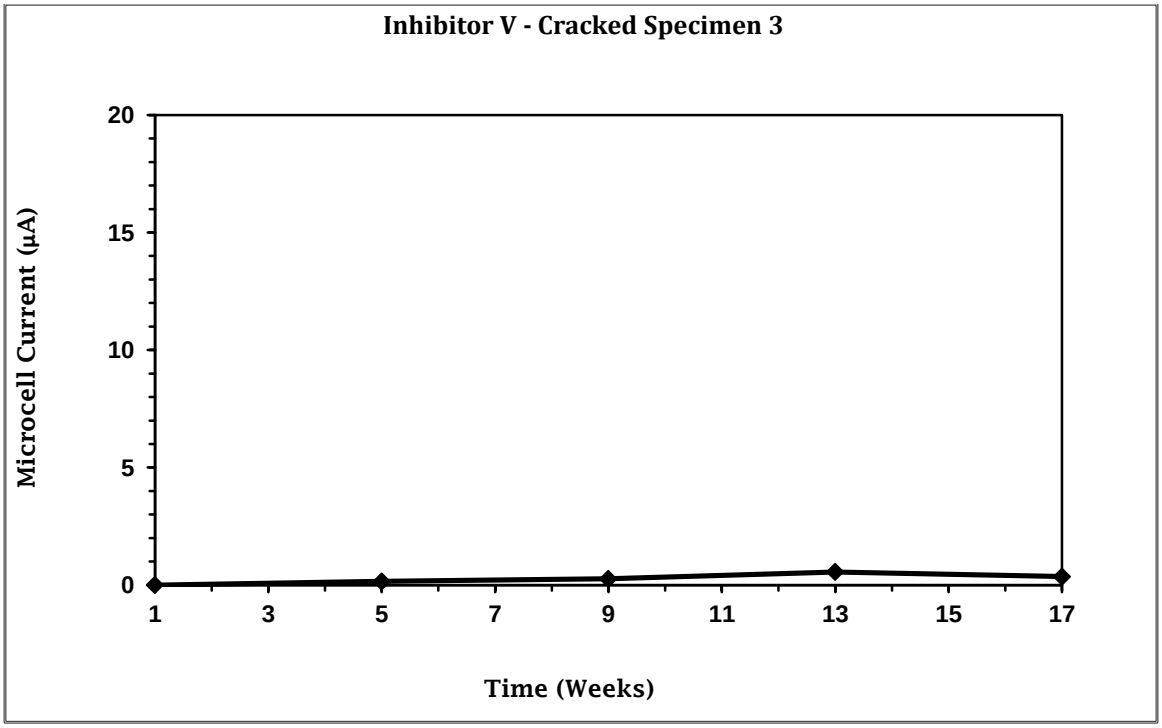


Figure C.18: Macro-Cell Current for Steel in Cracked Concrete Specimen (3) Made with Inhibitor V

## C.2 MACRO-CELL READINGS FOR CRACKED ASTM G109 SPECIMENS

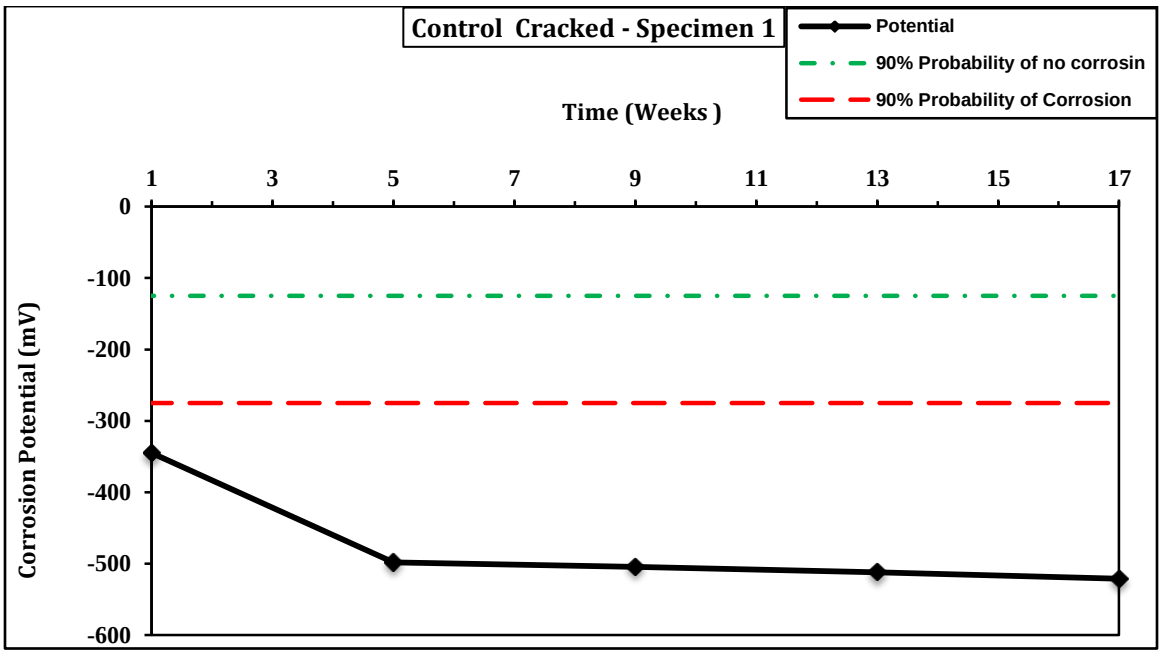


Figure C.19: Corrosion Potential for Steel in Control Cracked Concrete Specimen (1)

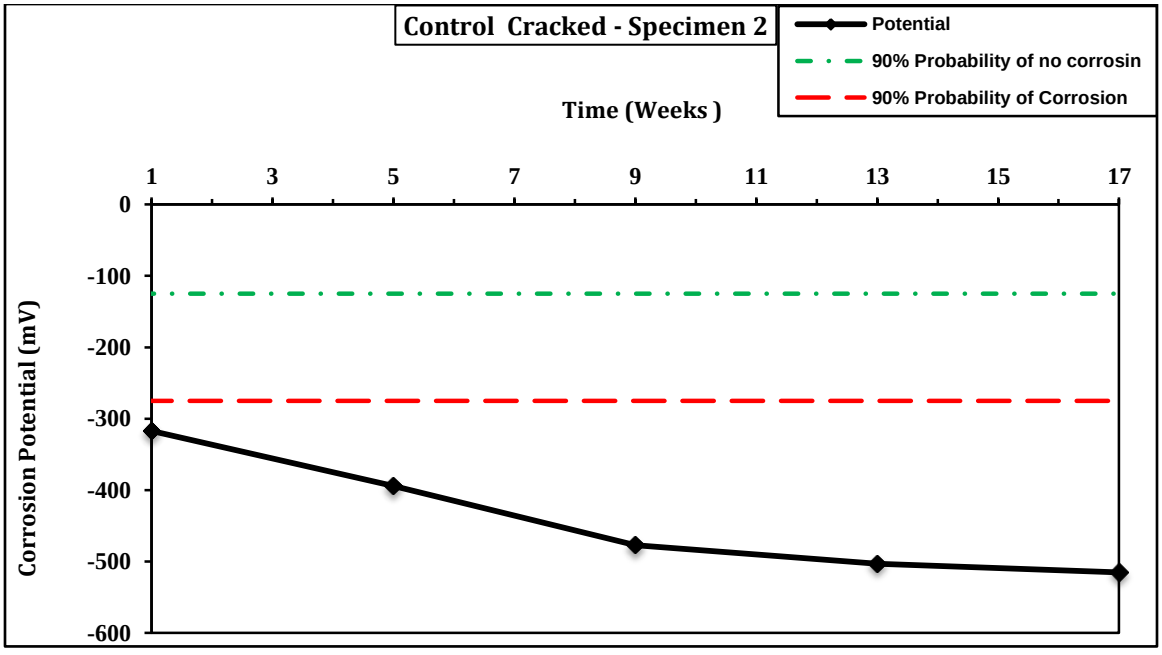


Figure C.20: Corrosion Potential for Steel in Control Cracked Concrete Specimen (2)

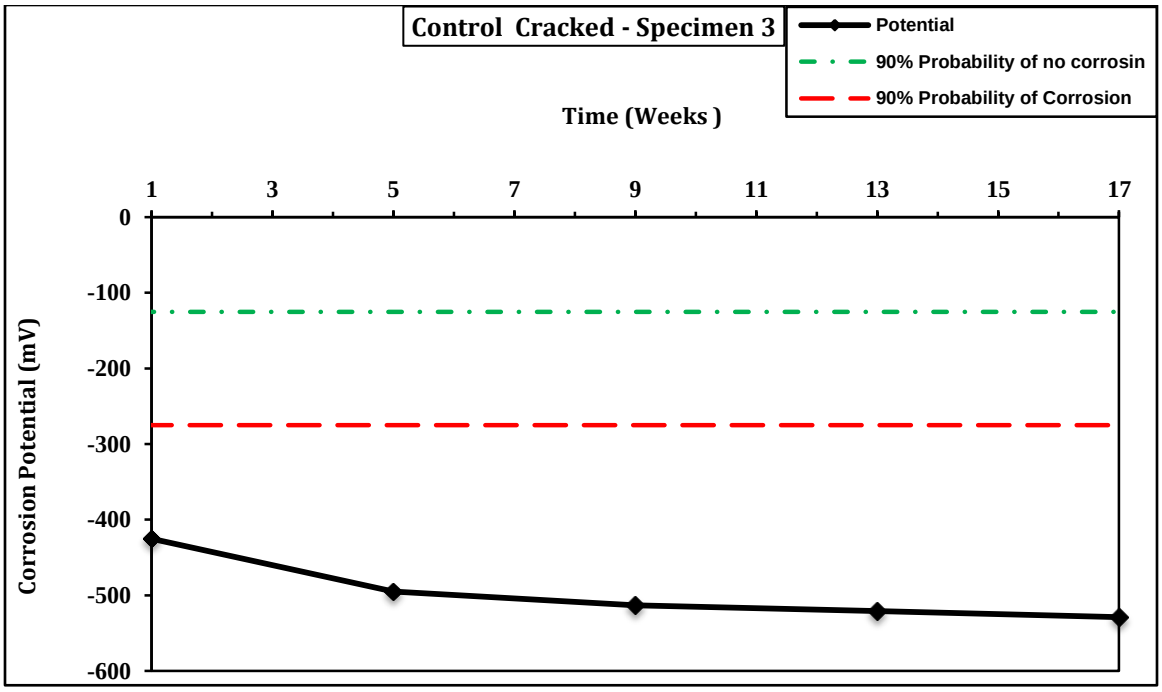


Figure C.21: Corrosion Potential for Steel in Control Cracked Concrete Specimen (3)

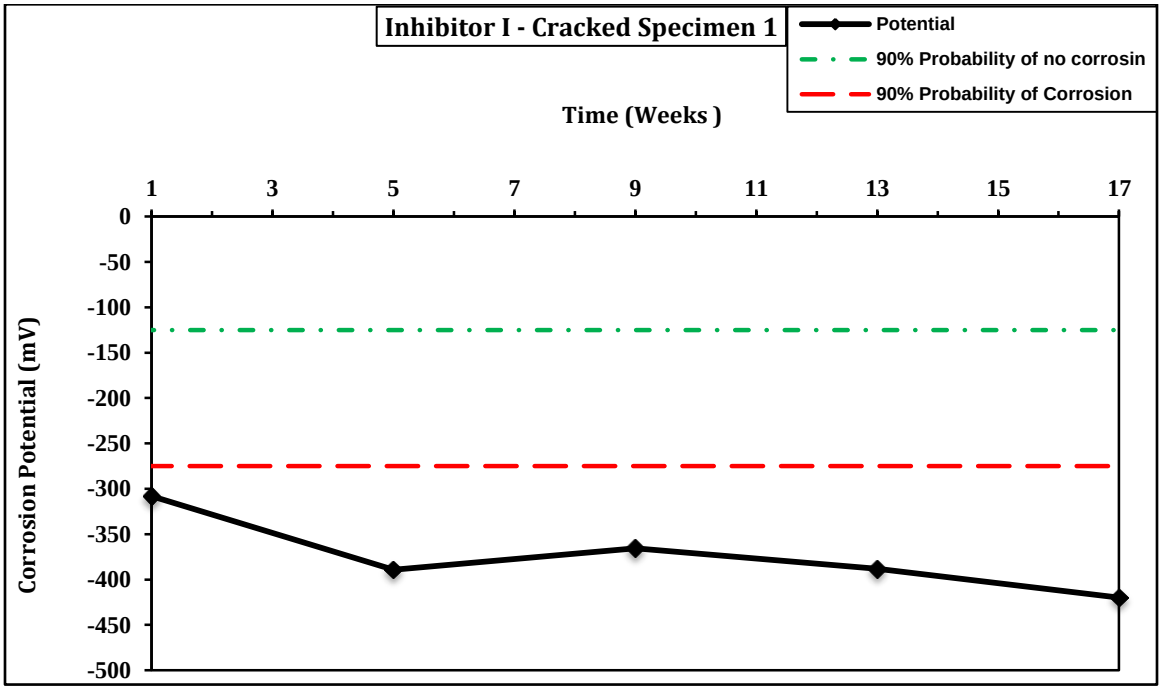


Figure C.22: Corrosion Potential for Steel in Cracked Concrete Specimen (1) Made with Inhibitor I

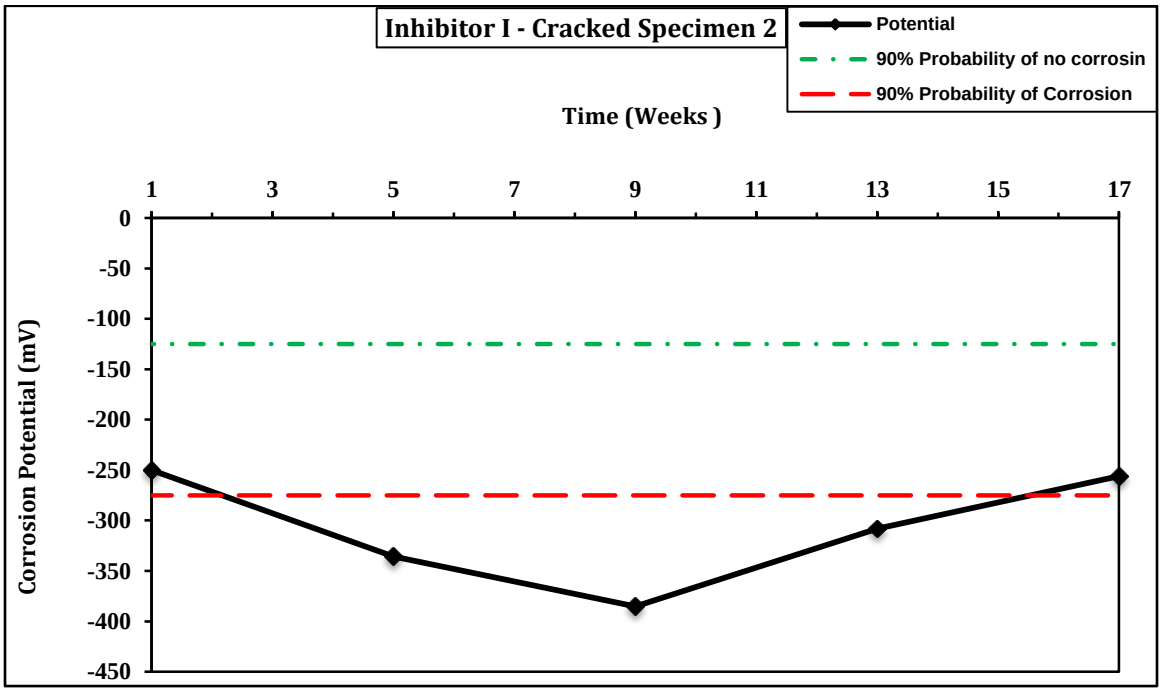


Figure C.23: Corrosion Potential for Steel in Cracked Concrete Specimen (2) Made with Inhibitor I

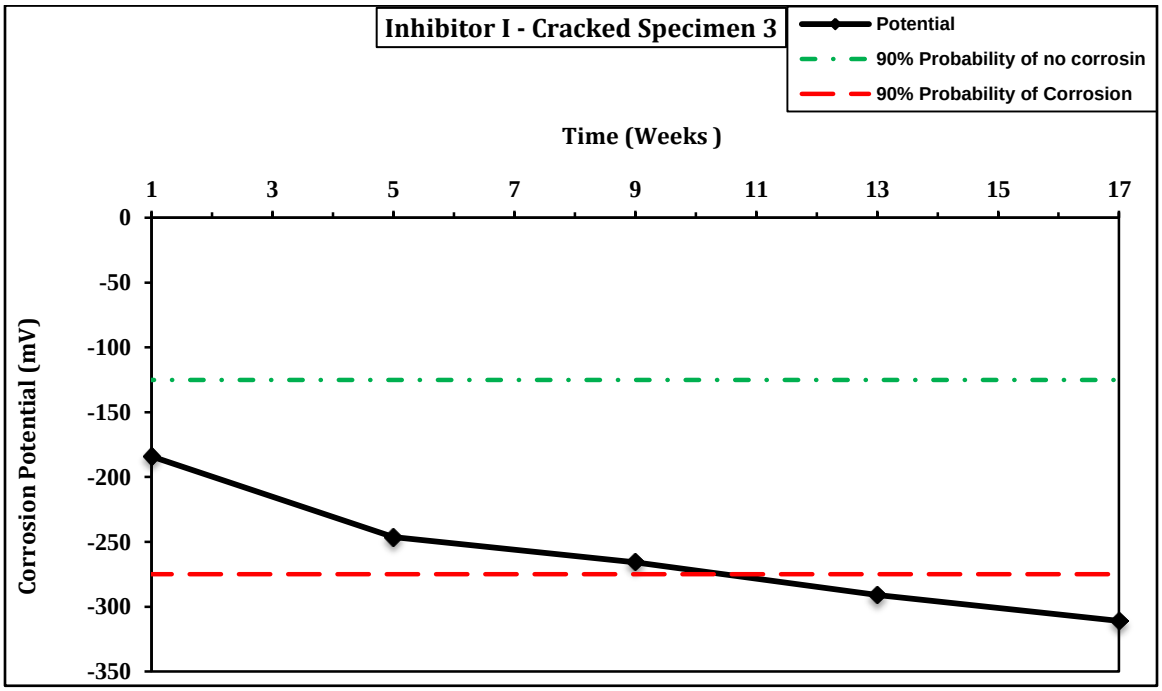


Figure C.24: Corrosion Potential for Steel in Cracked Concrete Specimen (3) Made with Inhibitor I

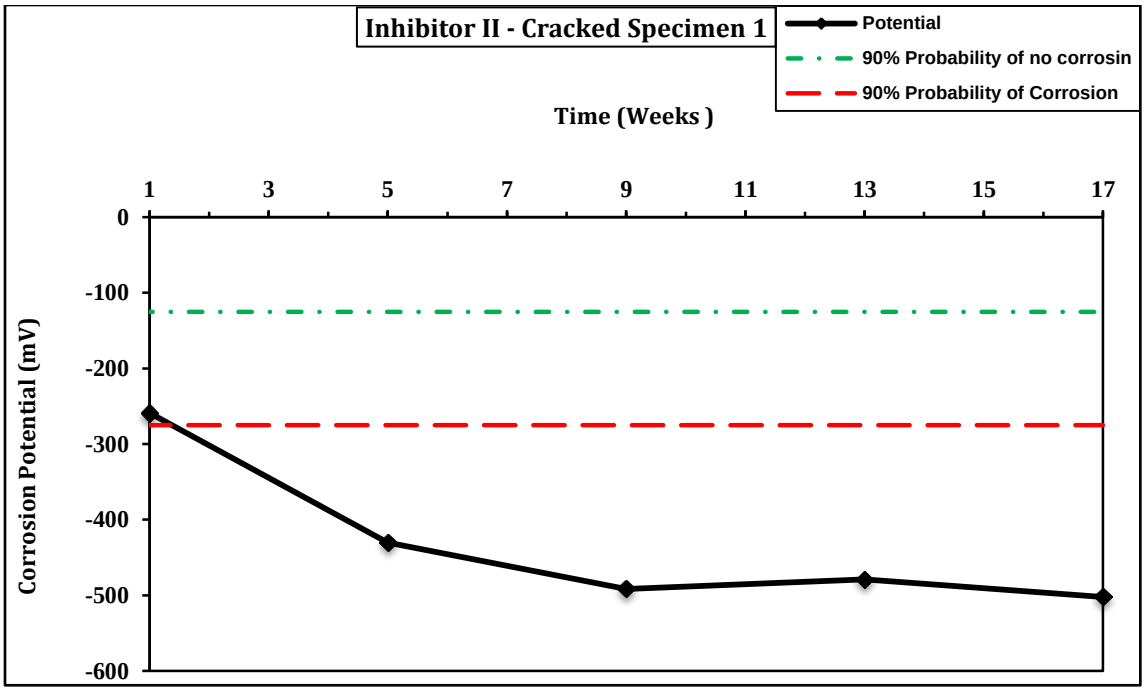


Figure C.25: Corrosion Potential for Steel in Cracked Concrete Specimen (1) Made with Inhibitor II

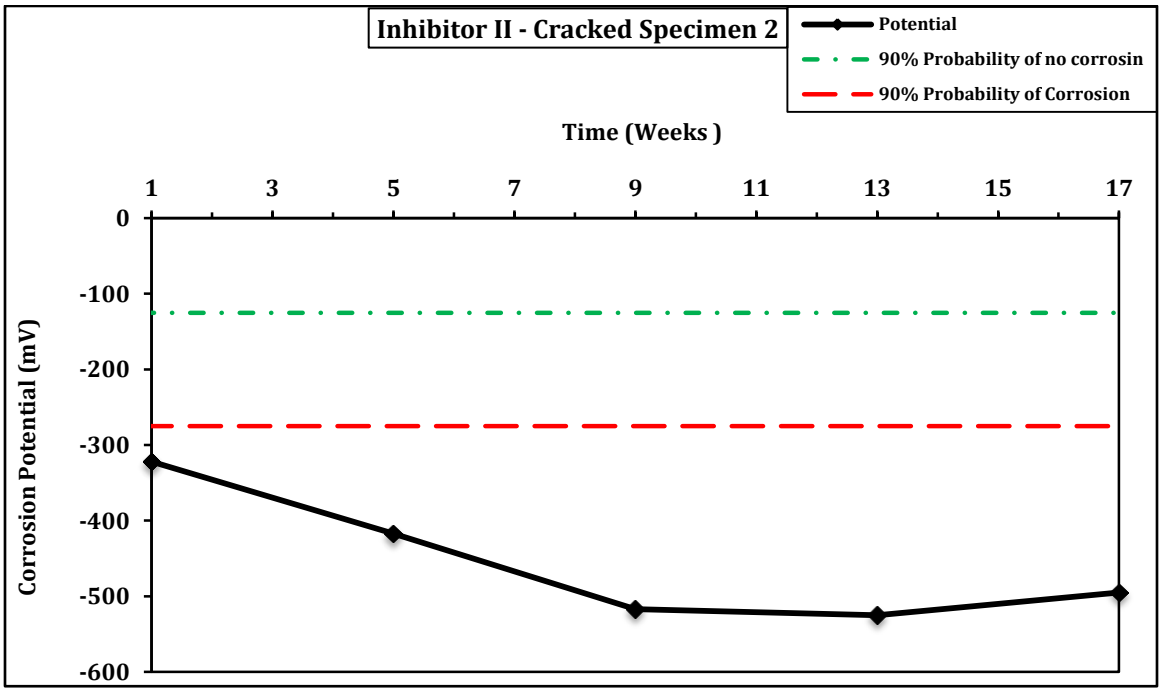


Figure C.26: Corrosion Potential for Steel in Cracked Concrete Specimen (2) Made with Inhibitor II

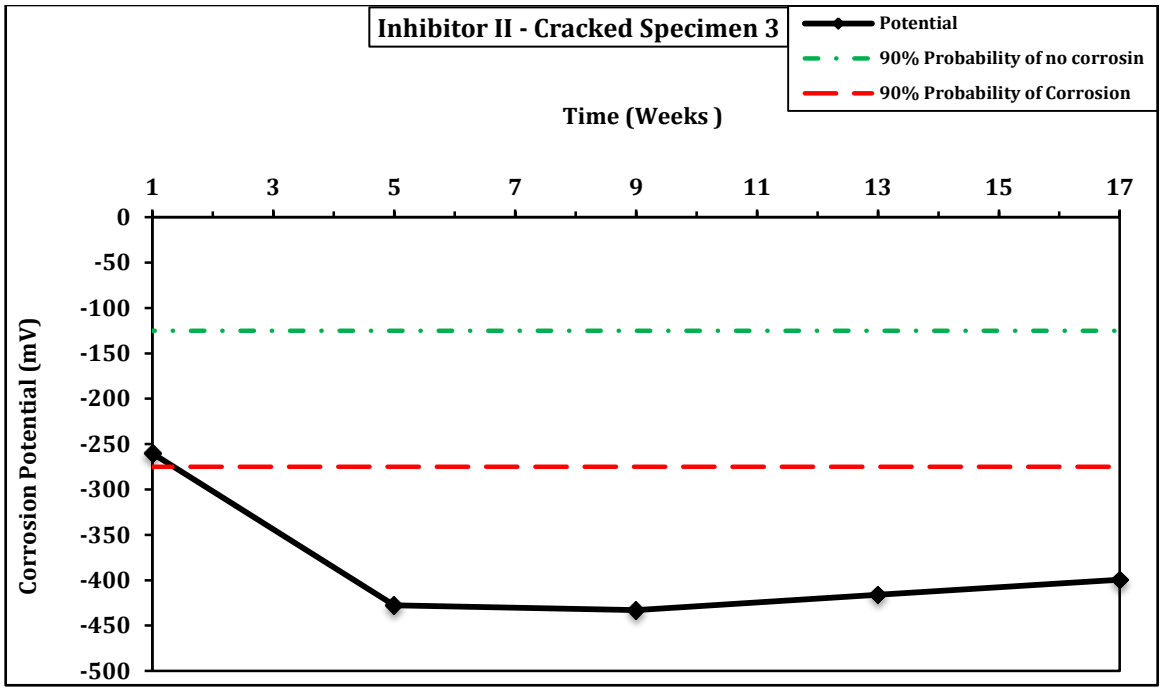


Figure C.27: Corrosion Potential for Steel in Cracked Concrete Specimen (3) Made with Inhibitor II

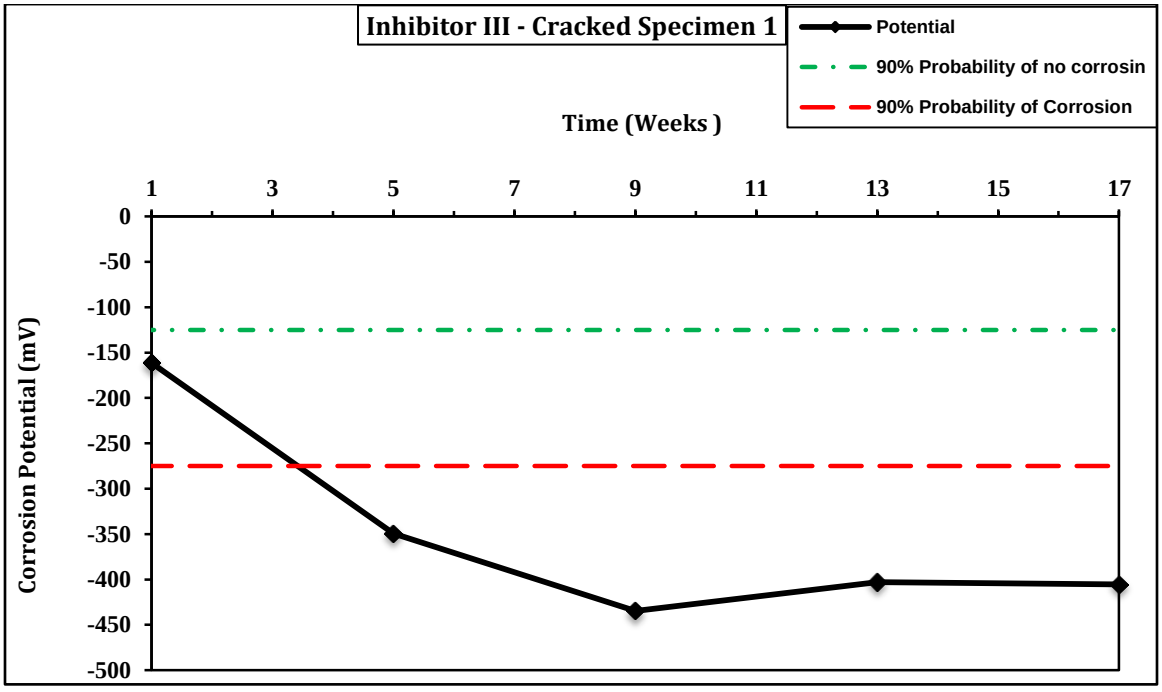


Figure C.28: Corrosion Potential for Steel in Cracked Concrete Specimen (1) Made with Inhibitor III

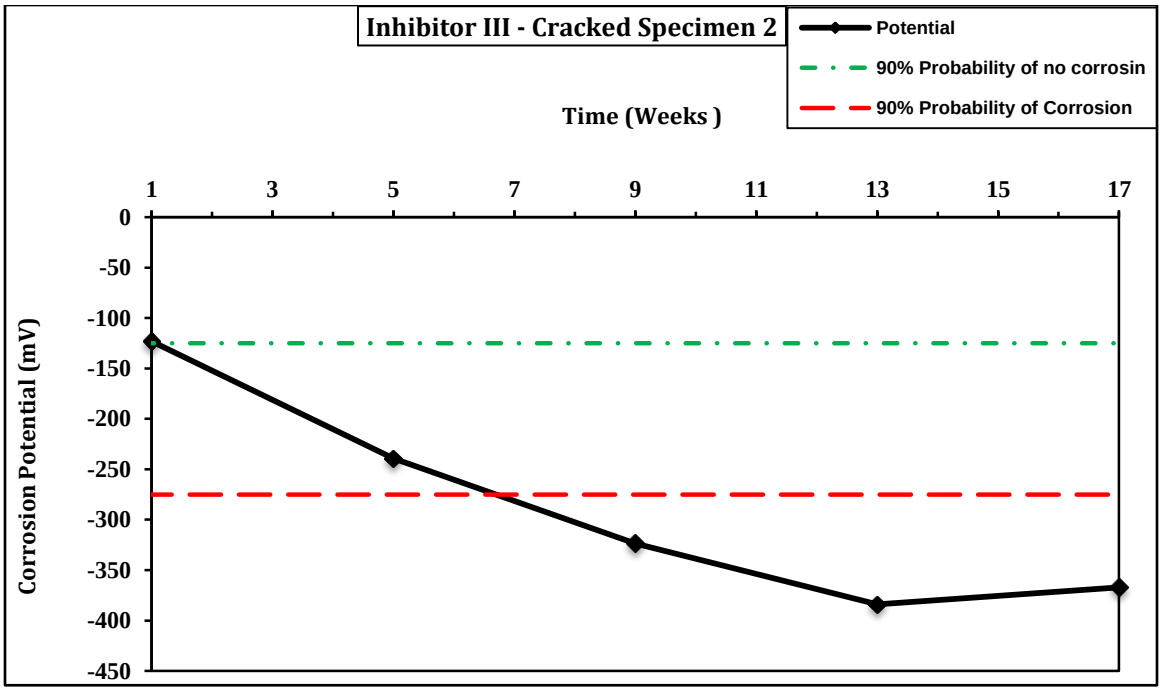


Figure C.29: Corrosion Potential for Steel in Cracked Concrete Specimen (2) Made with Inhibitor III

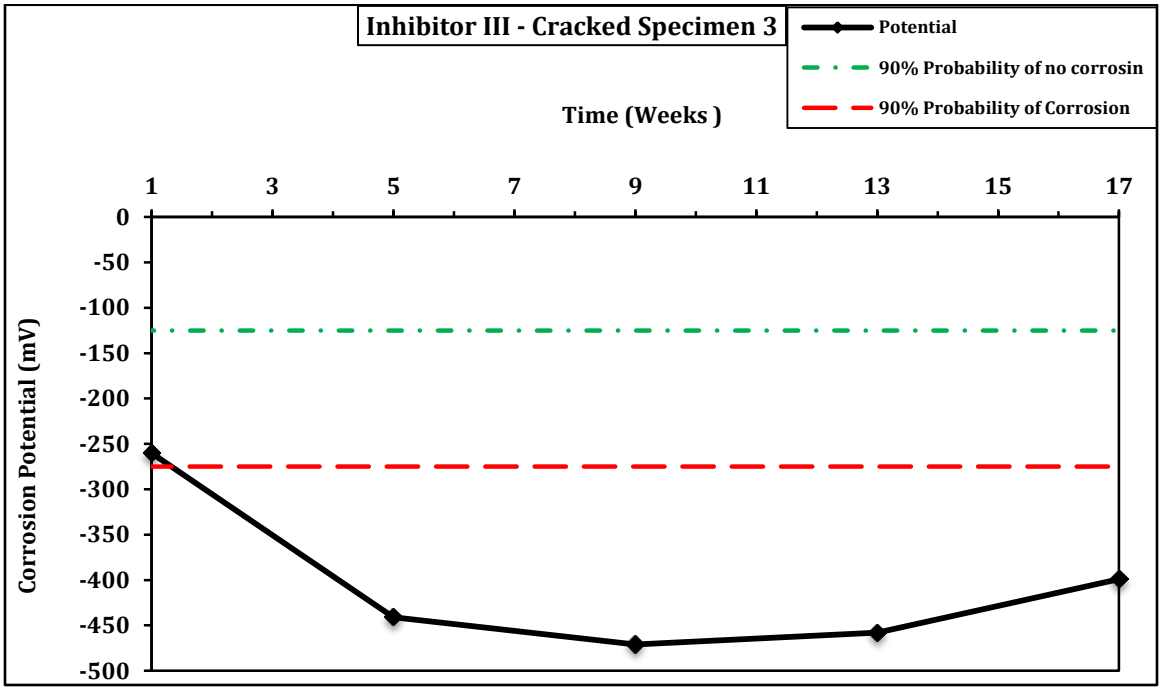


Figure C.30: Corrosion Potential for Steel in Cracked Concrete Specimen (3) Made with Inhibitor III

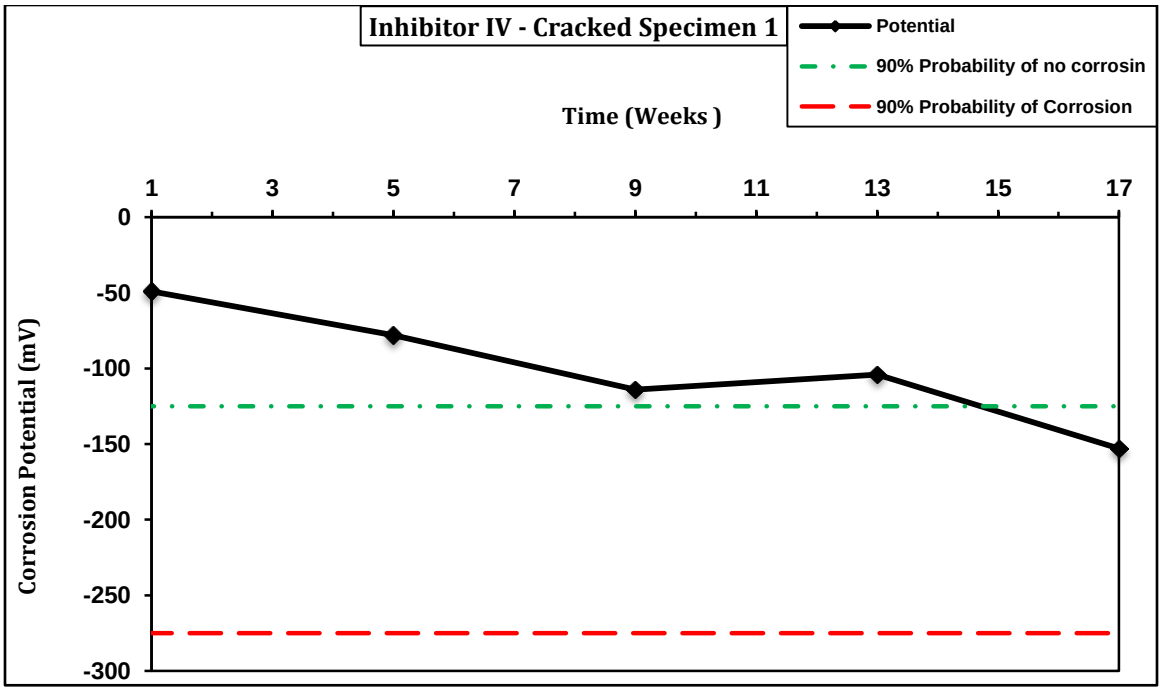


Figure C.31: Corrosion Potential for Steel in Cracked Concrete Specimen (1) Made with Inhibitor IV

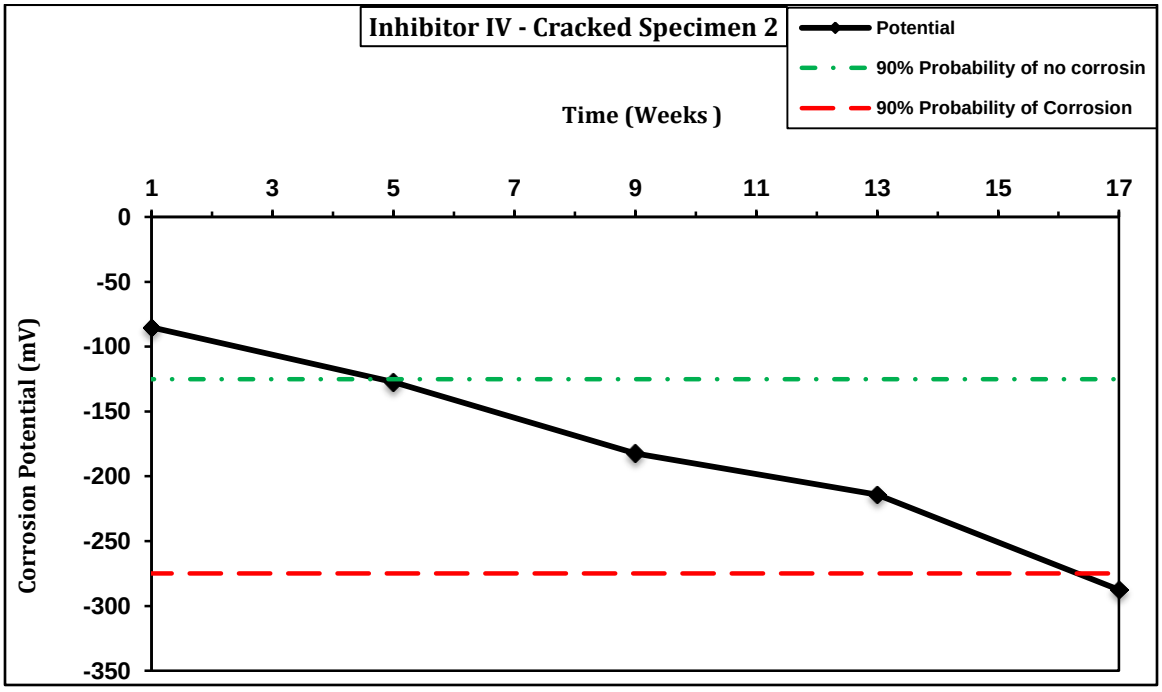


Figure C.32: Corrosion Potential for Steel in Cracked Concrete Specimen (2) Made with Inhibitor IV

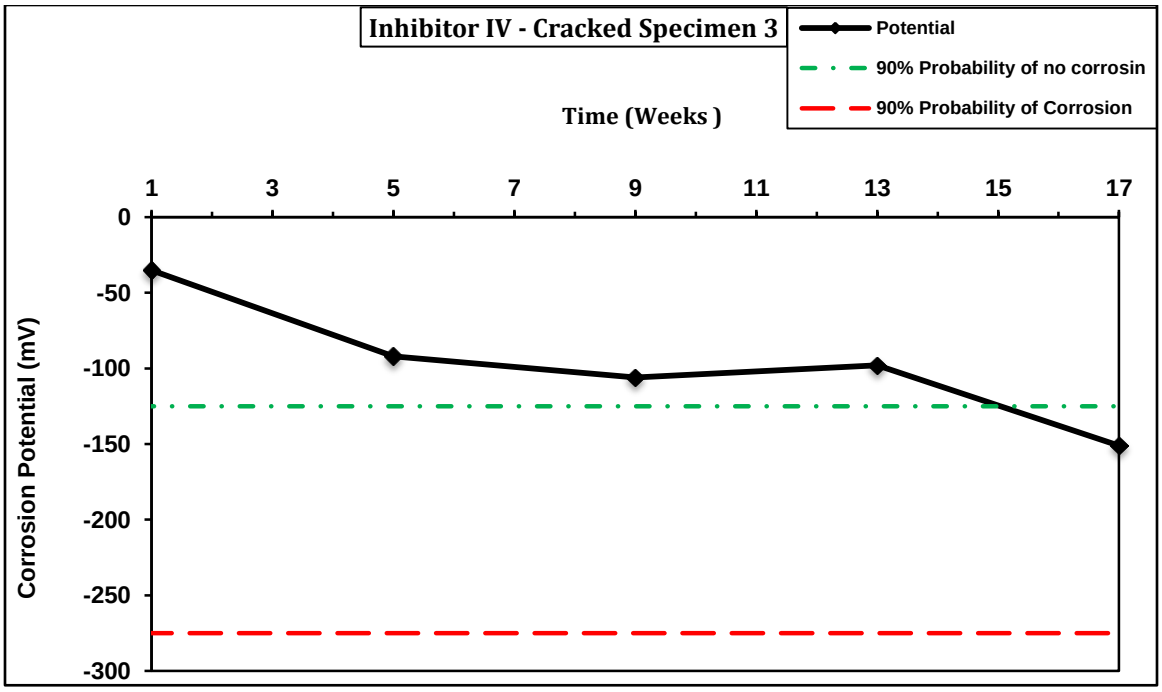


Figure C.33: Corrosion Potential for Steel in Cracked Concrete Specimen (3) Made with Inhibitor IV

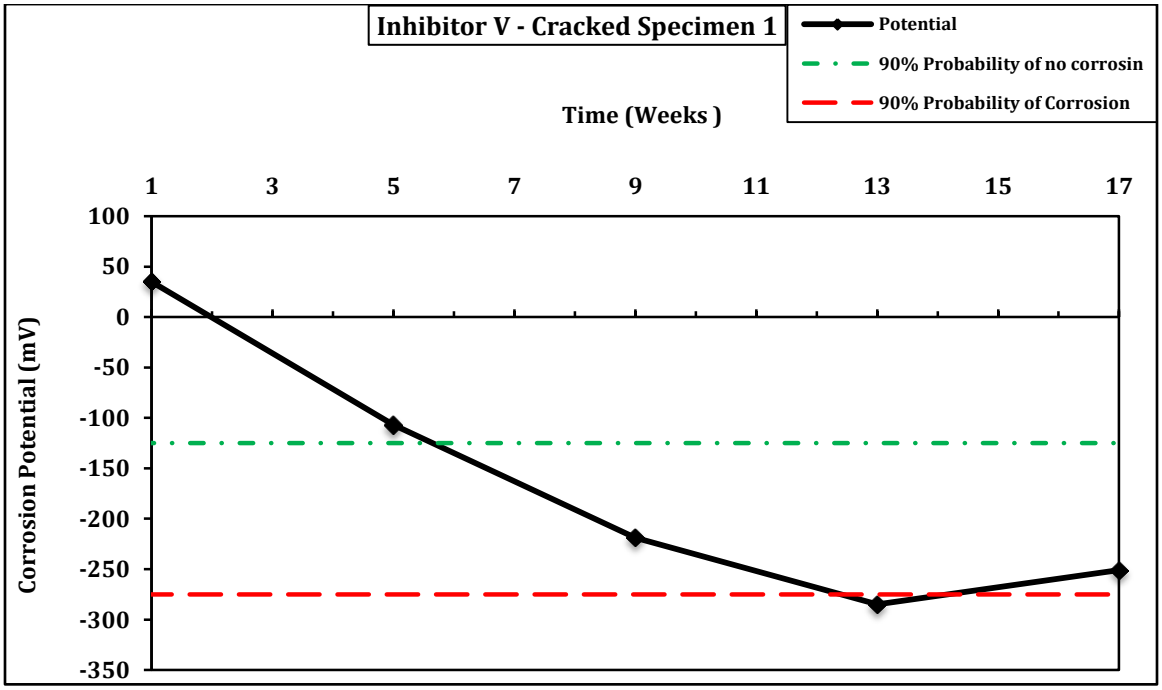


Figure C.34: Corrosion Potential for Steel in Cracked Concrete Specimen (1) Made with Inhibitor V

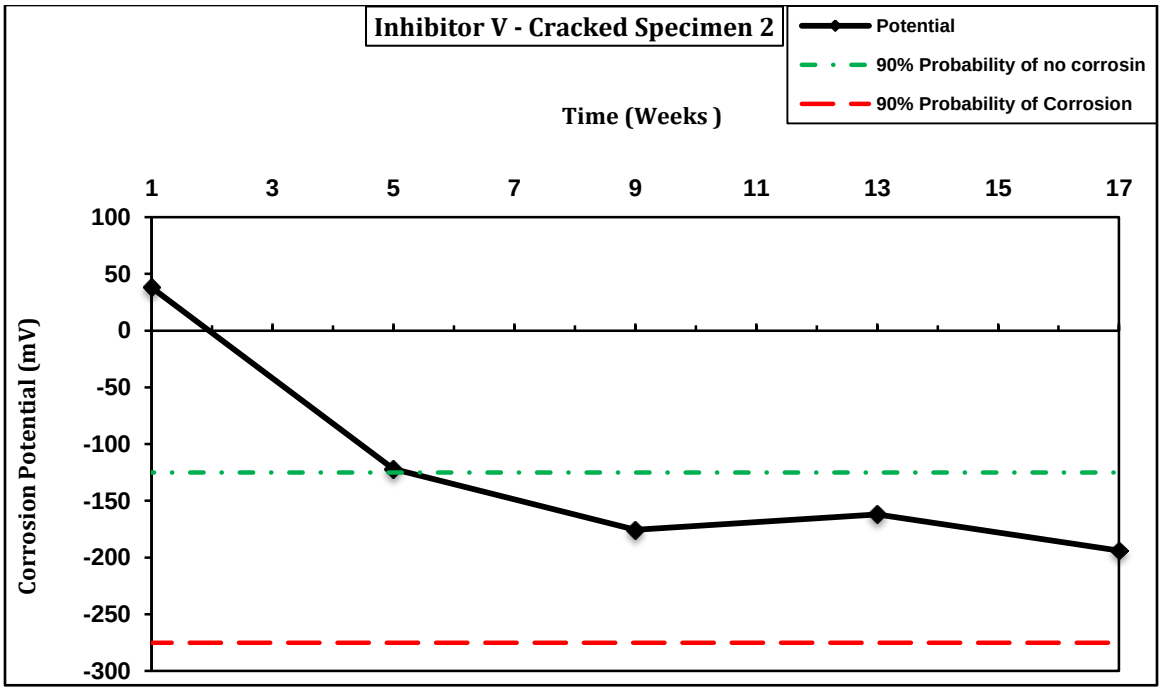


Figure C.35: Corrosion Potential for Steel in Cracked Concrete Specimen (2) Made with Inhibitor V

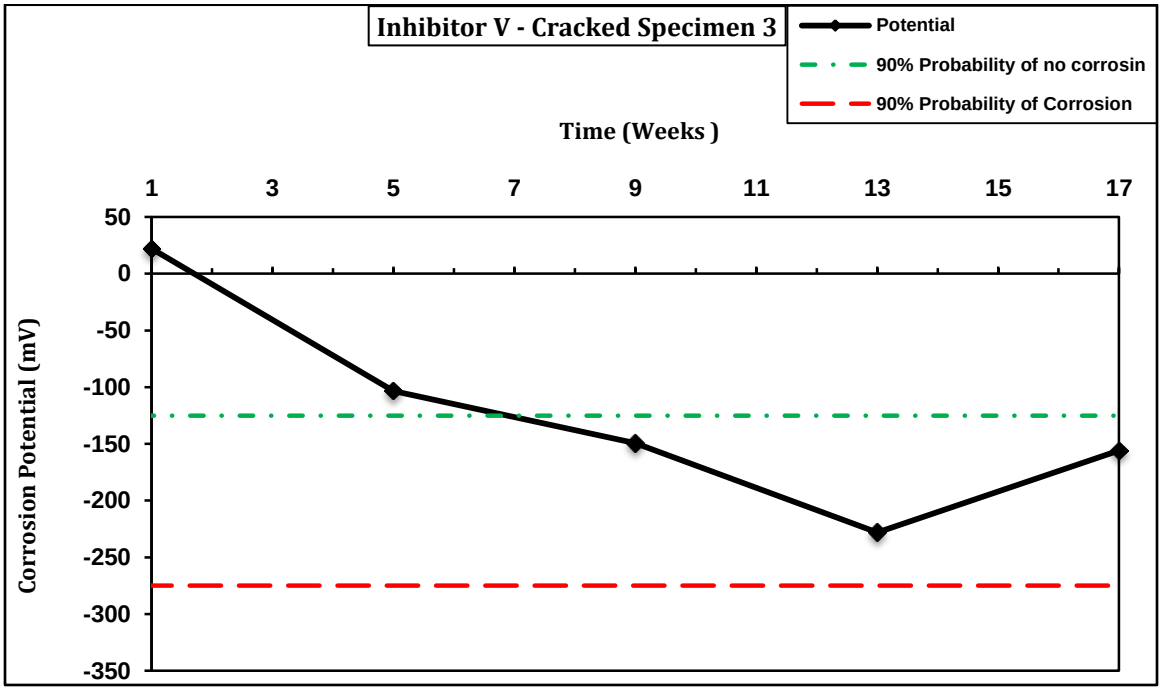


Figure C.36: Corrosion Potential for Steel in Cracked Concrete Specimen (3) Made with Inhibitor V

# REFERENCES


[1] MacGregor, J., Reinforced Concrete Mechanics and Design, 3rd edition, New Jersey, Prentice Hall, 1997.

[2] Maslehuddin, M., Rasheeduzzafar, Page, C. L. Al-Mana, A. I., **"**Influence of Some Parameters Relevant to Arabian Gulf Environment on Reinforcement Corrosion,**"** *Arabian Journal for Science and Engineering*: Theme Issue on Corrosion and Its Prevention, April 1995, pp. 239-257.

[3] Saricimen H., **"**Concrete Durability Problems in the Arabian Gulf Region- A Review,**"** *Proceedings, Fourth International Conference Deterioration and Repair of R.C. in the Arabian, Gulf,* Bahrain, 1993, pp. 943-959.

[4] Shameem, M., Maslehuddin, M., Saricimen, H., and Al-Mana, A. I., **"**Extending the Life of Reinforced Concrete Structures in the Arabian Gulf Environment,**"** *Proceedings, Structural Faults and Repairs Conference*, London, July 1995, pp. 115-126.

[5] Al-Amoudi, M., Elleithy, W. M., Maslehuddin, O. S. B. and Al-Sulaimani, G. J., **"**Use of Fusion-Bonded Epoxy-Coated Steel Bars: Needed Research,**"** *Proc., 4th Saudi Engineering Conference*, 1995, Jeddah, Vol. II, pp. 271-280.

[6] Al-Gahtani, A.S. and Maslehuddin, M., **"**Corrosion of Fusion-Bonded Epoxy Coated Bars in Chloride-Contaminated Plain and Silica Fume Cement Concretes Exposed to Varying Temperature,**"** *Proceedings, Structural Faults and Repair Conference*, Edinburgh, 10-12 June 2008.

[7] Al-Amoudi, O. S. B., Maslehuddin, M. and Ibrahim, M., **"**Long-Term Performance of FBEC Bars in Chloride-Contaminated Concrete,**"** *ACI Materials Journal*, Vol. 101, No. 4, July/August 2004, pp. 303-309.

[8] Maslehuddin, M., Saricimen, H., Al-Mana, A. I., and Shamim, M., **"**Performance of Concrete in A High Chloride-Sulfate Environment,**"** *American Concrete Institute, Special Publication SP-122*, 1990, pp. 469-494.

[9] Saricimen, H., Al-Tayyib, A. J., Maslehuddin, M., Shamim, M., **"**Concrete Deterioration in High Chloride-Sulfate Environment and Repair Strategies,**"** *American Concrete Institute, Special Publication, SP-128*, 1991, pp. 19-34.

[10] Fontana, M G., *Corrosion Engineering*, McGraw-Hill Book Company, New York, 1986

[11] Jones, Denny A., *Principles and Prevention of Corrosion*, Macmillan Publishing Company, New York, NY, 1992.

[12] Broomfield, John P., *Corrosion of Steel in Concrete: Understanding, Investigation and Repair,* St. Edmundsbury Press Limited, Bury St. Edmunds, Suffolk, Great Britain, 1997, 238 pp.

[13] Hausmann, D. A., "Steel Corrosion in Concrete, How does it Occur," *Materials Protection*, Nov. 1967, Vol. 6, pp. 19-23.

[14] Al-Amoudi, O. S. B., Rasheeduzzafar, Abdul Jauwad, S. N., and Maslehuddin, M., "Corrosion of Reinforcing Steel in Sabkha Environment", *King Saud University Journal for Science and Engineering*, Vol. 8, 1996, pp. 37-50.

[15] Holden W.R., Page C L., and Short N.R., "The Influence of Chloride And Sulfates on Concrete Durability," Corrosion of Reinforcement in Concrete Construction, Crane AP., Editor, *Society of Chemical Industry*, London, 1983, pp. 143-149.

[16] Al-Amoudi, O.S.B. and Maslehuddin, M., "The Effect of Chloride and Sulfate Ions on Reinforcement Corrosion", *Cement and Concrete Research*, 1993, Vol. 23, No 1, pp. 139-146.

[17] Mehta, P.K. and Gerwick, B.C., "Cracking-Corrosion Interaction in Concrete Exposed to Marine Environment," *Concrete International*, Vol. 4, No 10, October 1982, pp 45-51.

[18] STUVO (1986), *Concrete in Hot Countries*, Report of STUVO, Dutch member group of FIP, The Netherlands.

[19] Berke, N.S., and Hicks, M.C., "Calcium Nitrite Corrosion Inhibitor With and Without Epoxy-Coated Reinforcing Bar for Long Term Durability in the Gulf," *Concrete Durability in the Arabian Gulf* Macmillan, G.L. (Editor), Bahrain Society of Engineers, 1995, pp. 119-133.

[20] Matta, Z.G., and Giannetti, F., "The Use of Calcium Nitrite Admixtures in the Arabian Gulf," *Concrete Durability in the Arabian Gulf* Macmillan, G.L. (Editor), Bahrain Society of Engineers, 1995, pp. 157-171.

[21] Matta, R.G., and Berke, N.S., "The Use of Calcium Nitrite Corrosion Inhibiting Admixture to Extend the Life of Reinforced Concrete in the Arabian Gulf," *Proceedings, First Inter. Conference on Reinforced Concrete Materials in Hot Climates*, United Arab Emirates University, Al-ain, UAE, April, 1994, pp.24-27.

[22] Al-Amoudi, O.S.B., M. Maslehuddin, A.N. Lashari, and A.A. Almusallam, AA. (2003). "Effectiveness of Corrosion Inhibitors in Contaminated Concrete," *Cement & Concrete Composites*. Vol. 25, No. 4-5, pp. 439-450.

[23] Ramachandran, V.S. (1984). *Concrete Admixtures Handbook: Properties, Science and Technology*, Noyes Publications, Park Ridge, New Jersey.

[24] Zoltanetzky J.R., C. Gordon, and J. Parnes (1990). New Developments in Corrosion Inhibiting Admixture Systems for Reinforced Concrete. In: Page CL, Treadaway KWJ, Bamforth PB, editors. *Corrosion of Reinforcement in Concrete*. London: Elsevier Applied Science; pp. 825 – 850.

[25] Treadaway K.W.J. and A.D. Russell (1968). The Inhibition of the Corrosion of Steel in Concrete, *Highways and Public Works*; Vol. 36, pp. 40 – 41.

[26] Craig R.J., and L.E. Wood (1970). **"**Effectiveness of Corrosion Inhibitors and Their Influence on The Physical Properties of Portland Cement Corrosion Inhibitor in Concrete,**"** *Transportation Research Record*, No. 328; Highway Research Board p. 77 – 78.

[27] Gouda V.K. and W.Y. Halaka (1970). **"**Corrosion and Corrosion Inhibition of Reinforced Steel Embedded in Concrete,**"**. *British Corrosion Journal*, Vol. 5, pp. 204–208.

[28] Gaidis, JM. (2004). **"**Chemistry of Corrosion Inhibitors,**"** *Cement & Concrete Composites*, Vol. 26, No. 3, pp. 181-190.

[29] Griffin, D.F. (1975). **"**Corrosion Inhibitors for Reinforced Concrete,**"** *ACI Special Publication SP-49*, American Concrete Institute, Detroit, pp. 95-102.

[30] El-Jazairi, B., N.S. Berke, and W.R. Grace (1990). **"**The Use of Calcium Nitrate as A Corrosion Inhibiting Admixture to Steel Reinforcement in Concrete,**"** *Corrosion of Reinforcement in Concrete*, Elsevier Applied Science, London, 1990. pp. 571-585.

[31] Montes, P.T.W. Bremner, and D.H. Lister (2004). **"**Influence of Calcium Nitrate Inhibitor and Crack Width on Corrosion of Steel in High Performance Concrete Subjected To a Simulated Marine Environment,**"** *Cement & Concrete Composites*, Vol. 26, No. 3, pp. 243-254.

[32] Maeder, U.A. (1989). **"**A New Class of Corrosion Inhibitors,**"** *Proceedings, 3rd International Conference on Deterioration and Repair of Reinforced Concrete in the Arabian Gulf*, Bahrain, Vol. 1, pp. 119-133.

[33] Wombacher, F.U., U. Maeder and B. Marazzani (2004). **"**Aminoalchohol Based Mixed Corrosion Inhibitors,**"** *Cement & Concrete Composites*. Vol. 26, No. 3, pp. 209-216.

[34] Jamil, A., A. Shriri, A.R. Boulif, M.F. Montemor and M.G.S. Ferreira (2005). **"**Corrosion Behavior of Reinforcing Steel Exposed to An Aminoalcohol Based corrosion inhibitor,**"** *Cement & Concrete Composites,* Vol. 27, pp. 671–678.

[35] Scott, A., A. Civjan, J.M. Lafave, T. Joanna, D. Lovett, L. Jose, and D.W. Pfeifer (2005). **"**Effectiveness of Corrosion Inhibiting Admixture Combinations in Structural Concrete,**"** *Cement & Concrete Composites*, Vol. 27, pp. 688–703.

[36] Qian, S. and D. Cusson (2004). **"**Electrochemical Evaluation of The Performance of Corrosion-Inhibiting Systems in Concrete Bridges,**"** *Cement & Concrete Composites*, Vol. 26, pp. 217–233.

[37] Malik, A.U., F. Andijani, F. Al-Moali and G. Ozair (2004). **"**Studies on The Performance of Migratory Corrosion Inhibitors In Protection of Rebar Concrete in Gulf Seawater Environment,**"** *Cement & Concrete Composites*. Vol. 26, No. 3, pp. 243-252.

[38] Al-Mehthel, M., Al-Dulaijan, S. U., Al-Idi, S.H., Shameem, M., Ali, M.R. and Maslehuddin, M. (2009). **"**Performance of Generic and Proprietary Corrosion Inhibitors in Chloride-Contaminated Silica Fume Cement Concrete,**"** *Construction and Building Materials*, 23, Vol. 23, No. 5, pp. 1768-1774.

[39] Belew, Y.K. 1996 **"**New Products Evaluation Committee Laboratory Investigation of Five Corrosion Inhibitors,**"** *Indiana Department of Transportation*, Indianapolis, USA.

[40] Robertson I.N., Newtson C., (2009), **"**Performance of corrosion inhibitors in concrete exposed to marine environment, **"** In: Alexander, M.G., Beushausen, H.-D., Dehn, F., Moyo, P., (eds), Concrete Repair, Rehabilitation and Retrofitting II, Taylor & Francis Group, London, pp 901−906.

[41] Qian, S., and Cusson, D. (2007) **"**Accelerated Laboratory and Field Investigations of Corrosion Inhibiting Systems For Concrete Bridges,**"** *Northern Area Eastern Conference*, Ottawa , Ontario, pp. 1-5.

[42] Paredes, M.A., A.A. Carvallo, R. Kessler, Y.P.Virmani, A.A. Sagüés (2010) **"**Corrosion Inhibitors in Concrete Second Iinterim Report,**"** *Florida Department of Transportation*, University of South Florida, pp. 2959–2968.

[43] Thangavel, K., S. Muralidharan, V. Saraswathy, M. A.Quraishi, 2009 **"**Migration vs Admixed Corrosion Inhibitors for Steel in Portland, Pozzolona and Slag Cement Concretes Under Macro Cell Condition,**"** *The Arabian Journal for Science and* Engineering, Vol. 34, No. 2C, pp. 418 – 424.

[44] Dr. P. Balaguru, 2001, Evaluation of Corrosion Inhibitors, New Jersey Department of Transportation, USA, pp. 127-136.

[45] Shi, X., Yang, Z., Nguyen, T.A., Suo, Z., Avci, R., Song, S. 2012 **"**Electrochemical and Analytical Characterization of Three Corrosion Inhibitors of Steel in Simulated Concrete Pore Solutions,**"** *International Journal of Minerals, Metallurgy and Materials*, January, Vol. 19, No. 1, pp.38-46.

[46] P. Garcés, P. Saura, E. Zornoza, C. Andrade, 2011 **"**Influence of pH on The Nitrite Corrosion Inhibition of Reinforcing Steel in Simulated Concrete Pore Solution,**"** *Corrosion Science*, August, Vol. 53, pp 3991–4000.

[47] M. Pandiarajan, P. Prabhakar and S. Rajendran, 2012 **"**Corrosion Behavior of Mild Steel in Simulated Concrete Pore Solution Prepared in Rain Water, Well Water and Sea Water,**"** *Eur. Chem. Bull.*, Vol. 1, No.7, pp. 238-240.

[48] Mashal Sheban, Muna Abu-Dalo and Ayman Ababneh, 2007 **"**Effect of Benzotriazole Derivatives on the Corrosion of Steel in Simulated Concrete Pore Solutions**,"** Anti-Corrosion Methods and Materials, Vol. 54, No. 3, pp. 135–147.

[49] J. Hu,D. A. Koleva, J. H. W. de Wit, H. Kolev, and K. van Breugel, 2011 **"**Corrosion Performance of Carbon Steel in Simulated Pore Solution in the Presence of Micelles**,"** *Journal of The Electrochemical Society*, Vol. 158, No.3, pp. 76-87.

[50] Lijuan Feng, Huaiyu Yang, Fuhui Wang, 2011 **"**Experimental and Theoretical Studies for Corrosion Inhibition of By Imidazoline Derivative in 5% NaCl Saturated Ca(OH)2 Solution**,"** *Electrochimica Acta*, pp. 58 427– 436.

[51] Pereira, E.V., Figueira, R.B., Salta, M.M., and Fonseca, I.T.E., 2010 **"**Long-term Efficiency of Two Organic Corrosion Inhibitors for Reinforced Concrete**,"** *Materials Science Forum*, Vol. 636-637, pp. 1059-1064.

[52] Ormellese, M., Lazzari, L., Goidanich, S., Fumagalli, G., Brenna, A., 2009 **"**A study of Organic Substances as Inhibitors for Chloride-Induced Corrosion in Concrete**,"** Corrosion Science, Vol. 51, No. 12, pp.2959-2968.

[53] Mennucci, M. M., Banczek, E.P., Rodrigues, P.R.P, Costa, I., 2009 **"**Evaluation of Benzotriazole as Corrosion Inhibitor for Carbon Steel in Simulated Pore Solution**,"** *Cement and Concrete Composites,* Vol. 31, No. 6, July, pp. 418-424.

[54] Nguyen, T.A., Shi, X., 2009 **"**A Mechanistic Study of Corrosion Inhibiting Admixtures, 2009**"** *Anti-Corrosion Methods and Materials*, Vol. 56, No. 1, pp. 3-12.

**[**55**]** Song, H.W., Saraswathy, V., Muralidharan, S., Lee, C.H., Thangavel, K., 2009 **"**Role of Alkaline Nitrites in The Corrosion Performance of Steel in Composite Cements**,"** *Journal of Applied Chemistry*, Vol. 39, No. 1, January, pp. 15-22**.**

[56] Benzina Mechmeche, L., Dhouibi, L., Ben Ouezzdou, M., Triki, E., Zucchi, F., 2008 **"**Investigation of The Early Effectiveness of An Amino-Alcohol Based Corrosion Inhibitor Using Simulated Pore Solutions and Mortar Specimens**,"** *Cement and Concrete Composites*, Vol. 30, No. 3, March, pp. 167-173.

[57] Ann, K. Y. and Buenfeld, N. R., 2007 **"**The Effect of Calcium Nitrite on The Chloride-Induced Corrosion of Steel in Concrete**,"** *Magazine of Concrete Research*, Vol. 59, No. 9, November, pp. 689-697.

[58] Berke, N.S. and M.C. Hicks (2004). Predicting Long-term Durability of Steel Reinforced Concrete with Calcium Nitrate Corrosion Inhibitor, *Cement & Concrete Composites*. Vol. 26, No. 3, pp. 191-198.

[59] Justnes, H. and E.C. Hygaard (1994)., **"**The Influence of Technical Grade Calcium Nitrate Additions on The Chloride Binding Capacity of Cement And The Rate of Chloride Induced Reinforcement Corrosion of Steel Embedded in Mortars**,"** *Corrosion and Corrosion Protection of Steel in Concrete,* Swamy, R.N. Ed., Vol. 1, pp. 491-502.

[60] Nmai, C.K. (2004)., **"**Multi-Functional Organic Corrosion Inhibitor,**"** *Cement & Concrete Composites*, Vol. 26, No. 3, pp. 199-208.

[61] Meyer, Jessi Jackson "Report of Concrete Corrosion Inhibitor Testing," American Engineer Testing, June 4, 2003.

[62] ASTM C 876-91, **"**Standard Test Method for Half Cell Potentials of Reinforcing Steel in Concrete,**"** *Annual Book of ASTM Standards*, Volume 04.02.

[63] Stern, M., and Geary, A.L., 1957 **"**A Theoretical Analysis of the Slope of the Polarization,**"** *Curvesm Journal of The Electrochemical Society*, Vol. 104, No. 1, pp. 56-63

[64] Mansfield, F., 1977 **"**Polarization Resistance Measurements: Experimental Procedure and Evaluation of Data**"**, *Electrochemical Techniques for Corrosion*, NACE, Houston, pp. 18-26.

[65] Gonzalez, A.J., Feliu, S., Andrade, C., and Rodriguez, I., 1991 **"**On-site Detection of Corrosion of Reinforced Concrete Structures, **"** *Materials and Structures*, Vol. 24, pp. 346-350.

[66] Kapat, C., Pradhan, B., and Bhattacharjee, B. 2006. "Potentiostatic Study of Reinforcing Steel in Chloride Contaminated Concrete Powder Solution Extracts." Corros. Sci., Vol. 487, 1757–1769.

[67] ASTM C1152 / C1152M – 04 (2012) e1**"**Standard Test Method for Acid-Soluble Chloride in Mortar and Concrete,**"** *Annual Book of ASTM Standards*, American Society for Testing and Materials, Philadelphia.

[68] ASTM G 109 [2007] Standard Test Method for Determining Effects of Chemical Admixtures on Corrosion of Embedded Steel Reinforcement in Concrete Exposed to Chloride Environments. *Annual Book of ASTM Standards*, American Society for Testing and Materials, Philadelphia.

[69] Beeby, A.W., Development of a Corrosion Cell for the Study of the Influences of the Environment and the Concrete Properties on Corrosion, Cement and Concrete Association, Slough, U.K. October, 1985.

[70] M. Maslehuddin," Corrosion of Steel in Alkeline Media," *Bahrain Society of Engineers*, 6th Middle East Corrosion Conference, January 1994, Vol.5, pp. 597.

# VITAE

## Personal Information


**Name:** Khaled Ahmed Alawi Al-Sodani

**Marital Status:** Married with two children

**Nationality:** Yemeni

**Date of Birth:** 21th April 1981

**Permanent Address:** Engineers Street, Almosal, Rada'a City, Al-Baidha, Yemen

**Email:** khaas2015@yahoo.com

**Mobile:** +966-58-003-9374 & +967-733-733-470


## Educational Qualification

- Graduated from high school in 1999, scientific stream, Joman Secondary Boys School (1996-1999), Rada'a, Yemen.
- B.Sc. in Civil Engineering, Thamar University, July, 2001-July, 2005, Thamar-Yemen.
- Received a scholarship from the Ministry of Higher Education and Thamar University to join summer training for students of Arab Universities Union (2004), Minia University, Egypt.
- Received a scholarship from the Ministry of Higher Education and Thamar University to study M.S degree at KFUPM in 2011.
- M.S (Structures & Materials), King Fahd University of Petroleum and Minerals, September, 2011-May, 2014, Dhahran Saudia Araiba.

## Work and Experience

- In 2007, Assigned as as an Instructor at Thamar University in Yemen, College of Engineering and I am still working there as a faculty member.
- During the period from 2006 to 2010, I worked as a consultant and engineering designer for a lot of reinforced concrete projects, Yemen.

## Publication / Conference Attendance

- "Evaluation of Five Corrosion Inhibitors under the Combined Effect of Chloride and Sulfates", under review.

- "Evaluation of Five Corrosion Inhibitors on Corrosion of Mild Steel in Simulated Concrete Pore Solution for Hot and Aggressive Exposure", under review.

- "Performance of Corrosion inhibitors for Steel in Silica Fume Cement Concrete according to ASTM G109", under preparation.

- "Evaluation of three Corrosion Inhibitors for Corrosion under the Combined Effect of Chloride, Sulfate and Temperature", Abstract already submitted to the World's Largest Corrosion Conference & Expo (NACE 2015).

- "Effect of Corrosion Inhibitors on Corrosion of Mild Steel in Simulated Concrete Pore Solution for Hot and Aggressive Exposure", Abstract already submitted to the World's Largest Corrosion Conference & Expo (NACE 2015).